GAS-PHASE ION/ION REACTIONS FOR ENHANCED LIPID ANALYSIS

by

Caitlin Elizabeth Randolph

A Dissertation

Submitted to the Faculty of Purdue University

In Partial Fulfillment of the Requirements for the degree of

Doctor of Philosophy

Department of Chemistry

West Lafayette, Indiana

December 2020

THE PURDUE UNIVERSITY GRADUATE SCHOOL

STATEMENT OF COMMITTEE APPROVAL

Dr. Scott A. McLuckey, Chair

Department of Chemistry

Dr. Alexander Laskin

Department of Chemistry

Dr. Julia Laskin

Department of Chemistry

Dr. Shelley A. Claridge

Department of Chemistry

Approved by:

Dr. Christine A. Hrycyna

To Brandon,

for your unending love, patience, and support. Thank you for always understanding.

To my family,

for without them, none of this would be possible.

.

ACKNOWLEDGMENTS

First, I would like to express my sincere gratitude to my family. Brandon – thank you for loving, supporting, and encouraging me. I am forever thankful for your patience and strength. Mom and Dad – to you both I owe so much. No words will adequately express my appreciation for the sacrifices you both have made to help me get to this point. My successes are largely owed to the unequivocal love and support you both have given me throughout my life, this journey included. Cayley – thank you for being my best friend, through the good and the bad. I love that we could take on Purdue together. Life without you would be so incredibly dull. Poppy – I attribute my passion for learning to you, and because of you, I had the courage to take this leap.

To my friends and Uncommon family – I feel as though I can never adequately express my appreciation for you all. Each one of you has touched my heart in a special way. Pete – thank you for your patience and guidance. While you thought you were only teaching me to be a weightlifter, you have taught me so much more. Because of you, I know I am capable of things I never imagined. Jackie and Leasa – there is such love in my heart for you two. Our friendship is something rare – unique in every which way – and comes around only once in a lifetime. Between the tears, the hugs, and the endless laughs, my world is a much happier place with you two in it. Courtney – thank you for being an inspiration. Your hard work, dedication, and persistence are truly unparalleled.

To my labmates, former and present, thank you for the conversations and sharing your wisdom. I am so thankful to have worked with and known each of you. To my thesis advisor, Dr. Scott McLuckey, I am forever grateful for this opportunity. Thank you for listening, encouraging, and pushing me. Your dedication to your students is inspiring, and your passion for discovery is unmatched. To my collaborator, Dr. Steve Blanksby, thank you for sharing your knowledge with me. Thank you for your patience, answering my endless questions. Your guidance and support are invaluable.

TABLE OF CONTENTS

LIST OF TABLES 9
LIST OF FIGURES 10
LIST OF ABBREVIATIONS 20
ABSTRACT 22
CHAPTER 1. ENHANCING DETECTION AND CHARACTERIZATION OF LIPIDS USING CHARGE MANIPULATION IN ELECTROSPRAY IONIZATION-TANDEM MASS SPECTROMETRY 24
1.1 Introduction 24
1.2 Charge Switching 29
1.2.1 Negative to Positive Charge Inversion 30
Solution-Based Metal Cationization 30
Solution-Based Covalent Derivatization 34
Gas-Phase Charge Inversion 40
1.2.2 Positive to Negative Charge Inversion 42
Solution-Based Noncovalent Derivatization 42
Gas-Phase Charge Inversion 43
1.3 Charge Manipulation 45
1.3.1 Charge Manipulation of Cations 45
1.3.2 Charge Manipulation of Anions 48
1.4 Conclusions 49
1.5 References 50
CHAPTER 2. GAS-PHASE ION/ION REACTIONS INVOLVING TRIS-PHENANTHROLINE ALKALINE EARTH METAL COMPLEXES AS CHARGE INVERSION REAGENTS FOR THE IDENTIFICATION OF FATTY ACIDS 83
2.1 Introduction 83
2.2 Experimental 86
2.2.1 Reagents 86
2.2.2 Corn Oil Hydrolysis 86
2.2.3 Nomenclature 86

2.2.4 Mass Spectrometry 87
2.3 Results and Discussion 87
2.3.1 Gas-Phase Reaction of FA Anion with $[Cat(Phen)_3]^{2+}$ 87
2.3.2 Gas-Phase Fragmentation of Charge Inverted Saturated Fatty Acids 88
2.3.3 Characterization of Monounsaturated Fatty Acids 89
2.3.4 Characterization of Polyunsaturated Fatty Acids 91
2.3.5 Characterization of Fatty Acids in Corn Oil 95
2.4 Conclusions 96
2.5 References 96
CHAPTER 3. GENERATING FATTY ACID PROFILES IN THE GAS PHASE: FATTY ACID IDENTIFICATION AND RELATIVE QUANTITATION USING ION/ION CHARGE INVERSION CHEMISTRY 114
3.1 Introduction 114
3.2 Experimental 118
3.2.1 Materials 118
3.2.2 Preparation of nESI Solutions 118
3.2.3 Nomenclature 118
3.2.4 Mass Spectrometry 119
3.2.5 Development of Fatty Acid Mass Spectral Library 119
3.2.6 Relative Quantitation of Fatty Acid Isomers 120
3.3 Results and Discussion 121
3.3.1 Development of CID Mass Spectral Library 121
3.3.2 Relative Quantitation of Isomeric Fatty Acids 122
3.3.3 Fatty Acid Profiling of Bovine Liver Extract 125
3.4 Conclusions 127
3.5 References 128
CHAPTER 4. TOWARD COMPLETE STRUCTURE ELUCIDATION OF GLYCEROPHOSPHOLIPIDS IN THE GAS PHASE THROUGH CHARGE INVERSION ION/ION CHEMISTRY 141
4.1 Introduction 141
4.2 Experimental 144

4.2.1 Materials 144
4.2.2 Lipid Extraction and Preparation of nESI Solutions 145
4.2.3 Nomenclature 145
4.2.4 Mass Spectrometry 146
4.3 Results and Discussion 146
4.3.1 Generation of $[FA - H + MgPhen]^+$ Complex Cations from GPL Anions 146
4.3.2 Identification of Double Bond Position(s) in Synthetic GPL 147
4.3.3 Identification of Human Plasma Lipids 149
4.4 Conclusions 153
4.5 References 153
CHAPTER 5. STRUCTURAL ELUCIDATION OF ETHER GLYCEROPHOSPHOLIPIDS USING GAS-PHASE ION/ION CHARGE INVERSION CHEMISTRY 177
5.1 Introduction 177
5.2 Experimental 181
5.2.1 Materials 181
5.2.2 Lipid Extraction and Preparation of nESI Solutions 181
5.2.3 Nomenclature 181
5.2.4 Mass Spectrometry 182
5.3 Results and Discussion 183
5.3.1 Differentiation of Plasmenyl and Plasmanyl Glycerophospholipids 183
5.3.2 Identification of Fatty Acyl Double-Bond Position(s) in Ether GPL 186
5.3.3 Identification of Ether Lipids in Human Plasma 188
5.4 Conclusions 192
5.5 References 193
CHAPTER 6. PROTON TRANSFER REACTIONS FOR THE GAS-PHASE SEPARATION, CONCENTRATION, AND IDENTIFICATION OF CARDIOLIPINS 218
6.1 Introduction 218
6.2 Experimental 220
6.2.1 Materials 220
6.2.2 Mass Spectrometry 221
6.2.3 Nomenclature 221

6.3 Results and Discussion 222
6.3.1 Proton-Transfer Reactions to Facilitate the Characterization of Synthetic CL 222
6.3.2 Proton-Transfer Reactions for CL Class Separation 224
6.3.3 Proton-Transfer Reactions and Refill Experiments to Concentrate Charge-Reduced CL Anions 225
6.3.4 Identification of CLs in *E. coli* Extract Using Proton-Transfer Ion/Ion Reactions and Refill Experiments 227
6.4 Conclusions 229
6.5 References 231
CHAPTER 7. CHARGE-SWITCH DERIVATIZATION OF FATTY ACID ESTERS OF HYDROXY FATTY ACIDS VIA GAS-PHASE ION/ION REACTIONS 250
7.1 Introduction 250
7.2 Experimental 253
7.2.1 Reagents 253
7.2.2 Mass Spectrometry 254
7.2.3 Nomenclature 254
7.3 Results and Discussion 255
7.3.1 Charge Inversion Ion/Ion Strategies to Elucidate Saturated FAHFA Structures 255
7.3.2 Differentiation of Isomeric *n*-FAHFAs using Direct Charge Inversion Ion/Ion Strategies 258
7.3.3 Structure Elucidation of Unsaturated FAHFAs using Charge Inversion Ion/Ion Reactions 260
7.4 Conclusions 262
7.5 References 263
PUBLICATIONS 279

LIST OF TABLES

Table 2.1 Observed *m/z* values from CID of $[M - H + MgPhen]^+$ where M = 18:0. 102

Table 2.2 Observed *m/z* values from CID of $[M - H + MgPhen]^+$ for 18:2(9*Z*,12*Z*) and 18:2(9*Z*,11*Z*) fatty acid isomers shown in Figure 2.6. 108

Table 3.1 Fatty Acid Profile of Bovine Liver Phospholipidome (Polar Bovine Liver Extract) . 140

Table 4.1 Summary of Lipids Identified in Human Plasma Extract Using Gas-Phase Charge Inversion Ion/Ion Chemistry 171

Table 6.1 Cardiolipin profile for *E. coli* extract..... 241

LIST OF FIGURES

Figure 1.1 Common lipid categories with structural examples 65

Figure 1.2 General glycerophospholipid structure. Polar headgroup structures and names are given in the orange panel (top left corner). The headgroup composition determines GPL class. In the green panel (top right), example *sn*-1 radyl chains are portrayed, noting that the nature of the *sn*-1 linkage dictates GPL subclass. Explicitly, GPL contain either an acyl, 1-*O*-alkyl, or a 1-*O*-alk-1′-enyl group at the sn-1 position, indicating the diacyl, plasmanyl, or plasmenyl subclasses, respectively. 66

Figure 1.3 GPLs in human plasma samples. The measurements for PE, PC, and PI species were performed in quintuplicate and reported as the mean ± standard error of the mean (SEM). Adapted with permission from Reference 14. 67

Figure 1.4 FAB-MS/MS spectra of 22:6(4*Z*,7*Z*,10*Z*,13*Z*,16*Z*,19*Z*) (a) $[M - H + 2Li]^+$ and (b) $[M - H]^-$ ions. The product ions indicative of carbon-carbon double bond cleavage are indicated with double bond symbols. Reproduced with permission from Reference 52. 68

Figure 1.5 CID spectra of $[FA - H + 2Li]^+$ adducts of (a) 18:2(9, 12), (b) 18:3(9,12,15), and (c) 18:3(6,9,12). Reproduced with permission from Reference 78. 69

Figure 1.6 Product ion spectra of the $[M - H + 2Li]^+$ precursor ion of FA 18:1(9*Z*) obtained utilizing collisional activation via (a) HCD (30 eV collision energy) and (b) 193 nm UVPD (100 laser pulses per scan were performed with the HCD collision energy set at 2 eV). Reproduced with permission from Reference 79. 70

Figure 1.7 UPLC MRM chromatograms for the double bond positional isomers of FA 18:3 and FA 20:3 The isomer-specific transitions used for 18:3(*n*-3), 18:3(*n*-6), 20:3(*n*-6), and 20:3(*n*-3) were $415^+ \rightarrow 317^+$, $415^+ \rightarrow 307^+$, $443^+ \rightarrow 335^+$, and $443^+ \rightarrow 345^+$, respectively. Reproduced with permission from Reference 81. 71

Figure 1.8 Low-energy CID spectra of $[FA - H + Cu^{II}]^+$ ions for (a) 18:2(9*Z*,12*Z*) and (b) 18:2(9*E*, 12*E*). Reproduced with permission from Reference 83. 72

Figure 1.9 Negative ion mode CID spectra of (a) $[PI(3,4)P_2 - 2H]^{2-}$ (*m/z* 510.2360), (b) $[PI(3,5)P_2 - 2H]^{2-}$ (*m/z* 510.2360), and (c) $[PI(4,5)P_2 - 2H]^{2-}$ (*m/z* 510.2360). Positive ion mode CID spectra of charge-inverted (d) $[(LGa_2)_2(PI(3,4)P_2 - 7H)]^{3+}$ (*m/z* 811.2594), (e) $[(LGa_2)_2(PI(3,5)P_2 - 7H)]^{3+}$ (*m/z* 811.2594), and (f) $[(LGa_2)_2(PI(4,5)P_2 - 7H)]^{3+}$ (*m/z* 811.2594). The product ions that display at least a 3-fold increase abundance relative to corresponding identical ions in the CID spectra of the other two isomers are indicated with a red box. Reprinted with permission from Reference 85. 73

Figure 1.10 Positive ion mode CID spectra for (a) arachidonic acid (*i.e.*, FA 20:4(5*Z*,8*Z*,11*Z*,14*Z*), (b) 9(*S*)- Hydroperoxyoctadecadienoic acid (HPODE), and (c) stearic acid (*i.e.*, FA 18:0) derivatized with cholamine. Reprinted with permission from Reference 98. 74

Figure 1.11 Analysis of a commercially available FAME mixture using OzID in combination with charge-switch derivatization. OzID spectra of (a) AMPP-FA 16:1 (*m/z* 421) and (b) AMPP-FA 18:3 (*m/z* 445). Diagnostic product ions highlighted in (a) reveal the presence of FA 16:0(*n*-7). The red lines indicate peaks diagnostic for polyunsaturated FA 18:3(*n*-3, *n*-6, *n*-9), and black lines indicate peaks characteristic of FA 18:3(*n*-6, *n*-9, *n*-12) in (b). (c) CID product ion spectrum of AMPP-FA 18:3 (*m/z* 445). Adapted with permission from Reference 113. 76

Figure 1.12 Demonstration of gas-phase charge inversion ion/ion chemistry for the analysis of PE 36:2 in human plasma extract. (a) Structure of ionized PE 18:0/18:2(9,12). (b) Reaction scheme detailing identification procedure for the PE 18:0/18:2(9,12) anion. (c) Ion-trap CID spectrum resulting from activation of $[PE\ 36:2 - H]^-$. (d) Product ion spectrum following ion/ion reaction of fragment ions generated via activation of $[PE\ 36:2 - H]^-$ and $[MgPhen_3]^{2+}$ dications and subsequent beam-type CID. (e) CID spectrum of $[18:2 - H + MgPhen]^+$. (f) CID spectrum of $[18:1 - H + MgPhen]^+$. Adapted with permission from Reference 126. 78

Figure 1.13(a) Negative ion mode mass spectra of PC 16:0/18:1 from solutions containing 5 mM ammonium bicarbonate (NH_4HCO_3) and ammonium formate (NH_4COOH). (b) CID spectra (CE = 30 eV) of $[M + HCO_3]^-$ of PC 16:0/18:1 (*m/z* 820) and (c) $[M + HCO_3]^-$ of PC 18:1/16:0 (*m/z* 820). MS^3 product ion spectra obtained via (d) CID and (e) OzID of the product ions at *m/z* 419 from (b). The proposed structure of the product ion observed at *m/z* 419 derived from CID of $[M + HCO_3]^-$ of PC 16:0/18:1 is given in (f). Reprinted with permission from Reference 131. 79

Figure 1.14 Mass spectra of a bovine liver extract (0.5 μM total lipid concentration) obtained via (a) direct negative nano-ESI, (b) direct positive nano-ESI, and (c) charge inversion of the lipid cations shown in (b) with $[PDPA - 2H]^{2-}$ reagent dianions. Reprinted with permission from Reference 135. 81

Figure 1.15 Positive ion ESI-MS spectra of soybean asolectin solutions containing PE 31:1 as an internal standard (IS) within known concentration in methanol (a) without and (b) with the addition of 18C6. (c) The concentrations (μM) of major PEs found in soy asolectin (including isotopic corrections). Reprinted with permission from Reference 150. 82

Figure 2.1 Enlarged spectrum over the *m/z* region of 200 – 650 detailing the results of the ion/ion reaction between $[Mg(Phen)_3]^{2+}$ dications and singly deprotonated 18:1(9*Z*). In order to conclude that the ion/ion reaction is unit efficient, it is important to note that a proton deficient $[Mg(Phen)_3]^{2+}$, denoted $[Mg(Phen)_3 — H]^+$ at *m/z* 563, would indicate a proton transfer reaction between the singly deprotonated $[M — H]^-$ and the $[Mg(Phen)_3]^{2+}$. As there is no peak at *m/z* 563, the ion/ion reaction does not have competing reaction pathways. 101

Figure 2.2 Ion-trap CID spectrum of the $[M – H + MgPhen]^+$ complex generated via gas-phase ion/ion reaction between singly deprotonated 18:0 and $[Mg(Phen)_3]^{2+}$ dications. 103

Figure 2.3 Ion-trap CID of $[M — H + Cat]^+$ with M = 18:0 where (a) Cat = Ca^{2+} (b) Cat = Sr^{2+} (c) Cat = Ba^{2+} and (d) Cat = $MgPhen^{2+}$. The blue asterisk indicates a doubly hydrated CRF product ion. For the bare metal complexes (Cat = Ca^{2+}, Sr^{2+}, or Ba^{2+}), as the size of the cation increases, the relative abundance of the hydrated CRF ion series decreases. 104

Figure 2.4 Ion-trap CID of a series of isomeric 18:1 fatty acids. Ion-trap CID spectrum of $[M – H + MgPhen]^+$ where (a) M = 18:1(11*Z*), (b) M = 18:1(9*Z*), and (c) M = 18:1(6*Z*). The blue curve highlights the spectral pattern used to localize the double bond. 105

Figure 2.5 Ion-trap CID of $[M — H + Cat]^+$ derived from 18:1(11*Z*) where (a) Cat = Ca^{2+} (b) Cat = Sr^{2+} (c) Cat = Ba^{2+} and (d) Cat = $MgPhen^{2+}$. The blue curve highlights the spectral pattern used to identify the double bond position. The blue asterisk indicates a doubly hydrated CRF product ion. 106

Figure 2.6 Ion-trap CID of $[M – H + MgPhen]^+$ where (a) M = 18:2(9*Z*,12*Z*) and (b) M = 18:2(9*Z*,11*Z*). Comparison of the two CID spectra shows marked differences between diunsaturated FAs with homoconjugated and conjugated double bonds. 107

Figure 2.7 Ion-trap CID of $[M – H + MgPhen]^+$ derived from the gas-phase ion/ion reaction of singly deprotonated 20:2(8*Z*,14*Z*) and $[Mg(Phen)_3]^{2+}$. 109

Figure 2.8 Ion-trap CID of $[M – H + MgPhen]^+$ derived from the gas-phase ion/ion reaction of $[Mg(Phen)_3]^{2+}$ with singly deprotonated (a) 18:3(9*Z*,12*Z*,15*Z*) and (b) 18:3(6*Z*,9*Z*,12*Z*). 110

Figure 2.9 (a) Negative ion mode nESI of hydrolyzed corn oil. (b) Negative ion mode nESI of blank solvent extraction. FAs are known to be common contaminants found in glassware, plastics, and solvents. FAs observed in both the hydrolyzed corn oil and the blank solvent extraction are denoted in red, whereas FAs unique to corn oil are denoted in green. The 18:1 FA was found in both the hydrolyzed corn oil and the blank solvent extraction, yet the relative abundance of the 18:1 FA in the hydrolyzed corn oil is considerably greater than in the blank solvent extraction. Therefore, it can be presumed that the 18:1 FA is also present in the corn oil sample. 111

Figure 2.10 The CID spectrum of $[M – H + MgPhen]^+$ where M = 16:1 isolated from hydrolyzed corn oil (FA contaminant). Note that double bond stereochemistry cannot be ascertained using the presented method. However, as the *Z* geometry is most common biologically, the structure is depicted as such. 112

Figure 2.11 Ion-trap CID of $[M – H + MgPhen]^+$ where M = (a) 18:1, (b) 18:2, and (c) 18:3. Fatty acids were isolated from negative nESI of hydrolyzed corn oil. 113

Figure 3.1 CID spectra resulting from the activation of (a) [22:5(7*Z*, 10*Z*, 13*Z*, 16*Z*, 19*Z*) – H + $MgPhen]^+$ and (b) [22:5(4*Z*, 7*Z*, 10*Z*, 13*Z*, 16*Z*) – H + $MgPhen]^+$. (c) Difference plot ((*n*-6) – (*n*-3)) highlighting the distinguishing product ions for 22:5 isomer differentiation. 132

Figure 3.2 CID spectra representative of isomeric FA mixtures analyzed as the charge-inverted FA complex cation, $[FA – H + MgPhen]^+$. CID spectra of $[18:1 – H + MgPhen]^+$ for the isomeric mixture of 18:1 *n*-9/*n*-7 at the molar ratios of (a) 5/95 and (b) 95/5. CID spectra of $[18:3 – H + MgPhen]^+$ for the isomeric mixture of 18:3 *n*-3/*n*-6 at the molar ratios of (c) 15/85 and (d) 95/5. Product ions used for relative quantitation are shown in red. Calculated isomer compositions (mean ± standard deviation, *n* = 3) are shown in green. The lightning bolt signifies the precursor ion subjected to ion-trap CID. 133

Figure 3.3 Structure and fragmentation pattern of $[FA – H + MgPhen]^+$ ion where FA = 18:1(9*Z*) (*i.e.* the *n*-9 isomer). 134

Figure 3.4 Structure and fragmentation pattern of $[FA – H + MgPhen]^+$ ion where FA = 18:1(11*Z*) (*i.e.* the *n*-7 isomer). 135

Figure 3.5 Structure and fragmentation pattern of $[FA – H + MgPhen]^+$ ion where FA = 18:3(6*Z*,9*Z*,12*Z*) (*i.e.* the *n*-6 isomer). 136

Figure 3.6 Structure and fragmentation pattern of [FA – H + MgPhen]$^+$ ion where FA = 18:3(9*Z*,12*Z*,15*Z*) (*i.e.* the *n*-3 isomer). 137

Figure 3.7 Demonstration of gas-phase generation of fatty acyl anions from bovine liver extract. (a) Nano-ESI mass spectrum of 50 μM BLE obtained via direct negative ion mode ionization. (b) Fatty acid profile CID spectrum resulting from collisional activation of BLE precursors in the phospholipid range (*m*/*z* 650–900), followed by a subsequent collisional activation of remaining anions from *m*/*z* 400 to 650. (c) Enlargements of the fatty acid profile shown in panel (b) over the mass-to-charge range of 200–400. 138

Figure 3.8 Mass spectrum resulting from the gas-phase ion/ion reaction of [Mg(Phen)$_3$]$^{2+}$ dications with fatty acyl anions derived from bovine liver extract via the described ion/ion chemistry. Peaks labeled with the blue circle are not fatty acids, as confirmed by CID of the precursor ion..... 139

Figure 4.1 Sequence of MS events used to structurally interrogate synthetic PE 16:0/18:1(9*Z*). (a) Structure of ionized PE 16:0/18:1(9*Z*) (i.e., [PE – H]$^-$). The blue and red font indicate the *sn*-1 and *sn*-2 fatty acyls, respectively. (b) Reaction scheme detailing identification procedure for the PE 16:0/18:1(9*Z*) anion. (c) Ion-trap CID spectrum of [PE – H]$^-$ (*m*/*z* 716.5). (d) Charge inversion spectrum generation via the gas-phase ion/ion reaction between product ions generated from CID of the [PE – H]$^-$ precursor ion as shown in (c) and [MgPhen$_3$]$^{2+}$ dications. (e) Subsequent beam-type (BT) CID spectrum generated post-ion/ion reaction. (f) Ion-trap CID product ion spectrum following monoisotopic mass selection and collisional activation of [18:1(9*Z*) – H + MgPhen]$^+$ (*m*/*z* 485.3). Note that circles (●/○) indicate positive ion mode analysis, while squares (■/□) indicate negative ion mode analysis. 159

Figure 4.2 Sequence of MS events used to provide in-depth structural identification for synthetic PE 18:0/20:4(5*Z*, 8*Z*, 11*Z*,14*Z*) standard. The blue and red font indicate the *sn*-1 and *sn*-2 fatty acyl product ions respectively. (a) Ion-trap CID spectrum of [PE 18:0/20:4(5*Z*, 8*Z*, 11*Z*,14*Z*) – H]$^-$ (*m*/*z* 766.4). (b) Charge inversion spectrum generation via the gas-phase ion/ion reaction between product ions generated from CID of the [PE 18:0/20:4(5*Z*, 8*Z*, 11*Z*,14*Z*) – H]$^-$ precursor ion as shown in (a) and [MgPhen$_3$]$^{2+}$ dications. (c) Subsequent beam-type (BT) CID spectrum generated post-ion/ion reaction. (d) Ion-trap CID product ion spectrum following monoisotopic mass-selection and collisional activation of [20:4(5Z, 8Z, 11Z,14Z) – H + MgPhen]$^+$ (*m*/*z* 507.3). .. 160

Figure 4.3 Ion-trap CID spectrum resulting from collisional activation of [PC 16:0/18:1(9Z) + Cl]$^-$ (*m*/*z* 794.5). 161

Figure 4.4 Sequence of MS events used to provide in-depth structural identification for synthetic PC 16:0/18:1(9*Z*) standard. (a) Ion-trap CID spectrum of [PC 16:0/18:1(9*Z*) – CH$_3$]$^-$ (*m*/*z* 744.5). (b) Charge inversion spectrum generation via the gas-phase ion/ion reaction between product ions generated from CID of the [PC 16:0/18:1(9*Z*) – CH$_3$]$^-$ precursor ion as shown in (a) and [MgPhen$_3$]$^{2+}$ dications. (c) Subsequent beam-type (BT) CID spectrum generated post-ion/ion reaction. (d) Ion-trap CID product ion spectrum following monoisotopic mass-selection and collisional activation of [18:1(9Z) – H + MgPhen]$^+$ (*m*/*z* 485.3). 162

Figure 4.5 Sequence of MS events used to provide in-depth structural identification for synthetic PG 16:0/18:1(9*Z*) standard. (a) Ion-trap CID spectrum of [PG 16:0/18:1(9*Z*) – CH_3]$^-$ (*m/z* 747.5). (b) Charge inversion spectrum generation via the gas-phase ion/ion reaction between product ions generated from CID of the [PG 16:0/18:1(9*Z*) – H]$^-$ precursor ion as shown in (a) and [$MgPhen_3$]$^{2+}$ dications. (c) Subsequent beam-type (BT) CID spectrum generated post-ion/ion reaction. (d) Ion-trap CID product ion spectrum following monoisotopic mass-selection and collisional activation of [18:1(9Z) – H + MgPhen]$^+$ (*m/z* 485.3). 163

Figure 4.6 Ion-trap CID spectrum resulting from collisional activation of [PS 16:0/18:1(9Z) – H]$^-$ (*m/z* 760.5). 164

Figure 4.7 Sequence of MS events used to provide in-depth structural identification for synthetic PS 16:0/18:1(9*Z*) standard. (a) Ion-trap CID spectrum of [PS 16:0/18:1(9*Z*) – serine]$^-$ (*m/z* 760.5). (b) Charge inversion spectrum generation via the gas-phase ion/ion reaction between product ions generated from CID of the [PS 16:0/18:1(9*Z*) – serine]$^-$ precursor ion as shown in (a) and [$MgPhen_3$]$^{2+}$ dications. (c) Subsequent beam-type (BT) CID spectrum generated post-ion/ion reaction. (d) Ion-trap CID product ion spectrum following monoisotopic mass-selection and collisional activation of [18:1(9Z) – H + MgPhen]$^+$ (*m/z* 485.3). 165

Figure 4.8 Sequence of MS events used to provide in-depth structural identification for synthetic PA 16:0/18:1(9*Z*) standard. (a) Ion-trap CID spectrum of [PA 16:0/18:1(9*Z*) – CH_3]$^-$ (*m/z* 673.5). (b) Charge inversion spectrum generation via the gas-phase ion/ion reaction between product ions generated from CID of the [PA 16:0/18:1(9*Z*) – H]$^-$ precursor ion as shown in (a) and [$MgPhen_3$]$^{2+}$ dications. (c) Subsequent beam-type (BT) CID spectrum generated post-ion/ion reaction. (d) Ion-trap CID product ion spectrum following monoisotopic mass-selection and collisional activation of [18:1(9Z) – H + MgPhen]$^+$ (*m/z* 485.3). 166

Figure 4.9 Sequence of MS events used to provide in-depth structural identification for synthetic PI 16:0/18:1(9*Z*) standard. (a) Ion-trap CID spectrum of [PI 16:0/18:1(9*Z*) – CH_3]$^-$ (*m/z* 835.5). (b) Charge inversion spectrum generation via the gas-phase ion/ion reaction between product ions generated from CID of the [PI 16:0/18:1(9*Z*) – H]$^-$ precursor ion as shown in (a) and [$MgPhen_3$]$^{2+}$ dications. (c) Subsequent beam-type (BT) CID spectrum generated post-ion/ion reaction. (d) Ion-trap CID product ion spectrum following monoisotopic mass-selection and collisional activation of [18:1(9Z) – H + MgPhen]$^+$ (*m/z* 485.3). 167

Figure 4.10 Direct infusion negative ion mode nESI mass spectrum of human plasma extract. 168

Figure 4.11 Precursor ion scan of *m/z* 184 in positive ion mode used to identify PC lipids in human plasma extract. This scan also includes other choline-bearing lipids such as the [M + H]$^+$ ion of sphingomyelin SM (d34:1) at *m/z* 703.6 169

Figure 4.12 141 Da neutral loss scan in the positive ion mode used to identify PE lipids in human plasma extract. 170

Figure 4.13 Ion-trap CID spectrum resulting from collisional activation of [PC 34:2 + OAc]$^-$ (*m/z* 816.6) found in human plasma extract. 172

Figure 4.14 Demonstration of gas-phase charge inversion ion/ion chemistry for the analysis of PC 34:2 in human plasma extract. (a) Ion-trap CID spectrum resulting from activation of [PC 34:2 – CH_3]$^-$. (b) Product ion spectrum following ion/ion reaction of fragment ions generated via activation of [PC 34:2 – CH_3]$^-$ and [$MgPhen_3$]$^{2+}$ dications. (c) Beam-type CID product ion spectrum post-ion/ion reaction. (d) CID spectrum of [18:2 – H + MgPhen]$^+$. 173

Figure 4.15 CID spectrum resulting from collisional activation of [PC 34:2 – CH_3]$^-$ (*m/z* 742.5) found in human plasma extract. Enlargement of the spectrum from m/z 245 – 285 shows the major FA anions [16:0 – H]$^-$ (*m/z* 255.2) and [18:2 – H]$^-$ (*m/z* 279.2) and the minor FA anions [16:1 – H]$^-$ (*m/z* 253.2) and [18:1 – H]$^-$ (*m/z* 281.2). 174

Figure 4.16 Demonstration of gas-phase charge inversion ion/ion chemistry for the analysis of PI 38:4 extracted from human plasma. (a) Ion-trap CID spectrum resulting from activation of [PI 38:4 – H]$^-$ (*m/z* 885.5). (b) Product ion spectrum following ion/ion reaction of fragment ions generated via activation of [PI 38:4 – H]$^-$ and [$MgPhen_3$]$^{2+}$ dications and subsequent beam type CID. (c) CID spectrum of [20:4 – H + MgPhen]$^+$ (*m/z* 507.3). 175

Figure 4.17 Demonstration of gas-phase charge inversion ion/ion chemistry for the analysis of PE 36:2 in human plasma extract. (a) Ion-trap CID spectrum resulting from activation of [PE 36:2 – H]$^-$. (b) Product ion spectrum following ion/ion reaction of fragment ions generated via activation of [PE 36:2 – H]$^-$ and [$MgPhen_3$]$^{2+}$ dications and subsequent beam-type CID. (c) CID spectrum of [18:2 – H + MgPhen]$^+$. (d) CID spectrum of [18:1 – H + MgPhen]$^+$. 176

Figure 5.1 Schematic diagram (not to scale) of a QTRAP 4000 hybrid triple quadrupole/linear ion trap mass spectrometer (AB SCIEX, Concord, ON, Canada) previously modified for ion/ion reactions. 198

Figure 5.2 MS^2 product ion spectra obtained via ion-trap CID of (a) [PE *P*-18:0/18:1(9Z) – H]$^-$ (*m/z* 728.5), (b) [PE *O*-16:0/18:1(9Z) – H]$^-$ (*m/z* 702.5), and (c) [PE 16:0/18:1(9Z) – H]$^-$ (*m/z* 716.5). MS^3 product ion spectra obtained via ion-trap CID of (d) [PE *P*-18:0/18:1(9Z) – H – R_2'CH=C=O]$^-$ (*m/z* 464.3), (e) [PE *O*-16:0/18:1(9Z) – H – R_2'CH=C=O]$^-$ (*m/z* 438.3), and (f) [PE 16:0/18:1(9*Z*) – H – R_2'CH=C=O]$^-$ (*m/z* 452.3). The lightning bolt (□) indicates the ion subjected to ion-trap CID. 199

Figure 5.3 MS^2 product ion spectra obtained via ion-trap CID of (a) [PC *P*-18:0/18:1(9Z) – H]$^-$ (*m/z* 806.5), (b) [PC *O*-16:0/18:1(9Z) – H]$^-$ (*m/z* 780.5), and (c) [PC 16:0/18:1(9Z) – H]$^-$ (*m/z* 794.5). MS^3 product ion spectra obtained via ion-trap CID of (d) [PC *P*-18:0/18:1(9Z) – H – R_2CH=C=O]$^-$ (*m/z* 492.3), (e) [PC *O*-16:0/18:1(9Z) – H – R_2CH=C=O]$^-$ (*m/z* 466.3), and (f) [PC 16:0/18:1(9*Z*) – H – R_2CH=C=O]$^-$ (*m/z* 480.3). The lightning bolt (□) indicates the ion subjected to ion-trap CID. 200

Figure 5.4 Mutual storage product ion spectra resulting from ion/ion reaction between [PDPA – 2H]$^{2-}$ dianions and (a) [PE *P*-18:0/18:1(9Z) + H]$^+$ (*m/z* 730.5), (b) [PE *O*-16:0/18:1(9Z) + H]$^+$ (*m/z* 704.5), and (c) [PE 16:0/18:1(9Z) + H]$^+$ (*m/z* 718.5) cations 201

Figure 5.5 CID spectra of (a) [PE *P*-18:0/18:1(9*Z*) – H]$^-$ (*m/z* 728.5), (b) [PE *O*-16:0/18:1(9*Z*) – H]$^-$ (*m/z* 702.5), and (c) [PE 16:0/18:1(9*Z*) – H]$^-$ (*m/z* 716.5) obtained via charge inversion ion/ion reaction. Product ion spectra obtained via ion-trap CID of mass-selected (d) [PE *P*-18:0/18:1(9*Z*) – H – R_2'CH=C=O]$^-$ (*m/z* 464.3), (e) [PE *O*-16:0/18:1(9*Z*) – H – R_2'CH=C=O]$^-$ (*m/z* 438.3), and (f) [PE 16:0/18:1(9*Z*) – H – R_2'CH=C=O]$^-$ (*m/z* 452.3). The lightning bolt indicates the ion that was subjected to ion-trap CID..... 202

Figure 5.6 Mutual storage product ion spectra resulting from ion/ion reaction between [PDPA – 2H]$^{2-}$ dianions and (a) [PC *P*-18:0/18:1(9Z) + H]$^+$ (*m/z* 772.5), (b) [PC *O*-16:0/18:1(9Z) + H]$^+$ (*m/z* 746.5), and (c) [PC 16:0/18:1(9Z) + H]$^+$ (*m/z* 760.5) cations. 203

Figure 5.7 CID spectra of (a) [PC *P*-18:0/18:1(9Z) – CH_3]$^-$ (*m/z* 756.5), (b) [PC *O*-16:0/18:1(9Z) – CH_3]$^-$ (*m/z* 730.5), and (c) [PC 16:0/18:1(9Z) – CH_3]$^-$ (*m/z* 744.5) obtained via charge inversion ion/ion reaction. Product ion spectra obtained via ion-trap CID of mass-selected (d) [PC *P*-18:0/18:1(9Z) – CH_3 – R_2'CH=C=O]$^-$ (*m/z* 492.2), (e) [PC *O*-16:0/18:1(9Z) – CH_3 – R_2'CH=C=O]$^-$ (*m/z* 466.2), and (f) [PC 16:0/18:1(9*Z*) – CH_3 – R_2'CH=C=O]$^-$ (*m/z* 480.3)..... 204

Figure 5.8 Demonstration of ion/ion reactions to identify double-bond position(s) in the fatty acyl substituent of an unsaturated plasmalogen. (a) Product ion spectrum resulting from the ion/ion reaction between $[MgPhen_3]^{2+}$ dications and fragment ions generated via CID of [PE *P*-18:0/18:1(9*Z*) – H]$^-$. (b) Product ion spectrum generated by BT CID of the product ions shown in (a). (c) Ion-trap CID spectrum of mass-selected [18:1(9*Z*) – H + MgPhen]$^+$ (*m/z* 485.3)..... 205

Figure 5.9 Demonstration of ion/ion reactions to identify double bond position(s) in the fatty acyl substituent of unsaturated plasmanyl GPL. (a) Product ion spectrum resulting from the ion/ion reaction between $[MgPhen_3]^{2+}$ dications and fragment ions generated via CID of [PE *O*-16:0/18:1(9*Z*) – H]$^-$. (b) Product ion spectrum generated by BT CID of the product ions shown in (a). (c) Ion-trap CID spectrum of mass-selected [18:1(9*Z*) – H + MgPhen]$^+$ (*m/z* 485.3)..... 206

Figure 5.10 Demonstration of ion/ion reactions to identify double bond position(s) in the fatty acyl substituent of unsaturated plasmalogens. (a) Mutual storage product ion spectrum resulting from the ion/ion reaction between $[MgPhen_3]^{2+}$ dications and fragment ions generated via CID of [PC *P*-18:0/18:1(9*Z*) – H]$^-$. (b) Product ion spectrum generated by BT CID of the mutual storage product ions shown in (a). (c) Ion-trap CID spectrum of mass-selected [18:1(9*Z*) – H + MgPhen]$^+$ (*m/z* 485.3). 207

Figure 5.11 Demonstration of ion/ion reactions to identify double bond position(s) in the fatty acyl substituent of unsaturated plasmalogens. (a) Mutual storage product ion spectrum resulting from the ion/ion reaction between $[MgPhen_3]^{2+}$ dications and fragment ions generated via CID of [PC *O*-18:0/18:1(9*Z*) – H]$^-$. (b) Product ion spectrum generated by BT CID of the mutual storage product ions shown in (a). (c) Ion-trap CID spectrum of mass-selected [18:1(9*Z*) – H + MgPhen]$^+$ (*m/z* 485.3). 208

Figure 5.12 (a) Precursor ion scan of *m/z* 184 in positive ion mode used to identify PC lipids in human plasma extract. This scan also includes other choline-bearing lipids such as the [M + H]$^+$ ion of sphingomyelin SM. (b) 141 Da neutral loss scan in the positive ion mode used to identify PE lipids in human plasma extract. 209

Figure 5.13 Nano-ESI mass spectra of human plasma extract obtained via (a) direct infusion negative ionization and (b) direct infusion positive ionization. 210

Figure 5.14 (a) Mutual storage product ion/ion spectrum resulting from the charge inversion ion/ion reaction of mass-selected [PE *O*-38:5 + H]$^+$ (*m/z* 752.5) cations and [PDPA – 2H]$^{2-}$ dianions. Note that the mutual storage product ion denoted with an asterisk (*) at *m/z* 716.5 results from the charge inversion of a precursor ion coisolated with the *m/z* 752.5 cation population. (b) MS^3 ion-trap CID spectrum of the ion at *m/z* 750.5 obtained after ion/ion reaction 211

Figure 5.15 (a) Ion-trap CID spectrum of the ether-linked PE *O*-38:5 anion at *m/z* 750.5. (b) MS^3 product ion spectrum obtained via ion-trap CID of the mass-selected fragment ion observed at *m/z* 464.2 in panel (a). (c) Product ion spectrum obtained following the mutual storage charge inversion ion/ion reaction of the fragment ions observed in panel (a) with [MgPhen$_3$]$^{2+}$ dications and subsequent collisional activation with beam-type CID. 212

Figure 5.16 MS^3 product ion spectrum of the ion at *m/z* 480.2 derived from collisional activation of the [PE *O*-38:5 – H]$^-$ (*m/z* 730.5) ion from human plasma extract. 213

Figure 5.17 Ion-trap CID of mass-selected [20:4 – H + MgPhen]$^+$ from derived from PE *P*-18:0/20:4(5,8,11,14) extracted from human plasma. 214

Figure 5.18 (a) Product ion spectrum resulting from ion/ion reaction between [PDPA – 2H]$^{2-}$ dianions and [PC *O*-38:5 + H]$^+$ cations. (b) CID spectrum of the charge-inverted [PC *O*-38:5 + PDPA – H]$^-$ complex cation (*m/z* 1014.7). 215

Figure 5.19 (a) Product ion spectrum of [PC *O*-38:5 – CH$_3$]$^-$ (*m/z* 778.6) generated via charge inversion ion/ion reaction of mass-selected [PC *O*-38:5 + H]$^+$ (*m/z* 794.5) cations in human plasma and [PDPA – 2H]$^{2-}$ dianions with subsequent CID of the first generation [PC *O*-38:5 + PDPA – H]$^-$ complex anion (*m/z* 1014.7). (b) Ion-trap CID spectrum of the ion at *m/z* 492.2 shown in panel (a) obtained after ion/ion reaction. 216

Figure 5.20 (a) Ion-trap CID of mass-selected the [PC-*O* 38:5 + OAc]$^-$ anion (*m/z* 852.6) extracted from human plasma. (b) MS^3 product ion spectrum of [PC-*O* 38:5 – CH$_3$]$^-$ anion (*m/z* 778.6). (c) Product ion spectrum obtained following the mutual storage charge inversion ion/ion reaction of the fragment ions shown in panel (b) with [MgPhen$_3$]$^{2+}$ dications and subsequent collisional activation with beam-type CID. 217

Figure 6.1 Demonstration of proton-transfer reactions for the identification of synthetic CL 16:0/18:1/16:0/18:1. (a) Negative nESI of CL 16:0/18:1/16:0/18:1. (b) Mutual storage product ion spectrum resulting from the proton-transfer reaction between Proton-Sponge cations and CL dianions. (c) Ion-trap CID spectrum of charge-reduced CL 16:0/18:1/16:0/18:1. 234

Figure 6.2 MS^2 product ion spectrum of [CL 16:0/18:1/16:0/18:1 – 2H]$^{2-}$ (*m/z* 702). 236

Figure 6.3 MS^3 product ion spectrum of [PA 16:0/18:1 – H]$^-$ (*m/z* 673) from CL 16:0/18:1/16:0/18:1. 237

Figure 6.4 Demonstration of gas-phase proton-transfer ion/ion reactions for the identification of CL from *E. coli* extract. (a) Direct negative nESI mass spectrum of *E. coli* extract. (b) Product ion spectrum resulting from the gas-phase proton-transfer ion/ion reaction between anions shown in (a) and Proton-Sponge reagent cations. Note that both spectra represent an average of 20 scans. 238

Figure 6.5 Enlargement of *m/z* 600 – 900 region in the (a) direct negative nESI mass spectrum of *E. coli*. extract, and (b) mutual storage product ion spectrum resulting from the gas-phase proton transfer ion/ion reaction between anions shown in (a) and Proton-Sponge® reagent cations. .. 239

Figure 6.6 Normalized abundance cardiolipin profile for *E. coli* extract at the sum compositional level generated via proton-transfer ion/ion reactions..... 240

Figure 6.7 (a) Ion-trap CID spectrum of *m/z* 693.5 from *E. coli* lipid extract. (b) Mutual storage product ion spectrum resulting from the ion/ion reaction between mass-selected *m/z* 693.5 from *E. coli* lipid extract and Proton-Sponge reagent cations. (c) Ion-trap CID spectrum of *m/z* 693.5 from *E. coli* lipid extract after the proton-transfer ion/ion reaction. The lightning bolt indicates the ion subjected to ion-trap CID..... 242

Figure 6.8 Demonstration of selective transfer of charge-reduced $[CL - H]^-$ product ions to the LIT for storage following the proton-transfer ion/ion reaction between lipid anions derived from *E. coli*. extract and Proton-Sponge® cations and subsequent increase in q2 RF amplitude. 243

Figure 6.9 Demonstration of refill experiments to concentrate charge-reduced $[CL - H]^-$ product ion signals. All mutual storage product ion spectra result from the ion/ion reaction between lipid anions derived from *E. coli* extract and Proton-Sponge reagent cations, followed by an increase in q2 RF value. Note that all spectra represent an average of 20 scans. Product ion spectra obtained via (a) 1, (b) 2, and (3) 3 fill cycles. 244

Figure 6.10 (a) Ion-trap CID spectrum of the charge-reduced $[CL\ 70{:}3 - H]^-$ ion (*m/z* 1430) that has been concentrated in Q3 using a total of three fill cycles. (b) Enlargement of *m/z* 550–950 mass spectral region shown in (a). The lightning bolt indicates the ion subjected to ion-trap CID. ... 245

Figure 6.11 MS^3 product ion spectrum of the mass-selected product ion observed at *m/z* 673. 246

Figure 6.12 MS^3 product ion spectrum of the mass-selected product ion observed at *m/z* 699. 247

Figure 6.13 (a) Ion trap CID spectrum of the charge-reduced $[CL\ 70{:}3 - H]^-$ ion (*m/z* 1430) that has *not* been concentrated in Q3 using a refill experiments. (b) enlargement of *m/z* 550 – 950 mass spectral region shown in (a). 248

Figure 6.14 (a) Ion-trap CID spectrum of the charge-reduced $[CL\ 67{:}3 - H]^-$ ion (*m/z* 1388) that has been concentrated in Q3 using a total of three refill experiments. (b) Enlargement of the *m/z* 625–705 mass spectral region shown in (a). 249

Figure 7.1 Illustration of charge inversion ion/ion workflow used to identify site of esterification in 10-PAHSA. (a) Product ion spectrum resulting from mutual storage ion/ion reaction between $[10\text{-PAHSA} - H]^-$ anions (*m/z* 537.5) and $[MgPhen_3]^{2+}$ reagent dications. (b) Beam type CID spectrum post-ion/ion reaction. (c) Ion trap CID spectrum of mass-selected $[10\text{-HSA} - H - H_2O + MgPhen]^+$ (*m/z* 485.3). 268

Figure 7.2 (a) Direct negative nESI mass spectrum of 10-PAHSA. (b) Product ion spectrum resulting from the ion/ion reaction between $[MgPhen_3]^{2+}$ reagent dications and $[10\text{-PAHSA} - H]^-$ anions. 269

Figure 7.3 BT CID spectrum to generate the $[10\text{-PAHSA} - H + MgPhen]^+$ complex cation (*m/z* 741.5). 270

Figure 7.4 Ion-trap CID spectrum of mass-selected [10-PAHSA – H + MgPhen]$^+$ (*m/z* 741.5).271

Figure 7.5 Ozone-induced dissociation mass spectra of the [HSA - H_2O - H + MgPhen]$^+$ product ions from CID of *n*-PAHSA isomers where *n* = 5, 9, 12 and 16 (w). Data were obtained on a Thermo Scientific Orbitrap Elite (*R* = 240,000 at *m/z* 400) fitted with a Triversa NanoMate nano-electrospray source operating in positive polarity. [*n*-PAHSA + MgPhen]$^+$ cations were generated by nESI of a mixture of $MgCl_2$, 1,10-phenanthroline and the FAHFA standard. Ozone (220 g/Nm^3, external) was seeded in helium buffer gas and delivered to the segmented ion trap as previously described.[17] 272

Figure 7.6 Demonstration of charge inversion ion/ion reactions for the identification of ester position in FAHFA. (a) CID spectrum of mass selected [10-PAHSA – H]$^-$ (*m/z* 537.5). (b) Mutual storage product ion spectrum resulting from the charge inversion ion/ion reaction between [$MgPhen_3$]$^{2+}$ reagent diactions and the product anions shown in panel (a). (c) Product ion spectrum generated via energetic transfer (*i.e.*, beam-type CID) of the mutual storage product cations shown in panel (b) from q2 to Q3. (d) CID spectrum of mass-selected [10-HSA – H – H_2O + MgPhen]$^+$ (*m/z* 485.3)..... 274

Figure 7.7 BT CID spectra of charge-inverted FAHFA complex cations derived from (a) 5-PAHSA, (b) 9-PAHSA, (c) 10-PAHSA, (d) 12-PAHSA, and (e) 13-PAHSA. 275

Figure 7.8 CID spectra of isomeric [*n*-HSA – H – H_2O + MgPhen]$^+$ complex cations derived from (a) 13-PAHSA, (b) 12-PAHSA, (c) 9-PAHSA, and (d) 5-PAHSA. 276

Figure 7.9 (a) Product ion spectrum resulting from ion/ion reaction between [10-POHSA]$^-$ anions and [$MgPhen_3$]$^{2+}$ reagent dications and subsequent BT CID. Ion-trap CID spectra of (b) [10-HSA – H – H_2O + MgPhen]$^+$ (*m/z* 485.3) and (c) [16:1 – H + MgPhen]$^+$ (*m/z* 457.3). 277

Figure 7.10 (a) CID spectrum of [10-POHSA]$^-$ (*m/z* 535.5). (b) Product ion spectrum resulting from ion/ion reaction between the [10-POHSA]$^-$ product anions shown in (a) and [$MgPhen_3$]$^{2+}$ reagent dications followed by collisional activation via BT CID. 278

LIST OF ABBREVIATIONS

BT	Beam-type
CE	Collision energy
CL	Cardiolipin
CID	Collision-induced dissociation
Da	Dalton
EI	Electron Ionization
ESI	Electrospray Ionization
FA	Fatty acid
FAHFA	Fatty acid ester of hydroxy fatty acid
GC	Gas chromatography
GPL	Glycerophospholipid/phospholipid
HFA	Hydroxy fatty acid
HPLC	High Performance Liquid Chromatography
LC	Liquid chromatography
LIT	Linear Ion Trap
m/z	Mass-to-charge ratio
MS	Mass Spectrometry
MS/MS	Tandem Mass Spectrometry
MSAE	Mass Selective Axial Ejection
MS^n	Tandem Mass Spectrometry
nESI	nano Electrospray Ionization
NLS	Neutral loss scan
PA	Glycerophosphatidic Acid

PC	Glycerophosphocholine
PDPA	1,4-phenylenedipropionic acid
PE	Glycerophosphoethanolamine
PG	Glycerophosphoglycerol
Phen	Phenanthroline
PI	Glycerophosphoinositol
PIS	Precursor ion scan
PS	Glycerophosphoserine
QqQ	Triple Quadrupole

ABSTRACT

Heightened awareness regarding the implication of disturbances in lipid metabolism with respect to prevalent human-related pathologies demands analytical techniques that provide unambiguous structural characterization and accurate quantitation of lipids in complex biological samples. The diversity in molecular structures of lipids along with their wide range of concentrations in biological matrices present formidable analytical challenges. Modern mass spectrometry (MS) offers an unprecedented level of analytical power in lipid analysis, as many advancements in the field of lipidomics have been facilitated through novel applications of and developments in electrospray ionization tandem mass spectrometry (ESI-MS/MS). ESI allows for the formation of intact lipid ions with little to no fragmentation and has become widely used in contemporary lipidomics experiments due to its sensitivity, reproducibility, and compatibility with condensed-phase modes of separation, such as liquid chromatography (LC). Owing to variations in lipid functional groups, ESI enables partial chemical separation of the lipidome, yet the preferred ion-type is not always formed, impacting lipid detection, characterization, and quantitation. Moreover, conventional ESI-MS/MS approaches often fail to expose diverse subtle structural features like the sites of unsaturation in fatty acyl constituents or acyl chain regiochemistry along the glycerol backbone, representing a significant challenge for ESI-MS/MS. To overcome these shortcomings, various charge manipulation strategies, including charge-switching, have been developed to transform ion-type and charge state, with aims of increasing sensitivity and selectivity of ESI-MS/MS approaches. Importantly, charge manipulation approaches afford enhanced ionization efficiency, improved mixture analysis performance, and access to informative fragmentation channels.

Here, gas-phase ion/ion chemistry was developed to transform conventional lipid ion types formed upon direct ESI into structurally informative ion types entirely within the mass spectrometer. Explicitly, gas-phase anionic to cationic charge switching chemistries were first developed for fatty acid profiling, as unambiguous structural elucidation and relative quantitation were achieved. Extensions of this gas-phase charge switch derivatization strategy to glycerophospholipids (GPLs), including ether GPLs, and fatty acid esters of hydroxy fatty acids demonstrates the versatility and flexibility of the ion/ion platforms. In an alternate approach, gas-phase proton transfer ion/ion reactions were employed for the gas-phase separation, concentration,

and identification of cardiolipins (CLs) from total lipid extract. In total, benefits for lipid structure elucidation and enhanced detection efficiencies have been demonstrated utilizing the reported gas-phase ion/ion platforms.

CHAPTER 1. ENHANCING DETECTION AND CHARACTERIZATION OF LIPIDS USING CHARGE MANIPULATION IN ELECTROSPRAY IONIZATION-TANDEM MASS SPECTROMETRY

1.1 Introduction

Lipids are universal cellular components, playing central roles in all organisms ranging from the smallest microorganisms such as bacteria and algae to complex animals like humans.[1] Perhaps best known for their fundamental roles as architectural components of cellular membranes, lipids also perform vital functions as signaling and energy storage molecules.[1-3] Based on the classification scheme devised by the LIPID MAPS[4, 5] consortium, lipids are divided into eight distinct categories: fatty acids (FAs), glycerolipids, glycerophospholipids (GPLs), sphingolipids, sterol lipids, prenol lipids, saccharolipids, and polyketides (Figure 1.1). Noting that each individual lipid category also contains unique classes and subclasses of molecules, lipids exhibit extensive structural diversity. For example, just considering FAs, variations in aliphatic chain length, degree of unsaturation, site(s) of unsaturation, and modification such as hydroxylation[6], cyclopropanation[7, 8], nitrosylation[9, 10], and methyl chain branching[11] are observed. This structural complexity is further compounded as FAs serve as building blocks for complex lipids like GPLs. As illustrated with Figure 1.2, the general GPL structure includes a central glycerol backbone, a functionalized phosphate ester group, and fatty acyl (or alkyl ether) chains. Esterified at the *sn*-3 position of the glycerol backbone is a phosphate moiety. Also coupled to this phosphate group is a polar functional group (*e.g.,* choline, ethanolamine, serine, inositol, or glycerol), that is often referred to as the headgroup. The most common GPL structure observed in eukaryotes is the diacyl (phosphatidyl) subclass wherein fatty acids (FAs) are esterified at the *sn*-1 and *sn*-2 positions of the glycerol backbone, but additional GPL subclasses incorporate alkyl ether chains at the *sn*-1 position while a fatty acyl chain remains esterified at the sn-2 position (Figure 1.2).[2, 12] Explicitly, the plasmanyl and plasmenyl (*i.e.,* plasmalogen) GPL subclasses contain a 1-*O*-alkyl or a 1-*O*-alk-1′-enyl group, respectively, at the *sn*-1 position. In turn, a broad range of discrete GPL molecular structures arise from not only variations in fatty acyl constituents but also alterations both in the headgroup and *sn*-1 bond type.[13] While extensive lipid molecular structural diversity within a class itself presents a considerable challenge, lipidomics analysis of biological mixtures is further

complicated by the presence of multiple classes of lipids (*i.e.*, mixture complexity) over a wide range of concentrations. Figure 1.3 emphasizes the analytical requirements for lipidome analysis. In particular, noting that biological systems can contain many hundreds and perhaps even thousands of structurally diverse lipids at vastly different concentrations, mixture complexity and associated issues of dynamic range pose formidable challenges for modern lipidomics.[14, 15]

Recently, modifications to lipid composition and production, namely FAs and GPLs, have been associated with the onset and progression of numerous human-related genetic[16, 17], neurodevelopmental[18, 19], and metabolic disorders[20-22] in addition to various other chronic pathologies[23-25], including several types of cancer.[26-35] Therefore, many lipidomics studies aim to characterize and quantify lipids, including lipid profiling for biomarker discovery. For instance, Chen *et al*. profiled serum samples from patients with early-stage breast cancer using LC-ESI-MS/MS, unveiling significant fold changes in a combined total of 15 phosphatidylcholines and cholesterol ester species in comparison with benign breast disease samples that could serve as potential biomarkers for diagnosis of early stage breast cancer.[33] In a more recent example, the Xia group, while examining human plasma samples from breast cancer patients, discovered that the ratio of double bond positional lipid isomers may serve as reliable biomarkers for breast cancer.[36] Therefore, increasing evidence for the critical biochemical and physiological roles of lipids, specifically regarding their function in health and disease, has highlighted the demand for analytical techniques that facilitate the rapid, unambiguous identification and quantitation of lipids in complex biological samples.

Even though thin-layer chromatography (TLC)[37] and nuclear magnetic resonance (NMR)[38] have played significant roles in the advancement of lipid science, mass spectrometry has emerged as the premier tool for contemporary lipid analytics.[15, 39] Frequently coupled to some form of chromatography, mass spectrometry (MS) has largely facilitated the rapid expansion of the lipidomics field. Owing to unparalleled versatility, MS-based approaches have been widely adapted for lipid identification and quantitation, as mass spectrometry experiments allow for the individual selection and interrogation, by means of fragmentation, of target analytes in complex mixtures. Ideally, product ions generated via the dissociation of precursor lipid ion enables the reconstruction of original lipid structure, though notable limitations prohibit complete structural elucidation. Since the 1950s[40], the method of choice for FA analysis has been gas chromatography (GC). However, GC-based strategies are restricted to the analysis of volatile, low molecular weight

compounds. In turn, a rich history of derivatization chemistries have been developed to enhance FA volatility, improve chromatographic separation, and ameliorate chemo-selectivity of fragmentation.[41-43] Most commonly, GC is coupled to mass spectrometers equipped with electron ionization (EI) sources, as the combination with MS reduces ambiguity for FA identification when compared to GC alone.[39, 44] While powerful, growing interest in high molecular weight and structurally complex lipids demanded the development of alternate MS-based approaches, noting that GC approaches are not amendable to intact complex lipids analysis, as FAs must be hydrolyzed from complex lipid precursors prior to derivatization, resulting in the loss of valuable information concerning the molecular origin of fatty acyl constituents.

In the pursuit of enhanced lipid structural elucidation, Gross and co-workers laid the foundation for current understanding of lipid structural elucidation and fragmentation utilizing fast atom bombardment (FAB) in conjunction with tandem-MS (MS/MS).[45-55] Performed on sector instruments, initial studies showed that the collisional activation of lipid ions via high-energy CID (> 1keV) afforded the identification of both GPL and FA structures. In particular, FA carboxylate anions derived from the ionization of non-esterified FAs or liberated from a GPL precursor anion dissociate, revealing the presence and location(s) of a variety of functional groups such as carbon-carbon double bonds, acyl chain branching, cyclopropyl rings, epoxides, and hydroxyl groups. Explicitly, deprotonated FA anions undergo unimolecular 1,4-hydrogen eliminations to produce terminally unsaturated and structurally diagnostic carboxylate product ions in a process referred to as charge remote fragmentation (CRF).[46, 56-58] However, fatty acyl identification utilizing this approach is limited to FA structures with three of fewer sites of unsaturation, as underivatized PUFAs containing four or more double bonds decompose primarily by uninformative neutral losses such as decarboxylation (– 44 Da).[47]

To overcome these limitations, metal-cationized FAs were generated in the FAB source by doping the sample and matrix with selected salts. Once formed, these metal adduct ions were interrogated via high-energy CID. As the primary requirements for CRF were found to be a tightly localized charge site and access to keV collision energies, FA cationization with both alkali[52] and alkaline earth[54] metals yielded metal-adducted FA ions which upon interrogation via high-energy CID, generate product ion spectra that permit the localization of carbon-carbon double bonds and unambiguous isomeric discrimination. While high-energy CID of alkaline earth metal cationized FA ions affords identification of double bond position, the CID spectra of $[FA - H + 2Li]^+$ are

arguably more straightforward. In turn, the utilization of lithium as a cationization reagent are favored over alternate alkali and alkaline earth metal counterparts. To localize carbon-carbon double bond positions repeatable spectral patterns obtained via interrogation of the $[FA - H + 2Li]^+$ cation were exploited, as carbon−carbon single bond cleavage proximal (*i.e.*, on the carboxyl end of the aliphatic chain) and vinylic to the last double bond in the aliphatic chain produced the heaviest fragment ion (highest *m/z*).[52, 55] The advantages of FAB-MS/MS of charge-switched FAs are highlighted with Figure 1.4.

Despite the clear successes demonstrated by high-energy CID, both instrumentation and ionization methods traditionally utilized to access CRF have become less common. In addition, both the ionization and fragmentation efficiency were low (*cf*. the magnification of the diagnostic product ions to the precursor ion abundance in Figure 1.4). Specifically, modern lipidomics workflows have largely replaced multisector instruments with triple quadrupole (QqQ), quadrupole time-of-flight (Q-TOF), and linear ion trap (LIT) mass spectrometers that operate under low-energy CID conditions (*i.e.*, <100 eV) while FAB has been primarily replaced with ionization methods like electrospray ionization (ESI) that offer increased sensitivity. Tandem-TOF (TOF/TOF) instruments are a notable exception that can achieve collision energies comparable to those accessed by multisector mass spectrometric platforms.[59, 60] In their report, Trimpin *et al*. explore the dissociation of charge-switched FA ions on a TOF/TOF platform, reporting that CID of $[FA - H + 2Li]^+$, produced by matrix-assisted laser desorption ionization, results in CRF product ions that permit the assignment of subtle structural features such as carbon-carbon double bond position and acyl chain branching.[59] While this approach facilitates the characterization of a series of isomeric FA, not all carbon-carbon double bond positions in PUFAs, particularly those near the methyl end of the aliphatic chain, can be qualitatively assigned. Moreover, wide isolation windows on TOF/TOF instruments hinder complex mixture analysis and the fragmentation efficiency remains low.

As FAB-MS/MS provided limited sensitivity for lipidome analysis, recent advances and novel applications of ESI-MS and MS/MS technologies have greatly facilitated the expansion of lipidomics, improving upon many of the shortcomings associated with the aforementioned platforms.[2] Lipid extracts are admitted to a (tandem) mass spectrometer using liquid chromatography (LC) or directly infused via ESI employing an approach commonly referred to as shotgun lipidomics. Notably, ESI achieves partial fractionation of the lipidome, as differences in

lipid functional groups influence ionization efficiency, observed ion-type, and charge-state. In the absence of a fixed charge site, the preference for a lipid to form a protonated or deprotonated precursor ion is largely dictated by acid-base chemistry.[61] For example, acidic lipids like FAs, glycerophosphoethanolamines (PEs), glycerophosphoglycerols (PGs), glycerophosphoserines (PSs), glycerophosphoinositols (PIs), and glycerophosphatidic acids (PAs) are detected in the negative ion mode as singly deprotonated $[M - H]^-$ species.[61] In contrast, choline-containing lipids like glycerophosphocholines (PCs) and sphingomyelin (SM) incorporate a fixed positive charge and are readily detected as gas-phase cations. Independent of ionization mode, lipids precursor ions can be detected and identified at a sum compositional level via accurate mass measurements (*i.e.*, observed mass-to-charge (*m/z*) ratios). Moreover, utilizing collision-induced dissociation (CID), class-specific fragmentation, pertaining to headgroup composition, allows for the detection of individual GPL classes.[62]

Further lipid structural elucidation is enabled through conventional ESI-MS/MS or MS^n experiments.[63-71] For example, in negative ion mode, low-energy CID of deprotonated GPL anions results in the cleavage of ester bonds at the *sn*-1 and *sn*-2 positions of anionic GPL, liberating fatty acyl chains and yielding abundant carboxylate anions that permit the assignment of fatty acyl composition and, in some cases, GPL subclass. While informative, such experiments fail to fully elucidate GPL structure. Explicitly, conventional ESI-MS/MS experiments do not generate unique product ions to assign the relative position of acyl chains on the glycerol backbone (*i.e.*, *sn*-position) and subtle structural features within the acyl chain constituents, like the positions and geometries of carbon-carbon double bonds among others, are not revealed. Furthermore, it is widely recognized that the native ion types formed upon ESI are not always the most advantageous for lipid detection and identificaiton.[52, 72] For example, the favorable ionization mode for FAs is the negative ion mode, as the carboxylic acid moiety can be readily deprotonated. However, there are two major obstacles for ESI-MS/MS analysis of $[FA - H]^-$ anions. First, when considering LC-ESI-MS/MS approaches, the best chromatographic resolution for FAs is achieved under acidic mobile phase conditions, which unfortunately, suppresses FA ionization efficiency.[73-75] Second, singly deprotonated FA anions undergo undesirable fragmentation when collisionally activated via low-energy CID. Specifically, $[FA - H]^-$ product ion spectra are dominated by water and carbon dioxide neutral losses and are largely devoid of structurally informative product ions.[76] As a consequence, various charge manipulation techniques have been developed to enhance lipid

analysis. Reminiscent of early studies utilizing high-energy CID, charge manipulation of lipids in ESI, including charge-switching strategies, can provide (i) increased ionization efficiency; (ii) improved chemo-selectivity and dynamic range; and (iii) access to preferred fragmentation that afford enhanced structural elucidation. To access these benefits, several solution-based derivatizations have now become widely adopted for ESI-MS workflows in lipidomics. In these approaches the lipid analyte is either non-covalently or covalently modified prior to, or during, the introduction into the ESI source. In an alternative approach, lipids are first ionized via ESI and then derivatized post-ionization within the mass-spectrometer via gas-phase chemistries.

In this review, we examine the application and benefits of charge manipulation strategies, including charge-switching, for the mass spectrometric analysis of lipids. The approaches summarized herein are focused on those implemented with ESI as this ionization method is the most widely adopted for modern lipidomics experiments. We note, however, that many of the same chemistries can, and are, being translated to other ionization modalities, e.g., MALDI. Here we provide, an overview of both solution-based and gas-phase derivatization, with a focus on the transformation of lipid precursor ions, namely those derived from polar lipids including FAs and phospholipids. Collectively, the manipulation of lipid precursor ions via the modification of charge state or ion type provides the primary advantages of enhanced sensitivity, isomeric resolution, mixture analysis performance, and structural characterization.

1.2 Charge Switching

Most charge switching strategies for lipid analysis employ solution-based derivatization, as this form of derivatization is more widely accessible compared to their gas-phase counterparts that require instrument modifications. In particular, two main techniques have been developed in order to generate charge-switched lipid ions. While both strategies target lipid modification with a fixed-charge or easily ionizable functional group, the manner in which charge-switched derivatives are generated differs between the two described approaches. In the first approach, noncovalent lipid adducts are generated in solution prior to ionization, typically via lipid complexation with a metal cation. This is typically achieved by adding a dopant to the ESI spray solution and is thus an online modification. The second tactic involves covalent derivatization of the lipid at a marked functional group via wet-chemical modification. This approach predominantly requires additional preparative and even clean-up steps prior to sample injection into the mass spectrometer. Ultimately, in

combination with conventional mass spectrometers, both covalent and non-covalent charge-switched lipids provide increased ion currents and expanded structural information that in favorable cases, enables isomer discrimination. More recently charge-switch derivatization utilizing gas phase ion/ion reactions has been explored for lipid detection, characterization, and quantitation. As described in more detail below, gas-phase charge inversion chemistry offers a number of advantages over parallel solution-based approaches, including enhanced derivatization efficiency, specificity, and sensitivity.[77]

1.2.1 Negative to Positive Charge Inversion

Solution-Based Metal Cationization

As stated above, workflows to access CRF are uncommon with modern instrumentation that operate on relatively low kinetic energy ions. However, charge-switching strategies employing solution additives have been extensively explored with the aims of improving lipid detection, identification, and quantitation using contemporary mass spectrometers. Acidic lipids such as FA, PS, PI, PA, PG, PE, typically form abundant $[M - H]^-$ anions with negative mode ESI but can be charge-switched to the positive ion polarity employing numerous solution phase additives. Explicitly, alkali, alkaline earth, and transition metal cations have been demonstrated to complex with a variety of polar lipid structures, facilitating acidic lipid ionization in the positive ion mode, resulting in increased ionization efficiency and sensitivity. Furthermore, as the low-energy CID spectra of lipid adduct cations contain structurally informative product ions, negative to positive mode charge-reversal has proven highly advantageous for lipid structural elucidation.

Paralleling previous approaches that employ high-energy CID, formal lithium fixation to lipid ions provides the notable advantages of enhanced structural characterization of unsaturated GPL and FA structures under low-energy CID conditions. First described by Hsu and Turk[78], abundant charge-switched FA cations were generated upon direct positive ESI of a solution containing a FA standard and lithium acetate. Low-energy CID of $[FA - H + 2Li]^+$ ions gives rise to product ion spectra that facilitate the identification of carbon-carbon double bond position(s) and, in turn, unambiguous isomeric discrimination via direct interpretation of a reproducible and relatively straightforward spectral pattern (Figure 1.5). Explicitly, the CID spectra of dilithiated adduct ions of monounsaturated FAs contain a series of closed-shell product ions, spaced 14 Da

apart, signifying sequential carbon-carbon single bond cleavage along the hydrocarbon chain. As fragmentation approaches the unsaturation site, this pattern is terminated, as carbon-carbon bond cleavages distal to the double bond (*i.e.,* on the methyl end) are rarely observed. Moreover, an abundant product ion reflecting cleavage of the carbon–carbon single bond vinylic to the carbon–carbon double bond is observed in the resulting $[FA - H + 2Li]^+$ CID spectrum. When multiple double bonds are present and separated by a single methylene group, cleavages between double bonds yield abundant product ions reminiscent of those observed under high-energy CID conditions. However, congested spectra of $[FA - H + 2Li]^+$ cations resulting from non-selective fragmentation of the aliphatic chain can complicate carbon-carbon double bond localization, especially when examining complex mixtures where multiple isomers are often simultaneously present. In a recent example, the Reid group deployed 193 nm ultraviolet photodissociation tandem MS (UVPD-MS/MS), a selective fragmentation technique, to reduce the spectral complexity of dilithiated-FA cations.[79] Here, the UVPD MS/MS spectra of $[FA - H + 2Li]^+$ cations contain marked pairs of diagnostic product ions that readily facilitate the localization of double bond position(s), as shown in Figure 1.6. Notably, application of this strategy to colorectal cancer cell lines revealed relative changes in the ratio of FA double bond positional isomers without prior fractionation of the isomers.

Extending the lithium cationization strategy to intact GPL analysis, Hsu and Turk described the generation of mono-, di-, and tri-lithiated adduct ions by direct ESI and subsequent interrogation of the charge-switched lipid cations using a multiple stage LIT mass spectrometric approach.[70, 80] Ultimately, several factors influence the formation of lithium-adducted lipid cations, including GPL class, fatty acyl composition, and lithium cation concentration. In total, this strategy enabled the detailed structural elucidation of GPL, including the plasmalogen and lyso GPL subclasses. In particular, the MS^n (n = 2,3) spectra of lithium-adducted GPL cations permit the assignment of lipid class (*i.e.,* headgroup composition) and the identification of fatty acyl composition and the more abundant *sn*-regioisomer. To localize carbon-carbon double bond positions in unsaturated fatty acyl substituents, MS^n (n = 3,4) experiments performed on product ions that carry the unsaturated fatty acyl moiety are exploited. While effective, the propensity to form various lithiated adduct ion types and extensive fragmentation can complicate spectral interpretation particularly where multiple isomers are present. Moreover, as multiple stages of CID

are required to assign unsaturated GPL structures, longer integration times are required, making this approach more compatible with direct infusion (shotgun) rather than LC-MS workflows.

Barium has also been used as a cationization agent for FA analysis. In the first example, Zehethofer *et al.* developed a UPLC-MS/MS method in which aqueous barium acetate was added post-column via an HPLC system to facilitate the solution-based derivatization of FAs prior to ionization and introduction to a hybrid triple quadrupole/linear ion trap (QqLIT) via ESI.[81] The fragmentation behavior of $[FA - H + Ba]^+$ adduct ions are comparable to those observed upon interrogation of lithium adducted FA complex cations, as detailed above. Briefly, for monounsaturated FAs, the CRF product ion series terminates at carbon-carbon single bond cleavage proximal (*i.e.,* on the carboxyl side) and vinylic to the double bond, while additional carbon-carbon single bond cleavages between double bonds are observed for PUFAs. Importantly, $[FA - H + Ba]^+$ adduct ions fragment upon collisional activation with low-energy CID to provide isomer-specific product ions, and in turn, sensitive multiple reaction monitoring (MRM) transitions could be established to easily identify FAs in which LC separation could not be achieved, as highlighted with Figure 1.7. In an additional study, Krogh and coworkers report the utilization of barium ion chemistry to selectively identify carboxylic acids, including FA structures, directly in waste and surface water and without chromatographic fractionation.[82]

In an additional approach, ESI-MS/MS of copper (II) adducted FAs performed on an ion-trap mass spectrometer facilitated structural characterization and notably, the differentiation of stereochemical isomers (*i.e., cis* and *trans*). The CID spectra of $[FA - H + Cu(II)]^+$ ions contain product ions similar to those provided by CRF with high-energy CID. Specifically, the location of the unsaturation position is indicated by a pair diagnostic ions generated via carbon-carbon bond cleavage vinylic to the double bond with a characteristic mass differential of 26 Da. Interestingly, this approach also facilitates the discrimination amongst stereochemical isomers. Briefly, Afonso *et al*. report that Cu(II) coordination is seemingly dependent on double bond geometry. The copper dication is suggested to be coordinated by the carboxylate and double bond site(s) in unsaturated FA with *trans* double bond geometry, and as shown with Figure 1.8, this Cu(II)-coordination hinders the neutral loss of CO_2 (– 44 Da) from the $[FA - H + Cu(II)]^+$ ion with *trans* geometry.[83] In contrast, dissociation of the copper-containing unsaturated FA with *cis* geometry yields a dominant decarboxylated product ion, suggesting the presence of a free carboxylic group. While this stereospecific approach is effective, this strategy has not been extended to PUFAs containing

three or more double bonds. Moreover, the significant natural abundance of the ^{64}Cu isomer and extensive fragmentation of the $[FA - H + Cu(II)]^+$ adduct ion results in congested CID spectra that require deconvolution and, thus, complicates FA identification.

Other solution-based charge switching strategies have also been developed for complex lipid detection and identification. For example, Deng and coworkers described the metal cationization of PS, PE, and PG lipids with a series of mono- and di-valent metals, including Li^+, Na^+, K^+, Sr^{2+}, Ba^{2+}, and the first transition series (*i.e.*, Mn^{2+}, Fe^{2+}, Co^{2+}, Cu^{2+}, Ni^{2+}, and Zn^{2+}).[84] It was reported that the low-energy CID spectra of all transition metal adducted GPL studied afforded the identification of lipid class, fatty acyl composition, and location of acyl chain esterification along the glycerol backbone. In particular, cobalt (II) was found to be the best cationization reagent, as the CID spectra of cobalt-adducted GPL were more straightforward than those derived from alternate transition metal complex cations due, in part, to the presence of a single naturally occurring isotope. Although, the $[M - H + Co]^+$ adduct ions can be applied to the structural elucidation of some lipid classes the approach does not significantly extend the information acquired from CID of these lipids in their native $[M - H]^-$ polarity.

Svane *et al*. report the utilization of digallium and dizinc complexes to facilitate positive ion mode analysis of various GPL classes, including PA, PE, PC, PG, and three different types of PI phosphates (*i.e.*, mono-, di-, and triphosphorylated PIs).[85] It was discovered that PI and PA lipids can undergo solution-based charge switch derivatization upon reaction with digallium complexes, while dizinc complexes could charge invert PG and PE lipids, although with low efficiency. However, PCs did not complex with either metal reagent likely due to the fixed, positively charged headgroup. Notably, the derivatization of PA and PI lipids with digallium complex cations was found to be highly efficient and resulted in up to a 100-fold increase in ion signals relative to the unmodified phospholipids in negative ion-mode. Moreover, the CID spectra of charge-switched lipids with digallium complex cations provided complementary information, and in the case of PI phosphates superior data, when compared to the structural information obtained from the dissociation of unmodified lipids in the negative ion mode. Briefly, interrogation of digallium complex-bound lipid ions allowed for the discrimination of different PI bisphosphate (PIP) regioisomers that differ only in the location of the phosphate moieties on the inositol sugar. Importantly, such discrimination cannot be achieved in the negative ion mode via CID of the unmodified lipid anions, as shown in Figure 1.9. Conversely, CID of PE or PG complexed with

dizinc complexes did not provide additional information when compared to MS/MS experiments conducted on the underivatized lipid ions in negative ion mode.

While CID of metalated lipid ions has proven advantageous for lipid detection and identification, Yoo *et al*. investigated the utility of electron induced dissociation (EID) for FA characterization.[86] In short, EID involves interactions between singly charged analyte ions and free electrons. Metalated FA cations were first generated upon direct ESI of a FA solution doped with metal salts. Specifically, Li, Zn, Co, Ni, Mg, Ca, Fe, and Mn were used to derivatize the carboxylic acid moiety of FAs. The combination of metal-cationization with Mn (II) and EID proved to be particularly useful for the detailed structural elucidation of FAs. For example, the EID spectra of $[FA - H + Mn]^+$ adduct ions contains both even- and odd- electron product ions generated via charge-driven and charge-remote fragmentation. In turn, the resulting product ion spectra facilitated the identification of carbon-carbon double bonds in unsaturated FA, though the authors note structural assignments are restricted to FA structures containing three or fewer double bonds. However, this approach suffers from extreme spectral complexity and, due to limited fragmentation efficiency, diagnostic ions were only observed at low abundances. The combination of low sensitivity and high spectral complexity suggest that it is unlikely to be extended to biological mixture analysis.

Solution-Based Covalent Derivatization

While the above examples of anion to cation charge-switching relied exclusively on the generation of lipid-metal adduct ions, an extensive body of work has been undertaken in employing covalent derivatization of lipid structures with novel chemical tags to enhance ionization in the positive ion mode. To date, most derivatization procedures report the introduction of a functional chemical tag that contains an amine group. The high proton affinity of amines enhances ionization with conjugation chemistries target the carboxylic acid group common to the FA lipid class that includes the low abundance lipid mediators such as the eicosanoids. In particular, the benefits of this type of charge-switching are twofold. First, the incorporation of easily ionizable moieties into the lipid structure provides enhanced detection sensitivities and dynamic range, as ionization efficiency is dramatically improved. Second, charge-switched lipids fragment to form characteristic product ions that can be exploited for increased selectivity.

Two such derivatization tactics targeted modification of FA structures, linking a chemical modifier to the FA carboxylic acid group via an ester bond. FAs esterified to picolylamine[87] and dimethylaminoether (DMAE)[88] modifiers integrated easily chargeable amine tags and have been successfully deployed for LC-MS/MS of FAs with positive ion mode ESI. Notably, Li and Franke established a fast, sensitive LC-orbitrap MS method utilizing fatty acid-picolylamine derivatives (FA-PA). When compared to DMAE derivatization, chemical modification of FAs with 3-picolylamine demonstrated enhanced sensitivity and improved chromatographic resolution.[87] Later covalent modification strategies redesign the readily ionizable tag so that an amide bond links the derivatization reagent to the carboxylic acid moiety. In these applications, an amide bond is preferred over ester linkage to the analytic carboxylic acid since the former is often more resistant to fragmentation upon collisional activation and can thus promote charge-remote fragmentation which is more characteristic of the FA structure. Explicitly, such strategies covalently link 5-(dimethylamino)naphthalene-1-sulfonyl piperazine (Dns-PP)[89], aminoxy tandem mass tags (aminoxyTMTs)[90], 4-aminomethylquinoline (AMQ)[91], and 3-hydroxymethyl-1-methylpyridium[92] to the carboxylic acid group of FAs, while 2-dimethylaminoethylamine (DMED) was coupled to both FAs and eicosanoids.[93, 94] In the abovementioned studies, chemical labeling coupled with LC-ESI-MS/MS analysis ensures the identification and quantitation of carboxyl-containing lipids in complex biological samples in the positive ion mode. Explicitly, the covalent modifiers have been found to enhance chromatographic resolution, increase ionization efficiency, and promote selective fragmentation. For instance, in a recent report, short-chain fatty acids (SCFAs) were converted into amide derivatives with AMQ.[91] Here, Liu and co-workers injected AMQ-derivatized fecal samples into an LC-MS/MS system for analysis. Notably, AMQ charge-switching improved chromatographic performance, SCFA ionization efficiency, and SCFA stability. In a final example based on carbodiimide chemistry, FAs labeled with 2, 4-dimethoxy-6-piperazin-1-yl pyrimidine (DMPP) were shown to provide a 1000-fold signal increase, providing excellent signal enhancement capacity and sufficient chromatographic separation by a C8 column.[95] This derivatization strategy is simple, fast, and highly sensitive, and in turn, offers an effective strategy to enhance MS detection signals and lipid identification.

To further improve ionization efficiency, fixed charge tags have been covalently linked to the carboxylic acid moieties of FAs. In particular, quaternary amines contain fixed cationic charge sites, and in turn, the unique chemical derivatization strategies featuring this functional group

facilitate exceptional positive ESI efficiency. For example, the trimethylaminoethyl (TMAE) ester salts of FAs (*i.e.*, the quaternary ammonium analogue to DMAE-FA derivatives) enabled the precise and accurate identification and quantitation of FAs. Due to the fixed cation site, TMAE-derivatized FAs provided enhanced ion currents when compared to DMAE-FA derivatives, and in turn, this approach requires notably smaller sample volumes.[96] In an additional example, Kretschmer *et al*. utilized the bromine containing charge-switching reagent, (2-(4-(aminophenoxy)ethyl)4-bromophenethyl)-dimethylammonium bromide hydrobromide referred to as 4-APEBA to detect prostaglandins in positive ion mode.[97]

While the above-mentioned reagents incorporate quaternary amines, additional fixed-charge chemical tags have been crafted to include pyridinium motifs that enable efficient cation formation via positive ESI. Regnier and colleagues first described the development of an LC-MS/MS method for the identification and quantitation of FAs through derivatization with 3-acyl-oxymethyl-1-methylpyridinium (AMMP).[74] Here, esterification of FAs with AMMP increased detection sensitivity by a factor of 2500 when compared negative mode analysis of underivatized FAs. Importantly, the MS/MS spectra of AMMP-FA cations also allowed for the identification of carbon-carbon double bond position, a notable advantage to alternate covalent anion to cation charge switching strategies described above. However, the abundances of these structurally informative product ions are exceptionally low, as product ions reflective of fragmentation at the AMPP charge tag esterification site were predominantly observed. A similar strategy exploits a mild amidation coupling reaction to generate cholamine derivatives of targeted long-chain FAs (LCFAs) to quantify potential biomarkers in the asthma patient serum. Established by Bian *et al*., LC-MS/MS analysis of chomaline-FA derivatives resulted in up to a 2000-fold increase in sensitivity with limits of detection at the low femtogram level.[98] Moreover, despite low intensities of relevant product ions, the MS/MS spectra of cholamine-derivatized FAs enable the localization of double bond positions and/or other functional groups (Figure 1.10).

Although the covalent charge-switching strategies described above afforded improved ionization efficiency and increased sensitivity, structure elucidation via these derivatization strategies was typically limited by fragmentation centralized at the charge-switch tag. Consequently, detailed lipid structural elucidation is significantly hindered. Recognizing these shortcomings, Bollinger *et al.* designed and synthesized the novel charge-switch derivatization reagent *N*-(4-aminomethylphenyl)pyridinium (AMPP).[99] Following a mild amidation reaction,

AMPP is coupled to the carboxylic acid moiety of FA including lipid mediators. Positive ion ESI of the resulting pyridinium-derivatized lipids lead to an exceptional increase in sensitivity when compared to analysis of the underivatized lipid. Importantly, CID of the AMPP-FA cation induces fragmentation of carbon-carbon bonds within the FA hydrocarbon chain, affording structural characterization of FA structures, including the resolution of isomeric mixtures that are often incompletely resolved LC. The proposed dissociation mechanisms for AMPP-derivatized unsaturated FAs are highlighted with Scheme 1.1, utilizing FA 18:3(9,12,15) as an example.[100] Explicitly, the CID spectra of FA isomers derivatized with AMPP display significant spectral differences that permit the localization of subtle structural features like carbon-carbon double bond position(s), methyl chain branching, among others. Owning to the enhanced sensitivity and specificity, AMPP-derivatized lipids have been widely explored using both direct infusion and LC-MS/MS workflows for the identification and quantitation of nonesterified FAs from a number of biological samples (*i.e.*, mouse plasma, human plasma, and serum) as well as identification of unusual esterified FAs in extracts from bacteria.[100-104] In their report, Han and coworkers deployed a shotgun approach that exploits the charge-remote fragmentation patterns of AMPP-derivatized FA isomers to accurately determine the composition of the FA isomers extracted from human plasma.[102] In an additional example, Tatituri *et al*. adopted this charge-reversal strategy to profile the FAs in *Listeria monocytogenes*, a virulent food-borne pathogen. Here, alkaline hydrolysis of the lipid extract is first utilized to release FA substituents from a lipid extract, followed by conversion of the free FAs to the AMPP-derivative.[103] Positive ion mode mass spectrometry analysis of the liberated and charge-switched FA cations revealed that branched-chain FAs were the major fatty acid substituents found in all the lipid families analyzed. Despite successes, CID of FA-AMPP in complex isomeric or isobaric mixtures can be challenging to deconvolve. In response, a number of studies have combined AMPP with alternate mode of ion activation.

To mitigate limitations of low-energy CID of AMPP charge-switched FAs, novel ion activation methods such has ozone-induced dissociation (OzID) and photodissociation (PD) of fixed-charge pyridinium derivatives have been deployed. Briefly, OzID exploits gas-phase ion/molecule reactions between unsaturated lipid ions and neutral ozone within the mass spectrometer. The resulting OzID spectra reveal predictable neutral losses that can be used for assigning the position(s) of carbon-carbon double bonds and thus elucidation of lipid structure.[105-111] While effective, ion/molecule reactions can be slow, particularly regarding those conducted in

negative ion mode, impacting sensitivity. Notably, alkali metal adducted lipids have been shown to be more reactive to ozone, thus greatly enhancing OzID reaction efficiency.[112] Importantly, the OzID spectra of metalated lipid cations also revealed the site(s) of unsaturation and relative positions of unsaturated acyl chains along the glycerol backbone. Poad *et al*. combined AMPP modification and OzID in an automated data-dependent workflow to both enhance the detection and structural elucidation of FAs.[113] Here, OzID of $[FA + AMPP]^+$ cations dramatically reduced spectral complexity when compared to those obtained with low-energy CID. In turn, OzID product ion spectra were straightforward and readily facilitated the unambiguous localization of unsaturation sites in AMPP-derivatized FAs (Figure 1.11). Application of this workflow to *vernix caseosa* revealed the presence of a wide range of isomers previously indistinguishable with conventional platforms, indicative of the broad coverage and dynamic range of the developed method.

Expanding upon the work of presented by Julian and coworkers[114], the Blanksby group has also utilized PD and radical-directed dissociation (RDD) to elucidate a wide array of FA structures, employing two separate charge-reversal strategies. In either approach, suitable radical initiators, explicitly those incorporating aryl-iodide motifs, are first covalently linked to the lipid of interest. Following ionization of even-electron FA precursor ions via direct positive ESI, subsequent irradiation of the charge-switched FA cation with a laser at 266 nm produces abundant radical FA cations, resulting from the loss of atomic iodine. The first charge-reversal strategy coupled with photochemistry relies on the generation and photodissociation of sodium-adducted FAs ions derivatized as 4-iodobenzyl esters (*i.e.*, $[FAIBE + Na]^+$).[115] Laser-photolysis of $[FAIBE + Na]^+$ results predominantly in the generation of $[M + Na - I]^{\bullet+}$ radical cations, yet low-abundance product ions formed by homolysis of carbon–carbon bonds allylic to the unsaturation site afford the identification of carbon-carbon double bond position(s) in unsaturated FAs. Moreover, $[M + Na - I]^{\bullet+}$ radical cations can be further activated via CID to discriminate between different types of isomeric FAs, as RDD provides evidence for hydroxylation and methyl chain branching localization. In a subsequent study, Narreddula *et al*. conceived conceived 1-(3-(aminomethyl)-4-iodophenyl)pyridin-1-ium (4-I-AMPP^+) fixed-charge, photolabile tags to enhance the detection and characterization of FAs in LC-MS/MS workflows.[116, 117] Explicitly, the PD mass spectra of FA structures conjugated with 4-I-AMPP^+ reveal structurally diagnostic product ions that can be exploited to distinguish an array of isomeric FAs, including chain branching, unsaturation,

hydroxylation, and cyclopropanation. Owing to the fixed charge, FA derivatization with I-AMPP$^+$ motifs provided increased sensitivity when compared to the previous approach that relied on 4-iodobenzyl alcohol esterification and metal cation adduction for positive ion mode FA analysis. Recent application of I-AMPP$^+$ charge switching was also deployed for the identification of ultralong *O*-acyl hydroxy fatty acids (OAHFAs).[118] Here, Hancock *et al*. achieve near-complete structural characterization of OAHFAs derived from human meibomian gland secretions, as the RDD mass spectra of 4-I-AMPP-derivatized meibum OAHFAs elucidated sites of unsaturation, the stereochemical configuration of carbon-carbon double bonds, and ester linkage regiochemistry.

Like OzID and RDD, the Paternò−Büchi (PB) reaction in conjunction with low-energy CID has been used to great effect for unsaturated lipid analysis, as this strategy permits the identification and quantitation of double bond positional isomers.[36, 119-121] In the earliest studies, the Xia group subjected unsaturated FAs to photochemical tagging with acetone, though this photochemistry can be readily applied to complex lipids as well.[119, 120] Ensuing CID of acetone-tagged unsaturated lipids provided predictable pairs of diagnostic ions exhibiting 26 Da spacing that are specific to the locations of unsaturation sites. However in the negative ion mode (*i.e.*, preferential ionization mode for FAs), low ionization efficiency of unsaturated FA-PB reaction product ions and non-specific neutral losses such as decarboxylation (– 44 Da) and the loss of the acetone tag (– 58 Da) hinder FA analysis, particularly those with more than three degrees of unsaturation. Once more, solution-based charge switching strategies proved advantageous for circumventing these obstacles. For example, Ma *et al*. demonstrated that PB-MS/MS on lithiated adduct ions, denoted $[FA^{PB} + Li]^+$, generated the characteristic pairs of diagnostic ions indicative of double bond position.[121] In an additional example, Esch and Heiles replaced acetone as the PB reactive agent with 3-acetylpyridine (3-acpy), an easily protonated chemical modifier upon direct positive ESI.[122] Here, 254 nm ultraviolet (UV) light irradiates an emitter tip filled with the reaction mixture, resulting in the covalent attachment of 3-acypy to the carbon-carbon double bond of an unsaturated FA. Consequently, PB functionalization with 3-acypy enabled the detection of PB reaction products in the positive ion mode with ion signal enhancement factors of up to 631 and facilitated the localization of carbon-carbon double bonds in all unsaturated FAs examined, including those with more than three degrees of unsaturation. While effective, all PB functionalization strategies described above require the presence of at least one carbon-carbon double bond and are not amenable saturated lipid analysis. Recognizing this shortcoming, Wei and

co-workers developed a double derivatization strategy for the enhanced detection and characterization of FAs.[123] In this study, the carbon-carbon double bonds in unsaturated FAs are first labeled with acetone using the photochemical PB reaction. Next, the entire FA pool comprised of acetone-labeled unsaturated FAs and unlabeled saturated FAs are derivatized with N,N-diethyl-1,2-ethanediamine (DEEA). This secondary chemical modification step results in the amidation of FA carboxyl groups and the incorporation of a tertiary amine group which is readily protonated in positive mode ionization, resulting in a remarkable increase in analytic sensitivity. Importantly, the novel double derivatization procedure has the primary advantage of being able to comprehensively profile FAs, including saturated and unsaturated FAs with a high degree of sensitivity and selectivity.

Gas-Phase Charge Inversion

In contrast with the above-mentioned charge-switching strategies utilizing solution-based derivatization, gas-phase ion/ion reactions to derivatize lipid anions within the mass spectrometer has been explored. For example, charge inversion ion/ion reactions have been utilized to convert FA anions into structurally informative, metalated cations.[124-127] These experiments are performed on mass spectrometers that have been modified to perform ion/ion reactions, as oppositely charged ions are mutually stored within a designated reaction cell.[128] Briefly, the process of charge inversion proceeds through the generation a long-lived electrostatic complex. In some cases, the noncovalent interactions within the complex are strong enough to yield adducted lipid ions, as the lipid and reagent ions remain electrostatically bound. However, if the noncovalent interactions are not sufficiently strong to generate adduct ions, multiple charges are transferred within the complex prior to the separation of the reagent and lipid ions, noting that the number of charges transferred must exceed the number required to neutralize the lipid ion in order to observe charge inverted product ions. Gas-phase charge switching offers the primary advantage of decoupling of the initial ionization event from lipid derivatization, and therefore, by conducting lipid derivatization in the gas phase, each reagent can be individually optimized with regards to solution and electrospray conditions.

Charge inversion has been particularly useful for lipid analysis, as conventional lipid ion types formed upon direct ESI can be altered into structurally informative ion types entirely within the mass spectrometer. Using a shotgun approach, gas-phase anionic to cationic charge switching

chemistries were first developed for FA profiling.[124] Explicitly, tris-phenanthroline magnesium complexes have proven particularly advantageous for the selective derivatization of FA anions. Here, direct negative nESI of nonesterified (*i.e.*, free) FA or the decomposition of complex lipid precursors via solution-based hydrolysis or gas-phase collisional activation (broadband or single frequency) gives rise to $[FA - H]^-$ anions. Scheme 1.2 summarizes the ion/ion reaction. The resulting singly deprotonated FA anions are then transformed in the gas-phase following reaction with tris-phenanthroline magnesium reagent dications, yielding abundant $[FA - H + MgPhen]^+$ complex cations. The CID spectra of charge-inverted FA cations display isomer-specific and highly reproducible fragmentation patterns indicative of FA structure. For example, monounsaturated FA ions cationized with magnesium phenanthroline complexes dissociate to yield a characteristic spectral gap flanked by product ions arising from carbon−carbon cleavage allylic to the double bond, reminiscent of those spectral patterns observed with high-energy CID. While double bond localization in highly unsaturated FA was hindered due to rearrangements and congested CID spectra, discrimination amongst PUFAs can still be achieved. Explicitly, as the $[FA - H + MgPhen]^+$ CID spectra were both highly reproducible and isomer-specific, automated matching to spectra of standards in a FA library facilitated unambiguous isomeric distinction, and consequently the localization of carbon−carbon double bonds.[125] Importantly, the use of multiple linear regression analysis in conjunction with charge inversion ion/ion chemistry enables the relative quantitation of FA isomers over a broad dynamic range of molar ratios. Recent application of this charge-switch derivatization of fatty acid esters of hydroxy fatty acids (FAHFAs) via gas-phase ion/ion reactions facilitated the assignment of FA and HFA constituents, pinpointed unsaturation sites within the FA moiety, and elucidated ester linkage regiochemistry, demonstrating the versatility of charge inversion reactions for lipid identification.[129]

This gas-phase charge inversion chemistry was subsequently extended to intact GPL analysis. Importantly, this top-down approach afforded the near-complete elucidation GPL molecular structures.[126, 127] With this strategy, a single experiment facilitates assignment of the GPL headgroup, fatty acyl composition, carbon−carbon double bond position(s) in unsaturated fatty acyl chains, and, in some cases, fatty acyl *sn*-position and relative abundances for isomeric fatty acyl substituents. A notable advantage of conducting derivatization within the gas-phase (opposed to solution-based modification) is the ability to switch charge states and ion type on demand. In other words, ion/ion chemistry allows for facile, highly efficient, and structure-

selective derivatization conducted independent of the ionization event. In turn, this platform offers a highly flexible approach to GPL characterization, as MS/MS events can be performed in the desirable polarity where structurally informative products ions are most readily observed. Briefly, the GPL was first ionized in negative ion mode and collisionally activated to liberate $[FA - H]^-$ anions via fragmentation of the ester bonds at the *sn*-1 and *sn*-2 positions of the central glycerol backbone. Subsequent ion/ion reactions with $[MgPhen_3]^{2+}$ reagent dications yield abundant $[FA - H + MgPhen]^+$ cations. As detailed above, the CID spectra of charge-inverted fatty acyl complex cations yielded isomer-specific product ion spectra that permit (i) unambiguous assignment of carbon−carbon double bond position(s) and (ii) relative quantitation of isomeric fatty acyl substituents (Figure 1.12).[126] A recent report combines a systematic MS^n platform with gas-phase charge switching to elucidate ether GPL structures, providing increased isomeric resolution as both *sn*-1 bond type and sites of unsaturation in the *sn*-2 fatty acyl were confidently assigned.[127] Applications of both workflows to proposed biomarkers found in human blood plasma extract revealed that, in fact, these structures exist as a mixture of isomers that are often left unresolved when employing conventional ESI-MS/MS.

1.2.2 Positive to Negative Charge Inversion

Solution-Based Noncovalent Derivatization

Perhaps one of the most commonly exploited charge switching approaches involves the addition of millimolar concentrations of acetate, formate, bicarbonate, or chloride salts to lipid solutions to afford choline-containing lipid detection in negative ion mode.[72, 130-133] This approach also provides enhanced PC structural characterization, as charge-switching PC anions dissociate to yield structurally informative product ions. For example, due to the presence of the quaternary ammonium group in the phosphocholine headgroup, PCs readily ionize in the positive ion mode, yielding abundant protonated ions. However, CID of the protonated PC ion provides information that is restricted to the headgroup, as a dominant phosphocholine product ion is observed at *m/z* 184. Unfortunately, phosphocholine-containing lipids cannot be ionized in the negative polarity by deprotonation, and in turn, structural information regarding acyl chain composition cannot be readily accessed without solution-based derivatization. Explicitly, ionization in the negative ion mode is reliant on the formation of $[M + X]^-$ adduct ions, where $X = Cl^-$, HCO_2^-, HCO_3^-, or

$CH_3CO_2^-$. CID of PC adduct anions produces a demethylated PC anion (*i.e.*, $[PC - CH_3]^-$), generated via combined losses of the counteranion and a methyl cation from the quaternary ammonium group, which fragments via subsequent collisional activation to provide product ions informative of acyl chain composition. Notably as highlighted with Figure 1.13, Zhao *et al*. reported that CID of bicarbonate-adducted PC anions exhibited nearly a 20-fold increase in ion signal compared to the $[PC + HCO_2]^-$ ion and can be beneficial for assigning *sn*-position, as CID of the $[PC + HCO_3]^-$ ion generated *sn*-specific diagnostic ions can be exploited for the identification and quantitation of *sn*-positional isomers.[131]

Lipids containing fixed cationic sites can also detected in negative ion mode by exploiting the noncovalent complexation of choline-containing target lipid analytes with the photocaged radical precursor 4-iodobenzoate (IB). Here, Pham *et al*. generated charge-switched $[PC + IB]^-$ adduct ions by direct negative ESI of a methanolic solution containing the PC analyte and IB.[134] Irradiation with 266 nm laser light cleaves the UV-labile carbon-iodine bond in the $[PC + IB]^-$ adduct ion, giving rise to a reactive phenyl radical. Subsequent CID of the PD-derived $[PC + IB - I]^{\bullet -}$ ion resulted in the formation of a dominant product ion corresponding to the neutral loss of methyl benzoate (*i.e.*, $[PC - CH_3 - H]^{\bullet -}$). The CID product ion spectra of $[PC - CH_3 - H]^{\bullet -}$ radical anions revealed a wealth of structural information and rich fragmentation chemistry. Contrary to conventional tandem MS spectra, RDD spectra facilitated the discrimination of isomeric lipids differing in double bond position and methyl chain branching, as product ions resulting from intrachain carbon-carbon cleavages were readily observed. Similar results were also obtained for SM. Moreover, alternate phospholipid classes like PS and PE were also found to noncovalently complex with IB, though in the absence of a fixed positive charge, complexation was not nearly as efficient.

Gas-Phase Charge Inversion

While the above approaches effectively transform cations into structurally informative anions by doping chemical additives into lipid solutions, similar strategies have been developed to charge-switch lipid cations in the gas phase. Recently, the McLuckey group[127, 135-139] and others[140] have explored the utilization of gas-phase ion/ion reactions for the charge inversion of lipid cations. For example, Stutzman *et al*. described the charge inversion of PC monocations via ion/ion reaction with doubly deprotonated 1,4-phenylenedipropionic acid (PDPA) anions in efforts to

increase structural characterization of PCs.[137] Following the ion/ion reaction, the dominant product ion observed was a negatively charged complex anion comprised of the original PC lipid and PDPA (*i.e.*, $[PC + PDPA - H]^-$). Importantly, subsequent ion-trap CID of the $[PC + PDPA - H]^-$ adduct ion gave rise to a demethylated PC, which as described above, can be further interrogated via CID to produce abundant fatty acyl carboxylate anions, affording the identification of FA chain lengths and degree of unsaturation. Though outside the scope of this review, the Prentice group has recently utilized PDPA ion/ion reactions in MS imaging experiments to invert the polarity of PC ions generated by MALDI, alluding to the versatility of ion/ion approaches.[140] Charge inversion reactions with PDPA dianions have also been exploited to chemically separate isomeric PC and PE lipids in the gas-phase. Here, Betancourt *et al*. reported distinct reactivities of isomeric PC and PE ions with PDPA, attributing the unique charge inversion reactivities to differences in polar headgroup composition .[135] Specifically, $[PC + H]^+$ cations are transformed via ion/ion reactions with $[PDPA - 2H]^{2-}$ dianions to yield $[PC + PDPA - H]^-$ complex product anions, whereas protonated PEs undergo charge inversion via double proton transfer to the two carboxylate moieties, giving rise to $[PE - H]^-$ product ions. Scheme 1.3 summarizes the reaction behaviors between $[PC + H]^+$ and $[PE + H]^+$ cations with $[PDPA - 2H]^{2-}$ reagent dianions. As highlighted with Figure 1.14, isomeric/isobaric PC and PE cations are effectively separated on the *m/z* scale. Importantly, the developed positive to negative ion charge inversion chemistry provides several benefits compared to conventional analysis conducted exclusively in a single ion polarity. First, this approach takes advantage of lipid ionization in the positive ion mode, which can be more efficient particularly for PCs. As the ionization and derivatization steps are decouple, structural characterization can then be conducted in the negative ion polarity, where structurally informative product ions are readily observed. Second, when compared to direct negative ionization, the positive ion charge inversion approach was demonstrated to reduce chemical noise, minimize mixture complexities within an isolated precursor ion population, and offered lower detection limits.

Combinations of PDPA reactions with solution-based derivatization strategies have also been explored with the aims of further increasing isomeric resolution and mixture analysis performance. For example, Franklin *et al*. coupled PDPA charge inversion ion/ion reactions with photochemical derivatization of carbon-carbon double bonds in unsaturated GPLs via the Paternò−Büchi (PB) reaction.[136] Ultimately, this method provides the gas-phase separation of

isomeric/isobaric PC and PE lipids while also affording the assignment of fatty acyl composition and the localization of carbon-carbon double bond(s) in unsaturated fatty acyl chains. In an additional example, gas-phase ion/ion reactions of ^{13}C-diazomethane-modified PE, PS, PC, and SM cations with PDPA reagent dianions were shown to charge-invert the positively charged GPL ions to the negative mode, where fatty acyl composition could be revealed.[138] Additional details regarding trimethylation enhancement using ^{13}C-diazomethane (^{13}C-TrEnDi) are provided below. The combination of ^{13}C-TrEnDi modification, PB derivatization, and PDPA reactions in a single workflow permitted enhanced structural identification at the carbon-carbon double bond positional level, particularly for PE lipids in complex biological samples.[139]

1.3 Charge Manipulation

The concept of charge manipulation is not inherently new to MS-based approaches. For example, there is an expansive body of literature regarding its applications the analysis of ionized biomolecules, especially peptide and protein characterization.77 Therefore, it is not surprising that charge manipulation strategies have been adapted for lipid analysis. For example, chemical modification procedures and gas-phase chemistries that influence ion charging have been developed to aid in lipid ionization efficiency, enhance structural elucidation, and separate targeted lipid classes from co-existing lipid signals derived from alternate lipid classes.

1.3.1 Charge Manipulation of Cations

Many advancements in lipid detection and identification have been driven by the manipulation of lipid precursor cations charge states and/or ion types, achieved via complexation with metal cations or covalent modifications with novel derivatization reagents. Below, we will review the reported strategies for altering lipid structures that readily ionize in the positive ion mode upon ESI. Such lipids primarily include those with fixed, cationic charge sites like PCs. Although PE and PS lipids tend to yield deprotonated anions upon negative ESI, these anionic lipids can also be ionized in positive ion mode via protonation, though their ionization efficiency is substantially lowered in this modality. In turn, some charge manipulation strategies reviewed below include these lipid classes, though the majority of presented approaches will focus on choline-containing lipids.

In addition to charge-switching, metal cationization has been explored to transform ion-type of lipid precursors that already demonstrate a propensity to ionize in positive ion mode. Identical to the strategies for metal cationization described above, the formation of metal-lipid complex cations upon positive ESI again relies on the addition of metal salts to lipid solutions prior to ionization. In early studies, Hsu and Turk examined alkali metal-adducted PC cations. Sodium-cationized PCs were first investigated with ESI-MS/MS.[141] However, the resulting CID spectra of sodium-PC adduct ions were largely uninformative. Turning to lithium as a cationization reagent, Turk and co-workers noted that CID of lithiated PC adducts offers advantages over analysis of protonated or sodiated PC ions.[142] Explicitly, the CID spectra of $[PC + Li]^+$ adduct ions contain abundant product ions generated via the loss of fatty acyl substituents, affording the assignment of acyl chain composition. In contrast to the CID spectra of lithium-lipid metal complexes described above with anionic phospholipid classes, this approach does not facilitate the localization of carbon-carbon double bonds.

Besides monovalent metal cationization, doubly charged PC-metal complexes have been examined by multiple groups. In the first example, O'Hair and colleagues investigated PC lipids complexed with Cu^{2+}, Co^{2+}, Mg^{2+}, and Ca^{2+} using electron capture dissociation (ECD).[143] Here, the ECD spectra of divalent metal-lipid complexes, notably those incorporating Ca and Mg dications, provided head group composition, fatty acyl composition, and in some cases, *sn*-position. In a recent example, Becher *et al*. explored the dissociation patterns of utilizing various activation methods, including CID, ultraviolet photodissociation (UVPD), and higher-energy collisional dissociation (HCD).[144] In this work, PC lipids were reported to complex with Fe^{2+} ions in solution, yielding doubly charged Fe-adducted PC cations upon positive mode ESI. The HCD, CID, and UVPD spectra of positive doubly charged PC-metal ion complexes revealed abundant carboxylate product ions created by ester bond cleavage at the *sn*-1 and *sn*-2 positions of the central glycerol backbone. Importantly, CID and UVPD of $[PC\text{-}Fe]^{2+}$ cations resulted in preferential loss of the *sn*-2 fatty acyl chain, enabling relative quantitation of *sn*-positional isomers. Unfortunately, neither approach described above facilitated detailed structural elucidation, as additional features like carbon-carbon double bond position were not revealed. Moreover, both strategies are limited to PC analysis, as alternate lipid classes were not effectively complexed with divalent metal cations. We note that this structure-selective reactivity could be beneficially exploited to enable the mass spectrometric separation of PCs from alternate phospholipid classes.

The advantages of cationic lipid covalent derivatization has been explored to alter lipid cation ion type, demonstrating the notable benefits of enhanced ionization efficiency and mass spectrometric separation of lipid classes. One such example, trimethylation enhancement using diazomethane, commonly referred to as TrEnDi, was recently developed by the Smith group.[145] Here, phosphate moieties, carboxylic acids, and primary amines are exhaustively methylated following exposure to an solution of diazomethane and acid. Consequently, PC, PS, PE, and SM lipids are derivatized with a permanent, fixed positive charge. By doing so, the sensitivity of MS/MS experiments are markedly improved, as ionization efficiency was greatly enhanced. Moreover, TrEnDi modification resulted in the consolidation of ion fragmentation into at most two dissociation channels, generating class-specific product ions that readily identify polar headgroup composition. Employing ^{13}C-labeled diazomethane, Canez *et al*. demonstrated the effectiveness of ^{13}C-TrEnDi, noting that this approach has the notable advantage over derivatization with unlabeled diazomethane as isobaric PE and PCs are effectively resolved.[146] However, the CID spectra of TrEnDi-modified lipid cations in positive ion mode do not contain product ions that permit fatty acyl identification, though this limitation can be overcome when combined with additional gas-phase derivatizations as described above.[138, 139]

Alternate covalent derivatization of cationic lipids via modification with a fixed, net positively charged reagent have also been implemented by the Reid group.[147-149] In their work, Reid and co-workers developed a selective chemical derivatization strategy for the differentiation of phospholipid classes using a direct infusion positive ESI-MS/MS approach. Coupled with high-resolution MS, the aminophospholipids PS and PE are covalently modified with the d_6-S,S'-dimethylthiobutanoylhydroxysuccinimide ester (d_6-DMBNHS) reagent. As d_6-DMBNHS contains a fixed charge sulfonium ion, the developed derivatization strategy improved ionization efficiency, extending the dynamic range of aminophospholipid detection in crude lipid extracts. Furthermore, as d_6-DMBNHS-modified lipids display a 136.0829 Da shift from unmodified lipids, possible isobaric interferences, namely those attributed to PC, PA, and PG lipid ions, were minimized. In a subsequent report, Fhaner *et al*. improved the previous shotgun strategy by utilizing a combination of the ^{13}C-labeled version of the DMBNHS ester reagent (*i.e.*, ^{13}C-DMBNHS) and selective modification of the vinyl double bond within plasmenyl ether containing lipids using iodine and methanol to fully resolve isobaric aminophospholipids, including ether species, from choline-containing species.[147] Collectively, this approach enables the mass spectrometric resolution and

molecular characterization of plasmenyl lipids and offers an attractive strategy to crude lipid extract analysis.

In a final shotgun approach, Pham and Julian achieved the separation of isomeric PE and PC structures via the selective, noncovalent complexation between PEs and 18-crown-6-ether (18C6).[150] Not only does this solution-based derivatization procedure eliminate overlapping PE and PC signals by shifting the PE cation signals into a higher *m/z* range, but it also improves the sensitivity of PE detection by nearly an order of magnitude, as the protonated primary amine is stabilized by the noncovalent binding of 18C6 This strategy is highlighted with Figure 1.15. Moreover, the incorporation of an IB motif into the 18C6 derivative enabled the generation of PE radical cations upon photoactivation and subsequent application of RDD experiments. The resulting RDD spectra of $[PE + H + IB - 18C6 - I]^{\bullet +}$ radical cations contained rich fragmentation patterns that allowed for the discrimination of isomeric lipids such as those varying in carbon-carbon double bond and methyl chain branching sites.

1.3.2 Charge Manipulation of Anions

Contrary to the many charge-manipulation strategies presented for lipid cation detection above, seemingly few parallel tactics have been applied for anion analysis. In a recent example, the McLuckey group applied proton transfer ion/ion reactions for the gas-phase separation, concentration, and identification of cardiolipins (CLs) from total lipid extract, relying exclusively on gas-phase chemistries.[151] Briefly, CLs are characterized by the presence of two phosphatidyl moieties linked to a central glycerol backbone and four fatty acyl substituents and are present at naturally low abundances within the cellular lipidome. In turn, analysis of this unique dimeric class of GPLs demands both high specificity and sensitivity, and thus, there are significant challenges associated with CL detection and structural elucidation, particularly when examining total lipid extracts. Here, $[CL - 2H]^{2-}$ were reacted with proton transfer reagent monocations in the gas-phase, giving rise to charge-reduced $[CL - H]^{-}$ anions. Consequently, the CL class was effectively separated on the *m/z* scale from alternate acidic phospholipid classes, as charge-reduced CL anions were resolved from more abundant, isobaric GPL monoanions. Prior to MS^n experiments, multiple iterations of proton-transfer ion/ion reactions allowed for the selective accumulation of the desired CL product ions. The iterative process not only dramatically reduces the averaging time needed to achieve good S/N product ion ratios but also enhances sensitivity and improves mixture analysis

performance. Application of this workflow to *Escherichia coli* extract afforded detailed characterization of low abundant CLs directly from total biological extract, as MS^n of charge-reduced $[CL - H]^-$ anions that have been concentrated in the gas-phase unveiled the structural complexities of CL molecular structures, revealing the presence of multiple CL isomers within a single mass-selected CL precursor anion population.

1.4 Conclusions

The importance of lipid analysis has become apparent when considering the relationships between altered lipid metabolism and the onset and progression of deleterious pathologies. Recent advances in ESI-MS/MS have largely facilitated the expansion of modern lipidomics, allowing for a deeper dive into the biochemical and functional roles of lipids. Nevertheless, there are significant challenges associated with conventional ESI-MS strategies and the reliance on native lipid ion types. As a consequence, a variety of charge and ion-type manipulation techniques have been developed with the dual aims of increasing ionization efficiency and enhancing structural characterization. Of these, solution-based derivatization methods have received the most attention, as these procedures can be readily utilized in conjunction with current commercially available mass spectrometers and can provide a number of benefits for lipid analysis. However, ion manipulation reliant on wet-chemical modification or alteration of solution conditions increase sample preparation timescales; promote undesired side-reactions that lead to complex mass spectra; and suffer incomplete derivatization leading to degenerate signals and impacting sensitivity. Post-source ion manipulation achieved through gas-phase ion/ion reactions thus offers unique advantages over solution-based counterparts. While it does not directly address ionization efficiency of lipids, benefits for structure elucidation and enhanced detection efficiencies have been demonstrated. By conducting lipid derivatization in the gas-phase, the ionization and derivatization events are decoupled, enabling the optimization of individual reagent solutions with regards to solution and electrospray conditions and enhanced control of reaction outcomes. Moreover, gas-phase ion/ion reactions offer the undeniable power to switch between charge states on-demand and undertake facile highly efficient and structure-selective derivatization. In some cases, a combination of both condensed-phase and gas-phase approaches have been shown to be particularly powerful. Though ion/ion reactions have been used to effectively manipulate the ion-type formed upon ionization, widespread adaptation of this strategy is primarily limited by the

requirement of instrument modification. In total, regardless of derivatization method, charge manipulation, particularly charge inversion, in combination with ESI-MS/MS provides increased efficiency, access to alternate and desirable fragmentation channels, and enhanced detection and identification of lipids in complex biological samples. In total, due to the broad spectrum of lipid structures, mixture complexities, and associated issues of dynamic range, the answer to unlocking the intricacies of the cellular lipidome likely lies in a combination of techniques. Such a platform might call on a combination of advanced separation techniques (LC), condensed-phase chemistries, gas-phase ion/ion chemistries (*i.e.*, charge inversion), and alternative ion activation methods (*i.e.*, OzID).

1.5 References

1. Pulfer, M.; Murphy, R. C., Electrospray mass spectrometry of phospholipids. *Mass Spectrom. Rev.* **2003,** *22* (5), 332-364.

2. Han, X. L.; Gross, R. W., Shotgun lipidomics: Electrospray ionization mass spectrometric analysis and quantitation of cellular lipidomes directly from crude extracts of biological samples. *Mass Spectrom. Rev.* **2005,** *24* (3), 367-412.

3. Dowhan, W.; Bogdanov, M.; Mileykovskaya, E., Functional roles of lipids in membranes. *Biochemistry of Lipids, Lipoproteins Membr., 5th Edition* **2008**, 1-37.

4. Fahy, E.; Subramaniam, S.; Murphy, R. C.; Nishijima, M.; Raetz, C. R. H.; Shimizu, T.; Spener, F.; van Meer, G.; Wakelam, M. J. O.; Dennis, E. A., Update of the LIPID MAPS comprehensive classification system for lipids. *J. Lipid Res.* **2009,** *50*, S9-S14.

5. Fahy, E.; Subramaniam, S.; Brown, H. A.; Glass, C. K.; Merrill, A. H.; Murphy, R. C.; Raetz, C. R. H.; Russell, D. W.; Seyama, Y.; Shaw, W.; Shimizu, T.; Spener, F.; van Meer, G.; Van Nieuwenhze, M. S.; White, S. H.; Witztum, J. L.; Dennis, E. A., A Comphrensive Classification System For Lipids. *Handbook of Biochemistry and Molecular Biology, 5th Edition* **2018**, 298-321.

6. Oh, H. J.; Kim, S. U.; Song, J. W.; Lee, J. H.; Kang, W. R.; Jo, Y. S.; Kim, K. R.; Bornscheuer, U. T.; Oh, D. K.; Park, J. B., Biotransformation of Linoleic Acid into Hydroxy Fatty Acids and Carboxylic Acids Using a Linoleate Double Bond Hydratase as Key Enzyme. *Adv. Synth. Catal.* **2015,** *357* (2-3), 408-416.

7. Jiang, X. Q.; Duan, Y. Y.; Zhou, B. S.; Guo, Q. Q.; Wang, H. H.; Hang, X. D.; Zeng, L. P.; Jia, J.; Bi, H. K., The Cyclopropane Fatty Acid Synthase Mediates Antibiotic Resistance and Gastric Colonization of Helicobacter pylori. *J. Bacteriol.* **2019,** *201* (20).

8. Blevins, M. S.; Klein, D. R.; Brodbelt, J. S., Localization of Cyclopropane Modifications in Bacterial Lipids via 213 nm Ultraviolet Photodissociation Mass Spectrometry. *Anal. Chem.* **2019,** *91* (10), 6820-6828.

9. Iles, K. E.; Wright, M. M.; Cole, M. P.; Welty, N. E.; Ware, L. B.; Matthay, M. A.; Schopfer, F. J.; Baker, P. R. S.; Agarwal, A.; Freeman, B. A., Fatty acid transduction of nitric oxide signaling: nitrolinoleic acid mediates protective effects through regulation of the ERK pathway. *Free Radical Bio. Med.* **2009,** *46* (7), 866-875.

10. Batthyany, C.; Schopfer, F. J.; Baker, P. R. S.; Duran, R.; Baker, L. M. S.; Huang, Y.; Cervenansky, C.; Branchaud, B. P.; Freeman, B. A., Reversible post-translational modification of proteins by nitrated fatty acids in vivo. *J. Biol. Chem.* **2006,** *281* (29), 20450-20463.

11. Vlaeminck, B.; Fievez, V.; Cabrita, A. R. J.; Fonseca, A. J. M.; Dewhurst, R. J., Factors affecting odd- and branched-chain fatty acids in milk: A review. *Anim. Feed Sc. Technol.* **2006,** *131* (3-4), 389-417.

12. Dean, J. M.; Lodhi, I. J., Structural and functional roles of ether lipids. *Protein Cell* **2018,** *9* (2), 196-206.

13. Yetukuri, L.; Ekroos, K.; Vidal-Puig, A.; Oresic, M., Informatics and computational strategies for the study of lipids. *Mol. Biosyst.* **2008,** *4* (2), 121-127.

14. Quehenberger, O.; Armando, A. M.; Brown, A. H.; Milne, S. B.; Myers, D. S.; Merrill, A. H.; Bandyopadhyay, S.; Jones, K. N.; Kelly, S.; Shaner, R. L.; Sullards, C. M.; Wang, E.; Murphy, R. C.; Barkley, R. M.; Leiker, T. J.; Raetz, C. R. H.; Guan, Z. Q.; Laird, G. M.; Six, D. A.; Russell, D. W.; McDonald, J. G.; Subramaniam, S.; Fahy, E.; Dennis, E. A., Lipidomics reveals a remarkable diversity of lipids in human plasma. *J. Lipid Res.* **2010,** *51* (11), 3299-3305.

15. Blanksby, S. J.; Mitchell, T. W., Advances in Mass Spectrometry for Lipidomics. *Annual Rev. Anal. Chem., Vol 3*, Yeung, E. S.; Zare, R. N., Eds. 2010; Vol. 3, pp 433-465.

16. Malheiro, A. R.; da Silva, T. F.; Brites, P., Plasmalogens and fatty alcohols in rhizomelic chondrodysplasia punctata and Sjogren-Larsson syndrome. *J. Inherited Metab. Dis.* **2015,** *38* (1), 111-121.

17. Schrakamp, G.; Schutgens, R. B. H.; Wanders, R. J. A.; Heymans, H. S. A.; Tager, J. M.; Vandenbosch, H., The Cerebro-hepato-renal (Zellweger) Syndrome - Impaired de novo biosynthesis of plasmalogens in cultured skin fibroblasts. *Biochim. Biophys. Acta* **1985,** *833* (1), 170-174.

18. Antalis, C. J.; Stevens, L. J.; Campbell, M.; Pazdro, R.; Ericson, K.; Burgess, J. R., Omega-3 fatty acid status in attention-deficit/hyperactivity disorder. *Prostaglandins Leukotrienes Essent. Fatty Acids* **2006,** *75* (4-5), 299-308.

19. Richardson, A. J., Omega-3 fatty acids in ADHD and related neurodevelopmental disorders. *In. Rev. Psychiatry* **2006,** *18* (2), 155-172.

20. Graessler, J.; Schwudke, D.; Schwarz, P. E. H.; Herzog, R.; Shevchenko, A.; Bornstein, S. R., Top-Down Lipidomics Reveals Ether Lipid Deficiency in Blood Plasma of Hypertensive Patients. *Plos One* **2009,** *4* (7).

21. Donovan, E. L.; Pettine, S. M.; Hickey, M. S.; Hamilton, K. L.; Miller, B. F., Lipidomic analysis of human plasma reveals ether-linked lipids that are elevated in morbidly obese humans compared to lean. *Diabetol. Metab. Syndr.* **2013,** *5*.

22. Simopoulos, A. P., An Increase in the Omega-6/Omega-3 Fatty Acid Ratio Increases the Risk for Obesity. *Nutrients* **2016,** *8* (3), 17.

23. Han, X. L.; Holtzman, D. M.; McKeel, D. W., Plasmalogen deficiency in early Alzheimer's disease subjects and in animal models: molecular characterization using electrospray ionization mass spectrometry. *J. Neurochem.* **2001,** *77* (4), 1168-1180.

24. Hu, C. X.; van der Heijden, R.; Wang, M.; van der Greef, J.; Hankemeier, T.; Xua, G. W., Analytical strategies in lipidomics and applications in disease biomarker discovery. *J. Chromatogr. B: Anal. Technol. Biomed. Life Sc.* **2009,** *877* (26), 2836-2846.

25. Hampel, H.; O'Bryant, S. E.; Molinuevo, J. L.; Zetterberg, H.; Masters, C. L.; Lista, S.; Kiddle, S. J.; Batrla, R.; Blennow, K., Blood-based biomarkers for Alzheimer disease: mapping the road to the clinic. *Nat. Rev. Neurol.* **2018,** *14* (11), 639-652.

26. Kuhajda, F. P., Fatty-acid synthase and human cancer: New perspectives on its role in tumor biology. *Nutrition* **2000,** *16* (3), 202-208.

27. Kiebish, M. A.; Han, X. L.; Cheng, H.; Chuang, J. H.; Seyfried, T. N., Cardiolipin and electron transport chain abnormalities in mouse brain tumor mitochondria: lipidomic evidence supporting the Warburg theory of cancer. *J. Lipid Res.* **2008,** *49* (12), 2545-2556.

28. Min, H. K.; Lim, S.; Chung, B. C.; Moon, M. H., Shotgun lipidomics for candidate biomarkers of urinary phospholipids in prostate cancer. *Anal. Bioanal. Chem.* **2011,** *399* (2), 823-830.

29. Zhou, X. C.; Mao, J. H.; Ai, J. M.; Deng, Y. P.; Roth, M. R.; Pound, C.; Henegar, J.; Welti, R.; Bigler, S. A., Identification of Plasma Lipid Biomarkers for Prostate Cancer by Lipidomics and Bioinformatics. *Plos One* **2012,** *7* (11).

30. Li, F.; Qin, X. Z.; Chen, H. Q.; Qiu, L.; Guo, Y. M.; Liu, H.; Chen, G. Q.; Song, G. G.; Wang, X. D.; Li, F. J.; Guo, S.; Wang, B. H.; Li, Z. L., Lipid profiling for early diagnosis and progression of colorectal cancer using direct-infusion electrospray ionization Fourier transform ion cyclotron resonance mass spectrometry. *Rapid Commun. Mass Spectrom.* **2013,** *27* (1), 24-34.

31. Qiu, Y. P.; Zhou, B. S.; Su, M. M.; Baxter, S.; Zheng, X. J.; Zhao, X. Q.; Yen, Y.; Jia, W., Mass Spectrometry-Based Quantitative Metabolomics Revealed a Distinct Lipid Profile in Breast Cancer Patients. *Int. J. Mol. Sci.* **2013,** *14* (4), 8047-8061.

32. Sapandowski, A.; Stope, M.; Evert, K.; Evert, M.; Zimmermann, U.; Peter, D.; Page, I.; Burchardt, M.; Schild, L., Cardiolipin composition correlates with prostate cancer cell proliferation. *Mol. Cell. Biochem.* **2015,** *410* (1-2), 175-185.

33. Chen, X. L.; Chen, H. K.; Dai, M. Y.; Ai, J. M.; Li, Y.; Mahon, B.; Dai, S. M.; Deng, Y. P., Plasma lipidomics profiling identified lipid biomarkers in distinguishing early-stage breast cancer from benign lesions. *Oncotarget* **2016,** *7* (24), 36622-36631.

34. Skotland, T.; Ekroos, K.; Kauhanen, D.; Simolin, H.; Seierstad, T.; Berge, V.; Sandvig, K.; Llorente, A., Molecular lipid species in urinary exosomes as potential prostate cancer biomarkers. *Eur. J. Cancer* **2017,** *70*, 122-132.

35. Messias, M. C. F.; Mecatti, G. C.; Priolli, D. G.; Carvalho, P. D., Plasmalogen lipids: functional mechanism and their involvement in gastrointestinal cancer. *Lipids Health Dis.* **2018,** *17*.

36. Zhang, W. P.; Zhang, D. H.; Chen, Q. H.; Wu, J. H.; Ouyang, Z.; Xia, Y., Online photochemical derivatization enables comprehensive mass spectrometric analysis of unsaturated phospholipid isomers. *Nat. Comm.* **2019,** *10*, 1-9.

37. Fuchs, B.; Suss, R.; Teuber, K.; Eibisch, M.; Schiller, J., Lipid analysis by thin-layer chromatography-A review of the current state. *J. Chromatogr. A* **2011,** *1218* (19), 2754-2774.

38. Li, J. B.; Vosegaard, T.; Guo, Z., Applications of nuclear magnetic resonance in lipid analyses: An emerging powerful tool for lipidomics studies. *Progress Lipid Res.* **2017,** *68*, 37-56.

39. Mitchell, T. W.; Pham, H.; Thomas, M. C.; Blanksby, S. J., Identification of double bond position in lipids: From GC to OzID. *J. Chromatogr. B-: Anal. Technol. Biomed. Life Sci.* **2009,** *877* (26), 2722-2735.

40. James, A. T.; Martin, A. J. P., Gas-liquid partition chromatography - the separation and micro-estimation of volatile fatty acids from formic acid to dodecanoic acid. *Biochem. J.* **1952,** *50* (5), 679-690.

41. Ren, J. W.; Mozurkewich, E. L.; Sen, A.; Vahratian, A. M.; Ferreri, T. G.; Morse, A. N.; Djuric, Z., Total Serum Fatty Acid Analysis by GC-MS: Assay Validation and Serum Sample Stability. *Curr. Pharm. Anal.* **2013,** *9* (4), 331-339.

42. Beale, D. J.; Pinu, F. R.; Kouremenos, K. A.; Poojary, M. M.; Narayana, V. K.; Boughton, B. A.; Kanojia, K.; Dayalan, S.; Jones, O. A. H.; Dias, D. A., Review of recent developments in GC-MS approaches to metabolomics-based research. *Metabolomics* **2018,** *14* (11), 152.

43. Chiu, H. H.; Kuo, C. H., Gas chromatography-mass spectrometry-based analytical strategies for fatty acid analysis in biological samples. *J. Food Drug Anal.* **2020,** *28* (1), 60-73.

44. Hancock, S. E.; Poad, B. L. J.; Batarseh, A.; Abbott, S. K.; Mitchell, T. W., Advances and unresolved challenges in the structural characterization of isomeric lipids. *Anal. Biochem.* **2017,** *524*, 45-55.

45. Tomer, K. B.; Crow, F. W.; Gross, M. L., Location of double-bond position in unsaturated fatty-acids by negative-ion MS/MS. *J. Am. Chem. Soc.* **1983,** *105* (16), 5487-5488.

46. Jensen, N. J.; Tomer, K. B.; Gross, M. L.; Lyon, P. A., Fast-atom-bombardment combined with tandem mass-spectrometry for the study of collisionally induced remote charge site decompositions. *ACS Symposium Series* **1985,** *291*, 194-208.

47. Jensen, N. J.; Tomer, K. B.; Gross, M. L., Collisional activation decomposition mass-spectra for locating double-bonds in poly-unsaturated fatty-acids. *Anal. Chem.* **1985,** *57* (11), 2018-2021.

48. Jensen, N. J.; Tomer, K. B.; Gross, M. L., Fast-atom-bombardment and tandem mass-spectrometry of phosphatidylserine and phosphatidylcholine. *Lipids* **1986,** *21* (9), 580-588.

49. Jensen, N. J.; Gross, M. L., Fast-atom-bombardment and tandem mass-spectrometry for determining iso-fatty and anteiso-fatty acids. *Lipids* **1986,** *21* (5), 362-365.

50. Tomer, K. B.; Jensen, N. J.; Gross, M. L., Fast-atom-bombardment and tandem mass-spectrometry for determining structural modification of fatty-acids. *Anal. Chem.* **1986,** *58* (12), 2429-2433.

51. Jensen, N. J.; Gross, M. L., Mass-spectrometry methods for structural determination and analysis of fatty-acids. *Mass Spectrom. Rev.* **1987,** *6* (4), 497-536.

52. Adams, J.; Gross, M. L., Tandem mass-spectrometry for collisional acitivation of alkali-metal-cationized fatty-acids - A method for determining double-bond location. *Anal. Chem.* **1987,** *59* (11), 1576-1582.

53. Jensen, N. J.; Tomer, K. B.; Gross, M. L., FAB MS/MS For Phosphatidylinositol, -glycerol, phosphatidylethanolamine and other complex phospholipids. *Lipids* **1987,** *22* (7), 480-489.

54. Davoli, E.; Gross, M. L., Charge remote fragmentation of fatty-acids cationized with alkaline-earth metal-ions. *J. Am. Soc. Mass Spectrom.* **1990,** *1* (4), 320-324.

55. Crockett, J. S.; Gross, M. L.; Christie, W. W.; Holman, R. T., Collisional activation of a series of homoconjugated octadecadienoic acids with fast atom bombardment and tandem mass-spectrometry. *J. Am. Soc. Mass Spectrom.* **1990,** *1* (2), 183-191.

56. Gross, M. L., Charge-remote fragmentations - method, mechanism, and applications. *Int. J. Mass Spectrom. Ion Proc.* **1992,** *118*, 137-165.

57. Gross, M. L., Charge-remote fragmentation: an account of research on mechanisms and applications. *Int. J. Mass Spectrom.* **2000,** *200* (1-3), 611-624.

58. Cheng, C. F.; Gross, M. L., Applications and mechanisms of charge-remote fragmentation. *Mass Spectrom. Rev.* **2000,** *19* (6), 398-420.

59. Trimpin, S.; Clemmer, D. E.; McEwen, C. N., Charge-remote fragmentation of lithiated fatty acids on a TOF-TOF instrument using matrix-ionization. *J. Am. Soc. Mass Spectrom.* **2007,** *18* (11), 1967-1972.

60. Pittenauer, E.; Allmaier, G., The Renaissance of High-Energy CID for Structural Elucidation of Complex Lipids: MALDI-TOF/RTOF-MS of Alkali Cationized Triacylglycerols. *J. Am. Soc. Mass Spectrom.* **2009,** *20* (6), 1037-1047.

61. Thomas, M. C.; Mitchell, T. W.; Blanksby, S. J., A comparison of the gas phase acidities of phospholipid headgroups: Experimental and computational studies. *J. Am. Soc. Mass Spectrom.* **2005,** *16* (6), 926-939.

62. Brugger, B.; Erben, G.; Sandhoff, R.; Wieland, F. T.; Lehmann, W. D., Quantitative analysis of biological membrane lipids at the low picomole level by nano-electrospray ionization tandem mass spectrometry. *Proc. Natl. Acad. Sci., U. S. A.* **1997,** *94* (6), 2339-2344.

63. Hsu, F. F.; Turk, J., Characterization of phosphatidylinositol, phosphatidylinositol-4-phosphate, and phosphatidylinositol-4,5-bisphosphate by electrospray ionization tandem mass spectrometry: A mechanistic study. *J. Am. Soc. Mass Spectrom.* **2000,** *11* (11), 986-999.

64. Hsu, F. F.; Turk, J., Charge-driven fragmentation processes in diacyl glycerophosphatidic acids upon low-energy collisional activation. A mechanistic proposal. *J. Am. Soc.Mass Spectrom.* **2000,** *11* (9), 797-803.

65. Hsu, F. F.; Turk, J., Charge-remote and charge-driven fragmentation processes in diacyl glycerophosphoethanolamine upon low-energy collisional activation: A mechanistic proposal. *J. Am. Soc. Mass Spectrom.* **2000,** *11* (10), 892-899.

66. Hsu, F. F.; Turk, J., Studies on phosphatidylglycerol with triple quadrupole tandem mass spectrometry with electrospray ionization: Fragmentation processes and structural characterization. *J. Am. Soc. Mass Spectrom.* **2001,** *12* (9), 1036-1043.

67. Hsu, F. F.; Turk, J., Electrospray ionization/tandem quadrupole mass spectrometric studies on phosphatidylcholines: The fragmentation processes. *J. Am. Soc. Mass Spectrom.* **2003,** *14* (4), 352-363.

68. Hsu, F. F.; Turk, J., Studies on phosphatidylserine by tandem quadrupole and multiple stage quadrupole ion-trap mass spectrometry with electrospray ionization: Structural characterization and the fragmentation processes. *J. Am. Soc. Mass Spectrom.* **2005,** *16* (9), 1510-1522.

69. Hsu, F. F.; Turk, J.; Rhoades, E. R.; Russell, D. G.; Shi, Y. X.; Groisman, E. A., Structural characterization of cardiolipin by tandem quadrupole and multiple-stage quadrupole ion-trap mass spectrometry with electrospray ionization. *J. Am. Soc. Mass Spectrom.* **2005,** *16* (4), 491-504.

70. Hsu, F. F.; Turk, J., Structural Characterization of Unsaturated Glycerophospholipids by Multiple-Stage Linear Ion-Trap Mass Spectrometry with Electrospray Ionization. *J. Am. Soc. Mass Spectrom.* **2008,** *19* (11), 1681-1691.

71. Hsu, F. F.; Lodhi, I. J.; Turk, J.; Semenkovich, C. F., Structural Distinction of Diacyl-, Alkylacyl, and Alk-1-Enylacyl Glycerophosphocholines as M-15 (-) Ions by Multiple-Stage Linear Ion-Trap Mass Spectrometry with Electrospray Ionization. *J. Am. Soc. Mass Spectrom.* **2014,** *25* (8), 1412-1420.

72. Ekroos, K.; Ejsing, C. S.; Bahr, U.; Karas, M.; Simons, K.; Shevchenko, A., Charting molecular composition of phosphatidylcholines by fatty acid scanning and ion trap MS3 fragmentation. *J. Lipid Res.* **2003,** *44* (11), 2181-2192.

73. Jemal, M.; Zheng, O. Y.; Teitz, D. S., High performance liquid chromatography mobile phase composition optimization for the quantitative determination of a carboxylic acid compound in human plasma by negative ion electrospray high performance liquid chromatography tandem mass spectrometry. *Rapid Comm. Mass Spectrom.* **1998,** *12* (8), 429-434.

74. Yang, W. C.; Adamec, J.; Regnier, F. E., Enhancement of the LC/MS analysis of fatty acids through derivatization and stable isotope coding. *Anal. Chem.* **2007,** *79* (14), 5150-5157.

75. Higashi, T.; Ichikawa, T.; Inagaki, S.; Min, J. Z.; Fukushima, T.; Toyo'oka, T., Simple and practical derivatization procedure for enhanced detection of carboxylic acids in liquid chromatography-electrospray ionization-tandem mass spectrometry. *J. Pharm Biomed. Anal.* **2010,** *52* (5), 809-818.

76. Murphy, R. C., Tandem Mass Spectrometry of Lipids: Molecular Analysis of Complex Lipids. New Developments in Mass Spectrometry **2015,** (4), 1-280.

77. Foreman, D. J.; McLuckey, S. A., Recent Developments in Gas-Phase Ion/Ion Reactions for Analytical Mass Spectrometry. *Anal. Chem.* **2020,** *92* (1), 252-266.

78. Hsu, F. F.; Turk, J., Distinction among isomeric unsaturated fatty acids as lithiated adducts by electrospray ionization mass spectrometry using low energy collisionally activated dissociation on a triple stage quadrupole instrument. *J. Am. Soc. Mass Spectrom.* **1999,** *10* (7), 600-612.

79. Fang, M. X.; Rustam, Y.; Palmieri, M.; Sieber, O. M.; Reid, G. E., Evaluation of ultraviolet photodissociation tandem mass spectrometry for the structural assignment of unsaturated fatty acid double bond positional isomers. *Anal. Bioanal. Chem.* **2020,** *412* (10), 2339-2351.

80. Hsu, F. F.; Turk, J., Characterization of phosphatidylethanolamine as a lithiated adduct by triple quadrupole tandem mass spectrometry with electrospray ionization. *J. Mass Spectrom.* **2000,** *35* (5), 596-606.

81. Zehethofer, N.; Pinto, D. M.; Volmer, D. A., Plasma free fatty acid profiling in a fish oil human intervention study using ultra-performance liquid chromatography/electrospray ionization tandem mass spectrometry. *Rapid Commun. Mass Spectrom.* **2008,** *22* (13), 2125-2133.

82. Duncan, K. D.; Volmer, D. A.; Gill, C. G.; Krogh, E. T., Rapid Screening of Carboxylic Acids from Waste and Surface Waters by ESI-MS/MS Using Barium Ion Chemistry and On-Line Membrane Sampling. *J. Am. Soc. Mass Spectrom.* **2016,** *27* (3), 443-450.

83. Afonso, C.; Riu, A.; Xu, Y.; Fournier, F.; Tabet, J. C., Structural characterization of fatty acids cationized with copper by electrospray ionization mass spectrometry under low-energy collision-induced dissociation. *J. Mass Spectrom.* **2005,** *40* (3), 342-349.

84. Ho, Y. P.; Huang, P. C.; Deng, K. H., Metal ion complexes in the structural analysis of phospholipids by electrospray ionization tandem mass spectrometry. *Rapid Commun. Mass Spectrom.* **2003,** *17* (2), 114-121.

85. Svane, S.; Gorshkov, V.; Kjeldsen, F., Charge Inversion of Phospholipids by Dimetal Complexes for Positive Ion-Mode Electrospray Ionization Mass Spectrometry Analysis. *Anal. Chem.* **2015,** *87* (17), 8732-8739.

86. Yoo, H. J.; Hakansson, K., Determination of Double Bond Location in Fatty Acids by Manganese Adduction and Electron Induced Dissociation. *Anal. Chem.* **2010,** *82* (16), 6940-6946.

87. Li, X. N.; Franke, A. A., Improved LC-MS Method for the Determination of Fatty Acids in Red Blood Cells by LC-Orbitrap MS. *Anal. Chem.* **2011,** *83* (8), 3192-3198.

88. Johnson, D. W., Dimethylaminoethyl esters for trace, rapid analysis of fatty acids by electrospray tandem mass spectrometry. *Rapid Commun. Mass Spectrom.* **1999,** *13* (23), 2388-2393.

89. Jiang, R. Q.; Jiao, Y.; Zhang, P.; Liu, Y.; Wang, X.; Huang, Y.; Zhang, Z. J.; Xu, F. G., Twin Derivatization Strategy for High-Coverage Quantification of Free Fatty Acids by Liquid Chromatography-Tandem Mass Spectrometry. *Anal. Chem.* **2017,** *89* (22), 12223-12230.

90. Sun, F. X.; Choi, A. A.; Wu, R. H., Systematic Analysis of Fatty Acids in Human Cells with a Multiplexed Isobaric Tag (TMT)-Based Method. *J. Proteome Res.* **2018,** *17* (4), 1606-1614.

91. Han, J.; Lin, K.; Sequeira, C.; Borchers, C. H., An isotope-labeled chemical derivatization method for the quantitation of short-chain fatty acids in human feces by liquid chromatography-tandem mass spectrometry. *Anal. Chim. Acta* **2015,** *854*, 86-94.

92. Narayana, V. K.; Tomatis, V. M.; Wang, T.; Kvaskoff, D.; Meunier, F. A., Profiling of Free Fatty Acids Using Stable Isotope Tagging Uncovers a Role for Saturated Fatty Acids in Neuroexocytosis. *Chem. Biol.* **2015,** *22* (11), 1552-1561.

93. Zhu, Q. F.; Hao, Y. H.; Liu, M. Z.; Yue, J.; Ni, J.; Yuan, B. F.; Feng, Y. Q., Analysis of cytochrome P450 metabolites of arachidonic acid by stable isotope probe labeling coupled with ultra high-performance liquid chromatography/mass spectrometry. *J. Chromatogr. A* **2015,** *1410*, 154-163.

94. Zhu, Q. F.; Zhang, Z.; Liu, P.; Zheng, S. J.; Peng, K.; Deng, Q. Y.; Zheng, F.; Yuan, B. F.; Feng, Y. Q., Analysis of liposoluble carboxylic acids metabolome in human serum by stable isotope labeling coupled with liquid chromatography-mass spectrometry. *J. Chromatogr. A* **2016,** *1460*, 100-109.

95. Leng, J. P.; Wang, H. Y.; Zhang, L.; Zhang, J.; Wang, H.; Guo, Y. L., A highly sensitive isotope-coded derivatization method and its application for the mass spectrometric analysis of analytes containing the carboxyl group. *Anal. Chim. Acta* **2013,** *758*, 114-121.

96. Pettinella, C.; Lee, S. H.; Cipollone, F.; Blair, I. A., Targeted quantitative analysis of fatty acids in atherosclerotic plaques by high sensitivity liquid chromatography/tandem mass spectrometry. *J. Chromatogr. B: Anal. Technol. Biomed. Life Sci.* **2007,** *850* (1-2), 168-176.

97. Kretschmer, A.; Giera, M.; Wijtmans, M.; de Vries, L.; Lingeman, H.; Irth, H.; Niessen, W. M. A., Derivatization of carboxylic acids with 4-APEBA for detection by positive-ion LC-ESI-MS(/MS) applied for the analysis of prostanoids and NSAID in urine. *J. Chromatogr. B: Anal. Technol. Biomed. Life Sci.* **2011,** *879* (17-18), 1393-1401.

98. Bian, X. Q.; Sun, B. Q.; Zheng, P. Y.; Li, N.; Wu, J. L., Derivatization enhanced separation and sensitivity of long chain-free fatty acids: Application to asthma using targeted and non-targeted liquid chromatography-mass spectrometry approach. *Anal. Chim. Acta* **2017,** *989,* 59-70.

99. Bollinger, J. G.; Thompson, W.; Lai, Y.; Oslund, R. C.; Hallstrand, T. S.; Sadilek, M.; Turecek, F.; Gelb, M. H., Improved Sensitivity Mass Spectrometric Detection of Eicosanoids by Charge Reversal Derivatization. *Anal. Chem.* **2010,** *82* (16), 6790-6796.

100. Yang, K.; Dilthey, B. G.; Gross, R. W., Identification and Quantitation of Fatty Acid Double Bond Positional Isomers: A Shotgun Lipidomics Approach Using Charge-Switch Derivatization. *Anal. Chem.* **2013,** *85* (20), 9742-9750.

101. Bollinger, J. G.; Rohan, G.; Sadilek, M.; Gelb, M. H., LC/ESI-MS/MS detection of FAs by charge reversal derivatization with more than four orders of magnitude improvement in sensitivity. *J. Lipid Res.* **2013,** *54* (12), 3523-3530.

102. Wang, M.; Han, R. H.; Han, X. L., Fatty Acidomics: Global Analysis of Lipid Species Containing a Carboxyl Group with a Charge-Remote Fragmentation-Assisted Approach. *Anal. Chem.* **2013,** *85* (19), 9312-9320.

103. Tatituri, R. V. V.; Wolf, B. J.; Brenner, M. B.; Turk, J.; Hsu, F. F., Characterization of polar lipids of Listeria monocytogenes by HCD and low-energy CAD linear ion-trap mass spectrometry with electrospray ionization. *Anal. Bioanal. Chem.* **2015,** *407* (9), 2519-2528.

104. Liu, X. P.; Moon, S. H.; Mancuso, D. J.; Jenkins, C. M.; Guan, S. P.; Sims, H. F.; Gross, R. W., Oxidized fatty acid analysis by charge-switch derivatization, selected reaction monitoring, and accurate mass quantitation. *Anal. Biochem.* **2013,** *442* (1), 40-50.

105. Thomas, M. C.; Mitchell, T. W.; Harman, D. G.; Deeley, J. M.; Murphy, R. C.; Blanksby, S. J., Elucidation of double bond position in unsaturated lipids by ozone electrospray ionization mass spectrometry. *Anal. Chem.* **2007,** *79* (13), 5013-5022.

106. Thomas, M. C.; Mitchell, T. W.; Harman, D. G.; Deeley, J. M.; Nealon, J. R.; Blanksby, S. J., Ozone-induced dissociation: Elucidation of double bond position within mass-selected lipid ions. *Anal. Chem.* **2008,** *80* (1), 303-311.

107. Deeley, J. M.; Thomas, M. C.; Truscott, R. J. W.; Mitchell, T. W.; Blanksby, S. J., Identification of Abundant Alkyl Ether Glycerophospholipids in the Human Lens by Tandem Mass Spectrometry Techniques. *Anal. Chem.* **2009,** *81* (5), 1920-1930.

108. Thomas, M. C.; Mitchell, T. W.; Blanksby, S. J., Online Ozonolysis Methods for the Determination of Double Bond Position in Unsaturated Lipids. *Lipidomics: Vol 1: Methods Protoc.* **2009,** *579,* 413-441.

109. Poad, B. L. J.; Pham, H. T.; Thomas, M. C.; Nealon, J. R.; Campbell, J. L.; Mitchell, T. W.; Blanksby, S. J., Ozone-Induced Dissociation on a Modified Tandem Linear Ion-Trap: Observations of Different Reactivity for Isomeric Lipids. *J. Am. Soc. Mass Spectrom.* **2010,** *21* (12), 1989-1999.

110. Brown, S. H. J.; Mitchell, T. W.; Blanksby, S. J., Analysis of unsaturated lipids by ozone-induced dissociation. *Biochim. Biophys. Acta-Mol. Cell Bio. Lipids* **2011,** *1811* (11), 807-817.

111. Marshall, D. L.; Criscuolo, A.; Young, R. S.; Poad, B. L.; Zeller, M.; Reid, G. E.; Mitchell, T. W.; Blanksby, S. J., Mapping Unsaturation in Human Plasma Lipids by Data-Independent Ozone-Induced Dissociation. *J. Am. Soc. Mass Spectrom.* **2019**, 1-10.

112. Pham, H. T.; Maccarone, A. T.; Thomas, M. C.; Campbell, J. L.; Mitchell, T. W.; Blanksby, S. J., Structural characterization of glycerophospholipids by combinations of ozone- and collision-induced dissociation mass spectrometry: the next step towards "top-down" lipidomics. *Analyst* **2014,** *139* (1), 204-214.

113. Poad, B. L. J.; Marshall, D. L.; Harazim, E.; Gupta, R.; Naredrdula, V. R.; Young, R. S. E.; Duchoslav, E.; Campbell, J. L.; Broadbent, J. A.; Cvacka, J.; Mitchell, T. W.; Blanksby, S. J., Combining Charge-Switch Derivatization with Ozone-Induced Dissociation for Fatty Acid Analysis. *J. Am. Soc. Mass Spectrom.* **2019,** *30* (10), 2135-2143.

114. Tao, Y. Q.; Quebbemann, N. R.; Julian, R. R., Discriminating D-Amino Acid-Containing Peptide Epimers by Radical-Directed Dissociation Mass Spectrometry. *Anal. Chem.* **2012,** *84* (15), 6814-6820.

115. Pham, H. T.; Trevitt, A. J.; Mitchell, T. W.; Blanksby, S. J., Rapid differentiation of isomeric lipids by photodissociation mass spectrometry of fatty acid derivatives. *Rapid Commun. Mass Spectrom.* **2013,** *27* (7), 805-815.

116. Narreddula, V. R.; Boase, N. R.; Ailuri, R.; Marshall, D. L.; Poad, B. L. J.; Kelso, M. J.; Trevitt, A. J.; Mitchell, T. W.; Blanksby, S. J., Introduction of a Fixed-Charge, Photolabile Derivative for Enhanced Structural Elucidation of Fatty Acids. *Anal. Chem.* **2019,** *91* (15), 9901-9909.

117. Narreddula, V. R.; Sadowski, P.; Boase, N. R. B.; Marshall, D. L.; Poad, B. L. J.; Trevitt, A. J.; Mitchell, T. W.; Blanksby, S. J., Structural elucidation of hydroxy fatty acids by photodissociation mass spectrometry with photolabile derivatives. *Rapid Commun. Mass Spectrom.* **2020,** *34* (9), UNSP e8741.

118. Hancock, S. E.; Ailuri, R.; Marshall, D. L.; Brown, S. H. J.; Saville, J. T.; Narreddula, V. R.; Boase, N. R.; Poad, B. L. J.; Trevitt, A. J.; Willcox, M. D. P.; Kelso, M. J.; Mitchell, T. W.; Blanksby, S. J., Mass spectrometry-directed structure elucidation and total synthesis of ultra-long chain (O-acyl)-omega-hydroxy fatty acids. *J. Lipid Res.* **2018,** *59* (8), 1510-1518.

119. Stinson, C. A.; Xia, Y., A method of coupling the Paterno-Buchi reaction with direct infusion ESI-MS/MS for locating the C=C bond in glycerophospholipids. *Analyst* **2016,** *141* (12), 3696-3704.

120. Ma, X. X.; Xia, Y., Pinpointing Double Bonds in Lipids by Paterno-Buchi Reactions and Mass Spectrometry. *Angew. Chem. Int. Ed.* **2014,** *53* (10), 2592-2596.

121. Ma, X. X.; Chong, L.; Tian, R.; Shi, R. Y.; Hu, T. Y.; Ouyang, Z.; Xia, Y., Identification and quantitation of lipid C=C location isomers: A shotgun lipidomics approach enabled by photochemical reaction. *Proc. Natl. Acad. Sci. U. S. A.* **2016,** *113* (10), 2573-2578.

122. Esch, P.; Heiles, S., Charging and Charge Switching of Unsaturated Lipids and Apolar Compounds Using Patern-Buchi Reactions. *J. Am. Soc. Mass Spectrom.* **2018,** *29* (10), 1971-1980.

123. Xu, S. L.; Wu, B. F.; Oresic, M.; Xie, Y.; Yao, P.; Wu, Z. Y.; Lv, X.; Chen, H.; Wei, F., Double Derivatization Strategy for High-Sensitivity and High- Coverage Localization of Double Bonds in Free Fatty Acids by Mass Spectrometry. *Anal. Chem.* **2020,** *92* (9), 6446-6455.

124. Randolph, C. E.; Foreman, D. J.; Betancourt, S. K.; Blanksby, S. J.; McLuckey, S. A., Gas-Phase Ion/Ion Reactions Involving Tris-Phenanthroline Alkaline Earth Metal Complexes as Charge Inversion Reagents for the Identification of Fatty Acids. *Anal. Chem.* **2018,** *90* (21), 12861-12869.

125. Randolph, C. E.; Foreman, D. J.; Blanksby, S. J.; McLuckey, S. A., Generating Fatty Acid Profiles in the Gas Phase: Fatty Acid Identification and Relative Quantitation Using Ion/Ion Charge Inversion Chemistry. *Anal. Chem.* **2019,** *91* (14), 9032-9040.

126. Randolph, C. E.; Blanksby, S. J.; McLuckey, S. A., Towards Complete Structure Elucidation of Glycerophospholipids in the Gas Phase through Charge Inversion Ion/Ion Chemistry. *Anal. Chem.* **2020**, *92*, 1219-1227.

127. Randolph, C. E.; Shenault, D. M.; Blanksby, S. J.; McLuckey, S. A., Structural Elucidation of Ether Glycerophospholipids Using Gas-Phase Ion/Ion Charge Inversion Chemistry. *J. Am. Soc. Mass Spectrom.* **2020,** *31* (5), 1093-1103.

128. Yu, X.; Jin, W.; McLuckey, S. A.; Londry, F. A.; Hager, J. W., Mutual storage mode ion/ion reactions in a hybrid linear ion trap. *J. Am. Soc. Mass Spectrom.* **2005,** *16* (1), 71-81.

129. Randolph, C. E.; Blanksby, S. J.; McLuckey, S. A., Charge-switch derivatization of fatty acid esters of hydroxy fatty acids via gas-phase ion/ion reactions. Anal. Chim. Acta, **2020**, In press.

130. Zhang, X.; Reid, G. E., Multistage tandem mass spectrometry of anionic phosphatidylcholine lipid adducts reveals novel dissociation pathways. *Int. J. Mass Spectrom.* **2006,** *252* (3), 242-255.

131. Zhao, X.; Zhang, W. P.; Zhang, D. H.; Liu, X. W.; Cao, W. B.; Chen, Q. H.; Ouyang, Z.; Xia, Y., A lipidomic workflow capable of resolving sn- and CC location isomers of phosphatidylcholines. *Chem. Sci.* **2019,** *10* (46), 10740-10748.

132. Han, X. L.; Gross, R. W., Structural determination of picomole amounts of phospholipids via electrospray ionization tandem mass spectrometry. *J. Am. Soc. Mass Spectrom.* **1995,** *6* (12), 1202-1210.

133. Harrison, K. A.; Murphy, R. C., Negative electrospray ionization of glycerophosphocholine lipids: Formation of M-15 (-) ions occurs via collisional decomposition of adduct anions. *J. Mass Spectrom.* **1995,** *30* (12), 1772-1773.

134. Pham, H. T.; Ly, T.; Trevitt, A. J.; Mitchell, T. W.; Blanksby, S. J., Differentiation of Complex Lipid Isomers by Radical-Directed Dissociation Mass Spectrometry. *Anal. Chem.* **2012,** *84* (17), 7525-7532.

135. Rojas-Betancourt, S.; Stutzman, J. R.; Londry, F. A.; Blanksby, S. J.; McLuckey, S. A., Gas-Phase Chemical Separation of Phosphatidylcholine and Phosphatidylethanolamine Cations via Charge Inversion Ion/Ion Chemistry. *Anal. Chem.* **2015,** *87* (22), 11255-11262.

136. Franklin, E. T.; Betancourt, S. K.; Randolph, C. E.; McLuckey, S. A.; Xia, Y., In-depth structural characterization of phospholipids by pairing solution photochemical reaction with charge inversion ion/ion chemistry. *Anal. Bioanal. Chem.* **2019**, *411*, 4739-4749.

137. Stutzman, J. R.; Blanksby, S. J.; McLuckey, S. A., Gas-Phase Transformation of Phosphatidylcholine Cations to Structurally Informative Anions via Ion/Ion Chemistry. *Anal. Chem.* **2013,** *85* (7), 3752-3757.

138. Betancourt, S. K.; Canez, C. R.; Shields, S. W. J.; Manthorpe, J. M.; Smith, J. C.; McLuckey, S. A., Trimethylation Enhancement Using C-13-Diazomethane: Gas-Phase Charge Inversion of Modified Phospholipid Cations for Enhanced Structural Characterization. *Anal. Chem.* **2017,** *89* (17), 9452-9458.

139. Franklin, E. T.; Shields, S. W. J.; Manthorpe, J. M.; Smith, J. C.; Xia, Y.; McLuckey, S. A., Coupling Headgroup and Alkene Specific Solution Modifications with Gas-Phase Ion/Ion Reactions for Sensitive Glycerophospholipid Identification and Characterization. *J. Am. Soc. Mass Spectrom.* **2020,** *31* (4), 938-945.

140. Specker, J. T.; Prentice, B. M. In *Gas-phase separation and concentration of phosphatidylcholine lipids using charge inversion ion/ion reactions enabled on an FT-ICR mass spectrometer*, 68th American Society for Mass Spectrometry Conference on Mass Spectrometry and Allied Topics, 2020.

141. Fang, J. S.; Barcelona, M. J., Structural determination and quantitative analysis of bacterial phospholipids using liquid chromatography electrospray ionization mass spectrometry. *J. Microbiol. Methods* **1998,** *33* (1), 23-35.

142. Hsu, F. F.; Bohrer, A.; Turk, J., Formation of lithiated adducts of glycerophosphocholine lipids facilitates their identification by electrospray ionization tandem mass spectrometry. *J. Am. Soc. Mass Spectrom.* **1998,** *9* (5), 516-526.

143. James, P. F.; Perugini, M. A.; O'Hair, R. A. J., Electron capture dissociation of complexes of diacylglycerophosphocholine and divalent metal ions: Competition between charge reduction and radical induced phospholipid fragmentation. *J. Am. Soc. Mass Spectrom.* **2008,** *19* (7), 978-986.

144. Becher, S.; Esch, P.; Heiles, S., Relative Quantification of Phosphatidylcholine sn-Isomers Using Positive Doubly Charged Lipid-Metal Ion Complexes. *Anal. Chem.* **2018,** *90* (19), 11486-11494.

145. Wasslen, K. V.; Canez, C. R.; Lee, H.; Manthorpe, J. M.; Smith, J. C., Trimethylation Enhancement Using Diazomethane (TrEnDi) II: Rapid In-Solution Concomitant Quaternization of Glycerophospholipid Amino Groups and Methylation of Phosphate Groups via Reaction with Diazomethane Significantly Enhances Sensitivity in Mass Spectrometry Analyses via a Fixed, Permanent Positive Charge. *Anal. Chem.* **2014,** *86* (19), 9523-9532.

146. Canez, C. R.; Shields, S. W. J.; Bugno, M.; Wasslen, K. V.; Weinert, H. P.; Willmore, W. G.; Manthorpe, J. M.; Smith, J. C., Trimethylation Enhancement Using C-13-Diazomethane (C-13-TrEnDi): Increased Sensitivity and Selectivity of Phosphatidylethanolamine, Phosphatidylcholine, and Phosphatidylserine Lipids Derived from Complex Biological Samples. *Anal. Chem.* **2016,** *88* (14), 6996-7004.

147. Fhaner, C. J.; Liu, S.; Zhou, X.; Reid, G. E., Functional Group Selective Derivatization and Gas-Phase Fragmentation Reactions of Plasmalogen Glycerophospholipids. *Mass Spectrom. Soc. Japan*, **2012**; Vol. 2.

148. Fhaner, C. J.; Liu, S. C.; Ji, H.; Simpson, R. J.; Reid, G. E., Comprehensive Lipidome Profiling of Isogenic Primary and Metastatic Colon Adenocarcinoma Cell Lines. *Anal. Chem.* **2012,** *84* (21), 8917-8926.

149. Nie, S.; Fhaner, C. J.; Liu, S. C.; Peake, D.; Kiyonami, R.; Huang, Y. Y.; Reid, G. E., Characterization and multiplexed quantification of derivatized aminophospholipids. *Int. J. Mass Spectrom.* **2015,** *391*, 71-81.

150. Pham, H. T.; Julian, R. R., Mass Shifting and Radical Delivery with Crown Ether Attachment for Separation and Analysis of Phosphatidylethanolamine Lipids. *Anal. Chem.* **2014,** *86* (6), 3020-3027.

151. Randolph, C. E.; Fabijanczuk, K. C.; Blanksby, S. J.; McLuckey, S. A., Proton transfer reactions for the gas-phase separation, concentration, and identification of cardiolipins. *Anal. Chem*., **2020,** doi.org/10.1021/acs.analchem.0c02545.

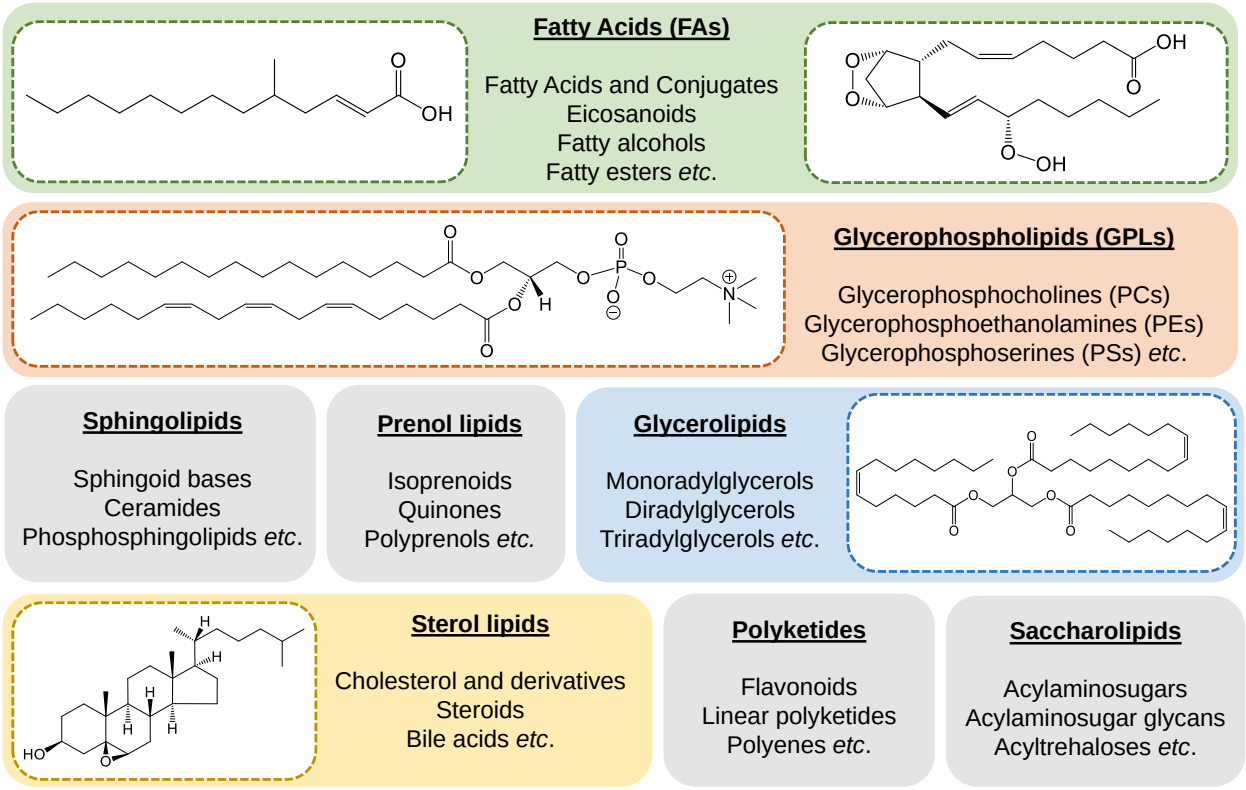

Figure 1.1 Common lipid categories with structural examples

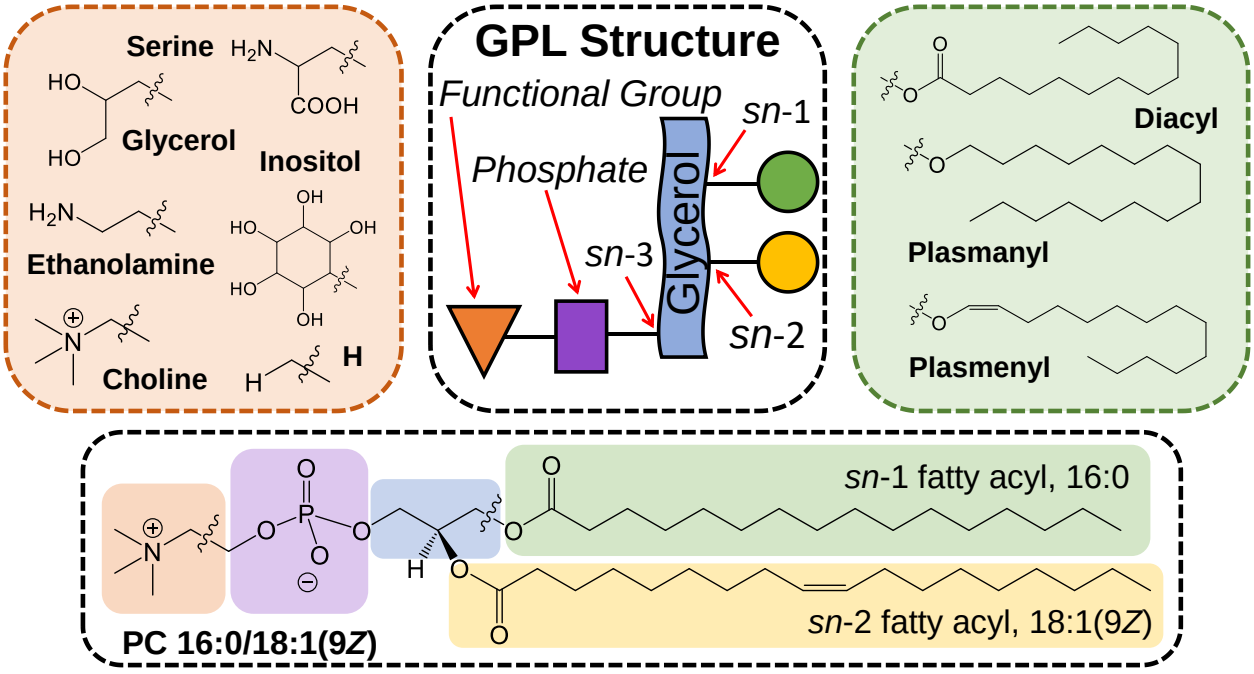

Figure 1.2 General glycerophospholipid structure. Polar headgroup structures and names are given in the orange panel (top left corner). The headgroup composition determines GPL class. In the green panel (top right), example *sn*-1 radyl chains are portrayed, noting that the nature of the *sn*-1 linkage dictates GPL subclass. Explicitly, GPL contain either an acyl, 1-*O*-alkyl, or a 1-*O*-alk-1′-enyl group at the sn-1 position, indicating the diacyl, plasmanyl, or plasmenyl subclasses, respectively.

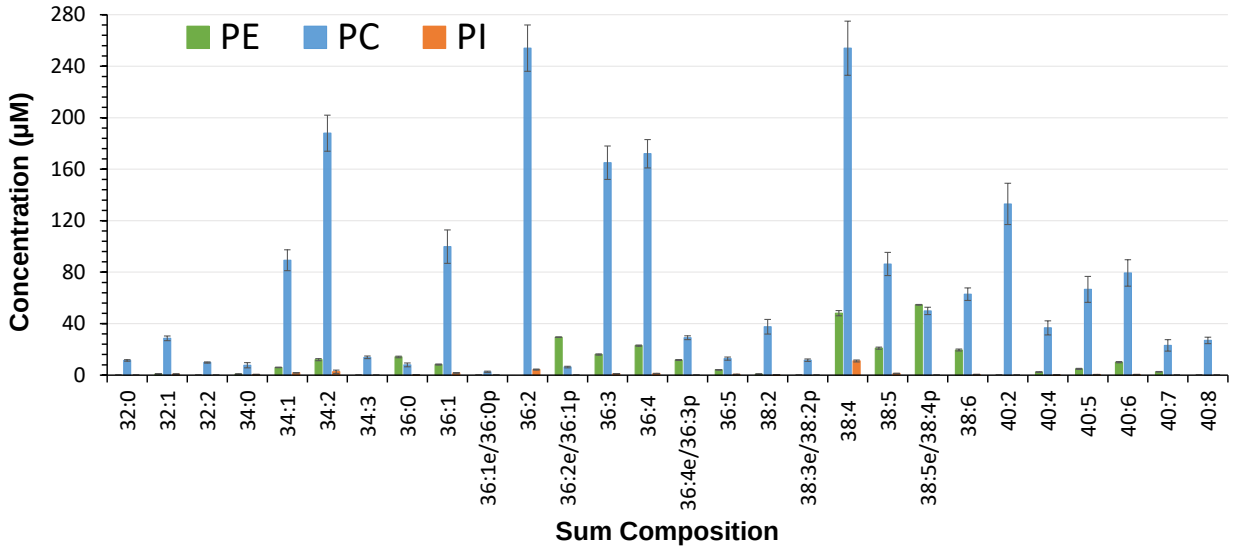

Figure 1.3 GPLs in human plasma samples. The measurements for PE, PC, and PI species were performed in quintuplicate and reported as the mean ± standard error of the mean (SEM). Adapted with permission from Reference 14.

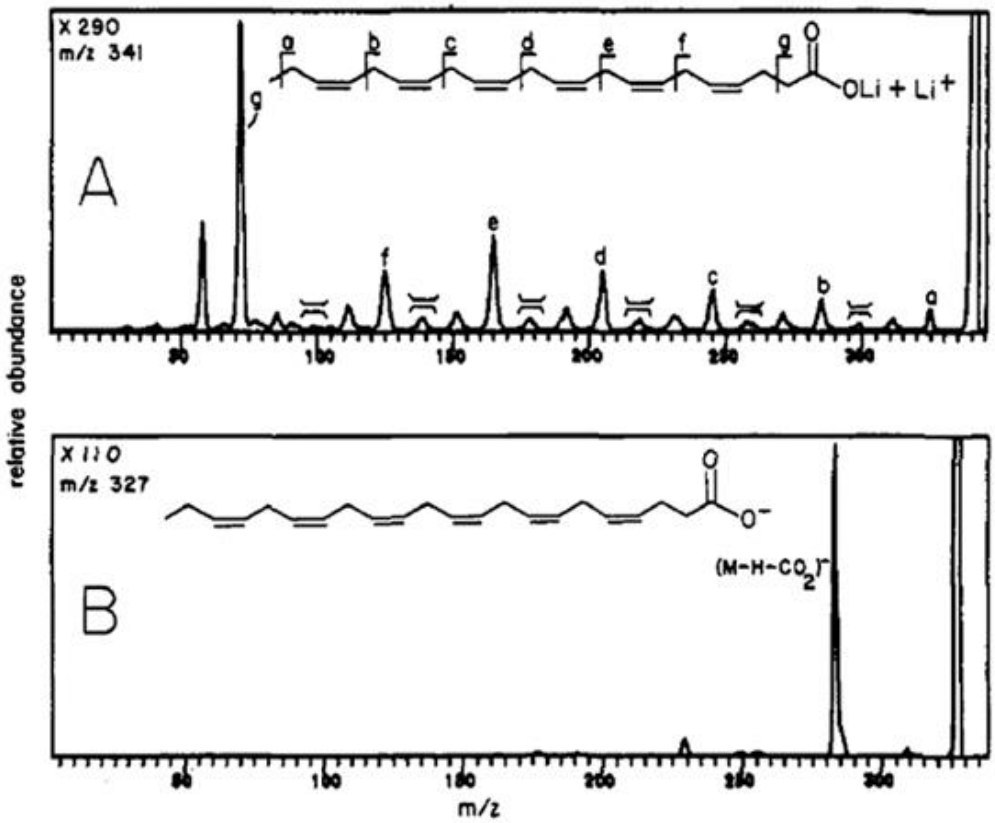

Figure 1.4 FAB-MS/MS spectra of 22:6(4*Z*,7*Z*,10*Z*,13*Z*,16*Z*,19*Z*) (a) $[M - H + 2Li]^+$ and (b) $[M - H]^-$ ions. The product ions indicative of carbon-carbon double bond cleavage are indicated with double bond symbols. Reproduced with permission from Reference 52.

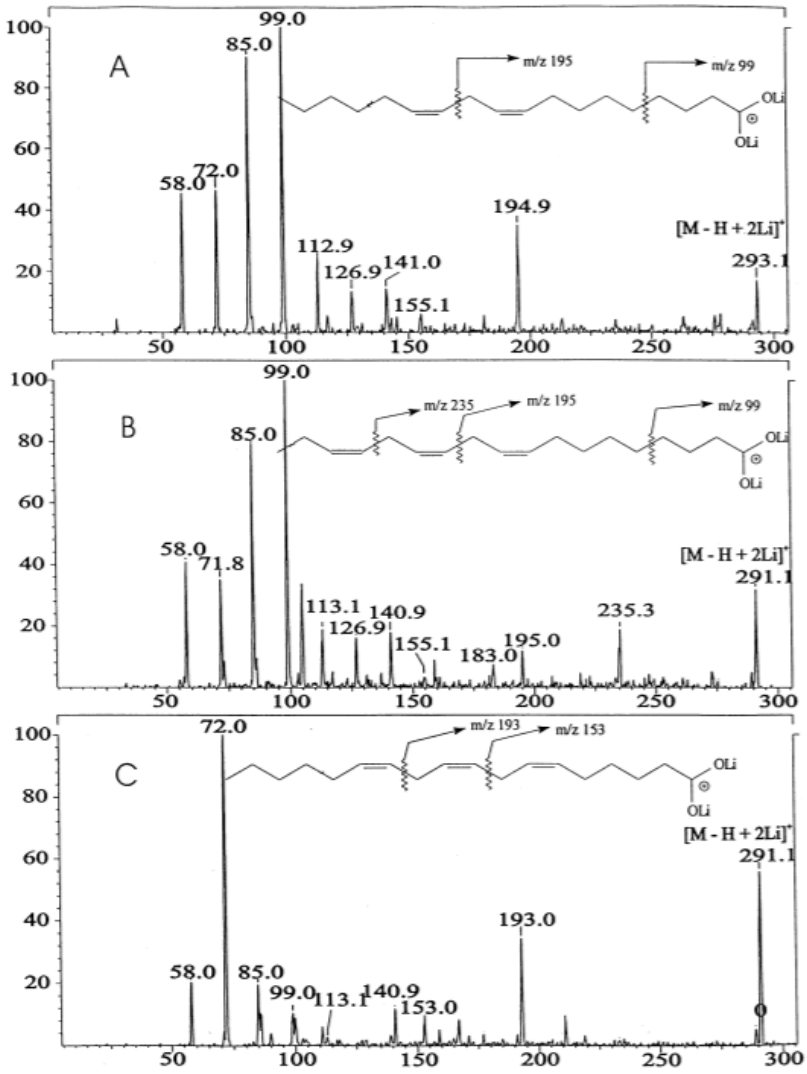

Figure 1.5 CID spectra of $[FA - H + 2Li]^+$ adducts of (a) 18:2(9, 12), (b) 18:3(9,12,15), and (c) 18:3(6,9,12). Reproduced with permission from Reference 78.

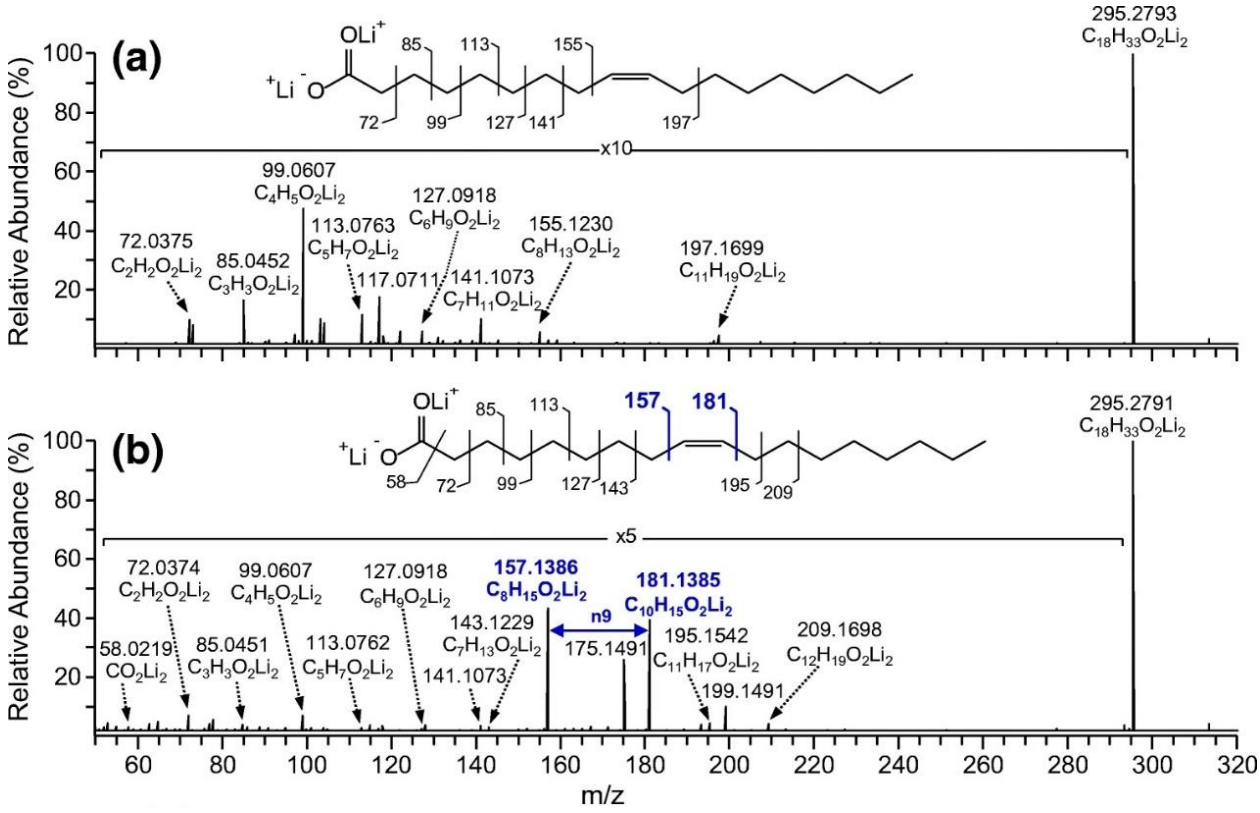

Figure 1.6 Product ion spectra of the $[M - H + 2Li]^+$ precursor ion of FA 18:1(9*Z*) obtained utilizing collisional activation via (a) HCD (30 eV collision energy) and (b) 193 nm UVPD (100 laser pulses per scan were performed with the HCD collision energy set at 2 eV). Reproduced with permission from Reference 79.

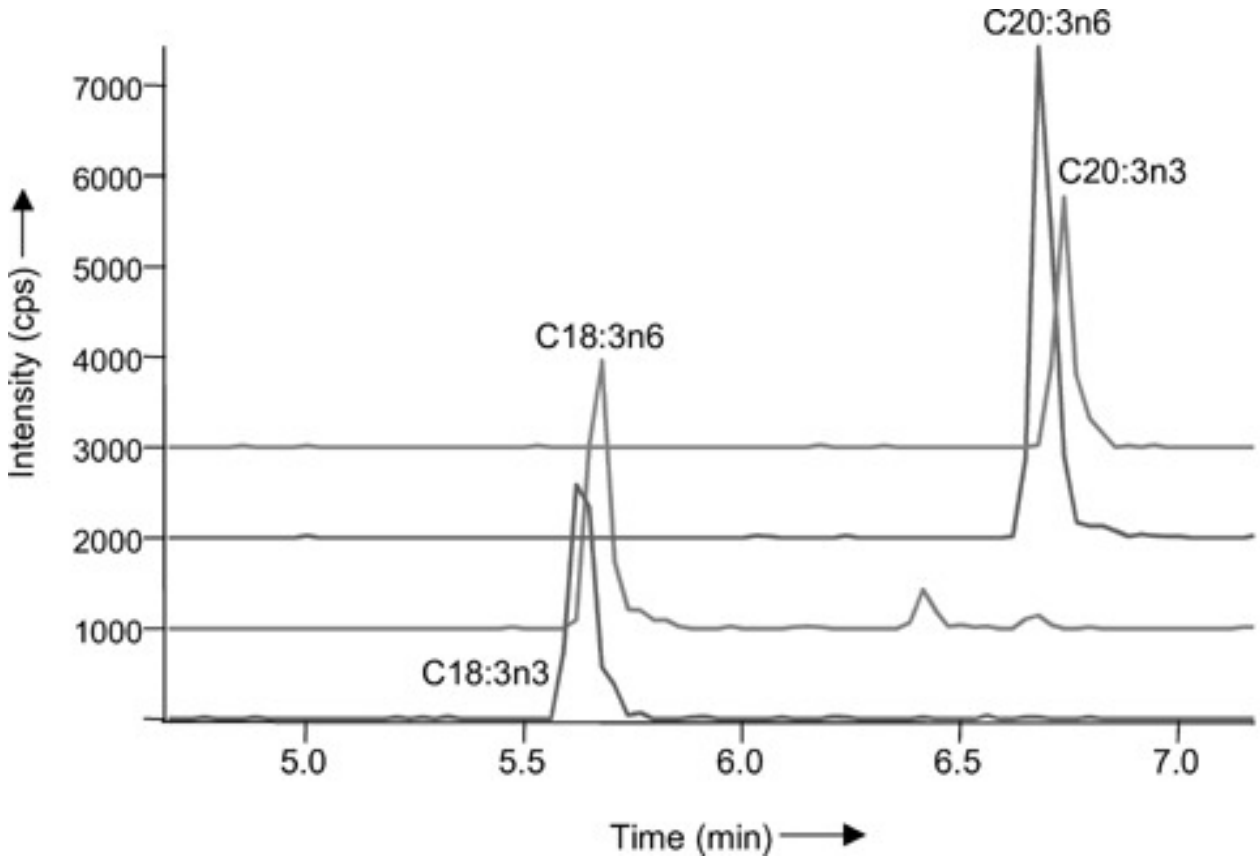

Figure 1.7 UPLC MRM chromatograms for the double bond positional isomers of FA 18:3 and FA 20:3 The isomer-specific transitions used for 18:3(*n*-3), 18:3(*n*-6), 20:3(*n*-6), and 20:3(*n*-3) were $415^+ \rightarrow 317^+$, $415^+ \rightarrow 307^+$, $443^+ \rightarrow 335^+$, and $443^+ \rightarrow 345^+$, respectively. Reproduced with permission from Reference 81.

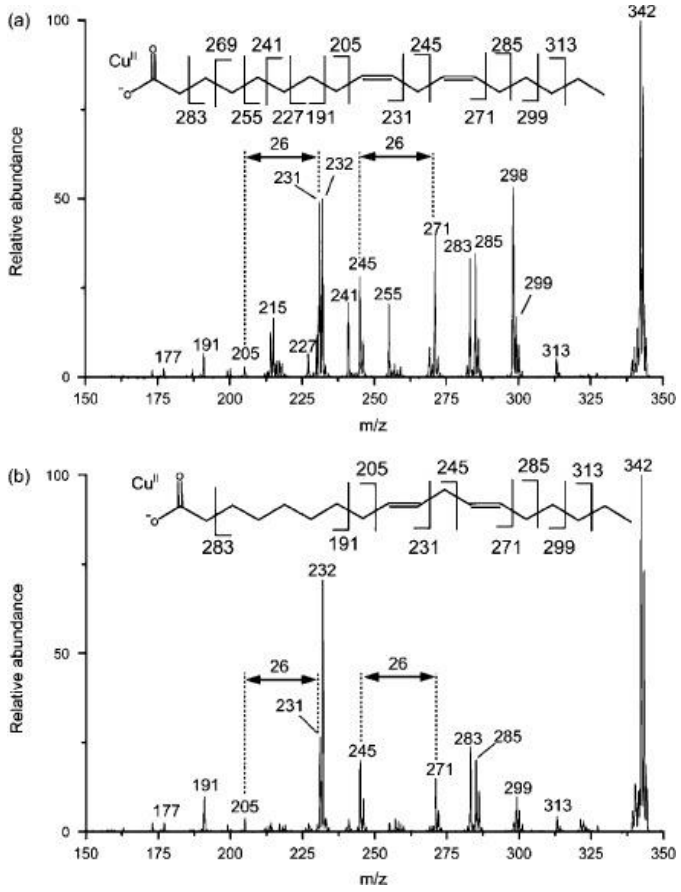

Figure 1.8 Low-energy CID spectra of $[FA - H + Cu^{II}]^+$ ions for (a) 18:2(9*Z*,12*Z*) and (b) 18:2(9*E*, 12*E*). Reproduced with permission from Reference 83.

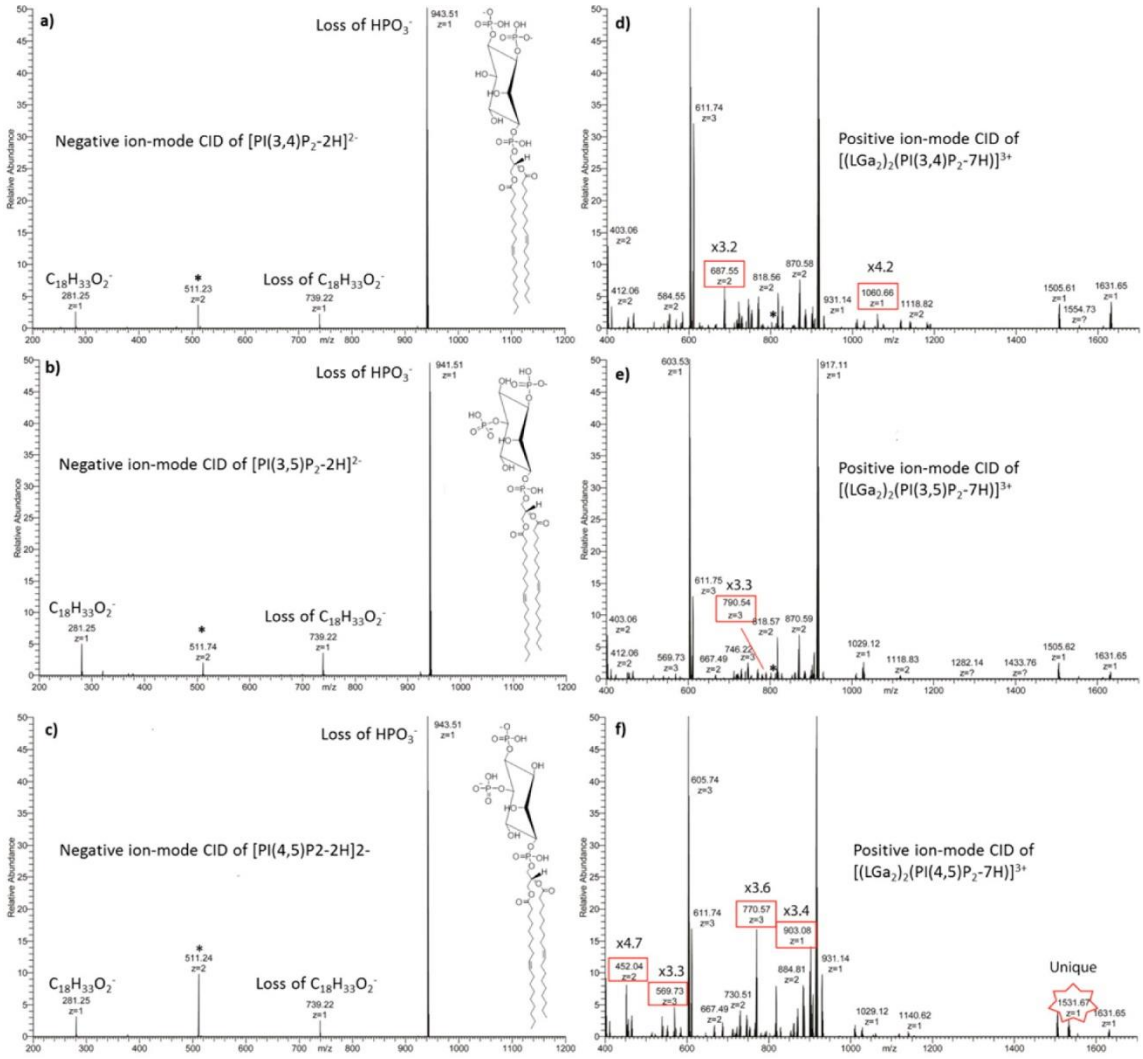

Figure 1.9 Negative ion mode CID spectra of (a) $[PI(3,4)P_2 - 2H]^{2-}$ (*m/z* 510.2360), (b) $[PI(3,5)P_2 - 2H]^{2-}$ (*m/z* 510.2360), and (c) $[PI(4,5)P_2 - 2H]^{2-}$ (*m/z* 510.2360). Positive ion mode CID spectra of charge-inverted (d) $[(LGa_2)_2(PI(3,4)P_2 - 7H)]^{3+}$ (*m/z* 811.2594), (e) $[(LGa_2)_2(PI(3,5)P_2 - 7H)]^{3+}$ (*m/z* 811.2594), and (f) $[(LGa_2)_2(PI(4,5)P_2 - 7H)]^{3+}$ (*m/z* 811.2594). The product ions that display at least a 3-fold increase abundance relative to corresponding identical ions in the CID spectra of the other two isomers are indicated with a red box. Reprinted with permission from Reference 85.

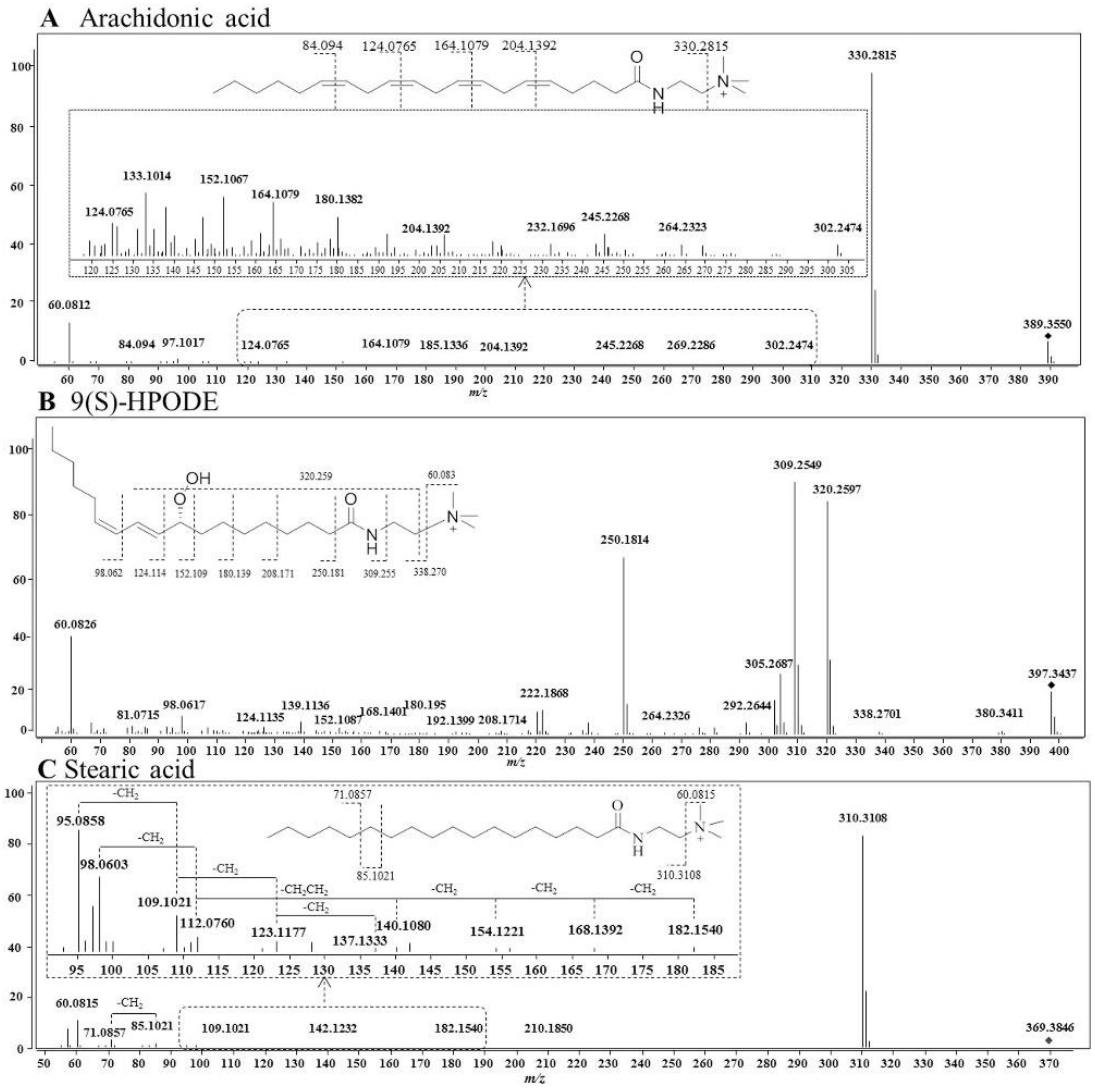

Figure 1.10 Positive ion mode CID spectra for (a) arachidonic acid (*i.e.*, FA 20:4(5*Z*,8*Z*,11*Z*,14*Z*), (b) 9(*S*)- Hydroperoxyoctadecadienoic acid (HPODE), and (c) stearic acid (*i.e.*, FA 18:0) derivatized with cholamine. Reprinted with permission from Reference 98.

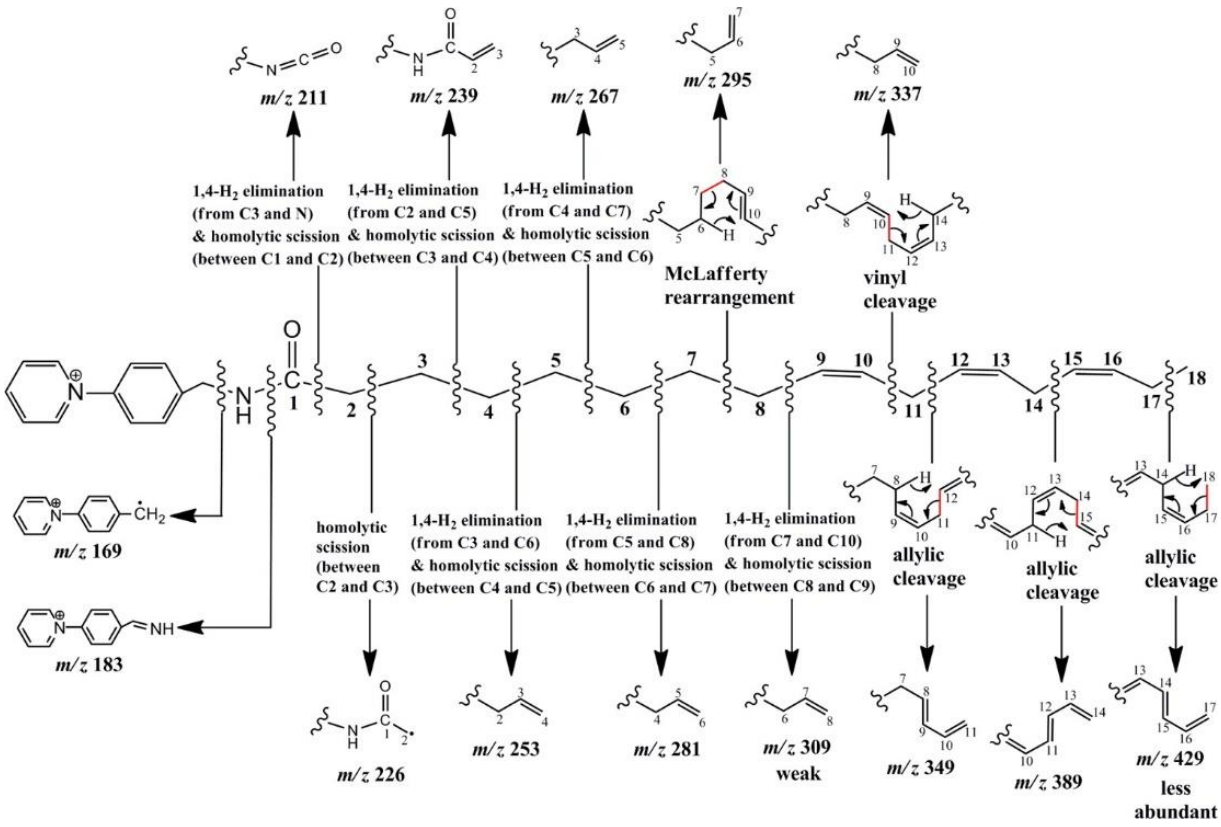

Scheme 1.1 Proposed fragmentation channels for unsaturated FA-AMPP cations. The fragmentation pathway for AMPP-derivatized 18:3(9,12,15) is presented. Note that carbon-carbon bonds highlighted in red indicate the site of cleavage. Reprinted with permission from Reference 100.

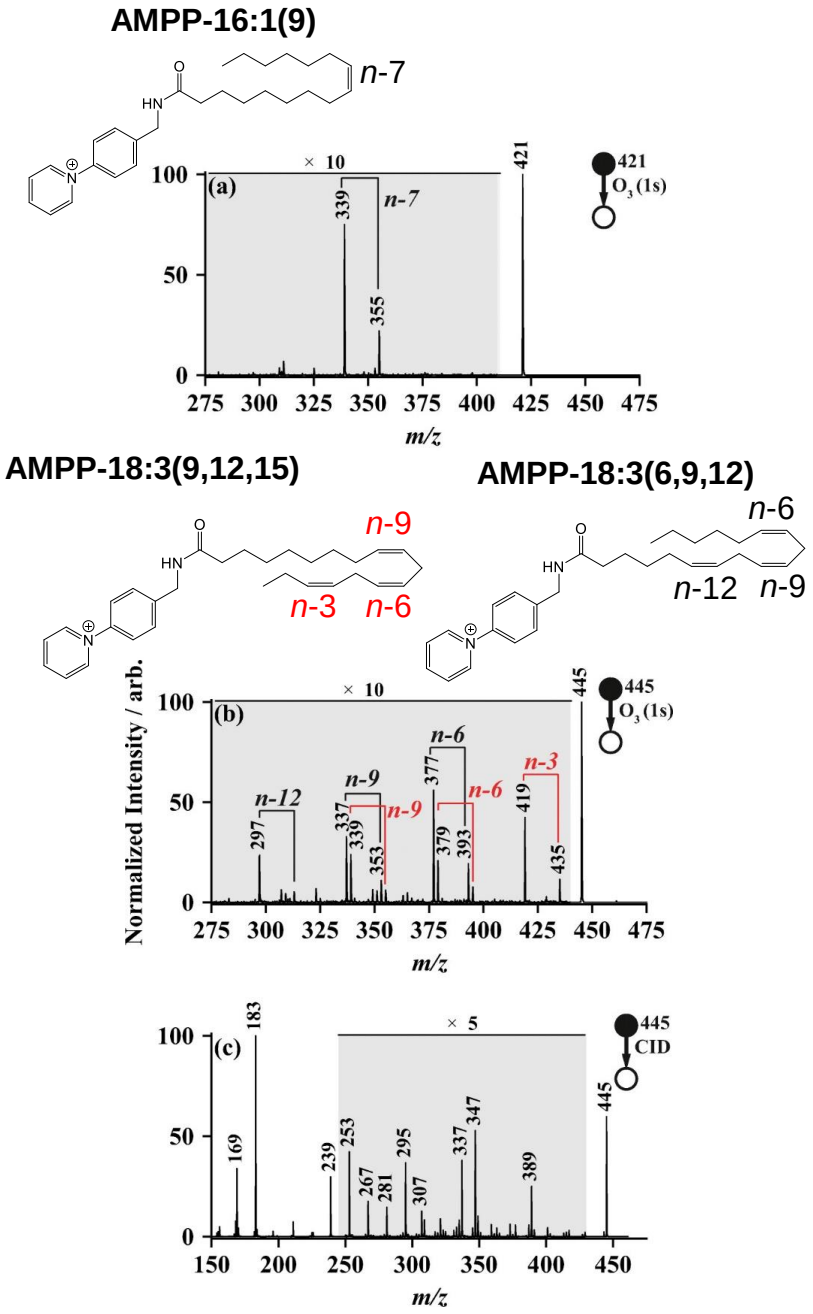

Figure 1.11 Analysis of a commercially available FAME mixture using OzID in combination with charge-switch derivatization. OzID spectra of (a) AMPP-FA 16:1 (*m/z* 421) and (b) AMPP-FA 18:3 (*m/z* 445). Diagnostic product ions highlighted in (a) reveal the presence of FA 16:0(*n*-7). The red lines indicate peaks diagnostic for polyunsaturated FA 18:3(*n*-3, *n*-6, *n*-9), and black lines indicate peaks characteristic of FA 18:3(*n*-6, *n*-9, *n*-12) in (b). (c) CID product ion spectrum of AMPP-FA 18:3 (*m/z* 445). Adapted with permission from Reference 113.

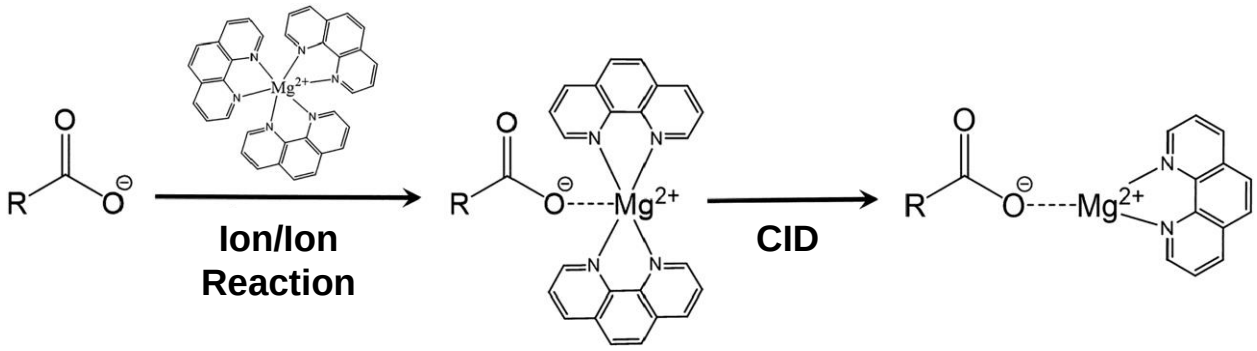

Scheme 1.2 Gas-Phase Charge Inversion Ion/Ion Reaction between $[FA - H]^-$ and $[MgPhen_3]^{2+}$ for the Generation of the $[FA - H + MgPhen]^+$ Ion. Adapted with permission from Reference 125.

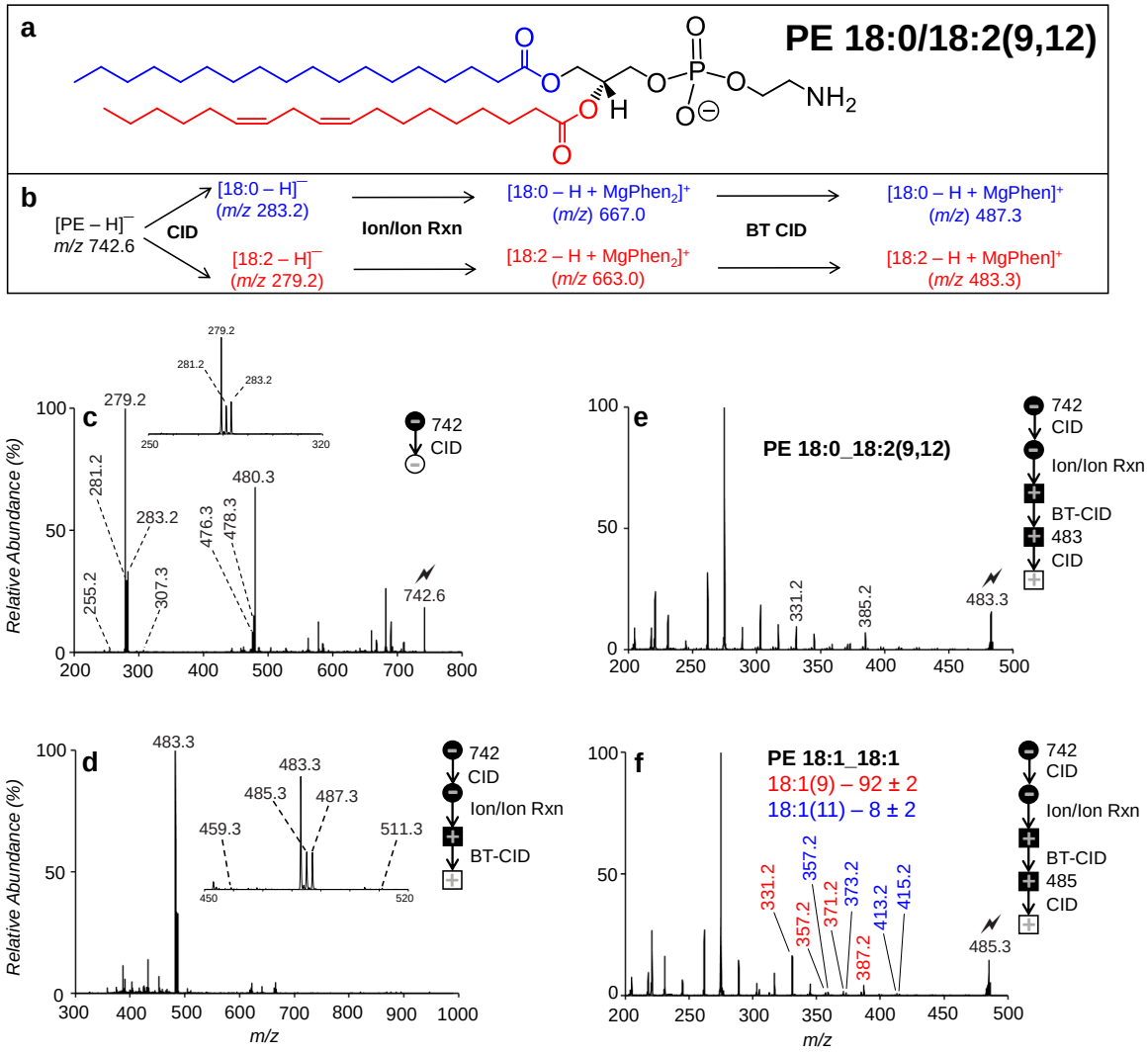

Figure 1.12 Demonstration of gas-phase charge inversion ion/ion chemistry for the analysis of PE 36:2 in human plasma extract. (a) Structure of ionized PE 18:0/18:2(9,12). (b) Reaction scheme detailing identification procedure for the PE 18:0/18:2(9,12) anion. (c) Ion-trap CID spectrum resulting from activation of $[PE\ 36:2 - H]^-$. (d) Product ion spectrum following ion/ion reaction of fragment ions generated via activation of $[PE\ 36:2 - H]^-$ and $[MgPhen_3]^{2+}$ dications and subsequent beam-type CID. (e) CID spectrum of $[18:2 - H + MgPhen]^+$. (f) CID spectrum of $[18:1 - H + MgPhen]^+$. Adapted with permission from Reference 126.

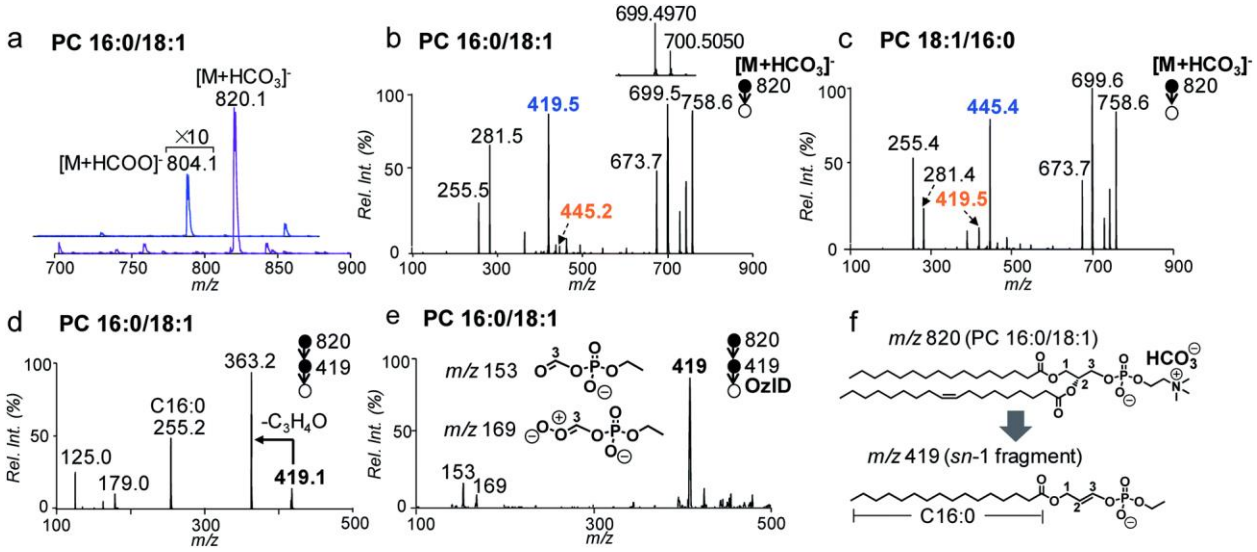

Figure 1.13(a) Negative ion mode mass spectra of PC 16:0/18:1 from solutions containing 5 mM ammonium bicarbonate (NH_4HCO_3) and ammonium formate (NH_4COOH). (b) CID spectra (CE = 30 eV) of $[M + HCO_3]^-$ of PC 16:0/18:1 (*m/z* 820) and (c) $[M + HCO_3]^-$ of PC 18:1/16:0 (*m/z* 820). MS^3 product ion spectra obtained via (d) CID and (e) OzID of the product ions at *m/z* 419 from (b). The proposed structure of the product ion observed at *m/z* 419 derived from CID of $[M + HCO_3]^-$ of PC 16:0/18:1 is given in (f). Reprinted with permission from Reference 131.

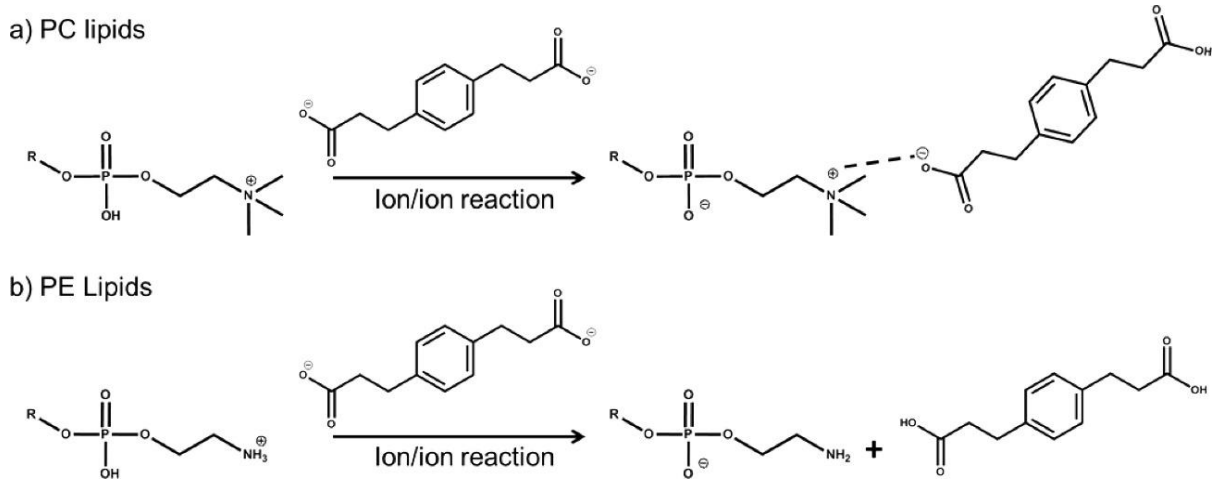

Scheme 1.3 Charge inversion ion/ion reactions of (a) $[PC + H]^+$ and (b) [PE + H]+ cations with doubly deprotonated PDPA reagent dianions. Reprinted with permission from Reference 135.

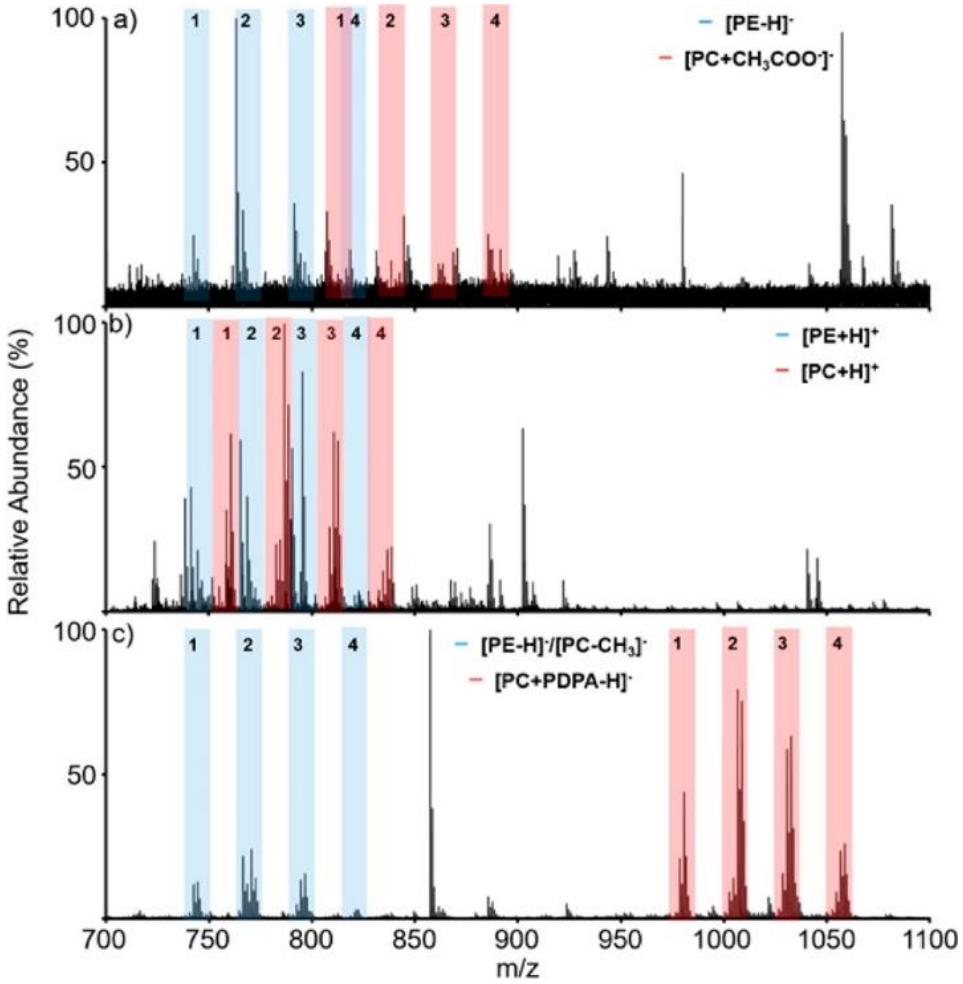

Figure 1.14 Mass spectra of a bovine liver extract (0.5 μM total lipid concentration) obtained via (a) direct negative nano-ESI, (b) direct positive nano-ESI, and (c) charge inversion of the lipid cations shown in (b) with $[PDPA - 2H]^{2-}$ reagent dianions. Reprinted with permission from Reference 135.

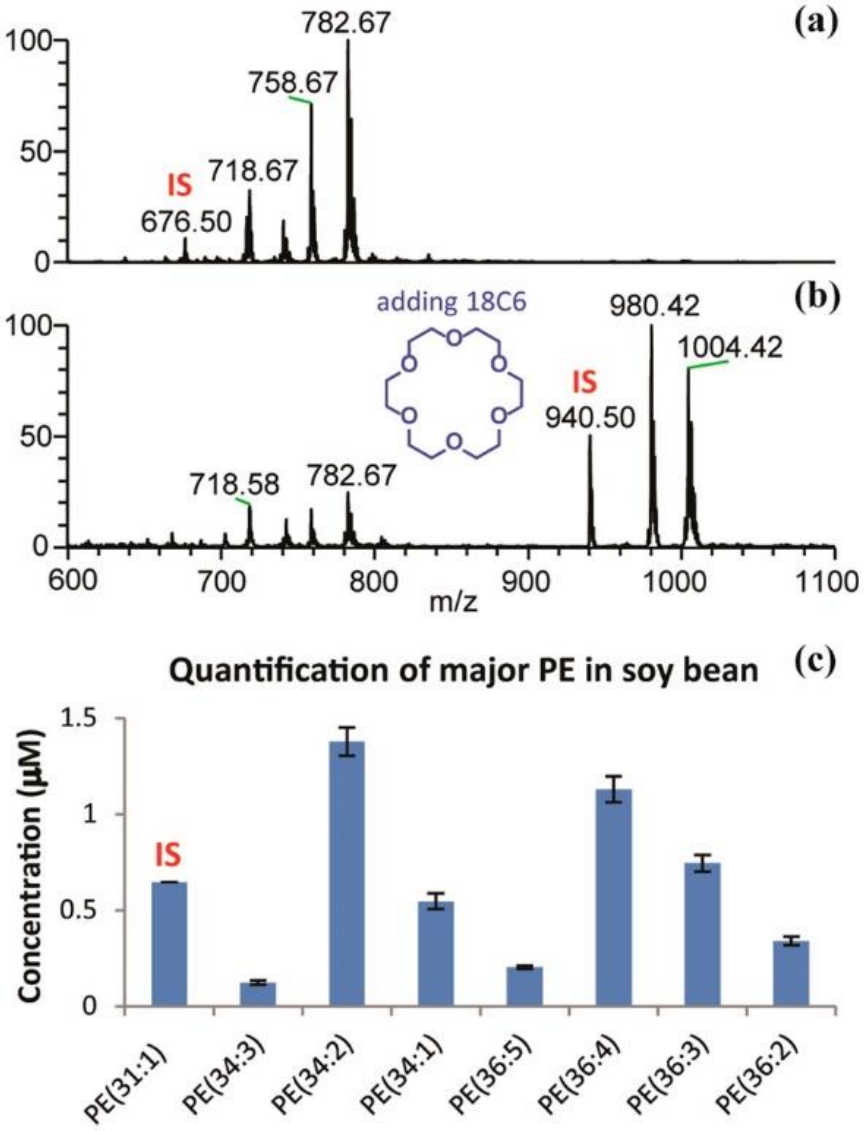

Figure 1.15 Positive ion ESI-MS spectra of soybean asolectin solutions containing PE 31:1 as an internal standard (IS) within known concentration in methanol (a) without and (b) with the addition of 18C6. (c) The concentrations (μM) of major PEs found in soy asolectin (including isotopic corrections). Reprinted with permission from Reference 150.

CHAPTER 2. GAS-PHASE ION/ION REACTIONS INVOLVING TRIS-PHENANTHROLINE ALKALINE EARTH METAL COMPLEXES AS CHARGE INVERSION REAGENTS FOR THE IDENTIFICATION OF FATTY ACIDS

2.1 Introduction

The fatty acid (FA) is the most fundamental lipid class and assumes vital biological roles in cellular structure, function, and metabolism.[1–3] FAs are widespread throughout nature and can appear as free circulating molecules or esterified within complex lipids such as triacyglycerols or phospholipids. While general FA composition includes an aliphatic chain and at least one carboxyl group, FAs exhibit extensive structural diversity through variations in the aliphatic chain length and variations in location, number, and geometry of double bonds. Like many biomolecules, FA structure dictates both physical properties (e.g., solubility, fluidity, thermodynamic stability) and biological function including FA metabolism. Furthermore, modification to FA composition and structure has been associated with adverse health effects, including the development and progression of chronic disease such as cardiovascular disease, diabetes, obesity, and cancer.[2–5] Specifically, variations in the ratio of essential *n*-3 and *n*-6 FAs have been linked with disease progression.[6] Similarly, the structure of FA and consequent composition of lipid extracts are critical in the optimization of desired physical and chemical properties for applications in a range of biocommodities (e.g., biodiesel).[7,8] Thus, the ability to probe FA structure is integral to the advancement of biomedical science and biotechnology, and in turn, efforts to characterize FAs have emerged as a principal focus in lipidomics.

Mass spectrometry (MS) has been deployed extensively to characterize FA. While traditional gas chromatography (GC)/MS of fatty acid methyl esters is still the most widely used strategy for this analysis, the resulting electron ionization mass spectra cannot distinguish closely related FA structures, especially lipid isomers.[9] In pursuit of detailed structure elucidation of FA, Gross and colleagues first described charge remote fragmentation (CRF).[10] In this approach, FAs were ionized and subjected to high energy (keV) collisions resulting in unimolecular 1,4-hydrogen eliminations to produce terminally unsaturated and structurally diagnostic carboxylate product ions.[11,12] Importantly, interruptions to the regular sequence of product ions could be used to identify site(s) of unsaturation or other important structural features of a FA.[13–17] Primary

requirements of CRF were found to be a localized charge site, which could be derived from FA cationization with a charge switching reagent (positive ion mode) or deprotonation of the carboxylic acid group (negative ion mode), and access to high collision energies. As multisector instruments operating in the keV regime became less prevalent, access to CRF became less common, with some recent reprise on tandem time-of-flight (TOF-TOF) instruments where dilithiated FA cations, $[M - H + 2Li]^+$, provided double bond position for a series of isomeric FAs.[18]

The preponderance of modern lipid analysis is undertaken using contemporary electrospray ionization-MS in conjunction with low energy collision-induced dissociation (CID). For such instruments, highly sensitive detection of FA can be achieved in negative ion mode; however, CID of the resulting $[M - H]^-$ anions provides relatively little structural information with spectra dominated by water and carbon dioxide neutral loss product ions and minimal structurally informative fragments observed.[12] Notably, however, Yang et al. report a method exploiting these small molecule losses (i.e., H_2O and CO_2 losses) following CID of FA $[M - H]^-$ anions in the negative ion mode to identify and quantify unsaturated FA isomers.[19] Overall, in order to surmount this limitation regarding FA characterization in the negative ion mode, two different derivatization strategies have been employed that can be considered in two classes. The first class targets derivatization of the functional groups within the FA chain (e.g., carbon−carbon double bonds) while the second group modifies the common carboxylic acid moiety itself. Examples of the first class include reactions between unsaturated lipids and ozone[20−25] or carbonyl reagents via the Paternò-Büchi reaction.[26,27] These methods are now achieving widespread adoption but do not provide insight into other structural features of FA (e.g., chain branching, cyclization, hydroxylation, etc.).

Efforts to modify the carboxylic acid functional group prior to ionization have been focused on promoting CRF at low collision energies and thereby generating rich structural details of FA. For example, Wang et al.[28] showed that solution-based covalent derivatization of FAs via amidation of the carboxylic moiety by the amine moiety on a N-(4-aminomethylphenyl) pyridinium (AMPP) yielded an AMPP-derivatized FA. The derivatized FA can readily be ionized in the positive ion-mode. Subsequent activation of the FA-AMPP precursor provided identification and quantification of FA double bond positional isomers utilizing CRF-like spectral patterns.[28,29] While powerful, these strategies rely on wet chemical derivatization prior to analysis. In contrast,

other investigators have doped salts into the ESI solution to obtain metalated FA cations. For example, Hsu and Turk showed that low-energy CID of dilithiated FA cations, $[M - H + 2Li]^+$, allowed for differentiation among unsaturated FA isomers in addition to double bond position identification as carbon−carbon single bond cleavage (C−C) proximal (i.e., on the carboxyl end of the aliphatic chain) and vinylic to the last double bond in the aliphatic chain produced the heaviest fragment ion (highest m/z).[30,31] Low-energy activation of copper(II) adducted FAs, $[M - H + Cu^{II}]^+$, allowed for the localization of one or two homoconjugated double bonds. In addition, CID spectra of $[M - H + Cu^{II}]^+$ provided a distinction between cis and trans FA isomers via exploitation of product ions related to the neutral loss of CO_2.[32] Divalent alkaline earth metals have received considerable recent attention as a means to ionize FA and drive diagnostic fragmentation of the resulting adduct ions.[33,34] The body of work to-date therefore suggests an advantageous approach to FA analysis would exploit the inherent propensity to ionize these analytes as $[M - H]^-$ anions and simultaneously harness the propensity of the corresponding metalated cation, $[M - H + Cat]^+$, to undergo CRF.

In this work, we demonstrate the gas-phase charge inversion of singly deprotonated fatty acid ions of the form $[M - H]^-$ with doubly charged tris-phenanthroline alkaline earth metal complexes, $[Cat(Phen)_3]^{2+}$ (Cat = Mg^{2+}, Ca^{2+}, Sr^{2+}, or Ba^{2+}). By conducting FA derivatization in the gas phase, each reagent solution can be individually optimized with regards to solution and electrospray conditions. Additionally, gas-phase ion/ion reactions allow for enhanced control of reaction outcomes when compared to analogous transformations conducted in solution.[35] Mutual storage ion/ion reaction resulted in alkaline earth metal cationization of the FA. As these complexes are inherently stable, the alkaline earth metal will not readily desorb from the carboxyl moiety upon CID providing CRF and detailed FA structural characterization.[17] To prove the utility of the method, hydrolyzed corn oil was examined. The fatty acid profile of corn oil has been linked with biodiesel quality and has been recognized as an indicator of corn oil purity.[7,36] The FA profile of corn oil can vary according to environmental and genetic factors, but the typical major FA constituents of corn oil include 16:0, 18:0, 18:1, 18:2, and 18:3, while minor FA components, reported at trace levels, include 14:0, 17:0, 20:0, 20:1, and 16:1.[8]

2.2 Experimental

2.2.1 Reagents

Chloroform, HPLC-grade methanol, and HPLC-grade water were purchased from Fisher Scientific (Pittsburgh, PA). All FA standards were purchased from Cayman Chemical (Ann Arbor, MI). United States Pharmacopeia (USP) reference standard corn oil, magnesium chloride, strontium acetate, calcium acetate, barium acetate, and 1,10-phenanthroline (Phen) were purchased from Sigma-Aldrich (St. Louis, MO). FA standards were prepared in methanol to a final concentration of 0.1 mg/mL (m/v). Tris-phenanthroline alkaline earth metal complexes were prepared by mixing the 1:1 (mol/mol) metal salt/Phen in methanol to final concentration of 0.1 mg/mL (m/v).[37,38]

2.2.2 Corn Oil Hydrolysis

As corn oil consists primarily of triacylglycerols, FAs were released via a TAG hydrolysis method as previously described.[13] Briefly, 200 mg of corn oil was hydrolyzed at 60 °C for 1 h with 800 μL of 98:2 (v/v) methanol/aqueous sodium hydroxide (1 M). FAs were then extracted using 2:1 (v/v) chloroform/methanol.

2.2.3 Nomenclature

We adopt the nomenclature for lipids recommended by the International Union of Pure and Applied Chemistry (IUPAC).[39] By convention, the first carbon (C1) in the aliphatic chain is the carboxyl carbon. The shorthand notation used denotes the number of carbon atoms followed by the number of carbon−carbon double bonds, designated after the colon, and definitive double bond position(s) indicated inside parentheses. For example, the shorthand notation 18:2 (9,12) represents an 18-carbon chain FA with 2 double bonds at the positions C9=C10 and C12=C13. Where known, the stereochemistry of carbon−carbon double bonds is assigned as *Z* (cis) and *E* (trans) (e.g., oleic acid is 18:1(9*Z*)), yet where unknown, only the position of unsaturation is indicated (e.g., 18:1(9)).40 The *n*−*x* classification system is also used where a FA is classified according the location of the first double bond located at the x^{th} carbon− carbon position from the methyl end of the aliphatic chain. For example, 18:3 *n*-3 has a double bond located at C15=C16.

2.2.4 Mass Spectrometry

All experiments were performed on a Sciex QTRAP 4000 hybrid triple quadrupole/linear ion trap mass spectrometer (SCIEX, Concord, ON, Canada) that has been modified to perform ion/ion reactions.[41] Alternately, pulsed nanoelectrospray ionization (nESI) allows for sequential injection of tris-phenanthroline alkaline earth metal complex dications, $[Cat(Phen)_3]2^+$ (Cat = Mg^{2+}, Ca^{2+}, Sr^{2+}, or Ba^{2+}), followed by singly deprotonated FA ions.[42] The 1:1 (mol/mol) metal salt/Phen solution was sprayed first, followed by isolation of $[Cat(Phen)_3]^{2+}$. $[Cat(Phen)3]2^+$ was then transferred to a high-pressure collision cell, q2, for storage. The FA was then ionized to an $[M - H]^-$ anion in the negative ion mode, isolated in Q1 in transient, and then transferred to q2. The FA anion and $[Cat(Phen)_3]^{2+}$ were mutually stored in q2 for 300 ms. The mutual storage product ions were then subjected to 18−21 V of dipolar direct current (DDC)−CID in q2 for 25 ms.[43] DDC−CID product ions were transferred to the low-pressure linear ion trap (LIT), Q3, for monoisotopic mass selection of $[M - H + Cat]^+$, which was then back-transferred to q2 following isolation. In q2, $[M - H + Cat]^+$ was collisionally activated for 50 ms at 200 mV via single frequency resonance excitation (q = 0.383 for unsaturated FAs, q = 0.317 for saturated FAs). Product ions generated from CID were transferred to Q3 and analyzed via mass-selective axial ejection.[44]

2.3 Results and Discussion

2.3.1 Gas-Phase Reaction of FA Anion with $[Cat(Phen)_3]^{2+}$

Gas-phase ion/ion reactions of FA $[M - H]^-$ anion with $[Cat(Phen)_3]^{2+}$ can charge invert FA anions to the positive ion mode. To do this experiment, $[Cat(Phen)_3]^{2+}$ (Cat = Mg^{2+}, Ca^{2+}, Sr^{2+}, or Ba^{2+}) was first ionized in the positive ion mode, isolated in Q1, stored in q2 followed by the ionization of the FA in the negative ion mode, which can also be isolated in Q1, and then transferred to q2. After 300 ms of mutual storage in q2, the singly deprotonated FA undergoes charge inversion generating a long-lived electrostatic complex, $[M - H + Cat(Phen)_2]^+$, produced via the replacement of a phenanthroline ligand with the FA anion. Scheme 2.1 shows the neutral loss of a phenanthroline ligand that occurs during the ion/ion reaction. All tris-phenanthroline alkaline earth metal complexes investigated herein produced the complex of interest. The charge inversion efficiency for the FA anion appears to be nearly unit efficient. The efficiency would be

less than unit efficient if FA anion neutralization were to take place through a proton-transfer reaction with the tris-phenanthroline alkaline earth metal complex, generating a singly charged, proton deficient $Cat(Phen)_3$ at *m/z* 563. As there is no *m/z* 563 peak in the ion/ion mass spectrum (Figure 2.1), it can be concluded that single proton transfer does not occur to a significant extent.

Scheme 2.1 also outlines results of q2 DDC−CID of the $[M - H + Cat(Phen)_2]^+$ complex. Fragmentation of the complex cation results in the loss of two phenanthroline ligands and generation of a metalated FA complex, $[M - H + Cat]^+$. However, DDC−CID of the $[M - H + Mg(Phen)_2]^+$ complex resulted in the neutral loss of only one phenanthroline ligand, giving rise to $[M - H + MgPhen]^+$.

2.3.2 Gas-Phase Fragmentation of Charge Inverted Saturated Fatty Acids

Saturated FA anions can undergo charge inversion when subjected to mutual storage with $[CatPhen_3]^{2+}$. The resulting reaction spectrum yields the $[M - H + Cat(Phen)_2]^+$ complex, which upon DDC−CID fragments to form the $[M - H + Cat]^+$ complex as described above. Collisional activation of metalated saturated FAs of the form $[M - H + Cat]^+$ (Cat = $MgPhen^{2+}$, Ca^{2+}, Sr^{2+}, or Ba^{2+}) generates a series of CRF ions, evenly spaced 14 Da apart, corresponding to carbon−carbon (C−C) single bond cleavages along the aliphatic chain. Figure 2.2 shows ion-trap CID of $[M - H + MgPhen]^+$ derived from gas-phase reaction of deprotonated octadecanoic acid (18:0) and $[Mg(Phen)_3]^{2+}$. The CID spectrum is dominated by a peak at m/z 221, signifying $[MgPhenOH]^+$. $[MgPhenO_2]^+$ at *m/z* 236 is one of two even mass product ions observed, representing the second most abundant product ion. Herein, we did not further investigate the mechanism underlying generation of the curious product ion $[MgPhenO_2]^+$, as this product ion does not provide information relevant to FA identification. The product ion $b^{+\bullet}$ (*m/z* 262), generated via homolytic C2−C3 cleavage, produces the only even mass, odd electron product ion derived from the aliphatic chain. Even electron, odd mass CRF ions, denoted with the prime notation (′), begin with C3−C4 fragmentation (c′ peak at *m/z* 289) and continue down the aliphatic chain. Relevant *m/z* values are tabulated in Table 2.1.

CID of $[M - H + Cat]^+$, resulting from the ion/ion reaction between deprotonated 18:0 and $[Cat(Phen)_3]^{2+}$ (Cat = Ca^{2+}, Sr^{2+}, or Ba^{2+}), generates CRF ions that readily adduct multiple water molecules.[45] Varying the q2 storage time of CRF ions resulted in a direct correlation between storage time and water adduction; i.e., longer storage times (up to 5000 ms) resulted in multiple

water adduction. In addition, DDC−CID of the trapped ions results in sequential removal of adducted water. In general, water adductions led to highly congested CID spectra when Cat = Ca^{2+}, Sr^{2+}, or Ba^{2+}. However, as the size of the metal cation increases (i.e., going down the alkaline earth metal group), the relative abundance of the hydrated CRF product ion series decreases. Thus, an inverse relationship between metal cation size and water adduction of the metal cationized FA and CRF ions is observed. This trend is highlighted by the decrease in relative abundance of the doubly hydrated CRF ion series displayed in Figure 2.3a-c as metal cation size increased sequentially, Ca^{2+}< Sr^{2+} < Ba^{2+}. The observed trend can be rationalized as an increased charge-to-size ratio of the metal cation would promote enhanced ion−dipole interactions between the metal cation and water molecules, and therefore, as the charge-to-size ratio decreases (i.e., cation size increases), the prominence of the hydrated CRF ion series decreases. Overall, the reagent cations Ca^{2+}, Sr^{2+}, and Ba^{2+} led to highly congested CID spectra complicated with water adductions. Conversely, CID spectra generated with the reagent cation $MgPhen^{2+}$ were straightforward, not displaying the series of water-adducted CRF ions. Thus, the reagent cation $MgPhen^{2+}$ proved to be the most useful charge inversion reagent as CID of saturated FA $[M - H + MgPhen]^+$ ions produced the most straightforward results.

2.3.3 Characterization of Monounsaturated Fatty Acids

Monounsaturated FAs ionized in the negative ion mode undergo gas-phase charge inversion via ion/ion reaction with $[Cat(Phen)_3]^+$ to produce the complex of interest, $[M - H + Cat]^+$. The presence of a repeatable spectral pattern influenced by double bond position revealed double bond location in monounsaturated fatty acids. Double bond localization for a series of monounsaturated octadecenoic acids is demonstrated in Figure 2.4 using the spectral pattern highlighted with the blue curve.

Figure 2.4a summarizes CID of $[M - H + MgPhen]^+$ where M = 18:1(11*Z*). The spectrum shows CRF ions of the same *m/z* as those observed with CID of charge-inverted 18:0 (see Figure 2.2) until fragmentation reaches the double bond position. The C5−C6 cleavage generates a doublet, not observed with the analysis of 18:0, composed of a CRF ion (e′ peak at *m/z* 303) and a terminally saturated product ion (e peak at *m/z* 305). Formation of the saturated product ion is suggested to occur through C5−C6 fragmentation and cyclization, forming a stable six-membered ring containing the carboxyl oxygen.[46]

To localize the double bond in Figure 2.4a, the presence of a spectral gap highlighted with the blue curve shown is used. Upon activation of the $[M - H + MgPhen]^+$ (M = 18:1(11*Z*)) complex, allylic C−C bond cleavages, both proximal (i.e., on the carboxyl side) and distal (i.e., on the methyl side) to the double bond, generated high abundance product ions flanking the spectral gap. Proximal allylic cleavage, C9−C10 cleavage, produced the CRF ion i′ (*m/z* 359), and distal allylic cleavage, C13−C14 cleavage, produced the doublet m′ (*m/z* 413) and m (*m/z* 415). In general, C−C cleavage proximal and allylic to the double bond generates a characteristic terminally unsaturated CRF ion, whereas distal allylic C−C cleavage generates a high intensity doublet composed of a CRF ion and a terminally saturated product ion. The observed spectral gap is the result of a dramatic suppression in product ion abundance related to product ions representing the C=C double bond and C−C cleavages vinylic to the double bond. Vinylic C−C bond cleavage, both proximal and distal to the double bond, produced two CRF ions observed at very low relative abundances. The C10−C11 cleavage (peak j′ at *m/z* 373) and the C12−C13 cleavage (peak l′ at m/z 399) represent vinylic cleavage proximal and distal to the C11=C12 double bond, respectively. Disruption of the 14 Da spacing is observed as an exceedingly small product ion representing the C11=C12 double bond (*m/z* 385) being spaced 12 Da from the CRF ion j′. Ultimately, perturbation of the 14 Da spacing further confirms double bond localization.

Ion-trap CID of $[M - H + Cat]^+$ (Cat = $MgPhen^{2+}$, Ca^{2+}, Sr^{2+}, or Ba^{2+}), demonstrated with 11*Z*-octadecenoic acid (18:1(11*Z*)) in Figure 2.5, provided double bond localization utilizing the spectral pattern described above. However, given the relative simplicity of utilizing $MgPhen^{2+}$ as the reagent due to a lack of hydrated CRF ions, data presented hereafter exclusively employed $MgPhen^{2+}$.

Distinction among FA double bond positional isomers is facilitated by direct spectral comparison. Double bond localization for a double bond positional isomer of 18:1(11*Z*) is first demonstrated with the analysis of 18:1(9*Z*). CID of the $[M - H + MgPhen]^+$ complex (M = 18:1(9*Z*)) is shown in Figure 2.4b. Though not entirely understood, analysis of this isomer via CID of the $[M - H + MgPhen]^+$ complex shows a dramatic decrease in the abundance of the $b^{+\bullet}$ (*m/z* 275) product ion relative to the CRF ion c′ (*m/z* 289). To localize the double bond for this isomer, the CID spectrum again displays a spectral gap flanked by allylic C−C cleavages. Allylic cleavage proximal to the double bond, C7−C8 cleavage, produced the CRF ion g′ at *m/z* 331. The characteristic doublet (k peak at *m/z* 387 and k′ peak at *m/z* 385) is produced via C11−C12 allylic

cleavage distal to the double bond. Vinylic cleavages are once more observed at lower relative abundances compared to allylic cleavages as shown with the CRF ions h′ (*m/z* 345) and j′ (*m/z* 371). Perturbation of the 14 Da spacing was also observed, as the *m/z* differential between h′ and the product ion representing the C9=C10 double bond is 12 Da.

Similarly, the gas-phase charge inversion of singly deprotonated 18:1(6Z) with $[Mg(Phen)_3]^{2+}$ generates the $[M - H + MgPhen]^+$ complex at *m/z* 485. CID of the $[M - H + MgPhen]^+$ complex where M = 18:1(6*Z*) provided double bond localization and distinction from the previous octadecenoic acid isomers investigated. When the double bond is located prior to C7, as in the case of 18:1(6*Z*), the double bond location can still be determined, but double bond localization relies solely on the spectral gap (Figure 2.4c). An unexpected doubly unsaturated product ion (peak e″ at *m/z* 301), denoted with the double prime notation (″), most likely originated from hydride migration and subsequent C5−C6 fragmentation, generating a terminally conjugated diene product ion; the presence of this product ion however did not hinder double bond localization, as the spectral gap was still maintained, albeit not as dramatically as with the other octadecenoic isomers shown above. The spectral gap (blue curve) is bordered by allylic cleavage product ions, g′ (*m/z* 289), h (*m/z* 343), and h′ (*m/z* 345). Once again, vinylic cleavages (peaks e″ and g′) are dramatically suppressed. The product ion corresponding to the C6=C7 double bond does not perturb the 14 Da spacing, but as this product ion is the least abundant CRF ion in the spectral gap, double bond localization is still obtained. Thus, exploitation of a spectral gap influenced by double bond position allowed for rapid, facile localization of the double bond for monounsaturated fatty acids and distinction between double bond positional FA isomers.

2.3.4 Characterization of Polyunsaturated Fatty Acids

The study of polyunsaturated fatty acids (PUFAs) was twofold, including an in-depth investigation of diunsaturated FAs and FAs with more than two degrees of unsaturation. Collisional activation of $[M - H + MgPhen]^+$ for diunsaturated FAs provided double bond localization again through repeatable spectral patterns indicative of double bond structure (e.g., homoconjugated, conjugated), similar to those described above.

Singly deprotonated 9*Z*,12*Z*-octadecadienoic acid (18:2-(9*Z*,12*Z*)), an *n*-6 essential fatty acid, reacted in the gas phase with $[Mg(Phen)_3]^{2+}$ producing the complex of interest, $[M - H + MgPhen]^+$ at *m/z* 483. Ion-trap CID of $[M - H + MgPhen]^+$ (M = 18:2(9*Z*,12*Z*)), shown in Figure

2.6a, provided bond localization through utilization of a repeatable spectral pattern. Observed *m/z* values for Figure 2.6 are tabulated in Table 2.2. For the first double bond location in 18:2(9*Z*,12*Z*), a spectral gap (blue curve) like that described for monounsaturated FA analysis is observed. Allylic cleavages proximal and distal to the first double bond generated product ions g′ (*m/z* 331) and k′ (*m/z* 385), respectively, flanking the spectral gap. Cleavage vinylic to the first double bond, represented by C8−C9 (peak h′ at *m/z* 345) and C10−C11 (peak j at *m/z* 373 and peak j′ at *m/z* 371) fragmentation, is suppressed, as is the product ion representing the C9=C10 double bond (*m/z* 359). While perturbation of the 14 Da spacing is not observed, the C9=C10 double bond can still be localized through exploitation of the spectral gap pattern.

To localize the second double bond in a homoconjugated diunsaturated FA, a secondary pattern is used. Once more, this is demonstrated with 18:2(9*Z*,12*Z*) analysis in Figure 2.6a and b. However, the pattern was also observed for numerous *n*-6 homoconjugated fatty acids analyzed via CID of the $[M - H + MgPhen]^+$ complex. The pattern indicative of homoconjugated double bonds consists of a series of doublets resulting from allylic and vinylic C−C cleavages distal to the double bond. Vinylic C−C cleavage distal to the double bond formed the doublet m′ (*m/z* 411) and m (*m/z* 413). Allylic C−C cleavage distal to the second double bond, represented by C14−C15 cleavage, produced a doublet of similar product ion intensity, n′ (*m/z* 425) and n (*m/z* 427). Fragmentation of the aliphatic chain after C15 is dramatically suppressed, as shown in Figure 2.6. Therefore, through the exploitation of a repeatable spectral pattern unique to homoconjugated, diunsaturated FAs, both double bond positions could be determined.

Examination of conjugated and homoconjugated diunsaturated FA structures resulted in distinct spectral differences upon CID of the $[M - H + MgPhen]^+$ complex. Direct spectral comparison of CID spectra of $[M - H + MgPhen]^+$ where M = 18:2(9*Z*,12*Z*) and M = 18:2(9*Z*,11*Z*), shown in Figure 2.6a,b respectively, resulted in marked spectral differences, predominantly regarding C11−C12 cleavage. For 18:2(9*Z*,12*Z*), C11−C12 cleavage represented a C−C single bond cleavage, producing the CRF ion k′ (*m/z* 385). However, for 18:2(9*Z*,11*Z*) (Figure 2.6b), C11−C12 cleavage represented C=C double bond cleavage. Therefore, a dramatic suppression in relative abundance of the C11=C12 product ion was expected and experimentally confirmed. Recognition of this suppressed product ion thus provides distinction among homoconjugated and conjugated double bond systems in diunsaturated fatty acids.

Biologically derived polyunsaturated FAs are commonly homoconjugated with conjugated systems also observed under certain conditions. However, some unusual FA structures have been reported where the double bonds are neither conjugated nor homoconjugated.[47] The gas-phase charge inversion of 8,14-eicosadienoic acid (20:2(8*Z*,14*Z*)) and subsequent analysis of the $[M - H + MgPhen]^+$ complex via CID provided double bond localization. Figure 2.7 shows the CID spectrum of the $[M - H + MgPhen]^+$ complex (M = 20:2(8*Z*,14*Z*)). Two spectral gaps are observed after CID of the $[M - H + MgPhen]^+$ complex (M = 20:2(8*Z*,14*Z*)). These spectral gaps were used to localize each double bond present in 20:2(8*Z*,14*Z*). For localization of the C8=C9 double bond, slight deviations from the monounsaturated FA spectral pattern were observed, specifically concerning C7−C8 cleavage. Typically, the peaks signifying C−C cleavages allylic to the double bond were more readily observed when compared to vinylic cleavage peaks. Yet, with the analysis of 20:2(8*Z*,14*Z*), C7−C8 cleavage resulted in a more abundant CRF ion g′ (*m/z* 331) compared to the C6−C7 allylic cleavage CRF ion f′ (*m/z* 317). However, this slight deviation in spectral pattern did not hinder localization of the first double bond. Ultimately, the dramatic reduction in peak intensity observed for the product ion representing the C8=C9 double bond (*m/z* 343) and the disruption of the 14 Da spacing provided double bond localization for the first double bond. As for localization of the C14=C15 double bond, the position of this double bond was determined again using the observed spectral gap. Flanking the second spectral gap in Figure 2.7 are product ions generated via cleavages allylic to the C14=C15 double bond, denoted by the doublet p *(m/z* 455) and p′ (*m/z* 453) and the CRF ion l′ (*m/z* 399). Cleavages vinylic to the second double bond are suppressed, as shown via CRF ions m′ (*m/z* 413) and o′ (*m/z* 439). Disruption of the 14 Da spacing is once again observed, confirming double bond localization, as the product ion representing the C14=C15 double bond (*m/z* 425) is spaced 12 Da from the CRF ion m′ (*m/z* 413). Thus, utilizing this secondary spectral gap and the disruption of the 14 Da spacing exhibited by CRF ions, the second double bond position can be localized.

As the degrees of unsaturation increase, overall fragmentation of the charge-inverted fatty acid $[M - H + MgPhen]^+$ complex increases as well. Thus, localization of the double bonds proved challenging. Nevertheless, distinction among FA isomers, specifically *n*-3 and *n*-6 double bond positional FA isomers, is readily achieved. This is demonstrated with the comparative analysis of octadecatrienoic acid (18:3) *n*-3 and *n*-6 isomers represented by 18:3(9*Z*,12*Z*,15*Z*) and 18:3-(6*Z*,9*Z*,12*Z*), respectively.

Ion-trap CID of $[M - H + MgPhen]^+$ where M = 18:3(9*Z*,12*Z*,15*Z*) resulted in clear spectral differences when compared to the CID spectrum of $[M - H + MgPhen]^+$ where M = 18:3(6Z,9Z,12Z), shown in Figure 2.8a and b, respectively. For both 18:3 isomers investigated, congested CID spectra suggest gas-phase double bond rearrangements, complicating double bond localization. While the localization of the double bonds is not readily visible with the CID spectrum, distinct tandem mass spectral differences allow for differentiation among the *n*-3 and *n*-6 18:3 isomers. CID spectral differences are predominately observed regarding fragmentation near the methyl end of the aliphatic chain, as highlighted in Figure 2.8 with the blue bar. Analysis of 18:3(9*Z*,12*Z*,15*Z*) via activation of the [M − H + MgPhen]+ complex (see Figure 2.8a) shows a doublet composed of two similarly intense peaks generated by C−C cleavage vinylic and distal to the C15=C16 double bond. The doublet, denoted by peaks n″ (*m/z* 423) and n′ (*m/z* 425), consists of a CRF ion and a CRF ion possessing an additional degree of unsaturation, suggested to form via hydride migrations and CRF. Likewise, the CID spectrum of [M − H + MgPhen]+ where M = 18:3(6*Z*,9*Z*,12*Z*) shows C11−C12 cleavage produces the doublet k″ (*m/z* 381) and k′ (*m/z* 383). Directly following the doublet, a single, intense CRF ion representing the final double bond is observed for both FA isomers, given by the peaks C15=C16 (*m/z* 437) and C12=C13 (*m/z* 395) for 18:3(9*Z*,12*Z*,15*Z*) and 18:3(6*Z*,9*Z*,12*Z*), respectively. The strong presence of this product ion reflecting the final double bond position suggests potential interaction and stabilization between the double bond and metal cation. CRF ion peaks, above the peaks representing the final double bond, are observed in decreasing relative abundance as fragmentation approaches the methyl end of the aliphatic chain. In total, despite difficulties localizing double bonds in the 18:3 isomers, clear spectral differences are observed in CID spectra obtained via activation of the described complex, providing distinction between the *n*-3 and *n*-6 isomers represented by 18:3(9*Z*,12*Z*,15*Z*) and 18:3(6*Z*,9*Z*,12*Z*).

Analysis of FAs with more than three degrees of unsaturation posed significant challenges for double bond localization. As the number of double bonds increases, fragmentation of the $[M - H + MgPhen]^+$ complex was more abundant, generating complex CID spectra. Despite complications experienced with highly unsaturated FA standards, this problem could be circumvented if an appropriate FA standard was readily available, as tandem mass spectra were highly reproducible using the proposed method. Construction of a spectral library with hopes of

applications utilizing spectral matching is under current investigation and represents the subject of future work.

2.3.5 Characterization of Fatty Acids in Corn Oil

To evaluate the utility of the method, hydrolyzed corn oil was examined. Negative ion mode analysis of hydrolyzed corn oil revealed the presence of the following FAs: 14:0, 15:0, 16:0, 17:0, 18:0, 16:1, 18:1, 18:2, and 18:3 (Figure 2.9) Subsequent negative ion mode analysis of a solvent blank subjected to the extraction procedure described above demonstrated the presence of FA contaminants in the hydrolyzed corn oil sample (Figure 2.9). The identified FA contaminants include: 12:0, 14:0, 15:0, 16:0, 18:0, 16:1, and 18:1. Comparison of the hydrolyzed corn oil and solvent blank nESI mass spectra shows the 18:1 FA is significantly more abundant in the hydrolyzed corn oil sample; thus, it can be reasonably concluded that the origin of the 18:1 FA can be attributed to both corn oil and sample contamination.

Application of the reported q2 mutual storage ion/ion reaction between mass selected hydrolyzed corn oil FA anions with $[Mg(Phen)_3]^{2+}$ generated the $[M - H + Mg(Phen)_2]^+$ complex. DDC−CID of the product ions resulted in the neutral loss of a phenanthroline ligand producing the $[M – H + MgPhen]^+$ complex. Ion-trap CID of the $[M - H + MgPhen]^+$ complex provided detailed FA characterization for the FAs in hydrolyzed corn oil.

Saturated FAs observed in hydrolyzed corn oil, though classified as contaminants due to their presence in the solvent blank, readily produced the $[M - H + MgPhen]^+$ complex upon mutual storage with $[Mg(Phen)_3]^{2+}$. CID of the resulting $[M - H + MgPhen]^+$ complex yielded similar CID spectra for all saturated FA with product ions equally spaced 14 Da apart. Numerous saturated FA contaminants were structurally confirmed via CID of the $[M - H + MgPhen]^+$ complex.

Characterization of unsaturated FAs, including PUFAs, in corn oil via gas-phase charge inversion provided double bond localization. Here, we report an observed 16:1(6) FA. As the 16:1(6) is unique to humans and excreted naturally from the skin,[48] corn oil sample contamination is suggested as the source for this fatty acid (Figure 2.10). The double bond in the 18:1 fatty acid observed in the corn oil sample was localized at C9=C10, classifying the FA as 18:1(9) (Figure 2.11a). Characterization of $[M - H + MgPhen]^+$ where M = 18:2 via ion-trap CID (Figure 2.11b) confirmed the FA as 18:2(9,12), exhibiting homoconjugated double bonds at C9=C10 and C12=C13. Furthermore, double bond localization in the observed 18:3 FA leads to the

identification of double bonds at positions C9=C10, C12=C13, and C15=C16 (Figure 2.11c), identifying this FA as 18:3(9,12,15), an *n*-3 fatty acid. The dynamic range of the method is highlighted by the ability to identify double bond position in the 18:3 which is, on average, a factor of 50 lower in abundance when compared to the 18:2 and according to previous reports less than 1% of corn oil FA by mass.[8] In total, while the FA profile of corn oil is relatively simple, the successes demonstrated here suggest the feasibility of significantly more complex sample analysis using the presented method.

2.4 Conclusions

FAs exhibit extensive structural diversity, and double bond localization has been proven to be difficult via conventional tandem mass spectrometry. Utilization of doubly charged trisphenanthroline alkaline earth metal complexes as charge inversion reagents led to the metal cationization of FA anions upon a q2 mutual storage ion/ion reaction followed by DDC−CID. While all alkaline earth metals explored provided FA characterization, the mass spectral simplicity observed with $[MgPhen]^{2+}$ strongly favors the usage of $[Mg(Phen)_3]^{2+}$ as the charge inversion reagent over $[Ca(Phen)_3]^{2+}$, $[Sr(Phen)_3]^{2+}$, and $[Ba(Phen)_3]^{2+}$.

Double bond localization was facile for monounsaturated and diunsaturated FAs, as a repeatable spectral gap generated via the presence of a double bond is observed, providing double bond position. Analysis of PUFAs with more than two degrees of unsaturation provided distinction among *n*-3 and *n*-6 fatty acid double bond positional isomers through direct spectral comparison. Complications were experienced with double bond localization in highly unsaturated FAs. However, tandem mass spectra of $[M - H + MgPhen]^+$ were highly reproducible. Thus, there is potential for unknown FA species to be identified via spectral comparison with known FA standards. Compared to previously reported analyses of solution-based derivations of FAs, the gas-phase charge inversion method provides a rapid approach to FA detailed characterization, including double bond localization.

2.5 References

1. Murphy, R. C. *In Tandem Mass Spectrometry of Lipids: Molecular Analysis of Complex Lipids*; Royal Society of Chemistry: London, **2015**; pp 1−39.

2. Cascio, G.; Schiera, G.; Di Liegro, I. *Curr. Diabetes Rev*. **2012**, 8, 2−17.

3. Kuhajda, F. P. *Nutrition* **2000**, 16, 202−208.

4. Jeppesen, C.; Schiller, K.; Schulze, M. B. *Curr. Diabetes Rep*. **2013**, 13, 279−288.

5. Martinez-Seara, H.; Rog, T.; Pasenkiewicz-Gierula, M.; Vattulainen, I.; Karttunen, M.; Reigada, R. *Biophys. J*. **2008,** 95, 3295−3305.

6. Simopoulos, A. P. Nutrients **2016**, 8, 128.

7. Ramos, M. J.; Fernandez, C. M.; Casas, A.; Rodriguez, L.; Perez, A. *Bioresour. Technol*. **2009**, 100, 261−268.

8. Dunlap, F. G.; White, P. J.; Pollak, L. M.; Brumm, T. J. *J. Am. Oil Chem. Soc*. **1995**, 72, 981−987.

9. Mitchell, T. W.; Pham, H.; Thomas, M. C.; Blanksby, S. J. *J. Chromatogr. B: Anal. Technol. Biomed. Life Sci*. **2009**, 877, 2722−2735.

10. Tomer, K. B.; Crow, F. W.; Gross, M. L. *J. Am. Chem. Soc.* **1983**, 105, 5487−5488.

11. Gross, M. L. *Int. J. Mass Spectrom. Ion Processes* **1992**, 118-119, 137−165.

12. Gross, M. L. *Int. J. Mass Spectrom*. **2000**, 200, 611−624.

13. Kerwin, J. L.; Wiens, A. M.; Ericsson, L. H. *J. Mass Spectrom*. **1996**, 31, 184−192.

14. Jensen, N. J.; Gross, M. L. *Mass Spectrom. Rev*. **1987**, 6, 497−536.

15. Jensen, N. J.; Tomer, K. B.; Gross, M. L. *Anal. Chem*. **1985**, 57, 2018−2021.

16. Adams, J.; Gross, M. L. *Anal. Chem*. **1987**, 59, 1576−1582.

17. Davoli, E.; Gross, M. L. *J. Am. Soc. Mass Spectrom*. **1990**, 1, 320−324.

18. Trimpin, S.; Clemmer, D. E.; McEwen, C. N. *J. Am. Soc. Mass Spectrom*. **2007**, 18, 1967−1967.

19. Yang, K.; Zhao, Z. D.; Gross, R. W.; Han, X. L. *Anal. Chem*. **2011**, 83, 4243−4250.

20. Brown, S. H. J.; Mitchell, T. W.; Blanksby, S. J. *Biochim. Biophys. Acta, Mol. Cell Biol. Lipids* **2011**, 1811, 807−817.

21. Poad, B. L. J.; Pham, H. T.; Thomas, M. C.; Nealon, J. R.; Campbell, J. L.; Mitchell, T. W.; Blanksby, S. J. *J. Am. Soc. Mass Spectrom*. **2010**, 21, 1989−1989.

22. Thomas, M. C.; Mitchell, T. W.; Blanksby, S. J. *J. Am. Chem. Soc*. **2006**, 128, 58−59.

23. Thomas, M. C.; Mitchell, T. W.; Blanksby, S. J. *Methods Mol. Biol*. **2009**, 579, 413−441.

24. Thomas, M. C.; Mitchell, T. W.; Harman, D. G.; Deeley, J. M.; Murphy, R. C.; Blanksby, S. J. *Anal. Chem*. **2007**, 79, 5013−5022.

25. Thomas, M. C.; Mitchell, T. W.; Harman, D. G.; Deeley, J. M.; Nealon, J. R.; Blanksby, S. J. *Anal. Chem*. **2008**, 80, 303−311.

26. Ma, X. X.; Chong, L.; Tian, R.; Shi, R. Y.; Hu, T. Y.; Ouyang, Z.; Xia, Y. *Proc. Natl. Acad. Sci. U. S. A.* **2016**, 113, 2573−2578.

27. Ma, X. X.; Xia, Y. *Angew. Chem., Int. Ed*. **2014**, 53, 2592−2596.

28. Wang, M.; Han, R. H.; Han, X. L. *Anal. Chem*. **2013**, 85, 9312−9320.

29. Yang, K.; Dilthey, B. G.; Gross, R. W. *Anal. Chem*. **2013**, 85, 9742−9750.

30. Hsu, F. F.; Turk, J. *J. Am. Soc. Mass Spectrom*. **1999**, 10, 600−612.

31. Hsu, F. F.; Turk, J. *J. Am. Soc. Mass Spectrom*. **2008**, 19, 1673−1680.

32. Afonso, C.; Riu, A.; Xu, Y.; Fournier, F.; Tabet, J. C. *J. Mass Spectrom*. **2005**, 40, 342−349.

33. Duncan, K. D.; Volmer, D. A.; Gill, C. G.; Krogh, E. T. *J. Am. Soc. Mass Spectrom*. **2016**, 27, 443−450.

34. Hale, O. J.; Cramer, R. *Anal. Bioanal. Chem*. **2018**, 410, 1435−1444.

35. Newton, K. A.; Amunugama, R.; McLuckey, S. A. *J. Phys. Chem. A* **2005**, 109, 3608−3616.

36. Catharino, R. R.; Haddad, R.; Cabrini, L. G.; Cunha, I. B. S.; Sawaya, A.; Eberlin, M. N. *Anal. Chem*. **2005**, 77, 7429−7433.

37. Barlow, C. K.; Hodges, B. D. M.; Xia, Y.; O'Hair, R. A. J.; McLuckey, S. A. *J. Am. Soc. Mass Spectrom*. **2008**, 19, 281−293.

38. Crizer, D. M.; Xia, Y.; McLuckey, S. A. *J. Am. Soc. Mass Spectrom*. **2009**, 20, 1718−1722.

39. IUPAC-IUB Commission on Biochemical Nomenclature (1967). *Eur. J. Biochem*. **1977**, 79, 11−21.

40. Liebisch, G.; Vizcaino, J. A.; Kofeler, H.; Trotzmuller, M.; Griffiths, W. J.; Schmitz, G.; Spener, F.; Wakelam, M. J. O. *J. Lipid Res*. **2013**, 54, 1523−1530.

41. Xia, Y.; Wu, J.; McLuckey, S. A.; Londry, F. A.; Hager, J. W. *J. Am. Soc. Mass Spectrom*. **2005**, 16, 71−81.

42. Liang, X. R.; Xia, Y.; McLuckey, S. A. *Anal. Chem*. **2006**, 78, 3208−3212.

43. Webb, I. K.; Londry, F. A.; McLuckey, S. A. *Rapid Commun. Mass Spectrom*. **2011**, 25, 2500−2510.

44. Londry, F. A.; Hager, J. W. *J. Am. Soc. Mass Spectrom*. **2003**, 14, 1130−1147.

45. Liu, H.; Yoo, H. J.; Hakansson, K. *J. Am. Soc. Mass Spectrom*. **2008**, 19, 799−808.

46. Fay, L.; Richli, U. *J. Chrom*. **1991**, 541, 89−98.

47. Ratnayake, W. M. N.; Chen, Z. Y. *Lipids* **1996**, 31, S279−S282.

48. Drake, D. R.; Brogden, K. A.; Dawson, D. V.; Wertz, P. W. *J. Lipid Res*. **2008**, 49, 4−11.

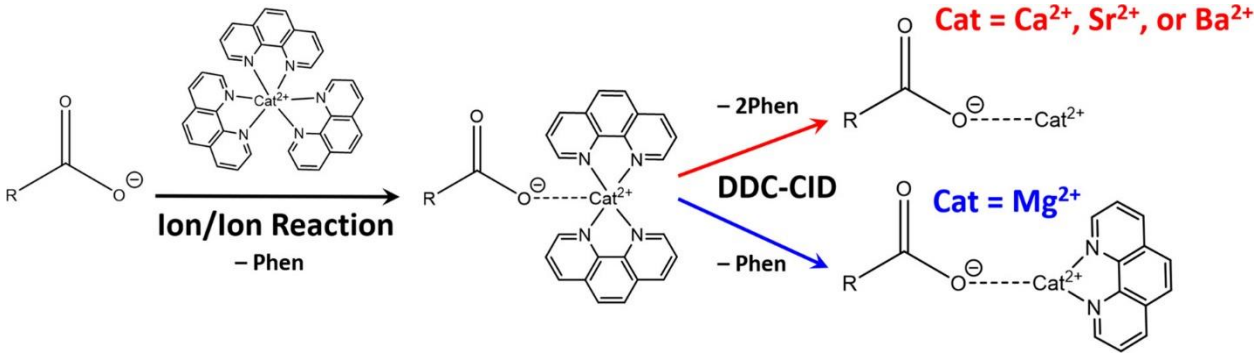

Scheme 2.1 Singly Deprotonated Fatty Acid Ion, $[M - H]^-$, Reacts with $[Cat(Phen)_3]^{2+}$ Dications in a Mutual Storage Ion/Ion Reaction To Produce the $[M - H + Cat(Phen)_2]^+$ Complex Where Cat = Ca^{2+}, Sr^{2+}, Ba^{2+}, or Mg^{2+}.

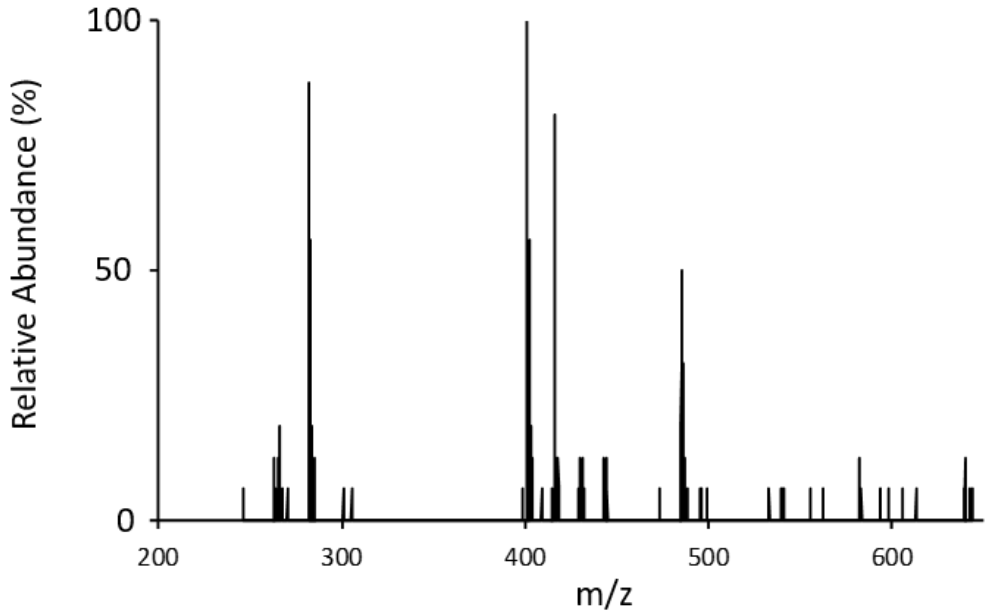

Figure 2.1 Enlarged spectrum over the *m/z* region of 200 – 650 detailing the results of the ion/ion reaction between $[Mg(Phen)_3]^{2+}$ dications and singly deprotonated 18:1(9*Z*). In order to conclude that the ion/ion reaction is unit efficient, it is important to note that a proton deficient $[Mg(Phen)_3]^{2+}$, denoted $[Mg(Phen)_3 — H]^+$ at *m/z* 563, would indicate a proton transfer reaction between the singly deprotonated $[M — H]^-$ and the $[Mg(Phen)_3]^{2+}$. As there is no peak at *m/z* 563, the ion/ion reaction does not have competing reaction pathways.

Table 2.1 Observed *m/z* values from CID of $[M - H + MgPhen]^+$ where M = 18:0.

Product Ion Observed	**Measured *m/z* value**
$[MgPhenOH]^+$	221
$[MgPhenO_2]^+$	236
$b^{+\bullet}$	263
c’	275
d’	289
e’	303
f’	317
g’	331
h’	345
i’	359
j’	373
k’	387
l’	401
m’	415
n’	429
o’	443
$[M - H + MgPhen]^+$	487

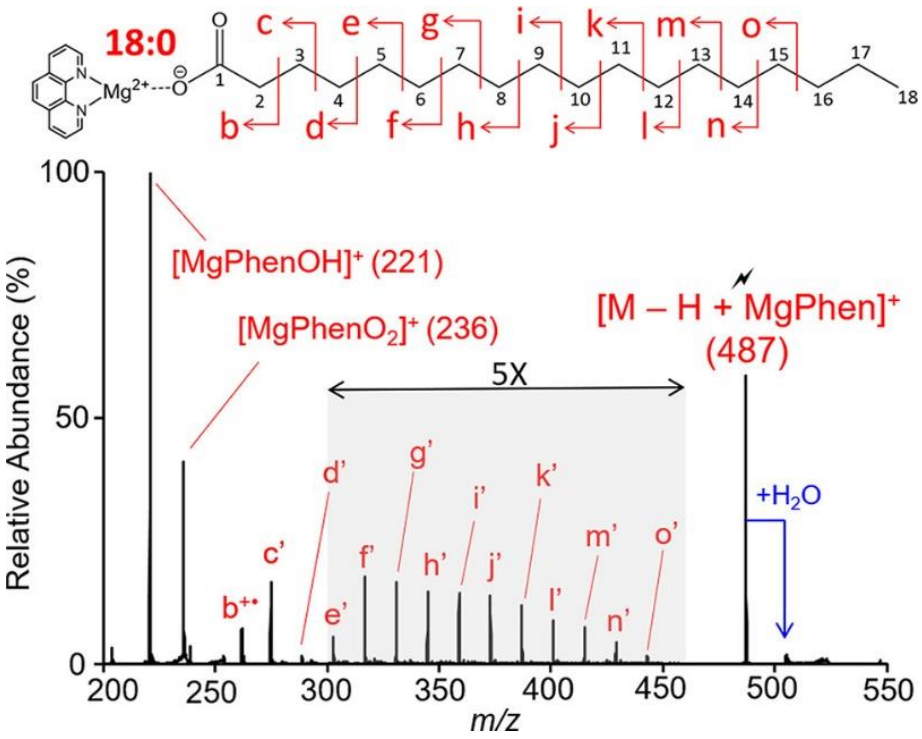

Figure 2.2 Ion-trap CID spectrum of the $[M - H + MgPhen]^+$ complex generated via gas-phase ion/ion reaction between singly deprotonated 18:0 and $[Mg(Phen)_3]^{2+}$ dications.

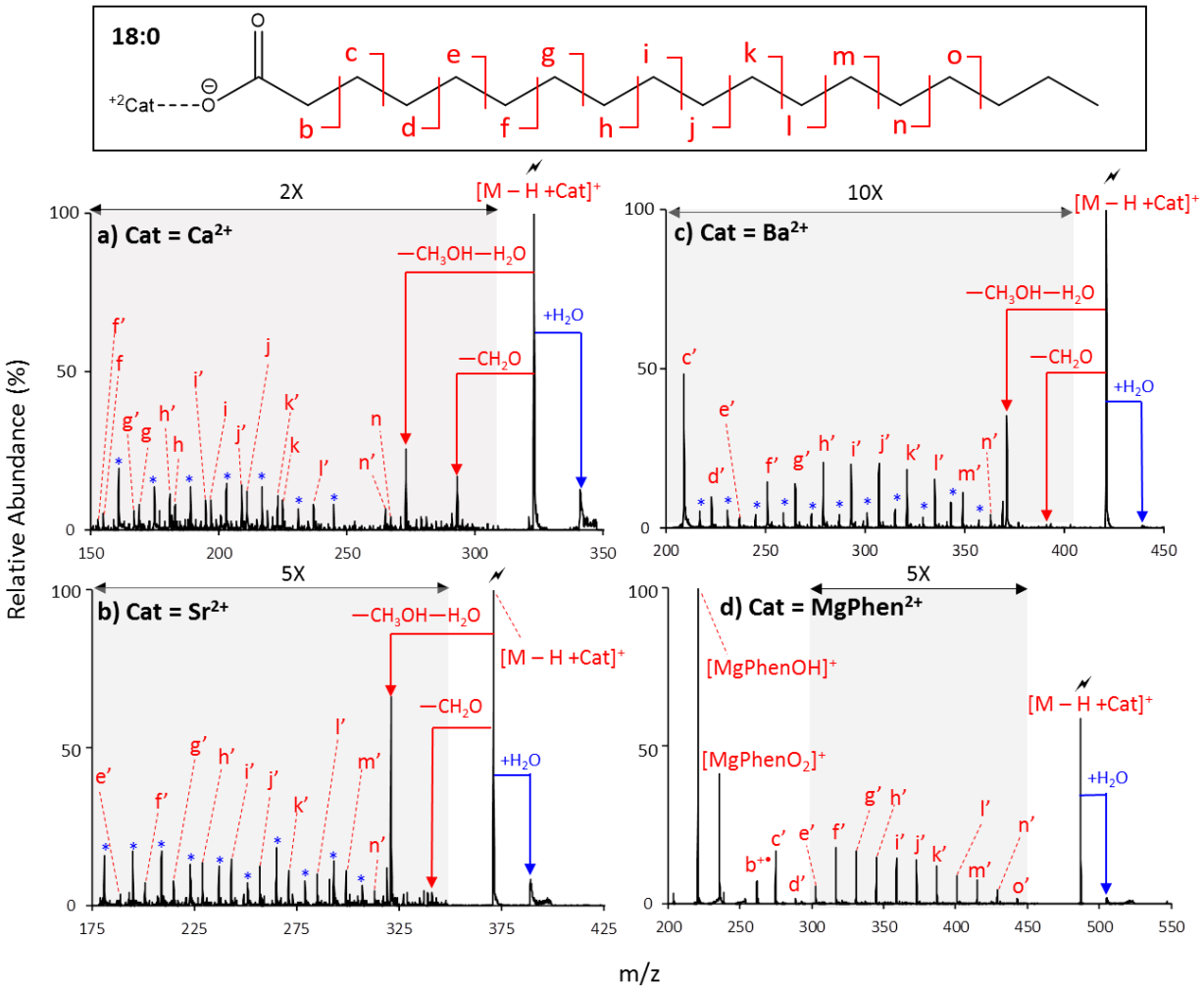

Figure 2.3 Ion-trap CID of $[M — H + Cat]^+$ with M = 18:0 where (a) Cat = Ca^{2+} (b) Cat = Sr^{2+} (c) Cat = Ba^{2+} and (d) Cat = $MgPhen^{2+}$. The blue asterisk indicates a doubly hydrated CRF product ion. For the bare metal complexes (Cat = Ca^{2+}, Sr^{2+}, or Ba^{2+}), as the size of the cation increases, the relative abundance of the hydrated CRF ion series decreases.

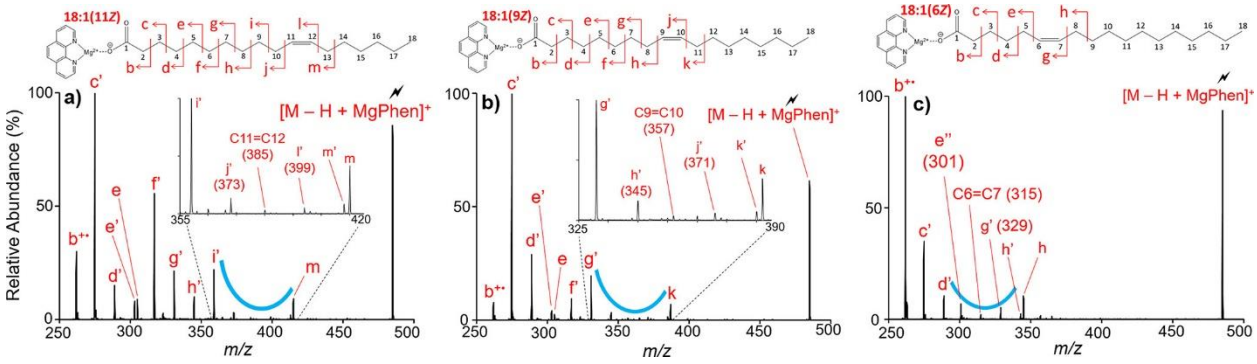

Figure 2.4 Ion-trap CID of a series of isomeric 18:1 fatty acids. Ion-trap CID spectrum of [M – H + MgPhen]$^+$ where (a) M = 18:1(11*Z*), (b) M = 18:1(9*Z*), and (c) M = 18:1(6*Z*). The blue curve highlights the spectral pattern used to localize the double bond.

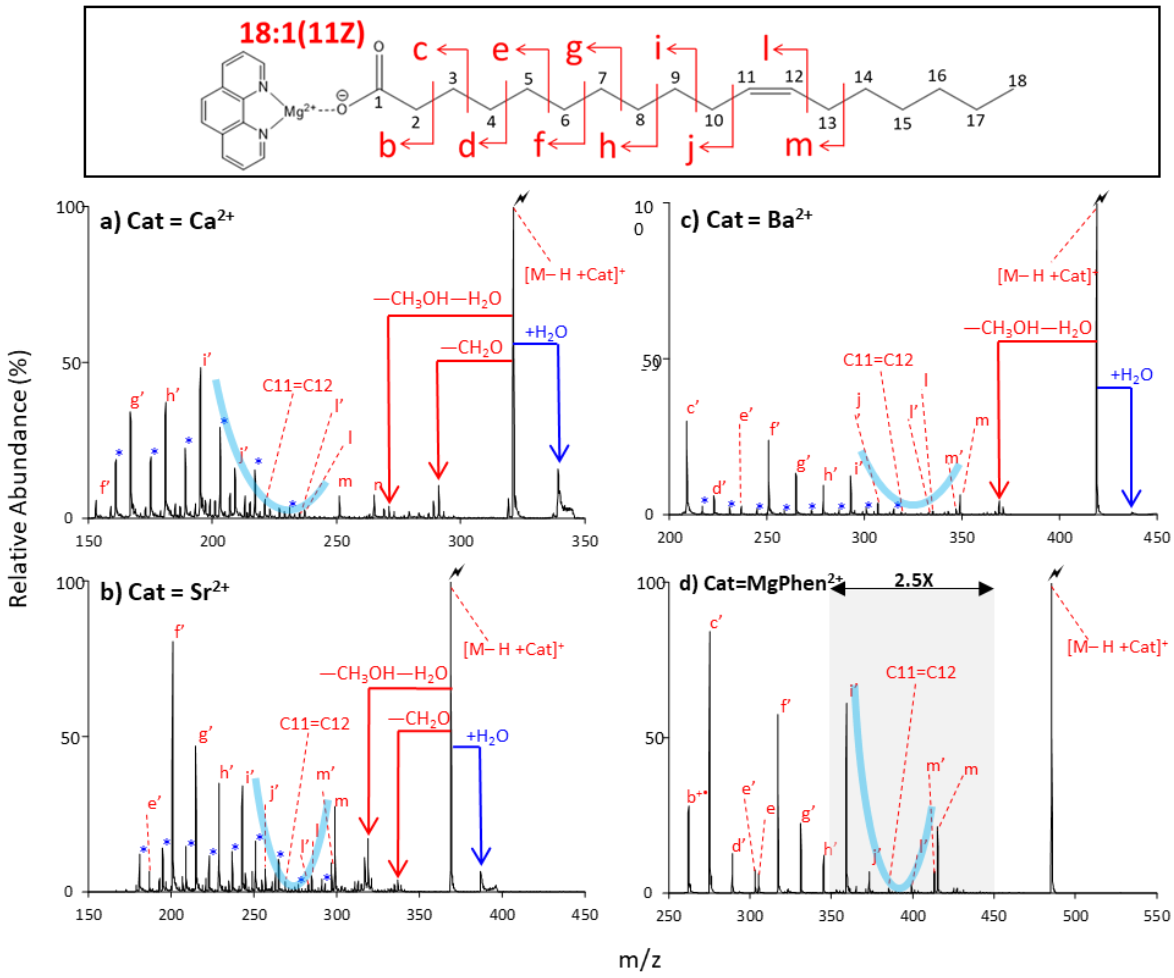

Figure 2.5 Ion-trap CID of $[M — H + Cat]^+$ derived from 18:1(11Z) where (a) Cat = Ca^{2+} (b) Cat = Sr^{2+} (c) Cat = Ba^{2+} and (d) Cat = $MgPhen^{2+}$. The blue curve highlights the spectral pattern used to identify the double bond position. The blue asterisk indicates a doubly hydrated CRF product ion.

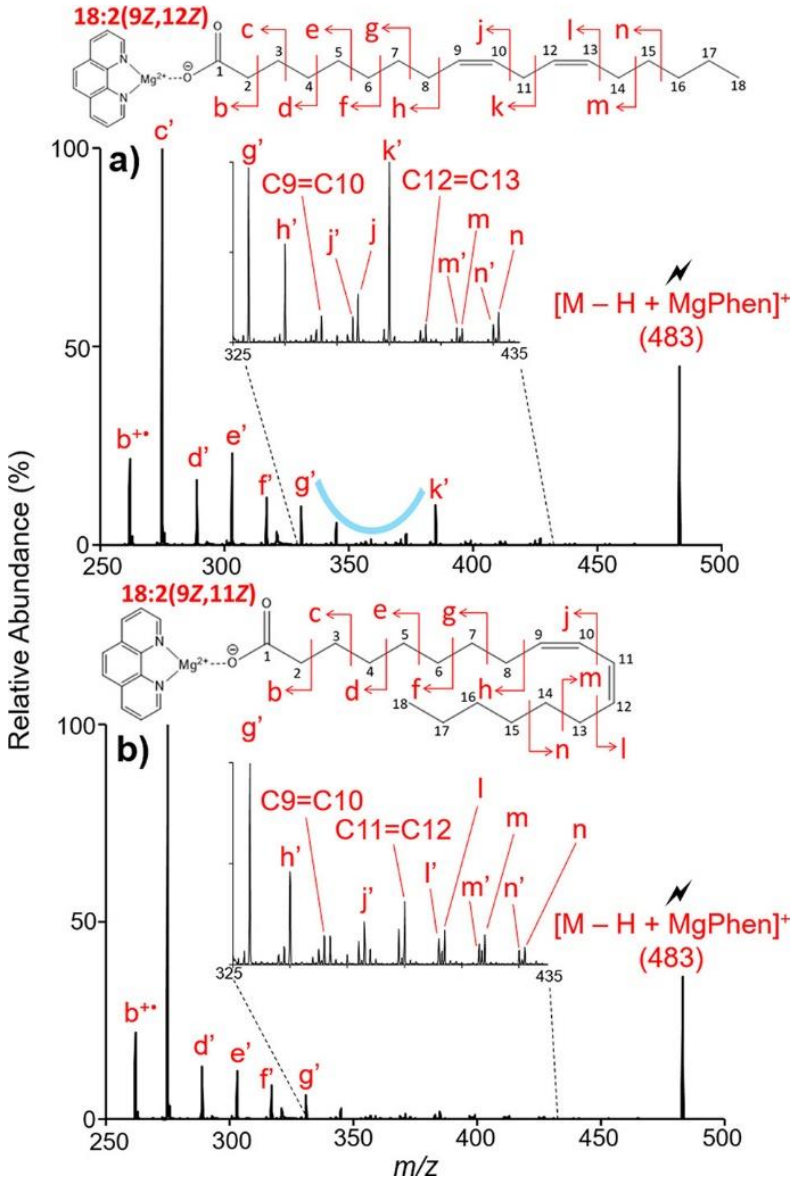

Figure 2.6 Ion-trap CID of $[M - H + MgPhen]^+$ where (a) M = 18:2(9*Z*,12*Z*) and (b) M = 18:2(9*Z*,11*Z*). Comparison of the two CID spectra shows marked differences between diunsaturated FAs with homoconjugated and conjugated double bonds.

Table 2.2 Observed *m/z* values from CID of $[M - H + MgPhen]^+$ for 18:2(9*Z*,12*Z*) and 18:2(9*Z*,11*Z*) fatty acid isomers shown in Figure 2.6.

Production Ion Observed	**m/z Value**	**Production Ion Observed**	**m/z Value**
FA 18:2(9*Z*,12*Z*)		FA 18:2(9*Z*,11*Z*)	
$b^{+\bullet}$	262	$b^{+\bullet}$	262
c′	275	c′	275
d′	289	d′	289
e′	303	e′	303
e	305	e	305
f′	317	f′	317
g′	331	g′	331
h′	345	h′	345
C9=C10	359	C9=C10	357
j′	371	j′	371
j	373	C11=C12	385
k′	385	l′	397
C12=C13	399	l	399
m′	411	m′	411
m	413	m	413
n′	425	n′	425
n	427	n	427
$[M - H + MgPhen]^+$	483	$[M - H + MgPhen]^+$	483

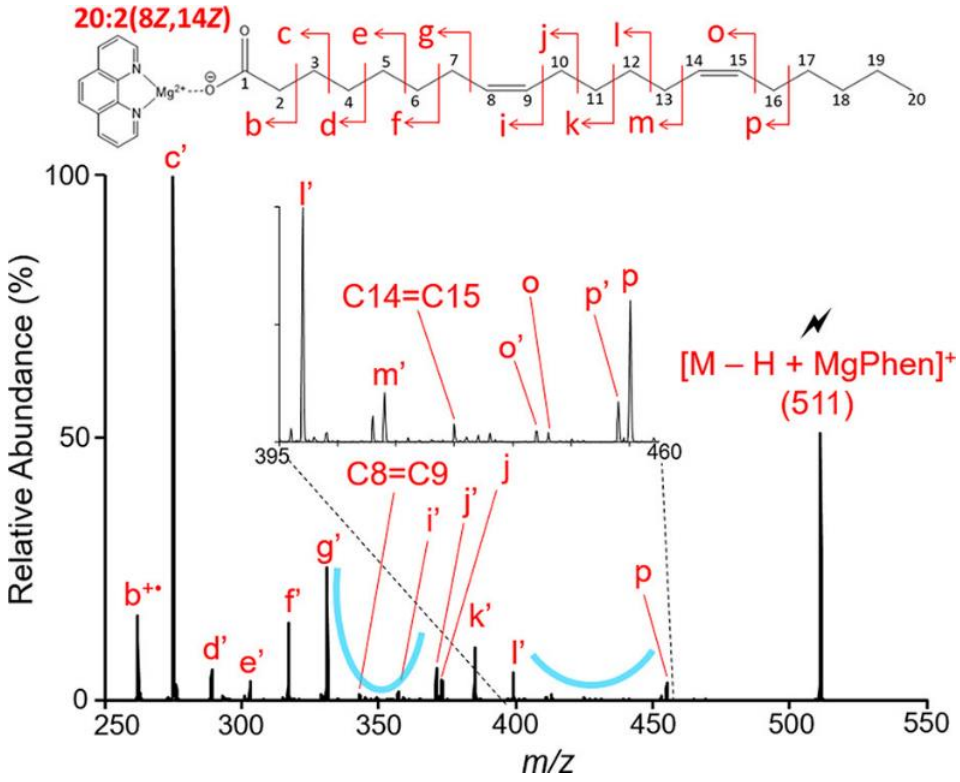

Figure 2.7 Ion-trap CID of $[M - H + MgPhen]^+$ derived from the gas-phase ion/ion reaction of singly deprotonated 20:2(8*Z*,14*Z*) and $[Mg(Phen)_3]^{2+}$.

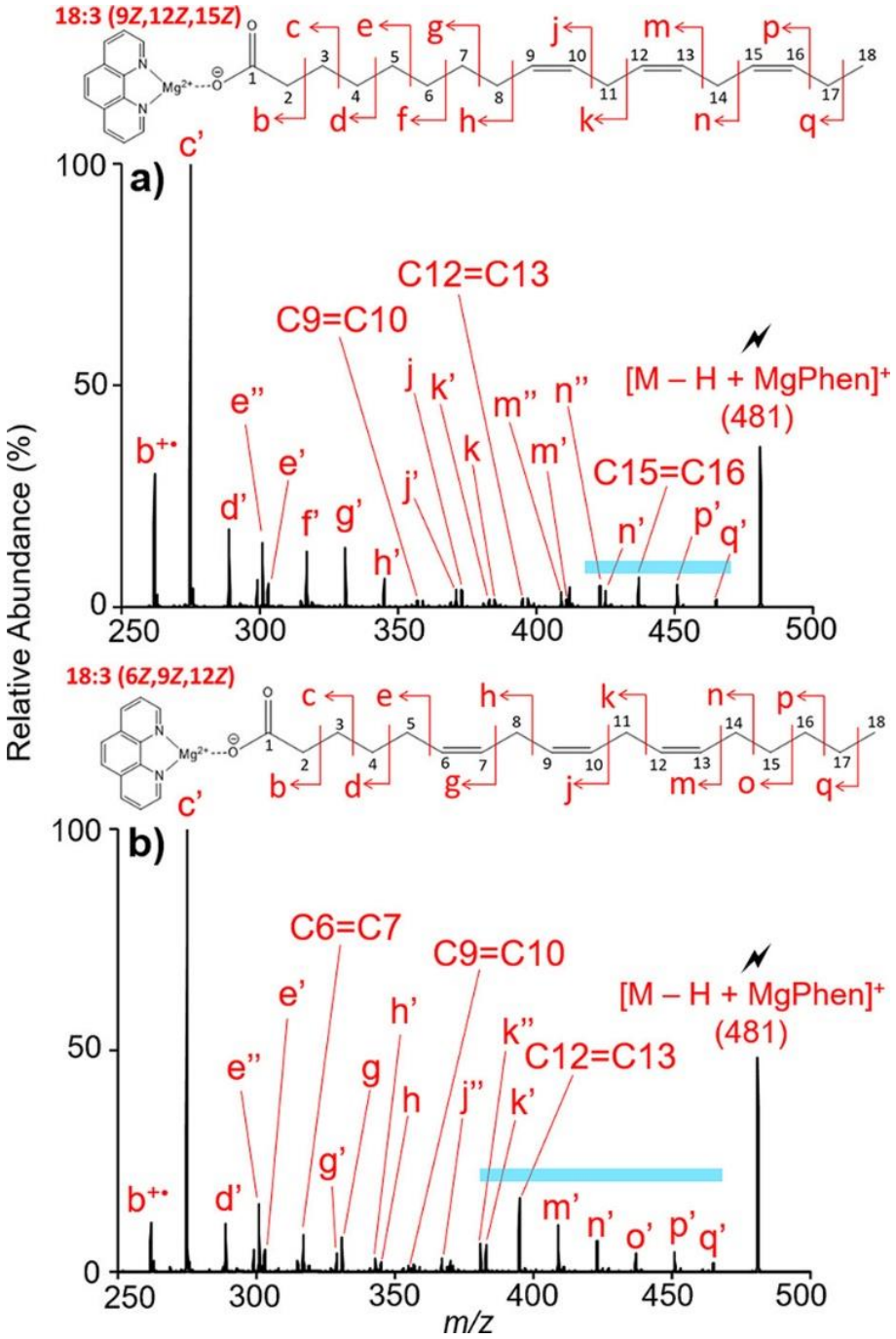

Figure 2.8 Ion-trap CID of $[M - H + MgPhen]^+$ derived from the gas-phase ion/ion reaction of $[Mg(Phen)_3]^{2+}$ with singly deprotonated (a) 18:3(9*Z*,12*Z*,15*Z*) and (b) 18:3(6*Z*,9*Z*,12*Z*).

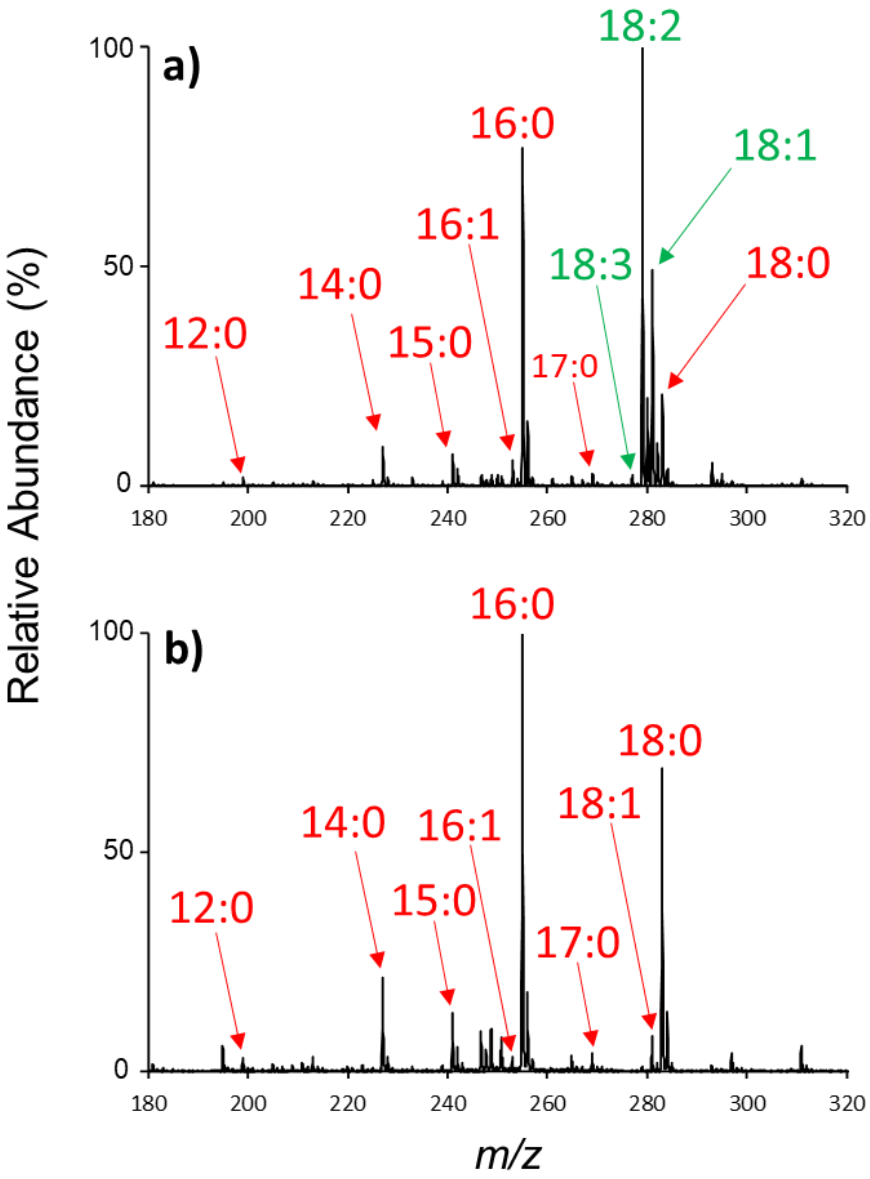

Figure 2.9 (a) Negative ion mode nESI of hydrolyzed corn oil. (b) Negative ion mode nESI of blank solvent extraction. FAs are known to be common contaminants found in glassware, plastics, and solvents. FAs observed in both the hydrolyzed corn oil and the blank solvent extraction are denoted in red, whereas FAs unique to corn oil are denoted in green. The 18:1 FA was found in both the hydrolyzed corn oil and the blank solvent extraction, yet the relative abundance of the 18:1 FA in the hydrolyzed corn oil is considerably greater than in the blank solvent extraction. Therefore, it can be presumed that the 18:1 FA is also present in the corn oil sample.

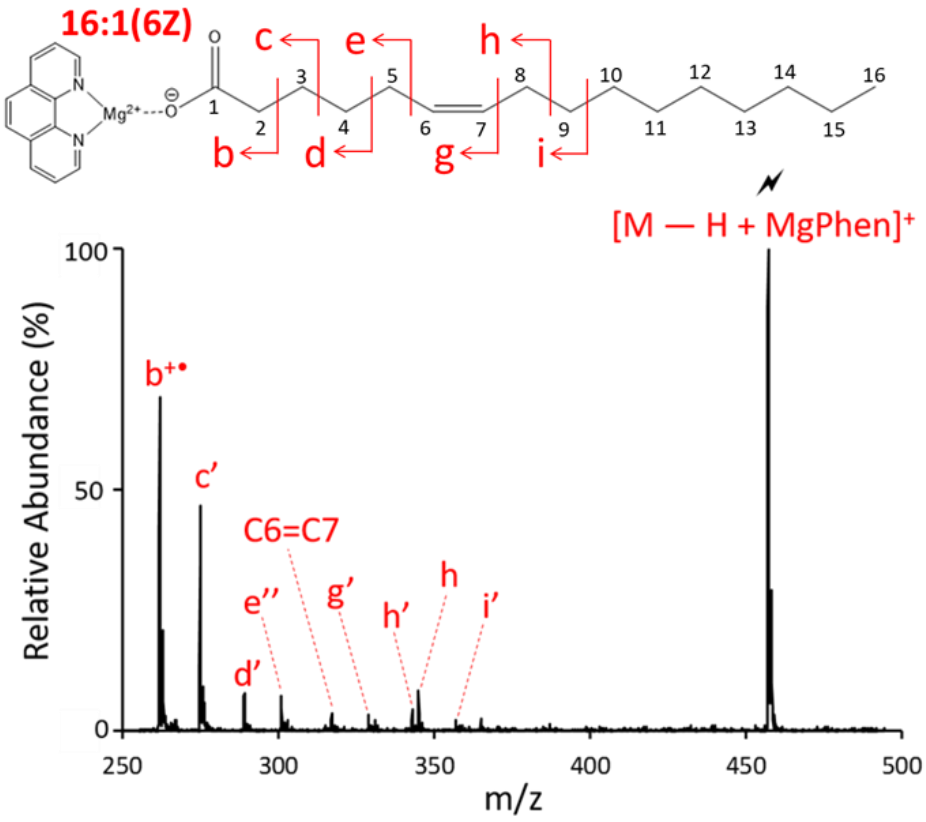

Figure 2.10 The CID spectrum of $[M - H + MgPhen]^+$ where M = 16:1 isolated from hydrolyzed corn oil (FA contaminant). Note that double bond stereochemistry cannot be ascertained using the presented method. However, as the *Z* geometry is most common biologically, the structure is depicted as such.

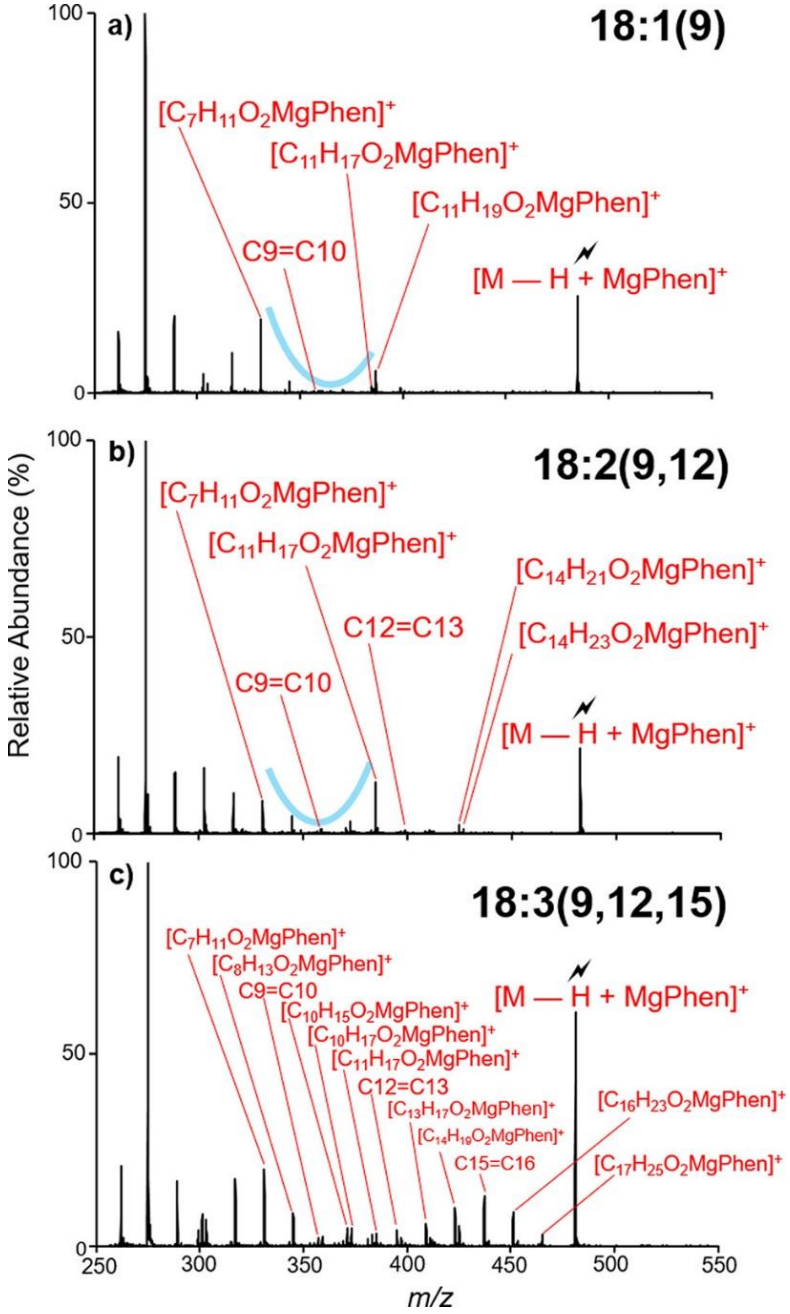

Figure 2.11 Ion-trap CID of $[M - H + MgPhen]^+$ where M = (a) 18:1, (b) 18:2, and (c) 18:3. Fatty acids were isolated from negative nESI of hydrolyzed corn oil.

CHAPTER 3. GENERATING FATTY ACID PROFILES IN THE GAS PHASE: FATTY ACID IDENTIFICATION AND RELATIVE QUANTITATION USING ION/ION CHARGE INVERSION CHEMISTRY

3.1 Introduction

Fatty acids (FAs) constitute a class of ubiquitous lipids, present in all living organisms. FAs are known to serve vital roles in cellular energy storage, cellular signaling, modification of proteins, and as key architectural components of complex lipids such as glycerophospholipids, sphingolipids, and sterol esters.[1–5] FA are comprised of at least one carboxylic acid moiety and an aliphatic chain. Despite their apparently simple composition, FA display dramatic structural diversity. Specifically, variations in aliphatic chain length, degree of unsaturation, site(s) of unsaturation, and modifications such as hydroxylation,[6] nitrosylation,[7] and methyl chain branching[8] are observed. Recently, alterations to FA structure and composition have been linked with the progression of numerous chronic diseases such as heart disease, diabetes, several types of cancer, and neurodevelopmental disorders like attention-deficit/hyperactivity disorder.[9–14] Therefore, efforts to both characterize and quantify FA are a principle focus of many recent research endeavors, including FA profiling for biomarker discovery.[14–17] Moreover, in a recent investigation profiling human plasma samples from patients with breast cancer and type 2 diabetes, Zhang et al. report that the ratio of lipid isomers differing on sites of unsaturation (so-called double bond positional isomers) could be of particular importance in lipid biomarker discovery.[14]

Mass spectrometry (MS) coupled with some form of chromatography represents the most widely adopted analytical platform for routine FA identification and quantitation. Gas chromatography (GC) and liquid chromatography (LC) are mainstays of FA analysis yet are not without their respective challenges. For instance, the analysis of FA via GC−MS first requires conversion of FA to their respective methyl esters. A significant disadvantage to GC−MS analysis of FA methyl esters is the inability to distinguish the resulting electron ionization mass spectra of lipid isomers, particularly highly unsaturated FA isomers.[18] Benefits of FA analysis with LC−MS/MS include no requirement of FA derivatization prior to analysis and validated methods for FA quantitation.[19] Once again, however, the resulting mass spectra (in this instance, collision-induced dissociation mass spectra) do not readily distinguish FA double bond positional isomers.

This restricts methods to those including LC workflows, but even the separation of some double bond positional FA isomers can only be achieved using silver-ion chromatography.[18]

Direct infusion electrospray ionization (ESI), commonly referred to as shotgun lipidomics, has gained popularity due to ease of use, reduced analysis time, and minimal sample volume requirements.[3,20] Briefly, shotgun lipidomics involves the direct infusion of crude lipid extract into the mass spectrometer without prior fractionation. Direct infusion under negative ESI conditions produces abundant $[M - H]^-$ anions of FA due to facile deprotonation of the carboxylic acid moiety. From accurate mass measurements of the $[M - H]^-$ ion mass-to-charge (*m/z*) ratio, FA sum composition information (i.e., aliphatic chain length, degree of unsaturation) can be determined. However, accurate mass measurements alone do not provide insight into FA structural characteristics, such as double bond position(s). Furthermore, reliance on tandem MS (MS/MS) methods for FA analysis, specifically low-energy collision induced dissociation (CID), has been minimally effective. In negative ion mode, activation of deprotonated FA anions results in CID spectra dominated by small molecule losses (i.e., carbon dioxide and water neutral losses) that do not provide insight into structural characteristics important in biochemical function such as double bond position(s).[21] Notably, relative abundances of water and carbon dioxide neutral losses are sensitive to structural features, which can further be exploited for FA identification and quantitation.[22]

To enhance the number of structurally informative product ions, two distinct strategies regarding FA derivatization are employed. The first approach involves derivatization of the double bond, while the second approach involves derivatization of the carboxylic acid moiety. Reactions used to derivatize the double bond include ozonolysis[18,23–28] and the Paternò–Büchi (PB) reaction.[29–31] Both strategies generate diagnostic product ions indicative of double bond position. Employing the PB reaction, Ma et al. demonstrated both relative and absolute quantitation of unsaturated lipids in rat brain tissue, reporting nearly one-half of the identified lipid species existing as mixtures of double bond positional isomers.[30] While absolute quantitation has yet to be explored with ozonolysis, relative changes in isomeric lipid concentration can be achieved.[32]

Charge-switching strategies represent the second approach to FA derivatization. Charge-switching derivatives directly target modification of the FA carboxyl group with a fixed, positively charged reagent. Wang et al. describe covalent modification of the carboxyl moiety via amidation of the carboxyl moiety with *N*-[4-(aminomethyl)phenyl]pyridinium (AMPP) ion in solution.[33]

ESI−MS/MS analysis of the AMPP-derivatized FA ion provided informative CID spectra that could be utilized for both structural elucidation and quantitation of FA. Specifically, Han and co-workers have shown that wet-chemical derivatization of fatty acids to AMPP conjugates followed by CID of the FA-AMPP ion can be used to undertake relative quantification of binary and ternary mixtures of fatty acid isomers utilizing a fitting routine similar to that outlined here.[33] Extending this approach, Yang et al. successfully quantified double bond positional isomers of AMPP-derivatized linolenic acid (i.e., 18:3(9,12,15), 18:3-(6,9,12)) originating from neutral lipids found human serum.[34] While effective, analysis of AMPP-derivatized FA relies on wet-chemical modification of free (i.e., nonesterified) FA. Thus, crude samples first require solution-based lipid extraction and hydrolysis to generate free FA prior to derivatization with AMPP and subsequent analysis.

In contrast to covalent modification of the carboxyl moiety, numerous investigators have exploited metal cation adducted FA.[35−44] Metal adducted FAs are typically generated prior to ionization via doping metal salts into ESI solution containing FA. It is well-known that charge-remote fragmentation (CRF) of alkali and alkaline earth metal cationized FA using high-energy CID is an effective method for structural elucidation of FA.[35−37] As high-energy CID operates in the keV kinetic regime, workflows to access CRF are uncommon, mostly due to the replacement of multisector instruments with triple quadrupole (QqQ) and quadrupole time-of-flight (Q-TOF) mass spectrometers that operate under low-energy CID conditions. More recently, product ion spectra generated via low-energy CID of dilithiated[40,41] (i.e., $[M - H + 2Li]^+$), copper(II) adducted[42] (i.e., $[M - H + Cu^{II}]^+$), and barium cationized lipids[43,44] (i.e., $[M - H + Ba]^+$, $[M + Ba]^{2+}$) have been advantageous in lipid structural analysis. However, the analysis of metalated lipid ions has been exploited solely for FA identification, and thus relative quantitation has remained unaddressed. Like AMPP-based methods, the construction of FA profiles utilizing metal adducted FA first requires the generation of free FA prior to metal cation adduction. Therefore, FA profiles developed from crude lipid extracts utilizing solution-based methods such as metal cation adduction or AMPP derivatization reflect the FA composition of all ester-linked lipids, unless lipid classes are first separated using additional fractionation steps prior to hydrolysis, derivatization, and analysis.

Recently, we reported the gas-phase charge inversion of FA anions via ion/ion reaction with tris-phenanthroline alkaline earth metal complex cations to identify the C=C double bond

position(s).[45] Gas-phase charge inversion of FA via ion/ion reactions offers the primary advantage of ionizing FA in the most efficient modality (i.e., negative ion mode), while characterizing the FA in the positive ion mode where structurally informative product ions are more readily observed. By conducting FA derivatization in the gas phase, electrospray and solution conditions can be optimized for each reactant.[46] Furthermore, when compared to FA derivatization methods reliant on wet chemistry (i.e., metal cation adduction, AMPP derivatization, etc.), gas-phase ion/ion reactions provide enhanced control of reaction outcomes including product generation and reaction efficiency. Singly deprotonated $[FA - H]^-$ anions and tris-phenanthroline magnesium complex dications react in the gas phase to form the long-lived electrostatic complex comprised of the deprotonated fatty acid, the magnesium dication, and a phenanthroline ligand. Collisional activation of the $[FA - H + MgPhen]^+$ ion generated reproducible spectral patterns that provided double bond position(s) for monounsaturated and diunsaturated FA. Double bond localization in highly unsaturated FA was hindered due to rearrangements and congested CID spectra; yet discrimination between isomeric polyunsaturated fatty acids (PUFA) was achieved.

Herein, we report the development of a mass spectral library, comprised of $[FA - H + MgPhen]^+$ product ion spectra. The FA library permits the confident identification of FA, including PUFA. Furthermore, in this study, we demonstrate the ability to sensitively determine relative abundances of isomeric FA using multiple linear regression analysis in conjunction with ion/ion chemistry. In addition, we applied the mass spectral library, relative quantitation algorithm, and an MS^n platform reliant entirely on gas-phase chemistries to develop a FA profile selectively for phospholipids present in bovine liver extract. Contrary to solution-based approaches, gas-phase FA profiling offers the ability to selectively release FA from the lipids ionized in negative ion mode permitting a quantitative profile of the fatty acid isomers carried by phospholipids. Within the literature, there is a growing awareness of the distinct profile of fatty acid isomers between lipid classes based on both traditional multistage fractionation[47] and next generation methods.[14] However, the method provided here is unique in that it provides a snapshot of the FA composition of phospholipids where changes will be related to membrane synthesis and function in isolation from changes to storage lipids such as triacylglycerols and cholesterol esters, which, in some contexts (i.e., plasma), will dominate total FA pool. To gain the same insights as provided by our approach utilizing wet-chemical methods, the lipid extract would need to be split in two, with one fraction subjected to intact phospholipid analysis while the other being hydrolyzed, derivatized,

and analyzed. Therefore, gas-phase FA profiling in conjunction with ion/ion chemistry as presented herein provides a detailed, isomer-specific profile of all FA released from the phospholipid fraction in the same infusion experiment. In turn, gas-phase FA profiling offers a rapid, sensitive, and selective approach to quantitative lipid profiling.

3.2 Experimental

3.2.1 Materials

HPLC-grade methanol and water were purchased from Fisher Scientific (Pittsburgh, PA). All FA standards were purchased from Cayman Chemical (Ann Arbor, MI) and used without further purification. Magnesium chloride and 1,10-phenanthroline (Phen) were purchased from Sigma-Aldrich (St. Louis, MO). Polar liver extract (bovine) was purchased from Avanti Polar Lipids, Inc. (Alabaster, AL).

3.2.2 Preparation of nESI Solutions

Solutions of FA standards were prepared in methanol to a final concentration of 10 μM (m/v). Similarly, solutions of bovine liver extract (polar) were prepared to a final concentration of 50 μM (m/v) in methanol with 10 mM ammonium acetate, assuming an average lipid molecular mass of 760 g/mol. Mixtures of FA isomers were prepared from individual isomer stock solutions in methanol. For relative quantitation, the total FA concentration was held constant (10 μM), while the molar ratio of FA isomers was varied. Tris-phenanthroline magnesium complexes were prepared by mixing the 1:1 (mol/mol) metal salt:Phen in methanol to a final concentration of 50 μM (m/v).

3.2.3 Nomenclature

The shorthand notation reported by Liebisch et al. is adopted to describe FA.[48] Before the colon, the number of carbon atoms is first indicated. After the colon, the number of carbon−carbon double bonds is designated with definitive double bond position(s), with respect to the carboxylic acid moiety, indicated within parentheses. If known, carbon−carbon double bond stereochemistry is further indicated as *Z* (*cis*) and *E* (*trans*). If unknown, only the double bond position is indicated. In some instances, the *n-x* terminology is also employed to classify FA isomers. The *n-x*

terminology describes the location of the first carbon−carbon double bond from the methyl end of the aliphatic chain.

3.2.4 Mass Spectrometry

All data were collected on a Sciex QTRAP 4000 hybrid triple quadrupole/linear ion trap mass spectrometer (SCIEX, Concord, ON, Canada) with modifications analogous to those previously described.[49] Alternately pulsed nanoelectrospray ionization (nESI) allows for sequential injection of the tris-phenanthroline magnesium dications, $[Mg(Phen)_3]^{2+}$, followed by singly deprotonated FA ions.[50] First, $[Mg(Phen)_3]^{2+}$ was generated in the positive ion mode, then mass-selected in Q1 and transferred to the high-pressure collision cell, q2, for storage. Next, $[FA - H]^-$ anions were generated in the negative ion mode, isolated in Q1 during transit, and transferred to q2 for storage. In q2, the $[FA - H]^-$ and $[Mg(Phen)_3]^{2+}$ ion were simultaneously stored for 300 ms. The mutual storage ion/ion reaction produced $[FA - H + Mg(Phen)_2]^+$. The $[FA - H + Mg(Phen)_2]^+$ ion was then subjected to 18 V of dipolar direct current (DDC)-CID for 25 ms, generating the $[FA - H + MgPhen]^+$ ion.[51] The resulting $[FA - H + MgPhen]^+$ ion was then transferred to the low-pressure linear ion trap (LIT), Q3, for monoisotopic isolation. Monoisotopically isolated $[FA - H + MgPhen]^+$ was then collisionally activated via single frequency resonance excitation (q = 0.383) for 150 ms. Product ions generated from CID were analyzed via mass-selective axial ejection (MSAE).[52]

As described in our original description of the charge inversion of FA with $[Mg(Phen)_3]^{2+}$,[45] both singly and doubly hydrated FA complex cations can be observed resulting from ion/molecule reactions in the collision cell with adventitious water. This occurs most readily with saturated FA. This phenomenon can lead to more complicated spectra and isobaric interferences. In our experience, this can be an issue after the instrument has been vented and shortly after pumping down.

3.2.5 Development of Fatty Acid Mass Spectral Library

A library of CID spectra of $[FA - H + MgPhen]^+$ ions of FA standards was constructed to aid in the identification of unknown FA. Automated spectral matching was conducted in the MATLAB numerical computing environment (Mathworks, Natick, MA). After normalization of

product ion intensities relative to the base peak, for both the library and the unknown $[FA - H + MgPhen]^+$ CID spectra obtained under identical conditions, the residuals were calculated between the normalized product ion intensities of unknown FA and each individually detected FA standard. Calculated residuals were then summed, and the minimum summed residual was returned. The FA standard from the developed library that generated the minimum summed residual when compared to the unknown FA represents the identity of the unknown FA.

3.2.6 Relative Quantitation of Fatty Acid Isomers

The MATLAB numerical computing environment (Mathworks, Natick, MA) was used to perform a multiple linear regression analysis modeled after that reported by Wang et al.[33] To generate relative quantities of isomeric components in a mixture, the library spectra of the standards, as described above, served as the predictors, while the normalized CID spectra of the $[FA - H + MgPhen]^+$ ions served as the responses. Herein, it is assumed that product ions observed in an isomeric mixture can be equated to a linear combination of individually detected isomer product ions. Under that assumption, the least-squares coefficients represent the relative composition of each individual isomer. Mathematically, this concept is represented by **equation 1**, where x_{isomer_j} signifies the composition of isomer *j* present in an isomeric mixture, $I_{ion_i isomer_j}$ represents the normalized product ion intensity of the specified product ion *i* from an individually detected isomer *j* sample, and $I_{ion_i mixture}$ indicates the normalized product ion intensity of the specified product ion *i* in an isomeric mixture. Note that the number of specified product ions *i* is strictly greater than the number of individual isomers j present in the isomeric mixture (i.e., $i = 1, 2, 3, ...n$ and $j = 1, 2, 3, ...m$ such that $n > m$). The least-squares coefficients were constrained such that the sum of all coefficients was one and all coefficients were greater than or equal to zero, as modeled by **equations 2** and **3**, respectively. Data are presented as the mean ± standard deviation from at least three individually prepared samples ($n = 3$). Calculated standard deviations are reported to one significant figure.

$$\Sigma x_{isomer_j} I_{ion_i isomer_j} = I_{ion_i mixture} \quad (1)$$

$$\Sigma x_{isomer_j} = 1 \quad (2)$$

$$x_{isomer_j} \geq 0 \quad (3)$$

3.3 Results and Discussion

3.3.1 Development of CID Mass Spectral Library

Singly deprotonated FA anions undergo charge inversion when reacted in the gas phase with tris-phenanthroline magnesium dications via a mutual storage ion/ion reaction.[45] The ion/ion reaction generates the $[FA - H + Mg(Phen)_2]+$ complex ion. DDC-CID of $[FA - H + Mg(Phen)_2]^+$ results in the neutral loss of one phenanthroline ligand, producing $[FA - H + MgPhen]^+$. The $[FA - H + MgPhen]^+$ fragments upon ion-trap collision-induced dissociation (CID) to generate product ion spectra indicative of double bond position(s). A priori double bond identification via direct interpretation of the $[FA - H + MgPhen]^+$ CID spectrum is achieved only for monounsaturated and diunsaturated FA. However, distinct spectral differences are observed for polyunsaturated $[FA - H + MgPhen]^+$ isomeric ions, as previously reported.[45]

To aid in the identification of FA, we constructed a library comprised of ion trap CID product ion spectra resulting from collisional activation of the $[FA - H + MgPhen]^+$ cations derived from the ion/ion charge inversion of the $[FA - H]^-$ anions of 40 unsaturated FA standards. Ion-trap CID of the $[FA - H + MgPhen]^+$ precursor ion generated CID spectra unique to individual FA isomers.

A notable advantage of the library matching approach is its ability to distinguish highly unsaturated FA isomers due to the fact that the CID spectra of the $[FA - H + MgPhen]^+$ ions are isomer-specific. As an illustration, two double bond positional isomers of FA 22:5 were examined using the described ion/ion chemistry. The reaction between $[Mg(Phen)_3]^{2+}$ dications and $[22:5 - H]^-$ anions generated the $[22:5 - H + MgPhen]^+$ complex cations (*m/z* 533.3). Product ion spectra for the 22:5 *n*-3 (i.e., 22:5(7*Z*, 10*Z*, 13*Z*, 16*Z*, 19*Z*)) and 22:5 *n*-6 (i.e., 22:5(4*Z*, 7*Z*, 10*Z*, 13*Z*, 16*Z*)) complex cations are shown in Figure 3.1a and b, respectively. To better visualize distinguishing product ions for 22:5 isomer differentiation, a difference plot was generated using Figure 3.1a and b, as illustrated with Figure 3.1c. To generate Figure 3.1c, the relative abundances of product ions produced via CID $[22:5 - H + MgPhen]^+$ for the *n*-3 isomer (Figure 3.1a) were subtracted from those obtained from the *n*-6 isomer (Figure 3.1b). Therefore, product ions with a higher relative abundance in, or unique to, the charge inverted 22:5 *n*-6 isomer fragmentation pattern are depicted with positive relative abundances (shown in blue font) in Figure 3.1c, while those with a higher relative abundance, or unique to, the fragmentation of the *n*-3 isomer are presented with negative relative abundances (shown in red font). Ultimately, distinct differences in the relative abundances

of fragment ions as well as product ions unique to individual isomers were observed between the CID spectra of the 22:5 FA ions. For example, the product ion generated via C2−C3 cleavage (*m/z* 262.1) is observed at a significantly higher relative abundance in the spectrum of the 22:5 *n*-6 isomer (Figure 3.1b) when compared to that of the 22:5 *n*-3 isomer (Figure 3.1a), as also highlighted with the difference plot (Figure 3.1c). This difference in *m/z* 262.1 fragment ion abundance is related to the proximity of the first double bond position relative to the carboxylate moiety; FA 22:5 *n*-6 contains a C4=C5, whereas the closest double bond to the carboxylate moiety in 22:5 *n*-3 is located at C7=C8. As the double bond moves closer to the carboxylate moiety, the relative abundance of the product ion *m/z* 262.1 increases. From Figure 3.1c, another example can be illustrated with the product ion at *m/z* 421.1, which is formed via C14−C15 cleavage. The product ion at *m/z* 421.1 is significantly more abundant in the 22:5 *n*-6 isomer. Carbon−carbon bond cleavages are correlated to double bond position(s), as the proximity to the charge site likely affects CRF. Numerous other reproducible differences in product ion relative abundances between the two isomeric ions are observed, many of which are highlighted in Figure 3.1c. Other notable differences include product ions at *m/z* 367.1, 393.2, 407.2, 433.2, 447.2, 455.3, and 461.2, which are significantly more abundant in the $[22{:}5(4Z, 7Z, 10Z, 13Z, 16Z) - H + MgPhen]^+$ CID spectrum (Figure 3.1b) than in the $[22{:}5(7Z, 10Z, 13Z, 16Z, 19Z) - H + MgPhen]^+$ CID spectrum (Figure 3.1a), as highlighted with the difference plot (Figure 3.1c). Conversely, product ions such as those observed at *m/z* 317.1, 331.1, 397.2, 409.2, 423.2, and 463.2 are indicative of the 22:5 *n*-3 isomer. By analogy with the comparison of Figure 3.1, all CID spectra of isomeric $[FA - H + MgPhen]^+$ ions in the library were sufficiently unique to allow for unambiguous identification and thus isomeric discrimination.

3.3.2 Relative Quantitation of Isomeric Fatty Acids

Qualitative and quantitative analysis remains a challenge with shotgun lipidomics, as the innate complexity of the cellular lipidome gives rise to a multitude of both isomeric and isobaric lipid species.[14,53,54] Therefore, methods to quantify relative compositions of FA isomers are of interest. We approach this issue using multiple linear regression analysis with the library data in conjunction with data derived from mixtures. It is assumed that the product ions generated from fragmentation of the $[FA - H + MgPhen]^+$ precursor ion population containing multiple FA isomers can be represented by a linear combination of spectra from individual components.

Relative quantitation is first illustrated with octadecenoic (18:1) isomers. Oleic (18:1 *n*-9) and vaccenic (18:1 *n*-7) acids were dissolved in methanol at varying molar ratios, while the total FA concentration was held constant (10 μM). The following theoretical molar ratios of the *n*-9 to *n*-7 18:1 FA (denoted 18:1 *n*-9/n-7) were used: 5/95, 15/85, 50/50, 85/15, and 95/5. Isomeric FA mixtures of 18:1 *n*-9/*n*-7 were ionized in the negative ion mode and transformed in the gas phase to $[18:1 - H + MgPhen]^+$ complex cations (*m/z* 485.2) as detailed above. CID spectra of $[18:1 - H + MgPhen]^+$ generated from 18:1 FA isomer mixtures and individual isomer standards were acquired under identical CID conditions, and product ion abundances were normalized to the base peak in all cases. Normalized product ion abundances from the 18:1 FA isomer mixture were used as responses, while the normalized product ion abundances from individually analyzed 18:1 isomer standards were used as predictors for the multiple linear regression analysis described by equations 1, 2, and 3. Specific diagnostic product ions, referred to as the ion set, were chosen as the basis of quantitation. The ion set utilized represents product ions indicative of double bond position for each 18:1 isomer. The ion set used for 18:1 *n*-9/*n*-7 relative quantitation includes the following product ions (depicted in red font in Figure 3.2a and b): *m/z* 345.1, 357.1, 359.2, 371.2, 373.2, 385.2, 387.2, 399.2, 413.3, and 415.3. Other ion sets were explored, including utilization of all product ions; however, the reported ion set yielded the most accurate results. Figure 3.3 and Figure 3.4 provide structures for the $[18:1 - H + MgPhen]^+$ ions, along with product ion *m/z* ratios from fragmentation of the complex cation for the *n*-9 and *n*-7 isomers, respectively.

The multiple linear regression approach yielded 18:1 *n*-9/*n*-7 isomer ratios of (mean ± standard deviation, $n = 3$) 5.0 ± 0.2/95.0 ± 0.2 (Figure 3.2a), 14 ± 2/86 ± 2, 46 ± 1/54 ± 1, 86.3 ± 0.9/13.7 ± 0.9, and 95.0 ± 0.2/5.0 ± 0.2 (Figure 3.2b), for the expected 18:1 *n*-9/*n*-7 isomeric ratios of 5/95, 15/85, 50/50, 85/15, and 95/5, respectively. The results show relative errors <9% and relative standard deviations <2% over a relatively wide dynamic range of molar ratios (i.e., 5/95 to 95/5). Ultimately, for isomeric monounsaturated FA, we are confident in the ability of the multiple linear regressions approach coupled with gas-phase ion/ion chemistry to both reliably and accurately calculate relative isomeric composition over a broad range of molar ratios for binary mixtures.

FA relative quantitation using multiple linear regression analysis was extended to the analysis of isomeric polyunsaturated fatty acids (PUFA). To illustrate, the *n*-3 and *n*-6 isomers of linolenic acid (18:3) were examined. Again, ion/ion reactions of $[18:3 - H]^-$ anions and

$[Mg(Phen)_3]^{2+}$ dications were used to generate $[18:3 - H + MgPhen]^+$ (*m/z* 481.2) from both isomeric mixtures and individual authentic isomer standards. The isomer ratios investigated for the relative quantitation of 18:3 *n*-3/*n*-6 isomers were identical to those utilized in the 18:1 experiments described above (i.e., 5/95, 15/85, 50/50, 85/15, and 95/5). For relative quantitation of 18:3 *n*-3/*n*-6 isomeric mixtures, the ion set that provided the best results includes product ions at *m/z* 317.1, 329.1, 331.1, 343.1, 345.2, 367.1, 371.2, 381.2, 383.2, 395.2, 397.2, 409.2, 423.2, and 425.2. $[18:3 - H + MgPhen]^+$ CID spectra for the 95/5 and 15/85 isomer ratios of 18:3 *n*-3/*n*-6 are shown in Figure 3.2c and d, respectively. Representative $[FA - H + MgPhen]^+$ structures and fragmentation patterns for the *n*-3 and *n*-6 isomers of FA 18:3 are shown in Figures 3.5 and 3.6, respectively. The results obtained from the analysis of the 15/85, 50/50, 85/15, and 95/5 isomeric ratios of FA 18:3 *n*-3/*n*-6 were (mean ± standard deviation, $n = 3$) 14 ± 2/86 ± 2 (Figure 3.2c), 48 ± 3/52 ± 3, 86 ± 2/14 ± 2, and 96.3 ± 0.4/3.7 ± 0.4 (Figure 3.2d). Again, our results show reasonable accuracy with most relative errors <5% and relative standard deviation <3% for these given isomeric molar ratios. Unfortunately, we were unable to reliably calculate the isomer ratio for the theoretical 5/95 *n*-3/*n*-6 18:3 isomer mixture, as the calculated isomer composition was 1 ± 1/99 ± 1. Thus, the observed limit of relative quantitation was 10% (mol) for the *n*-3 isomer as the minor component. However, this limit was not observed when the *n*-6 isomer was the minor component. The observed limit of relative quantitation for low molar ratios of the *n*-3 isomer relative to the *n*-6 isomer is most likely due the ratio of diagnostic ion abundance to the structurally uninformative product ion abundances. For the 18:3 *n*-3 FA, fewer diagnostic ions are generated relative to structurally uninformative product ions as compared to the relative abundance of diagnostic product ions for the 18:3 *n*-6 isomer.

We attempted to extend the approach to the relative quantitation of a three-component 18:1 isomer mixture. We used the *n*-7, *n*-9, and *n*-12 18:1 FA isomers for these experiments. However, using our approach, we were only able to achieve relative quantitation for isomeric mixtures with high concentrations of the *n*-9 isomer relative to that of the *n*-7 and *n*-12 isomers. A similar difference in diagnostic product ion generation relative to structurally uninformative product ion generation was also observed among the 18:1 isomers. Of the three 18:1 isomers, the *n*-9 isomer had the lowest ratio of diagnostic ions generated in relation to structurally uninformative product ions. Comparatively, the *n*-7 and *n*-12 isomers demonstrated increased ratios for the generation of diagnostic ions relative to structurally uninformative product ions. This decrease in the ratio of

diagnostic ions to structurally uninformative product ions for the *n*-9 isomer equates to reliable relative quantitation only at high concentrations of the *n*-9 isomer relative to the other two 18:1 FA isomers. Furthermore, we also attempted to extend the approach to the relative quantitation of highly unsaturated FA isomers; however, due to extensive fragmentation, these efforts were also unsuccessful.

3.3.3 Fatty Acid Profiling of Bovine Liver Extract

To demonstrate the capabilities of the presented method, we applied ion/ion charge inversion chemistry, the FA library, and the relative quantitation algorithm for the profiling of FA in bovine liver extract (BLE). FA profiles reported are representative of the fraction of lipids ionizable in the negative ion mode (i.e., phosphatidylethanolamine, phosphatidylinositol, phosphatidylserine, etc.). In this polarity, it is important to recognize that phosphatidylcholine (PC) lipids ionize as chloride or acetate adducts; therefore, PC ionization is likely to be less efficient in the negative ion mode relative to some of the other lipid classes. For comparison, our approach is most closely analogous to multistage chromatography for lipid class separation (i.e., TLC) with subsequent hydrolysis and fatty acid analysis (i.e., GC). However, as described above, the entirely gas-phase profiling experiment presented herein is unique in that information regarding the intact phospholipidome and a quantitative, isomer-specific FA profile of the phospholipidome can be obtained from a single experiment. Specifically, we first achieve fractionation of the lipidome via direct ionization of the lipid extract in the negative ion mode, as nonpolar lipids are not readily ionized in this modality. FA identification and relative quantitation are then achieved via an MS^n platform paired with ion/ion charge inversion chemistry. Although not demonstrated here, it is plausible that gas-phase FA profiling via precursor ion scanning could be used to identify lipid precursors for subsequent targeted analysis by ion/ion charge inversion.

To generate the FA profile for BLE, total lipid extract is first ionized in the negative ion mode, as illustrated with Figure 3.7a. To obtain $[FA - H]^-$ anions from complex lipid anions, we employ ion-trap CID over a broad range of m/z ratios. To do so, the excitation frequency is fixed (114.06 kHz) while the RF amplitude in q2 is scanned, producing what is referred to as a ramped ion-trap CID experiment. Over the phospholipid *m/z* range (*m/z* 650−900), ramp CID was used to generate fatty acyl anions directly from the ionized lipid precursor. A second ramp CID was applied over the range of *m/z* 400−650 toproduce [FA − H]− from remaining product ions

generated via the first ramp CID experiment. The result of both ramp CID experiments for BLE is shown in Figure 3.7b. The resulting product ion spectrum is representative of the FA profile of all precursor lipids ionizable in negative ion mode and is enlarged in Figure 3.7c over the *m/z* range of 200−400 (i.e., the FA anion range).

Following generation of FA anions from ionized lipids, positive ion nESI directly generated $[Mg(Phen)_3]^{2+}$ dications. In q2, a mutual storage reaction between the $[FA - H]^-$ anions and the $[Mg(Phen)_3]^{2+}$ dications followed by q2 DDCCID of the resulting mutual storage product ion generated the complexes of interest, $[FA - H + MgPhen]^+$ (Figure 3.8). Note that the *m/z* range in Figure 3.8 is equivalent to that shown in Figure 3.7c. Unidentified product ions were also generated following the ion/ion reaction, as marked in Figure 3.8 with blue circles. Mass-selection and collisional activation of each unidentified product ion (blue circles) indicated that these species were not FA because the fragmentation patterns were inconsistent with those observed via CID of a charge-inverted FA. Additionally, both singly and doubly hydrated product ions are observed following the mutual storage ion/ion reaction and DDC-CID. This observation is discussed in more detail below. To identify FA present in BLE, $[FA - H + MgPhen]^+$ ions were transferred to Q3. Once in Q3, $[FA - H + MgPhen]^+$ complex cations were monoisotopically isolated and subsequently activated via ion-trap CID (q = 0.383). The resulting CID spectra were used to identify FA in BLE via automated spectral matching with the FA library as described above. If applicable, relative compositions of FA isomers were determined using multiple linear regression analysis, also as described above.

The FA profile of BLE is summarized in Table 3.1. To generate the FA profile of BLE, each charge-inverted FA complex cation with a relative abundance >1% (Figure 3.8) was mass-selected and subjected to ion-trap CID. Saturated FAs in BLE include 16:0, 17:0, and 18:0, as confirmed via CID of $[FA - H + MgPhen]^+$. The following polyunsaturated FAs (PUFA) were identified in BLE in the pure *n*-6 form: 18:2(9,12), 20:3(8,11,14), 20:4(5,8,11,14), and 22:4(7,10,13,16). FA 22:5(7,10,13,16,19) existed in the pure *n*-3 form. Thus, all PUFA present in BLE were found to be "pure" (i.e., no double bond positional isomers detectable). The 18:1 FA in BLE existed as a mixture of 18:1(9) and 18:1(11) isomers (i.e., *n*-9 and *n*-7 isomers). Employing our relative quantitation approach, the relative composition of 18:1 isomers was calculated to be 88.4 ± 0.7 and 11.6 ± 0.7 for the 18:1(9) and 18:1(11) isomers, respectively. Our results are in good agreement with a previously developed lipid profile for BLE.[55]

A challenge for any shotgun lipidomics approach arises from the presence of isobaric FA species. In the present case, the ramped CID approach generates FA from all phospholipids in the BLE. We found that using a relatively wide mass isolation for the $[Mg(Phen)_3]^{2+}$ reagent led to isobaric overlap between $[18:1 - H + {}^{24}MgPhen]^+$ and $[18:2 - H + {}^{26}MgPhen]^+$ at *m/z* 485.3, for example. Fortunately, this did not lead to isobaric product ions and did not affect the ability to quantitate 18:1 isomers in BLE, as relative quantitation is based on specific product ions unique to the $[18:1 - H + {}^{24}MgPhen]^+$ precursor ion. Nevertheless, this was confirmed by repeating the experiment using isolated $[{}^{24}Mg(Phen)_3]^{2+}$ reagent ions. While is it straightforward to isolate $[{}^{24}Mg(Phen)_3]^{2+}$ reagent ions prior to reaction, other isobaric interferences can arise when all phospholipids undergo ramped CID with collection of all FA. An alternate approach would be a top-down shotgun lipidomics workflow that would entail the direct negative mode ionization of a complex lipid (or lipid extract), followed by mass-selection of a specific lipid precursor anion. Using traditional MS/MS, class information (phospholipid headgroup) and fatty acyl anions could be obtained from the mass-selected phospholipid precursor ion. Subsequent ion/ion reaction of $[FA - H]^-$ derived from a mass-selected lipid precursor with the $[Mg(Phen)_3]^{2+}$ dications permits identification of FA double bond position(s). This workflow is currently under investigation and is the subject of a future report.

3.4 Conclusions

In this work, we have demonstrated a unique shotgun approach for selective FA profiling of the that provides composition, double bond, and relative quantity (for binary isomeric mixtures) information regarding the phospholipidome. The workflow begins with the generation of phospholipids in the negative ion mode, thereby selecting for polar lipids, followed by ramped CID (i.e., a broad-band activation approach) of all of the lipid anions to release and capture the FA anions from the phospholipids in the precursor ion mixture. All FA anions are then simultaneously subjected to reactions with $[Mg(Phen)_3]^{2+}$ to generate $[FA - H + MgPhen]^+$ cations. Ion trap CID spectra generated from the mixture are then compared to library CID spectra derived from the $[FA - H + MgPhen]^+$ cations of 40 standards. Confident identification of even highly unsaturated FA could be made via the library comparison approach. Furthermore, we demonstrated a method to determine relative compositions of FA double bond positional isomers in binary mixtures via a multiple linear regression approach applied to $[FA - H + MgPhen]^+$ cations. In this case, library

CID spectra serve as predictors, while the spectrum of a mixture serves as the response. A significant advantage of a multiple linear regressions approach is rapid analysis time, as external calibration curve construction is not required; thus, both sample volume requirements and analysis times are greatly reduced. Collectively, the approach provides a relatively rapid and sensitive approach for lipid profiling that provides composition, double bond location, and relative abundance information for binary isomeric mixtures. Variations of this workflow, such as the addition of a precursor ion scan or the use of ion/ion reactions after lipid anion isolation and activation could also, in principle, provide lipid class information.

3.5 References

1. Murphy, R. C. *Tandem Mass Spectrometry of Lipids: Molecular Analysis of Complex Lipids*; RSC Publishing: UK, **2015**; pp 1−39.

2. Murphy, R. C.; Axelsen, P. H. *Mass Spectrom. Rev*. **2011**, 30, 579−599.

3. Han, X. L.; Gross, R. W. *Mass Spectrom. Rev*. **2005**, 24, 367−412.

4. Melo, T.; Montero-Bullon, J.-F.; Domingues, P.; Domingues, M. R. *Redox Biol*. **2019**, 101106−101106.

5. Batthyany, C.; Schopfer, F. J.; Baker, P. R. S.; Duran, R.; Baker, L. M. S.; Huang, Y.; Cervenansky, C.; Branchaud, B. P.; Freeman, B. A. *J. Biol. Chem*. **2006**, 281, 20450−20463.

6. Oh, H. J.; Kim, S. U.; Song, J. W.; Lee, J. H.; Kang, W. R.; Jo, Y. S.; Kim, K. R.; Bornscheuer, U. T.; Oh, D. K.; Park, J. B. *Adv. Synth. Catal*. **2015**, 357, 408−416.

7. Iles, K. E.; Wright, M. M.; Cole, M. P.; Welty, N. E.; Ware, L. B.; Matthay, M. A.; Schopfer, F. J.; Baker, P. R. S.; Agarwal, A.; Freeman, B. A. *Free Radical Biol. Med*. **2009**, 46, 866−875.

8. Vlaeminck, B.; Fievez, V.; Cabrita, A. R. J.; Fonseca, A. J. M.; Dewhurst, R. J. *Anim. Feed Sci. Technol.* **2006**, 131, 389−417.

9. Cascio, G.; Schiera, G.; Di Liegro, I. *Curr. Diabetes Rev*. **2012**, 8, 2−17.

10. Simopoulos, A. P. *Nutrients* **2016**, 8, 17.

11. Kuhajda, F. P. *Nutrition* **2000**, 16, 202−208.

12. Antalis, C. J.; Stevens, L. J.; Campbell, M.; Pazdro, R.; Ericson, K.; Burgess, J. R. *Prostaglandins, Leukotrienes Essent. Fatty Acids* **2006**, 75, 299−308.

13. Richardson, A. J. *Int. Rev. Psychiatry* **2006**, 18, 155−172.

14. Zhang, W. P.; Zhang, D. H.; Chen, Q. H.; Wu, J. H.; Ouyang, Z.; Xia, Y. *Nat. Commun*. **2019**, 10, 10.

15. Hu, C. X.; van der Heijden, R.; Wang, M.; van der Greef, J.; Hankemeier, T.; Xua, G. W. *J. Chromatogr. B-Anal. Technol. Biomed. Life Sci*. **2009**, 877, 2836−2846.

16. Li, F.; Qin, X. Z.; Chen, H. Q.; Qiu, L.; Guo, Y. M.; Liu, H.; Chen, G. Q.; Song, G. G.; Wang, X. D.; Li, F. J.; Guo, S.; Wang, B. H.; Li, Z. L. *Rapid Commun. Mass Spectrom*. **2013**, 27, 24−34.

17. Min, H. K.; Lim, S.; Chung, B. C.; Moon, M. H. *Anal. Bioanal. Chem*. **2011**, 399, 823−830.

18. Mitchell, T. W.; Pham, H.; Thomas, M. C.; Blanksby, S. J. *J. Chromatogr. B: Anal. Technol. Biomed. Life Sci*. **2009**, 877, 2722−2735.

19. Hewawasam, E.; Liu, G.; Jeffery, D. W.; Muhlhausler, B. S.; Gibson, R. A. *Prostaglandins, Leukotrienes Essent. Fatty Acids* **2017**, 125, 1−7.

20. Han, X. L.; Yang, K.; Gross, R. W. *Mass Spectrom. Rev*. **2012**, 31, 134−178.

21. Kerwin, J. L.; Wiens, A. M.; Ericsson, L. H. *J. Mass* Spectrom. **1996**, 31, 184−192.

22. Yang, K.; Zhao, Z.; Gross, R. W.; Han, X. *Anal. Chem*. **2011**, 83, 4243−4250.

23. Brown, S. H. J.; Mitchell, T. W.; Blanksby, S. J. *Biochim. Biophys. Acta, Mol. Cell Biol. Lipids* **2011**, 1811, 807−817.

24. Poad, B. L. J.; Pham, H. T.; Thomas, M. C.; Nealon, J. R.; Campbell, J. L.; Mitchell, T. W.; Blanksby, S. J. *J. Am. Soc. Mass Spectrom*. **2010**, 21, 1989−1999.

25. Thomas, M. C.; Mitchell, T. W.; Blanksby, S. J. *J. Am. Chem. Soc*. **2006**, 128, 58−59.

26. Thomas, M. C.; Mitchell, T. W.; Harman, D. G.; Deeley, J. M.; Murphy, R. C.; Blanksby, S. J. *Anal. Chem*. **2007**, 79, 5013−5022.

27. Thomas, M. C.; Mitchell, T. W.; Harman, D. G.; Deeley, J. M.; Nealon, J. R.; Blanksby, S. J. *Anal. Chem*. **2008**, 80, 303−311.

28. Thomas, M. C.; Mitchell, T. W.; Blanksby, S. J. *Methods Mol. Biol*. **2009**, 579, 413−441.

29. Ma, X. X.; Xia, Y. *Angew. Chem., Int. Ed*. **2014**, 53, 2592−2596.

30. Ma, X. X.; Chong, L.; Tian, R.; Shi, R. Y.; Hu, T. Y.; Ouyang, Z.; Xia, Y. *Proc. Natl. Acad. Sci. U. S. A.* **2016**, 113, 2573−2578.

31. Stinson, C. A.; Xia, Y. *Analyst* **2016**, 141, 3696−3704.

32. Paine, M. R. L.; Poad, B. L. J.; Eijkel, G. B.; Marshall, D. L.; Blanksby, S. J.; Heeren, R. M. A.; Ellis, S. R. *Angew. Chem., Int. Ed.* **2018**, 57, 10530−10534.

33. Wang, M.; Han, R. H.; Han, X. L. *Anal. Chem*. **2013**, 85, 9312−9320.

34. Yang, K.; Dilthey, B. G.; Gross, R. W. *Anal. Chem*. **2013**, 85, 9742−9750.

35. Adams, J.; Gross, M. L. *Anal. Chem*. **1987**, 59, 1576−1582.

36. Davoli, E.; Gross, M. L. *J. Am. Soc. Mass Spectrom*. **1990**, 1, 320−324.

37. Gross, M. L. *Int. J. Mass Spectrom. Ion Processes* **1992**, 118, 137−165.

38. Hsu, F. F.; Turk, J. *J. Am. Soc. Mass Spectrom*. **2010**, 21, 657−669.

39. Trimpin, S.; Clemmer, D. E.; McEwen, C. N. *J. Am. Soc. Mass Spectrom*. **2007**, 18, 1967−1972.

40. Hsu, F. F.; Turk, J. *J. Am. Soc. Mass Spectrom*. **1999**, 10, 600−612.

41. Hsu, F. F.; Turk, J. *J. Am. Soc. Mass Spectrom*. **2008**, 19, 1673−1680.

42. Afonso, C.; Riu, A.; Xu, Y.; Fournier, F.; Tabet, J. C. *J. Mass Spectrom*. **2005**, 40, 342−349.

43. Duncan, K. D.; Volmer, D. A.; Gill, C. G.; Krogh, E. T. *J. Am. Soc. Mass Spectrom*. **2016**, 27, 443−450.

44. Hale, O. J.; Cramer, R. *Anal. Bioanal. Chem*. **2018**, 410, 1435−1444.

45. Randolph, C. E.; Foreman, D. J.; Betancourt, S. K.; Blanksby, S. J.; McLuckey, S. A. *Anal. Chem*. **2018**, 90, 12861.

46. Newton, K. A.; Amunugama, R.; McLuckey, S. A. *J. Phys. Chem. A* **2005**, 109, 3608−3616.

47. Astudillo, A. M.; Meana, C.; Guijas, C.; Pereira, L.; Lebrero, P.; Balboa, M. A.; Balsinde, J. *J. Lipid Res*. **2018**, 59, 237−249.

48. Liebisch, G.; Vizcaino, J. A.; Kofeler, H.; Trotzmuller, M.; Griffiths, W. J.; Schmitz, G.; Spener, F.; Wakelam, M. J. O. *J. Lipid Res*. **2013**, 54, 1523−1530.

49. Yu, X.; Jin, W.; McLuckey, S. A.; Londry, F. A.; Hager, J. W. J. *Am. Soc. Mass Spectrom*. **2005**, 16, 71−81.

50. Xia, Y.; Liang, X. R.; McLuckey, S. A. *J. Am. Soc. Mass Spectrom*. **2005**, 16, 1750−1756.

51. Webb, I. K.; Londry, F. A.; McLuckey, S. A. *Rapid Commun. Mass Spectrom*. **2011**, 25, 2500−2510.

52. Londry, F. A.; Hager, J. W. *J. Am. Soc. Mass Spectrom*. **2003**, 14, 1130−1147.

53. Sansone, A.; Tolika, E.; Louka, M.; Sunda, V.; Deplano, S.; Melchiorre, M.; Anagnostopoulos, D.; Chatgilialoglu, C.; Formisano, C.; Di Micco, R.; Mennella, M. R. F.; Ferreri, C. *Plos One*. **2016**, 11, 11.

54. Shevchenko, A.; Simons, K. *Nat. Rev. Mol. Cell Biol*. **2010**, 11, 593−598.

55. Franklin, E. T.; Betancourt, S. K.; Randolph, C. E.; McLuckey, S. A.; Xia, Y. *Anal. Bioanal. Chem*. **2019**, 1 DOI: 10.1007/s00216-018-1537-1.

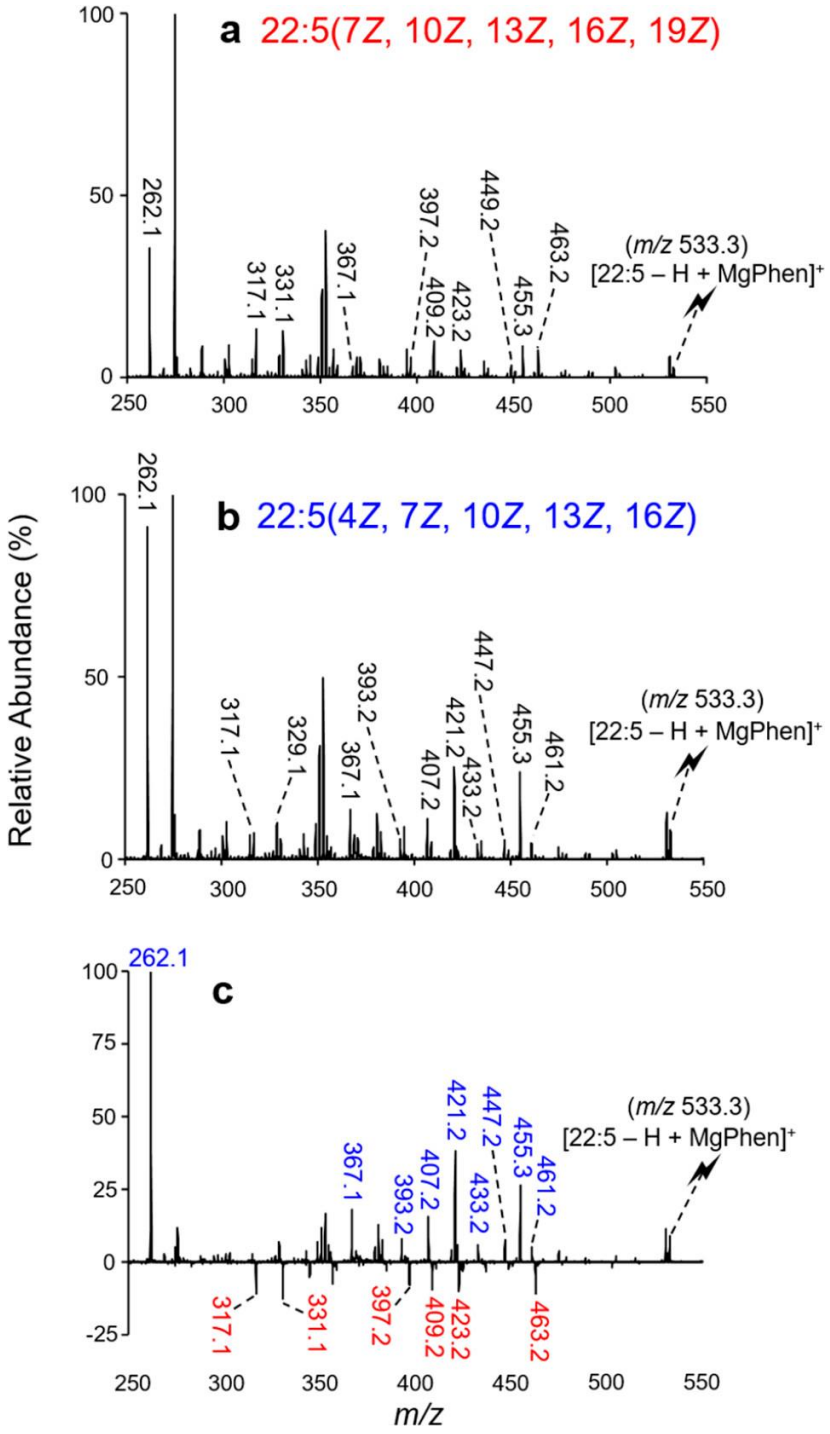

Figure 3.1 CID spectra resulting from the activation of (a) [22:5(7*Z*, 10*Z*, 13*Z*, 16*Z*, 19*Z*) – H + MgPhen]$^+$ and (b) [22:5(4*Z*, 7*Z*, 10*Z*, 13*Z*, 16*Z*) – H + MgPhen]$^+$. (c) Difference plot ((*n*-6) – (*n*-3)) highlighting the distinguishing product ions for 22:5 isomer differentiation.

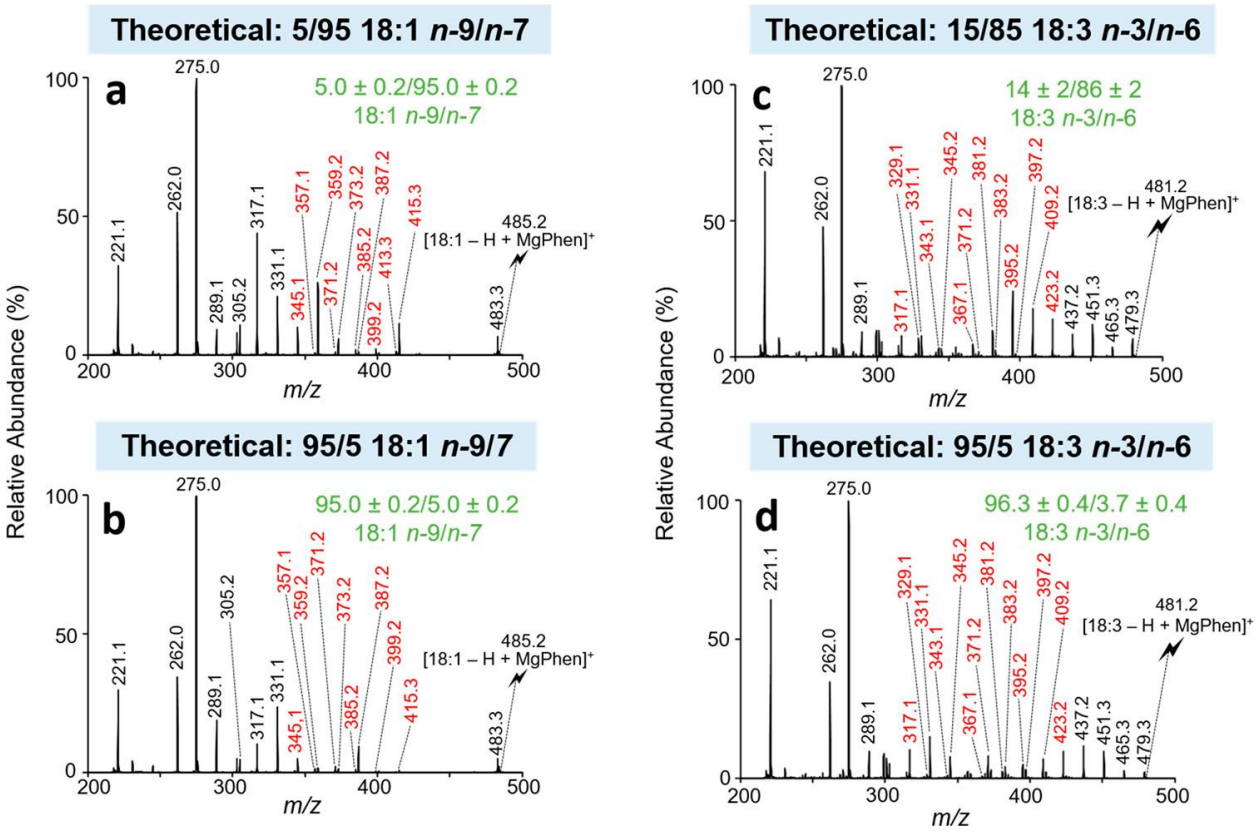

Figure 3.2 CID spectra representative of isomeric FA mixtures analyzed as the charge-inverted FA complex cation, $[FA - H + MgPhen]^+$. CID spectra of $[18:1 - H + MgPhen]^+$ for the isomeric mixture of 18:1 *n*-9/*n*-7 at the molar ratios of (a) 5/95 and (b) 95/5. CID spectra of $[18:3 - H + MgPhen]^+$ for the isomeric mixture of 18:3 *n*-3/*n*-6 at the molar ratios of (c) 15/85 and (d) 95/5. Product ions used for relative quantitation are shown in red. Calculated isomer compositions (mean ± standard deviation, $n = 3$) are shown in green. The lightning bolt signifies the precursor ion subjected to ion-trap CID.

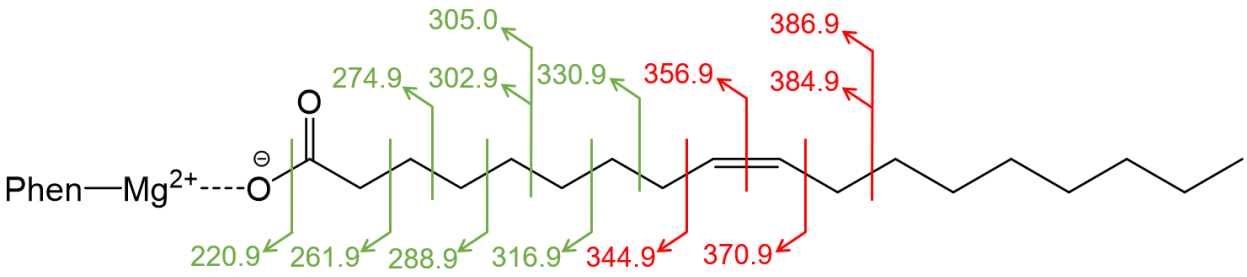

Figure 3.3 Structure and fragmentation pattern of $[FA - H + MgPhen]^+$ ion where FA = 18:1(9*Z*) (*i.e.* the *n*-9 isomer).

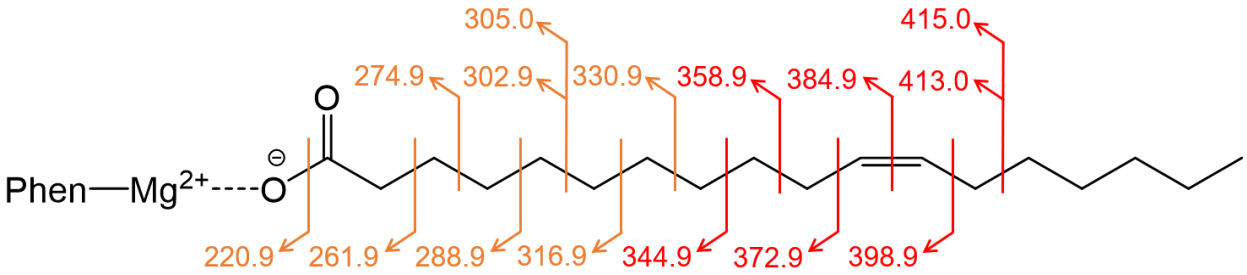

Figure 3.4 Structure and fragmentation pattern of [FA – H + MgPhen]$^+$ ion where FA = 18:1(11*Z*) (*i.e.* the *n*-7 isomer).

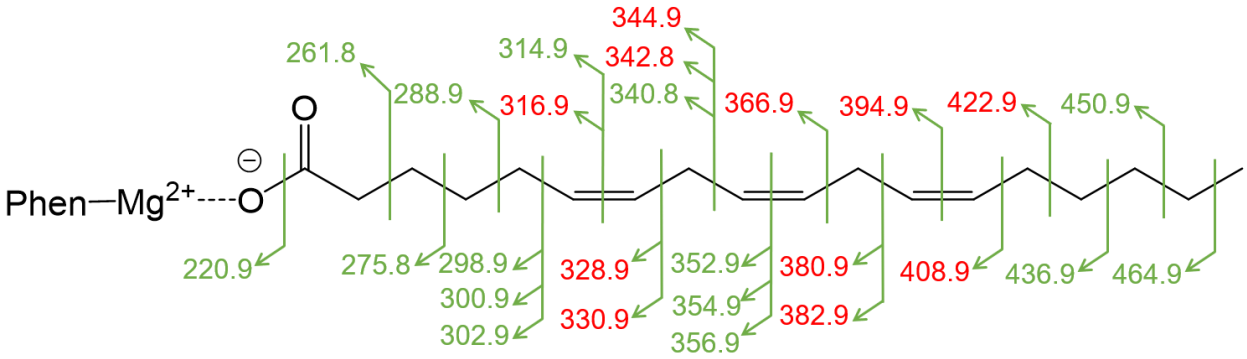

Figure 3.5 Structure and fragmentation pattern of $[FA - H + MgPhen]^+$ ion where FA = 18:3(6*Z*,9*Z*,12*Z*) (*i.e.* the *n*-6 isomer).

Figure 3.6 Structure and fragmentation pattern of $[FA - H + MgPhen]^+$ ion where FA = 18:3(9*Z*,12*Z*,15*Z*) (*i.e.* the *n*-3 isomer).

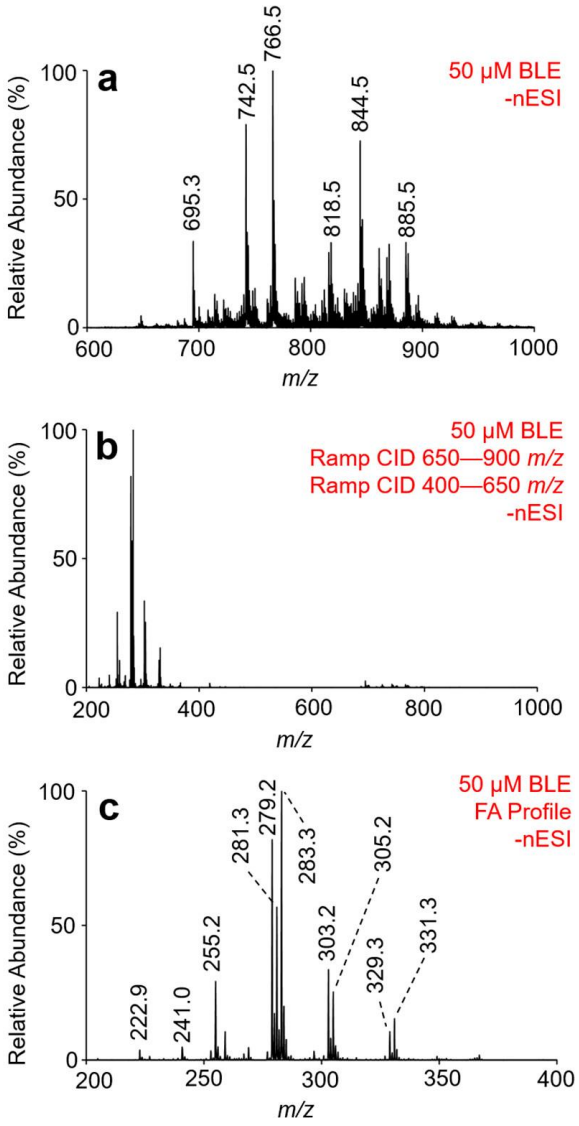

Figure 3.7 Demonstration of gas-phase generation of fatty acyl anions from bovine liver extract. (a) Nano-ESI mass spectrum of 50 μM BLE obtained via direct negative ion mode ionization. (b) Fatty acid profile CID spectrum resulting from collisional activation of BLE precursors in the phospholipid range (*m*/*z* 650–900), followed by a subsequent collisional activation of remaining anions from *m*/*z* 400 to 650. (c) Enlargements of the fatty acid profile shown in panel (b) over the mass-to-charge range of 200–400.

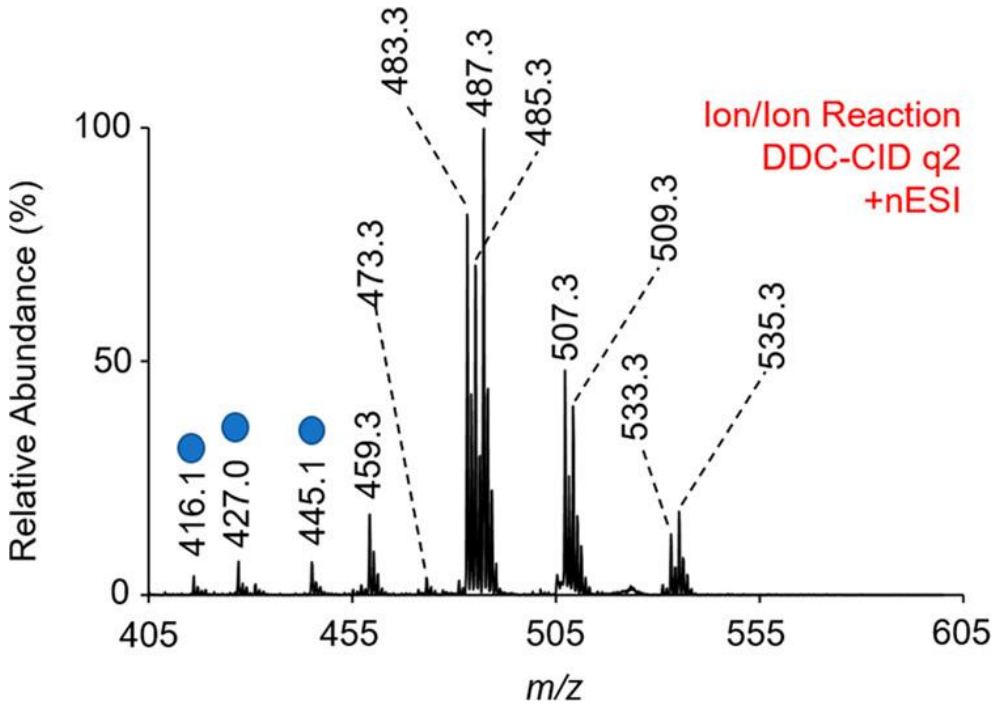

Figure 3.8 Mass spectrum resulting from the gas-phase ion/ion reaction of $[Mg(Phen)_3]^{2+}$ dications with fatty acyl anions derived from bovine liver extract via the described ion/ion chemistry. Peaks labeled with the blue circle are not fatty acids, as confirmed by CID of the precursor ion.

Table 3.1 Fatty Acid Profile of Bovine Liver Phospholipidome (Polar Bovine Liver Extract)

m/z	Fatty Acid Composition	Double Bond Position(s)	Relative Abundance (mean ± SD)
459.3	16:0	N/A	—
473.3	17:0	N/A	—
487.3	18:0	N/A	—
485.3	18:1	9 and 11	88.4 ± 0.7 and 11.6 ± 0.7
483.3	18:2	9, 12	—
509.3	20:3	8, 11, 14	—
507.3	20:4	5, 8, 11, 14	—
535.3	22:4	7, 10, 13, 16	—
533.3	22:5	7, 10, 13, 16, 19	—

CHAPTER 4. TOWARD COMPLETE STRUCTURE ELUCIDATION OF GLYCEROPHOSPHOLIPIDS IN THE GAS PHASE THROUGH CHARGE INVERSION ION/ION CHEMISTRY

4.1 Introduction

Glycerophospholipids (GPLs) are universal cellular components, accounting for nearly 60 mol% of lipid mass in eukaryotic cells.[1] The primary role of GPLs is to define the lipid bilayer (cellular membrane), which encompasses not only individual cells but also intracellular organelles.[2] While most cellular GPLs serve as architectural components of the lipid bilayer, GPLs also function as energy storage and signaling molecules.[2] The general GPL structure includes three main components: a glycerol backbone, a functionalized phosphate ester group, and fatty acyl (or alkyl ether) chains. The phosphate moiety is esterified at the *sn*-3 position of the glycerol backbone and is also coupled to a polar functional group (e.g., choline, ethanolamine, serine, inositol, or glycerol), commonly referred to as the headgroup. The most commonly observed GPL structure in eukaryotes is the diacyl (phosphatidyl) subclass wherein fatty acids (FAs) are esterified at the *sn*-1 and *sn*-2 positions of the glycerol backbone. Thus, extensive molecular diversity results from variations both in the headgroup and the fatty acyl substituents where composition can vary based on chain length, degree of unsaturation, site(s) of unsaturation, and stereochemistry. Considering just the commonly occurring headgroups and a pool of just 40 fatty acids, thousands of theoretical GPL structures can be constructed, including a multitude of isomeric or isobaric molecular structures.[3]

Mass spectrometry (MS) has proven to be a useful tool for both quantitative and qualitative analysis of lipids, including GPLs. Early MS studies of GPL used soft ionization methods such as fast-atom bombardment (FAB),[4,5] chemical ionization,[6] and field desorption.[7,8] However, these ionization methods were largely supplanted by electrospray ionization (ESI).[1] ESI readily generates both the $[M - H]^-$ and $[M + H]^+$ ions for GPLs in the negative ion and positive ion modes, respectively. The preference for a GPL to form protonated or deprotonated molecules is dictated by acid−base chemistry (or, in the case of choline, the existing fixed positive charge) of the polar headgroup, and thus, there exists a strong propensity of an individual GPL class to be detected in positive or negative ion mode ESI.[1,2,9] Specifically, anionic GPLs including phosphatidylethanolamine (PE), phosphatidylglycerol (PG), phosphatidylserine (PS),

phosphatidylinositol (PI), and phosphatic acid (PA) are readily observed in the negative ion mode as $[M - H]^-$ species. Conversely, phosphatidylcholines (PCs) lipids are neutral polar molecules, possessing a quaternary ammonium moiety that permits efficient ionization of PC in positive ion mode, generating $[M + H]^+$ ions. PC ionization in negative ion mode can also be achieved and relies on the addition of a dopant to the ESI solution to facilitate formation of an adduct ion (e.g., $[M + X]^-$ where X = Cl or CH_3CO_2).

While liquid chromatography (LC) coupled to MS has been a mainstay in lipid analysis, shotgun electrospray ionization tandem mass spectrometry (ESI-MS/MS) has gained popularity due to ease of use, reduced sample volumes, and shorter analysis times.[1] Utilizing ESI-MS/MS, collision-induced dissociation (CID) of GPL ions provides information regarding the GPL headgroup and fatty acyl composition. GPL classes can be individually detected via exploitation of neutral loss and precursor ion scans.[10] Additionally, in negative ion mode, CID of the GPL anion cleaves ester bonds at the *sn*-1 and *sn*-2 positions, liberating fatty acyl chains as abundant carboxylate product ions. The information extracted from such ESI-MS/MS experiments can facilitate assignment of the lipid subclass and acyl chain composition of a given GPL, resulting in a so-called molecular lipid assignment (e.g., PC 16:0_18:1).[11] While informative, the molecular lipid assignment fails to define both (i) the relative position of acyl chains on the glycerol backbone (i.e., sn-position) or (ii) the site(s) of carbon−carbon double bonds in an unsaturated acyl chain. The absence of this structural information is problematic for a number of reasons. First, failing to define *sn*- and double bond locations masks the possible presence of multiple isomeric contributors and thus fails to represent the natural diversity of a given GPL. Second, alterations in chemical structure influence both biophysical and biochemical properties of lipids. For example, differences in double bond position(s) in fatty acyl substituents can have profound effects on GPL physical properties such as solubility, fluidity, and thermodynamic stability that have consequences for their biological function(s).[12−14] Furthermore, a growing body of research suggests that alterations in the relative abundances of lipid isomers – indistinguishable by conventional ESI-MS/MS – could be sensitive markers for the onset and progression of numerous chronic diseases such as type-2 diabetes,[15] cardiovascular disease,[16] obesity,[17] neurodegenerative disease,[18] and several types of cancer.[19−23] Thus, analytical methods capable of providing more complete structural assignments of GPL are integral to furthering current understanding of lipid biochemistry and the roles of lipids in health and disease.[24]

As carbon−carbon double bond localization in unsaturated GPLs cannot be readily achieved with ESI-MS/MS methods relying on traditional, low-energy CID, a number of solution-based derivatization strategies and gas-phase ion chemistries have been explored to assign sites of unsaturation in GPLs. Pioneered by the Xia group, the solution phase Paternò−Büchi (PB) reaction involves derivatization of unsaturated lipids via selective addition of acetone to carbon−carbon double bond(s) (C=C) upon exposure to 254 nm ultraviolet radiation.[25−28] Low-energy CID of PB-modified lipids generates a pair of diagnostic product ions revealing the location of each double bond. Ultimately, while effective, the PB reaction is reliant on wet-chemical modification of unsaturated lipids and can suffer from low reaction yields. In turn, low derivatization efficiency can lead to partially modified or unreacted lipid species. As an alternate approach, recent work suggests solution-based epoxidation of unsaturated lipids can be achieved with high efficiency.[29] CID of the epoxidated lipid ion provides C=C location(s), yet this approach is largely unexplored compared to its PB counterpart and still reliant on solution-based lipid derivatization.

Based on gas-phase chemistry, ozone-induced dissociation (OzID) has received considerable attention for the structural elucidation of unsaturated lipids.[30−32] Specifically, OzID is a unique ion-activation method that exploits ion/molecule reactions between mass-selected unsaturated lipid ions and ozone vapor. Often in tandem with low-energy CID, OzID permits the identification of not only sites of unsaturation but also assignment of the *sn*-position of fatty acyl chains in GPLs, and in some instances, double bond geometry (i.e., *E*/*Z*) has been assigned.[33] Despite a wealth of structural information obtained using OzID, ion−molecule reactions can be slow, due to low reagent molecule densities and/or small rate constants, leading to low product ion abundances, and thus, longer integration times can be required, impacting sensitivity. While recent implementations of OzID have exploited higher pressure regions within the mass spectrometer to improve reaction efficiency, ion−ion reactions have potential advantages over ion−molecule chemistries for efficient structural characterization in the gas phase.[34,35]

Recently, we reported the use of gas-phase ion/ion charge inversion reactions for the structural elucidation of fatty acids.[36,37] In comparison to solution-based strategies, use of gas-phase ion/ion reactions for lipid analysis presents several advantages. For example, electrospray and solution conditions can be optimized for each reagent, including lipid analytes. Furthermore, gas-phase ion/ion reactions provide the ability to switch between charge states on-demand and undertake facile, highly efficient, and structure-selective derivatization. For instance, we have

previously reported that singly deprotonated FA anions (i.e., $[FA - H]^-$) react in the gas phase with trisphenanthroline magnesium dications, $[MgPhen_3]^{2+}$, to form the long-lived electrostatic complex ion composed of the magnesium dication, phenanthroline ligand, and deprotonated fatty acid (i.e., $[FA - H + MgPhen]^+$). Low-energy CID of $[FA - H + MgPhen]^+$ permits unambiguous FA identification and consequent isomer discrimination and relative quantitation.[37] Herein, we describe a top-down shotgun lipidomics approach toward in-depth GPL structural elucidation utilizing gas-phase ion/ion charge inversion and derivatization chemistries. To do this experiment, the GPL was first ionized, mass-selected, and collisionally activated in negative ion mode to liberate fatty acyl carboxylate anions (i.e., $[FA - H]^-$) carried by the glycerophospholipid precursor. Subsequent ion/ion reaction between these product anions and the charge inversion reagent dications (i.e., $[MgPhen_3]^{2+}$) resulted in the generation of $[FA - H + MgPhen]^+$ ions. Reisolation and CID of charge-inverted FA complex cations yield diagnostic spectra permitting confident assignment of FA double bond position(s) and calculation of the relative composition of isomeric FA mixtures. In total, this experiment provides near-complete structural information on the initial mass-selected GPL including information headgroup assignment, fatty acyl composition, site(s) of unsaturation, and, in some cases, relative abundances of isomeric fatty acyl substituents. Application of the developed ion/ion method to the analysis of targeted GPLs in human plasma extracts reveals the presence of isomeric GPLs that would be unresolved by conventional ESI-MS/MS platforms.

4.2 Experimental

4.2.1 Materials

HPLC-grade methanol, water, and chloroform were purchased from Fisher Scientific (Pittsburgh, PA). Magnesium chloride, ammonium acetate, 1,10-phenanthroline (Phen), and citrated human blood plasma were purchased from Sigma-Aldrich (St. Louis, MO). All lipid standards were purchased from Avanti Polar Lipids, Inc. (Alabaster, AL).

4.2.2 Lipid Extraction and Preparation of nESI Solutions

Solutions of lipid standards were prepared in methanol to a final concentration of 5 μM. Magnesium chloride and 1,10-phenanthroline were combined in methanolic solution to a final concentration of 20 μM.

Lipids were extracted from human plasma according to the Folch method.[38] Briefly, 50 μL of human plasma was added to 375 μL of methanol and vortexed for 30 s. Then, 750 μL of chloroform was added to the mixture. The resulting mixture was incubated for 1 h at room temperature in a shaker. Next, 312.5 μL of water was added to induce phase separation. After sitting for 10 min at room temperature, the mixture was centrifuged at 1000g for 10 min. Following centrifugation, the chloroform (lower) layer was collected and subsequently dried in a vacuum centrifuge. The dried organic phase was reconstituted in 1000 μL of methanol with 10 mM ammonium acetate prior to MS analysis.

4.2.3 Nomenclature

When possible, we adopt the shorthand notation recommended by Liebisch et al.[11] Briefly, GPL classes are abbreviated as follows: phosphatidylcholine (PC), phosphatidylethanolamine (PE), phosphatidylglycerol (PG), phosphatidylinositol (PI), phosphatidylserine (PS), and phosphatidic acid (PA). Fatty acyl substituents are described by the total number of carbons, as indicated before the colon, the total number of double bonds, as indicated after the colon, and identified double bond position(s), as indicated within parentheses (i.e., 18:1(9) represents an 18-carbon chain with 1 double bond between carbon-9 and -10 as numbered from the carboxylate moiety). If geometry is known, the double bond positional number is followed by *Z* for cis or *E* for trans, e.g., 18:1(9*Z*). Where regiochemistry of fatty acyl chains is identified, the fatty acyl substituents reported before and after a forward slash (i.e., PC 16:0/18:1) represent the fatty acids esterified to the *sn*-1 and *sn*-2 positions of the glycerol backbone, respectively. However, if regiochemistry is unknown, the fatty acyl substituents are separated by an underscore (i.e., PC 16:0_18:1).

4.2.4 Mass Spectrometry

All data were collected on a Sciex QTRAP 4000 hybrid triple quadrupole/linear ion-trap mass spectrometer (SCIEX, Concord, ON, Canada) with modifications analogous to those previously described.[39] Alternately pulsed nanoelectrospray ionization (nESI) allows for sequential injection of lipid anions and tris-phenanthroline magnesium dications, $[Mg(Phen)_3]^{2+}$.[40] First, the lipid anion was generated in negative ion mode via nESI. The lipid anion was then isolated during transit through Q1 and sent to the high-pressure collision cell, q2, for storage. In q2, ion-trap CID of the lipid anion generated the fatty acyl anions, denoted $[FA - H]^-$. Next, direct positive nESI was used to generate $[Mg(Phen)_3]^{2+}$. Following ionization, $[Mg(Phen)_3]^{2+}$ was mass-selected in Q1 and transferred to q2 for storage. In q2, product ions resulting from collisional activation of the lipid anion, including $[FA - H]^-$ anions, and $[Mg(Phen)_3]^{2+}$ dications were simultaneously stored for 500 ms. The ion/ion reaction produced charge-inverted product ions. Next, beam-type CID was used to simultaneously collisionally activate product ions and transfer them to the low-pressure linear ion trap (LIT), Q3. Charge-inverted FA complex cations (i.e., $[FA - H + MgPhen]^+$) were then mass-selected using a 1 Th window and subjected to collisional activation via single frequency resonance excitation (q = 0.383). Product ions generated from CID were analyzed via mass-selective axial ejection (MSAE).[41]

4.3 Results and Discussion

4.3.1 Generation of $[FA - H + MgPhen]^+$ Complex Cations from GPL Anions

Scheme 4.1 illustrates the generation of $[FA - H + MgPhen]^+$ complex cations from the gas-phase ion/ion reaction between reagent dications and fatty acyl carboxylate anions liberated from a GPL precursor anion. In negative ion mode, GPLs are first ionized via direct negative nESI, generating abundant $[M - H]^-$ for the classes PE, PS, PI, PG, and PA. Due to the quaternary ammonium moiety of PC, ionization of PC lipids in the negative ion mode required generation of the chloride or acetate adduct ion (i.e., $[PC + X]^-$ where X = Cl or CH_3CO_2). Next, the GPL anion was mass-selected during transit through Q1 and then transferred to the high-pressure collision cell q2. Once in q2, single frequency resonance excitation was used to collisionally activate the lipid precursor anion. Ion-trap CID of the mass-selected $[M - H]^-$ ion for unsaturated PE, PI, PG, and PA synthetic standards directly generated $[FA - H]^-$ anions via cleavage of the ester bonds at

the *sn*-1 and *sn*-2 positions. Consistent with previous reports,[42–47] additional fragment ions reflecting neutral losses of the *sn*-1 and *sn*-2 substituents as acids and ketenes were also observed. To release FA anions from PC and PS lipid precursor anions, two q2 CID steps were required. Specifically, CID of $[PC + X]^-$ (X = Cl or CH_3CO_2) generated the demethylated PC anion (i.e., $[PC - CH_3]^-$), while activation of $[PS - H]^-$ produced a fragment ion derived from neutral loss of the serine headgroup (loss of $C_4H_5NO_2$, 87 Da). Subsequent ion-trap CID of the $[PC - CH_3]^-$ and $[PS - H - C_4H_5NO_2]^-$ ions resulted in cleavage of the *sn*-1 and *sn*-2 ester bonds and generation of $[FA - H]^-$ anions.

To generate charge-inverted FA complex cations, all fragment ions, including $[FA - H]^-$ ions, were allowed to react with the tris-phenanthroline magnesium dications. The $[FA - H]^-$ anions are transformed in the gas phase to $[FA - H + MgPhen_2]^+$ by ion/ion reaction, as previously described.[36,37] All ion/ion product ions were then activated via beam-type CID (BT CID). BT CID resulted mostly in the formation of $[FA - H + MgPhen]^+$ ions, and ultimately, fatty acyl double bond positions can be pinpointed from $[FA - H + MgPhen]^+$ CID spectral matching to a previously constructed FA library.[37]

4.3.2 Identification of Double Bond Position(s) in Synthetic GPL

We first demonstrate the overall approach using synthetic PE 16:0/18:1(9*Z*). Direct negative ion nESI of PE 16:0/18:1(9*Z*) generated abundant $[PE - H]^-$ anions at *m/z* 716.5 (Figure 4.1a). To probe fatty acyl composition of this reference compound, ion-trap CID of $[PE - H]^-$ was employed. The MS/MS spectrum of PE 16:0/18:1(9Z), as shown in Figure 4.1c, displays structurally informative product ions relating to the fatty acyl substituents. Consistent with previous reports,[42] product ions arising from losses of both fatty acyl substituents were observed. For example, the product ions observed at *m/z* 478.3 and 452.3 reflect losses of the *sn*-1 (i.e., $[PE - H - R_1CH{=}C{=}O]^-$) and sn-2 (i.e., $[PE - H - R_2'\ CH{=}C{=}O]^-$) acyl chains as ketenes, whereas those observed at *m/z* 460.3 and 434.3 represent losses of the *sn*-1 and *sn*-2 acyl chains as fatty acids, denoted $[PE - H - R_1COOH]^-$ and $[PE - H - R_2COOH]^-$, respectively (Figure 4.1c). Dominating the CID spectrum are the $[16:0 - H]^-$ (*m/z* 255.2) and $[18:1 - H]^-$ (*m/z* 281.2) carboxylate fragment anions reflective of the fatty acyl substituents carried by the PE precursor ion at the *sn*-1 and *sn*-2 positions, respectively. The greater abundance of the $[18:1 - H]^-$ fragment ion relative to the $[16:0 - H]^-$ ion is in good agreement with previous observations,[42] suggesting

the formation of the carboxylate anion from the *sn*-2 acyl substituent. It is important to note that for unknown lipids, the relative abundances of the carboxylate anions alone (or related ketene and fatty acid loss fragments) are insufficient to quantitatively assign fatty acyl regiochemistry (i.e., *sn*-1 or *sn*-2) without calibration to standards. It can, however, provide a useful guide as to the dominant regiochemistry (i.e., the most abundant regioisomer).[48]

The charge inversion process begins with the product ions generated from CID of $[PE - H]^-$ (shown in Figure 4.1c). All fragment ions generated via activation of the deprotonated PE anion (Figure 4.1c) were subjected to ion/ion reaction with the $[MgPhen_3]^{2+}$ dications. Charge inversion proceeds via the formation of long-lived electrostatic complexes comprised of the anion, two phenanthroline ligands, and the magnesium metal dication. The product ion spectrum resulting from the ion/ion reaction between the fragment ions of $[PE\ 16:0/18:1 - H]^-$ and $[MgPhen_3]^{2+}$ is shown in Figure 4.1d. The dominant mutual storage product ions observed are the charge-inverted FA cations $[16:0 - H + MgPhen_2]^+$ (*m/z* 639.3) and $[18:1(9Z) - H + MgPhen_2]^+$ (*m/z* 665.4). Notably, the relative abundances of the FA anions (i.e., $[FA - H]^-$ from Figure 4.1c) and the charge-inverted FA cations (i.e., $[FA - H + MgPhen_2]^+$ from Figure 4.1d) were conserved. More so, FA anion charge inversion appears to be nearly unit efficient, as there was no evidence for FA anion neutralization via proton-transfer reaction with tris-phenanthroline magnesium complex cations.[36] Charge-inverted product ions reflecting the loss of the *sn*-1 fatty acyl as a fatty acid (i.e., $[PE - H - R_1COOH + MgPhen_2]^+$) and a ketene (i.e., $[PE - H - R_1'\ CH{=}C{=}O + MgPhen_2]^+$) were also observed at *m/z* 844.4 and 862.4, respectively. Similarly, the product ions representing *sn*-2 fatty acyl loss as both a fatty acid, $[PE - H - R_2COOH + MgPhen_2]^+$ (*m/z* 818.4), and ketene, $[PE - H - R_2'\ CH{=}C{=}O + MgPhen_2]^+$ (*m/z* 836.4), were also charge-inverted via ion/ ion reaction with $[MgPhen_3]^{2+}$ dications. Following the ion/ ion reaction, BT CID was then employed, yielding the spectrum shown in Figure 4.1e. The dominant product ions observed in Figure 4.1e are [18:1(9*Z*) − H + MgPhen]+ (*m/z* 485.3) and [16:0 − H + MgPhen]+ (*m/z* 459.3), generated via the neutral loss of a phenanthroline ligand from each of the analogous charge-inverted FA cations observed in Figure 4.1d. Also depicted in Figure 4.1e are a variety of low-abundance product ions reflecting neutral losses of the ethanolamine headgroup and a phenanthroline ligand from their respective charge-inverted mutual storage product ions. Specifically, these fragment ions were assigned as $[PE - H - R_1'\ CH{=}C{=}O - CH_2CH_2NH + MgPhen]^+$ (*m/z* 639.3), $[PE - H - R_1COOH - CH_2CH_2NH + MgPhen]+$ (*m/z* 621.3), $[PE - H - R_2'\ CH{=}C{=}O - CH_2CH_2NH + MgPhen]^+$

(*m/z* 613.3), and [PE − H − R_2COOH − CH_2CH_2NH + MgPhen]$^+$ (*m/z* 595.3). Lastly, to assign the double bond position unambiguously, the desired [FA − H + MgPhen]$^+$ ion was mass-selected with unit resolution and activated via ion-trap CID. In the case of PE 16:0/18:1(9*Z*), the C9=C10 double bond position was confirmed via observation of the spectral gap (highlighted in green shading) in the resulting CID product ion spectrum of [18:1(9*Z*) − H + MgPhen]$^+$ (Figure 4.1f).[36] Briefly, the spectral gap shown in Figure 4.1f results from dramatic suppression in the abundance of product ions arising from carbon−carbon cleavages vinylic to the double bond (i.e., *m/z* 345.2 and 371.2) and fragmentation of the C9=C10 double bond (i.e., *m/z* 357.2). More so, perturbation of the 14 Da spacing further confirms the C9=C10 double bond position, as the differential between *m/z* 345.2 and *m/z* 357.2 is 12 Da.

In total, the workflow first relies on ionization and collisional activation of the GPL precursor ion in negative ion mode to release fatty acyl substituents as carboxylate anions. As all GPL classes can be ionized in negative ion mode, fatty acyl anions can be liberated from any GPL precursor anion regardless of headgroup composition using low-energy CID. Thus, gas-phase ion/ion chemistry can be applied to assign GPL structure, including double bond position(s), independent of the polar headgroup present. To demonstrate, this method was applied to analyze the following synthetic GPL standards of varying headgroup and fatty acyl composition: PE 18:0/20:4(5*Z*,8*Z*,11*Z*,14*Z*), PC 16:0/18:1(9*Z*), PS 16:0/18:1(9*Z*), PI 16:0/18:1(9*Z*), PG 16:0/18:1(9*Z*), and PA 16:0/18:1(9*Z*). Data for these experiments are shown in Figures 4.2−4.9. As previously noted,[42−47] each GPL class (i.e., PE, PS, PC, etc.) exhibits some class-specific fragmentation behavior upon collisional activation, and charge inversion behavior is consequently influenced. That said, all GPL classes yield abundant fatty acyl anions, and thus, other variations in CID behavior do not interfere with the ability to confidently pinpoint carbon−carbon double bond position(s) across all species. Indeed, the final CID mass spectra of [18:1(9*Z*) − H + MgPhen]$^+$ derived by ion/ion chemistries from PC, PS, PI, PG, and PA complex lipids are identical and can further be matched explicitly to reference spectra previously generated from unesterified oleic acid.

4.3.3 Identification of Human Plasma Lipids

Human blood plasma is an exceedingly complex biological fluid rich in lipids, as more than 1500 lipids have been putatively identified.[49,50] Recently, characterization of the human blood

plasma lipidome has received much attention, as changes in the plasma lipidome have been widely studied with hopes of identifying potential disease biomarkers. Specifically, plasma lipid biomarkers have been proposed for a variety of disease pathologies including prostate cancer, Alzheimer's disease, cardiovascular disease, and many others.[51] However, many of these potential plasma lipid biomarkers have only been identified at the sum compositional level, neglecting to clearly differentiate among potential isomeric structures that likely exist. To demonstrate the utility of gas-phase ion/ion chemistry for the structural characterization of GPL, we applied this approach to examine GPL extracted from human plasma. Results obtained from the analysis of human plasma extract via direct negative ionization are shown in Figure 4.10. As mentioned above, precursor ion or neutral loss scanning can be used to detect individual GPL classes at the sum compositional level exploiting class-specific fragmentations.[1] For example, in positive ion mode, PCs were identified using precursor ion scanning of *m/z* 184 (Figure 4.11), while neutral loss scanning of 141 Da detected PEs (Figure 4.12). Information from these scan modalities can be compiled to generate targeted lists of GPL, which, in turn, can be used to guide subsequent structural interrogation via ion/ion chemistry. Herein, we report the detailed structural identification of three GPL extracted from human plasma. Explicitly, PC 34:2, PI 38:4, and PE 36:2 were investigated using the gas phase charge inversion MS^n process. Table 4.1 summarizes the structural identities of targeted GPL confirmed with ion/ion chemistry.

Upon direct negative mode ionization of the human plasma extract, the most abundant GPL-related anions were found to be derived from PC 34:2. Using the gas-phase workflow described here, PC 34:2 was found to be composed of at least two isomers. Following mass selection of the $[PC\ 34{:}2 + OAc]^-$ anion (*m/z* 816.6), collisional activation via ion-trap CID generated $[PC\ 34{:}2 - CH_3]^-$ (*m/z* 742.5) (Figure 4.13). Subsequent CID of the demethylated PC 34:2 anion is illustrated in Figure 4.14a and reveals the presence of at least two isomeric species. From Figure 4.14a, the dominant product ions observed at *m/z* 255.2 and 279.2 reflect the 16:0 and 18:2 fatty acyl carboxylate anions, respectively. As a result, PC 16:0_18:2 was found to be the major contributor to the PC 34:2 sum composition. The product ion observed at *m/z* 480.3 was generated by the neutral loss of the 18:2 fatty acyl as a ketene from the demethylated PC 34:2 anion (i.e., $[PC\ 34{:}2 - CH_3 - C_{16}H_{29}CH{=}C{=}O]-$). Importantly, this product ion is significantly more abundant than the corresponding $[PC\ 34{:}2 - CH_3 - C_{14}H_{27}CH{=}C{=}O]-$ ion at *m/z* 504.3 (see inset of Figure 4.15), indicating that the dominant regiochemistry can be assigned as PC 16:0/18:2.

This assignment is consistent with a recent study of human plasma that found the ratio of PC 16:0/18:2 to PC 18:2/16:0 to be 89:11.[52] The $[16:1 - H]^-$ (*m/z* 253.2) and $[18:1 - H]^-$ (*m/z* 281.2) anions were also observed at very low abundances, signifying the presence of PC 16:1_18:1 as the minor isomeric constituent (Figure 4.15).

To pinpoint double bond position(s) in unsaturated fatty acyl substituents, all product ions generated via CID of the $[PC\ 34:2 - CH_3]^-$ anion (Figure 4.14a) were subjected to reaction with $[MgPhen_3]^{2+}$ dications. The dominant product ions observed were the charge-inverted fatty acyl anions, denoted $[18:2 - H + MgPhen2]^+$ (*m/z* 663.3) and $[16:0 - H + MgPhen_2]^+$ (*m/z* 639.3), as shown in Figure 4.14b. Additional product ions observed at *m/z* 864.4 and 1126.8 represent $[PC\ 34:2 - CH_3 - C_{16}H_{29}CH{=}C{=}O + MgPhen_2]^+$ and $[PC\ 34:2 - CH_3 + MgPhen_2]^+$, respectively. Beam-type CID was then employed to generate the $[18:2 - H + MgPhen]^+$ (*m/z* 483.3) and $[16:0 - H + MgPhen]^+$ (*m/z* 459.3) complex cations (Figure 4.14c). Subsequent unit mass selection and ion-trap CID of the $[18:2 - H + MgPhen]^+$ ion at *m/z* 483.3 provided identification of double bond positions for the 18:2 fatty acyl, as highlighted in Figure 4.14d. The 18:2 fatty acyl was identified based on de novo spectral analysis and comparison to a reference spectrum derived from linoleic acid as 18:2(9,12). In turn, the major isomeric component of PC 34:2 was identified as PC 16:0/18:2(9,12). Note that the $[18:1 - H + MgPhen]^+$ (*m/z* 485.3) and $[16:1 - H + MgPhen]^+$ (*m/z* 457.3) complex cations were also generated, but the relative abundances of these product ions were extremely small, prohibiting further interrogation via CID and identification of unsaturation sites. In sum, our assignment of the dominant isomeric of PC 34:2 in plasma is in good agreement with previous reports of both *sn*-positional and carbon−carbon double bond assignments.[35,52]

As mentioned above, the human plasma lipidome has been widely investigated with hopes of identifying lipid biomarkers for a multitude of disease pathologies.[51] Thus, as additional examples, we chose to investigate two GPL proposed as plasma biomarkers. First, serum-based PIs have been reported to have a significant association with bipolar disorder (BD).[53] Specifically, alterations in PI levels have been observed in patients exhibiting BD when compared to non-diseased individuals. In our study, we identified the double bond positions in plasma PI 38:4 as PI 18:0_20:4(5,8,11,14) using the gas-phase ion/ion procedure described above (Figure 4.16). Furthermore, the relative abundance of the $[PI\ 38:4 - H - 20:4]^-$ ion at *m/z* 581.3 in the negative ion CID (Figure 4.16a) indicates the dominant regioisomer to be the canonical PI 18:0/20:4(5,8,11,14), noting that contributions from the alternate *sn*-isomer are not excluded based

upon these data. Based on this single experiment, PI 18:0/20:4(5,8,11,14) appears to be the only major contributor to PI 38:4.

In an additional example, we interrogated plasma-based PE 36:2. Recently, PE 36:2 has been recognized as a potential biomarker for lung cancer.54 Using the ion/ion reaction approach, we identified numerous isomeric contributors for PE 36:2. CID of the deprotonated PE 36:2 anion (i.e., $[PE\ 36:2 - H]^-$) at *m/z* 742.6) exposed the presence of at least three isomeric lipids (Figure 4.17a). PE 18:0_18:2 comprises the major fatty acyl contributor to PE 36:2, as indicated by the dominant 18:0 and 18:2 fatty acyl carboxylate anions observed at *m/z* 283.2 and 279.2. Furthermore, the fragment ion observed at *m/z* 480.3 was generated via the neutral loss of the 18:2 fatty acyl as a ketene from the deprotonated PE 36:2 anion. Two additional minor isomeric contributors were also identified. Explicitly, the $[18:1 - H]^-$ (*m/z* 281.2) fatty acyl anion can be attributed to PE 18:1_18:1, while the $[16:0 - H]^-$ (*m/z* 255.2) and $[20:2 - H]^-$ (*m/z* 307.3) carboxylate anions indicate PE 16:0_20:2. Sites of unsaturation were identified using gas-phase ion/ion chemistry, and results of the ion/ion reaction and subsequent BT CID are displayed in Figure 4.17b. Using mass selection and CID of the $[18:2 - H + MgPhen]^+$ cation (*m/z* 483.3), as detailed in Figure 4.17c, we confidently determine the structure of the major isomeric contributor to be PE 18:0_18:2(9,12). Upon interrogation of the $[18:1 - H + MgPhen]^+$ complex cation via ion-trap CID, the 18:1 fatty acyl was found to be an isomeric mixture of 18:1(11) and 18:1(9) (Figure 4.17d). From Figure 4.17d, the product ions denoted in red indicate the 18:1(9) isomer, while those depicted in blue signify the 18:1(11) isomer. Exploiting the previously developed multiple linear regressions approach in conjunction with library spectra generated from *cis*-vaccenic (18:1(11*Z*)) and oleic (18:1(9*Z*)) acids,[37] relative abundances of the 18:1(9) and 18:1(11) fatty acyls were calculated to be 92 ± 2 and 8 ± 2, respectively. It is important to note that we cannot distinguish among isomeric contributors such as PE 18:1(9)_18:1(9), PE 18:1(9)_18:1(11), or PE 18:1(11)_18:1(11) using the ion/ion method presented here. Furthermore, while we can identify the presence of PE 16:0_20:2 in human plasma, we were unable to localize double bond positions in the 20:2 fatty acyl substituent, as the charge-inverted 20:2 fatty acyl complex cation was too low in abundance for subsequent interrogation. Based on these results, it is clear that plasma biomarkers identified only at the sum compositional level can exist as isomeric mixtures, suggesting a need for isomeric discrimination biomarker discovery research.

4.4 Conclusions

In this work, we demonstrated a top-down shotgun lipidomics approach employing gas-phase charge inversion ion/ion chemistry that provides detailed structural characterization of glycerophospholipids. The glycerophospholipid, originating either from an authentic standard or lipid extract, is first ionized and mass-selected in the negative ion mode. Subsequent collisional activation of the isolated lipid anion liberates fatty acyl carboxylate anions carried by the GPL precursor at the *sn*-1 and *sn*-2 positions. Following generation of $[FA - H]^-$ anions from the GPL precursor, fatty acyl anions are transformed in the gas-phase to $[FA - H + MgPhen]^+$ complex cations via ion/ion reaction with $[MgPhen_3]^{2+}$ dications. These charge-inverted FA complex cations can be individually mass-selected and collisionally activated to produce product ion spectra that enable confident identification of double bond positions(s) and calculation of relative compositions of isomeric contributors. In total, charge inversion ion/ion chemistry offers a sensitive, rapid, and entirely gas-phase MS^n process for detailed structural elucidation of GPL. Key advantages of this strategy include (i) the ability to use spectral libraries based upon readily available fatty acid standards to characterize and quantitate the fatty acyl chains present in GPLs where standards are rare and expensive and (ii) the ability to assign – in some instances – *sn*-position and double bond position. The latter is particularly significant, as it represents a key step toward complete structure elucidation of GPLs in complex mixtures. As demonstrated with the analysis of three GPLs found in human plasma, the incorporation of ion/ion chemistry enables the identification of major, and some minor, isomeric contributors that are unresolved using conventional ESI-MS/MS experiments. Furthermore, these results indicate that a previously suggested plasma biomarker for lung cancer exists as a mixture of isomeric components, indicating the possible need for isomer differentiation during biomarker discovery.

4.5 References

1. Han, X. L.; Gross, R. W. *Mass Spectrom. Rev*. **2005**, *24* (3), 367−412.
2. Pulfer, M.; Murphy, R. C. *Mass Spectrom. Rev*. **2003**, *22* (5), 332−364.
3. Yetukuri, L.; Ekroos, K.; Vidal-Puig, A.; Oresic, M. *Mol. BioSyst*. **2008**, *4* (2), 121−127.
4. Kayganich, K. A.; Murphy, R. C. *Anal. Chem*. **1992**, *64* (23), 2965−2971.

5. Murphy, R. C.; Harrison, K. A. *Mass Spectrom. Rev*. **1994**, *13* (1), 57−75.

6. Haroldsen, P. E.; Murphy, R. C. *Biomed. Environ. Mass Spectrom*. **1987**, *14* (10), 573−578.

7. Lehmann, W. D.; Kessler, M. *Biomed. Mass Spectrom*. **1983**, *10* (3), 220−226.

8. Sugatani, J.; Kino, M.; Saito, K.; Matsuo, T.; Matsuda, H.; Katakuse, I. *Biomed. Mass Spectrom*. **1982**, *9* (7), 293−301.

9. Thomas, M. C.; Mitchell, T. W.; Blanksby, S. J. *J. Am. Soc. Mass Spectrom*. **2005**, *16* (6), 926−939.

10. Brugger, B.; Erben, G.; Sandhoff, R.; Wieland, F. T.; Lehmann, W. D. *Proc. Natl. Acad. Sci. U. S. A.* **1997**, *94* (6), 2339−2344.

11. Liebisch, G.; Vizcaino, J. A.; Kofeler, H.; Trotzmuller, M.; Griffiths, W. J.; Schmitz, G.; Spener, F.; Wakelam, M. J. O. *J. Lipid Res*. **2013**, *54* (6), 1523−1530.

12. Martinez-Seara, H.; Rog, T.; Pasenkiewicz-Gierula, M.; Vattulainen, I.; Karttunen, M.; Reigada, R. *J. Phys. Chem. B* **2007**, *111* (38), 11162−11168.

13. Martinez-Seara, H.; Rog, T.; Pasenkiewicz-Gierula, M.; Vattulainen, I.; Karttunen, M.; Reigada, R. *Biophys. J*. **2008**, *95* (7), 3295−3305.

14. Leekumjorn, S.; Cho, H. J.; Wu, Y. F.; Wright, N. T.; Sum, A. K.; Chan, C. *Biochim. Biophys. Acta, Biomembr*. **2009**, *1788* (7), 1508−1516.

15. Razquin, C.; Toledo, E.; Clish, C. B.; Ruiz-Canela, M.; Dennis, C.; Corella, D.; Papandreou, C.; Ros, E.; Estruch, R.; Guasch-Ferre, M.; Gomez-Gracia, E.; Fito, M.; Yu, E.; Lapetra, J.; Wang, D.; Romaguera, D.; Liang, L. M.; Alonso-Gomez, A.; Deik, A.; Bullo, M.; Serra-Majem, L.; Salas-Salvado, J.; Hu, F. B.; Martinez-Gonzalez, M. A. *Diabetes Care* **2018**, *41* (12), 2617−2624.

16. Mundra, P. A.; Barlow, C. K.; Nestel, P. J.; Barnes, E. H.; Kirby, A.; Thompson, P.; Sullivan, D. R.; Alshehry, Z. H.; Mellett, N. A.; Huynh, K.; et al. *Jci Insight* **2018**, *3* (17), e121326.

17. Huynh, K.; Barlow, C. K.; Jayawardana, K. S.; Weir, J. M.; Mellett, N. A.; Cinel, M.; Magliano, D. J.; Shaw, J. E.; Drew, B. G.; Meikle, P. J. *Cell Chemical Biology* **2019**, *26* (1), 71.

18. Hampel, H.; O'Bryant, S. E.; Molinuevo, J. L.; Zetterberg, H.; Masters, C. L.; Lista, S.; Kiddle, S. J.; Batrla, R.; Blennow, K. *Nat. Rev. Neurol*. **2018**, *14* (11), 639−652.

19. Li, F.; Qin, X. Z.; Chen, H. Q.; Qiu, L.; Guo, Y. M.; Liu, H.; Chen, G. Q.; Song, G. G.; Wang, X. D.; Li, F. J.; Guo, S.; Wang, B. H.; Li, Z. L. *Rapid Commun. Mass Spectrom.* **2013**, *27* (1), 24−34.

20. Min, H. K.; Lim, S.; Chung, B. C.; Moon, M. H. *Anal. Bioanal. Chem*. **2011**, *399* (2), 823−830.

21. Qiu, Y. P.; Zhou, B. S.; Su, M. M.; Baxter, S.; Zheng, X. J.; Zhao, X. Q.; Yen, Y.; Jia, W. *Int. J. Mol. Sci*. **2013**, *14* (4), 8047−8061.

22. Yu, Z. T.; Chen, H. K.; Zhu, Y.; Ai, J. M.; Li, Y.; Gu, W.; Borgia, J. A.; Zhang, J. C.; Jiang, B.; Chen, W.; Deng, Y. P. *Oncol. Lett*. **2018**, *16* (1), 761−768.

23. Zhou, X. C.; Mao, J. H.; Ai, J. M.; Deng, Y. P.; Roth, M. R.; Pound, C.; Henegar, J.; Welti, R.; Bigler, S. A. *PLoS One* **2012**, *7* (11), e48889.

24. Hancock, S. E.; Poad, B. L. J.; Batarseh, A.; Abbott, S. K.; Mitchell, T. W. *Anal. Biochem*. **2017**, *524*, 45−55.

25. Franklin, E. T.; Betancourt, S. K.; Randolph, C. E.; McLuckey, S. A.; Xia, Y. *Anal. Bioanal*. Chem. **2019**, *411*, 4739.

26. Ma, X. X.; Xia, Y. *Angew. Chem., Int. Ed*. **2014**, *53* (10), 2592−2596.

27. Stinson, C. A.; Xia, Y. *Analyst* **2016**, *141* (12), 3696−3704.

28. Zhang, W. P.; Zhang, D. H.; Chen, Q. H.; Wu, J. H.; Ouyang, Z.; Xia, Y. *Nat. Commun*. **2019**, *10*, 79.

29. Feng, Y.; Chen, B. M.; Yu, Q. Y.; Li, L. J. *Anal. Chem*. **2019**, *91* (3), 1791−1795.

30. Thomas, M. C.; Mitchell, T. W.; Harman, D. G.; Deeley, J. M.; Murphy, R. C.; Blanksby, S. J. *Anal. Chem*. **2007**, 79 (13), 5013−5022.

31. Thomas, M. C.; Mitchell, T. W.; Harman, D. G.; Deeley, J. M.; Nealon, J. R.; Blanksby, S. J. *Anal. Chem*. **2008**, *80* (1), 303−311.

32. Thomas, M. C.; Mitchell, T. W.; Blanksby, S. J. *Methods Mol. Biol*. **2009**, *579*, 413−441.

33. Poad, B. L. J.; Pham, H. T.; Thomas, M. C.; Nealon, J. R.; Campbell, J. L.; Mitchell, T. W.; Blanksby, S. J. *J. Am. Soc. Mass Spectrom*. **2010**, *21* (12), 1989−1999.

34. Vu, N.; Brown, J.; Giles, K.; Zhang, Q. B. *Rapid Commun. Mass Spectrom*. **2017**, *31* (17), 1415−1423.

35. Marshall, D. L.; Criscuolo, A.; Young, R. S.; Poad, B. L.; Zeller, M.; Reid, G. E.; Mitchell, T. W.; Blanksby, S. J. *J. Am. Soc. Mass Spectrom.* **2019**, *30*, 1621.

36. Randolph, C. E.; Foreman, D. J.; Betancourt, S. K.; Blanksby, S. J.; McLuckey, S. A. *Anal. Chem.* **2018**, *90* (21), 12861−12869.

37. Randolph, C. E.; Foreman, D. J.; Blanksby, S. J.; McLuckey, S. A. *Anal. Chem.* **2019**, *91* (14), 9032−9040.

38. Matyash, V.; Liebisch, G.; Kurzchalia, T. V.; Shevchenko, A.; Schwudke, D. *J. Lipid Res.* **2008**, *49* (5), 1137−1146.

39. Xia, Y.; Wu, J.; McLuckey, S. A.; Londry, F. A.; Hager, J. W. *J. Am. Soc. Mass Spectrom.* **2005**, *16* (1), 71−81.

40. Xia, Y.; Liang, X. R.; McLuckey, S. A. *J. Am. Soc. Mass Spectrom.* **2005**, *16* (11), 1750−1756.

41. Londry, F. A.; Hager, J. W. *J. Am. Soc. Mass Spectrom.* **2003**, *14* (10), 1130−1147.

42. Hsu, F. F.; Turk, J. *J. Am. Soc. Mass Spectrom.* **2000**, *11* (10), 892−899.

43. Hsu, F. F.; Turk, J. *J. Am. Soc. Mass Spectrom.* **2000**, *11* (11), 986−999.

44. Hsu, F. F.; Turk, J. *J. Am. Soc. Mass Spectrom.* **2000**, *11* (9), 797−803.

45. Hsu, F. F.; Turk, J. *J. Am. Soc. Mass Spectrom.* **2001**, *12* (9), 1036−1043.

46. Hsu, F. F.; Turk, J. *J. Am. Soc. Mass Spectrom.* **2003**, *14* (4), 352−363.

47. Hsu, F. F.; Turk, J. *J. Am. Soc. Mass Spectrom.* **2005**, *16* (9), 1510−1522.

48. Ekroos, K.; Ejsing, C. S.; Bahr, U.; Karas, M.; Simons, K.; Shevchenko, A. *J. Lipid Res.* **2003**, *44* (11), 2181−2192.

49. Bowden, J. A.; Heckert, A.; Ulmer, C. Z.; Jones, C. M.; Koelmel, J. P.; Abdullah, L.; Ahonen, L.; Alnouti, Y.; Armando, A. M.; Asara, J. M.; et al. *J. Lipid Res.* **2017**, *58* (12), 2275−2288.

50. Quehenberger, O.; Armando, A. M.; Brown, A. H.; Milne, S. B.; Myers, D. S.; Merrill, A. H.; Bandyopadhyay, S.; Jones, K. N.; Kelly, S.; Shaner, R. L.; Sullards, C. M.; Wang, E.; Murphy, R. C.; Barkley, R. M.; Leiker, T. J.; Raetz, C. R. H.; Guan, Z. Q.; Laird, G. M.; Six, D. A.; Russell, D. W.; McDonald, J. G.; Subramaniam, S.; Fahy, E.; Dennis, E. A. J. *Lipid Res*. **2010**, *51* (11), 3299−3305.

51. Vvedenskaya, O.; Wang, Y.; Ackerman, J. M.; Knittelfelder, O.; Shevchenko, A. *TrAC, Trends Anal. Chem*. **2019**, *120*, 115277.

52. Zacek, P.; Bukowski, M.; Rosenberger, T. A.; Picklo, M. *J. Lipid Res*. **2016**, *57* (12), 2225−2234.

53. Knowles, E.; Meikle, P.; Huynh, K.; Goring, H.; Olvera, R.; Mathias, S.; Duggirala, R.; Almasy, L.; Blangero, J.; Curran, J.; Glahn, D. *Eur. Neuropsychopharmacol*. **2017**, *27*, S452−S453.

54. Fahrmann, J. F.; Grapov, D.; DeFelice, B. C.; Taylor, S.; Kim, K.; Kelly, K.; Wikoff, W. R.; Pass, H.; Rom, W. N.; Fiehn, O.; Miyamoto, S. *Cancer Biomarkers* **2016**, *16* (4), 609−617.

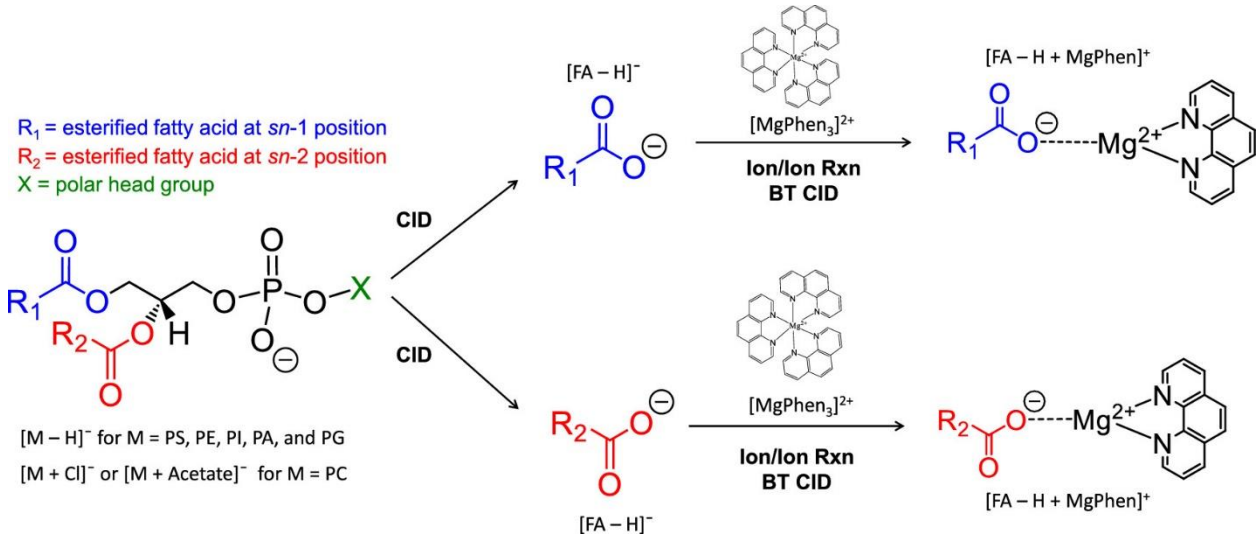

Scheme 4.1 Generation of Charge-Inverted FA Complex Cations, $[FA - H + MgPhen]^+$, Derived Directly from the GPL Anion in the Gas Phase via Ion/Ion Reaction between $[FA - H]^-$ Anions Released from a GPL Precursor Ion and $[MgPhen_3]^{2+}$ Reagent Dications

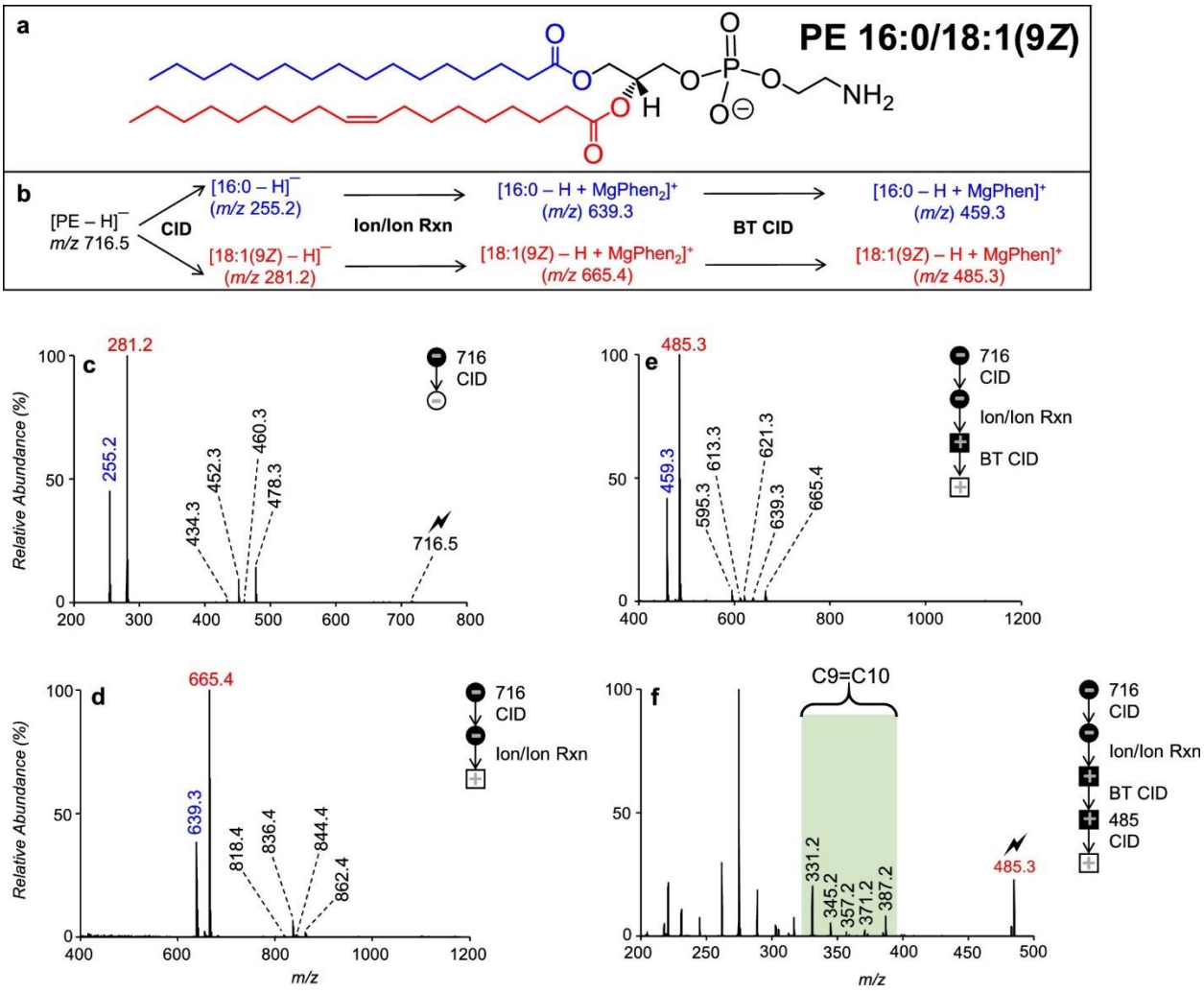

Figure 4.1 Sequence of MS events used to structurally interrogate synthetic PE 16:0/18:1(9*Z*). (a) Structure of ionized PE 16:0/18:1(9*Z*) (i.e., $[PE - H]^-$). The blue and red font indicate the *sn*-1 and *sn*-2 fatty acyls, respectively. (b) Reaction scheme detailing identification procedure for the PE 16:0/18:1(9*Z*) anion. (c) Ion-trap CID spectrum of $[PE - H]^-$ (*m*/*z* 716.5). (d) Charge inversion spectrum generation via the gas-phase ion/ion reaction between product ions generated from CID of the $[PE - H]^-$ precursor ion as shown in (c) and $[MgPhen_3]^{2+}$ dications. (e) Subsequent beam-type (BT) CID spectrum generated post-ion/ion reaction. (f) Ion-trap CID product ion spectrum following monoisotopic mass selection and collisional activation of $[18:1(9Z) - H + MgPhen]^+$ (*m*/*z* 485.3). Note that circles (●/○) indicate positive ion mode analysis, while squares (■/□) indicate negative ion mode analysis.

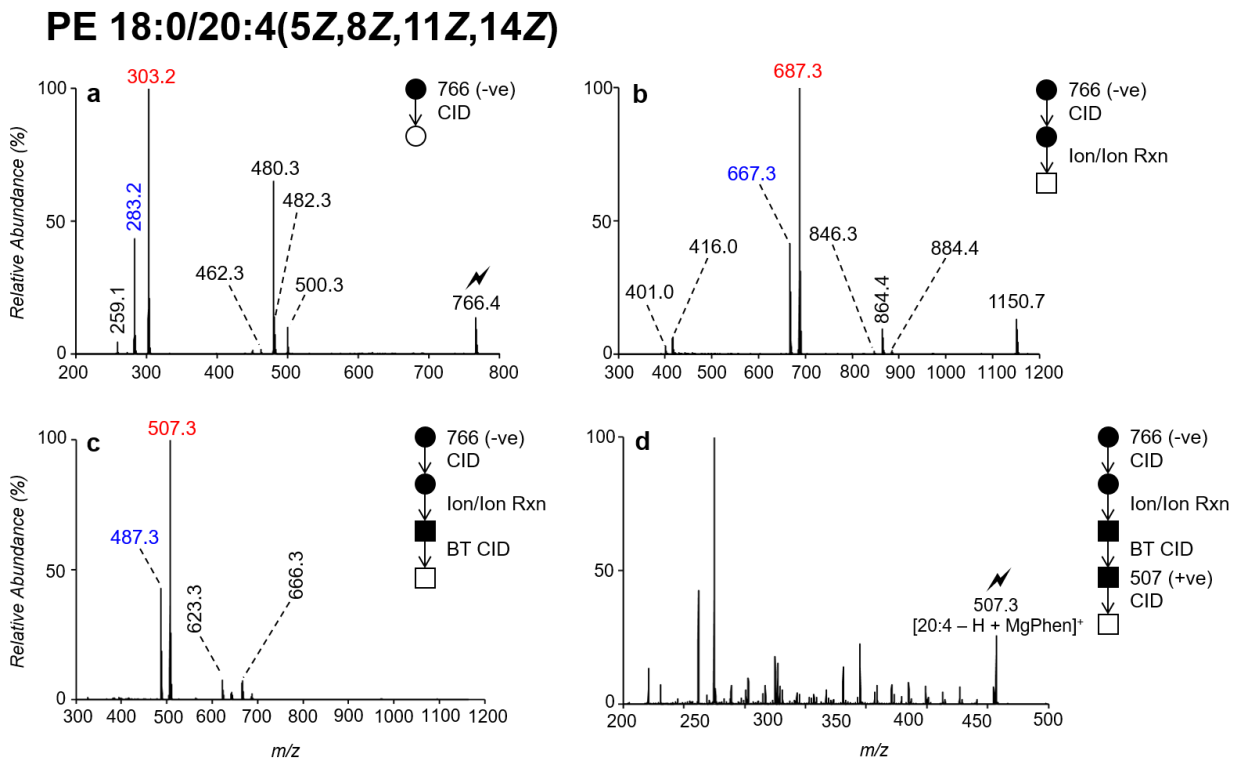

Figure 4.2 Sequence of MS events used to provide in-depth structural identification for synthetic PE 18:0/20:4(5*Z*, 8*Z*, 11*Z*,14*Z*) standard. The blue and red font indicate the *sn*-1 and *sn*-2 fatty acyl product ions respectively. (a) Ion-trap CID spectrum of [PE 18:0/20:4(5*Z*, 8*Z*, 11*Z*,14*Z*) – H]$^-$ (*m/z* 766.4). (b) Charge inversion spectrum generation via the gas-phase ion/ion reaction between product ions generated from CID of the [PE 18:0/20:4(5*Z*, 8*Z*, 11*Z*,14*Z*) – H]$^-$ precursor ion as shown in (a) and $[MgPhen_3]^{2+}$ dications. (c) Subsequent beam-type (BT) CID spectrum generated post-ion/ion reaction. (d) Ion-trap CID product ion spectrum following monoisotopic mass-selection and collisional activation of [20:4(5Z, 8Z, 11Z,14Z) – H + MgPhen]$^+$ (*m/z* 507.3).

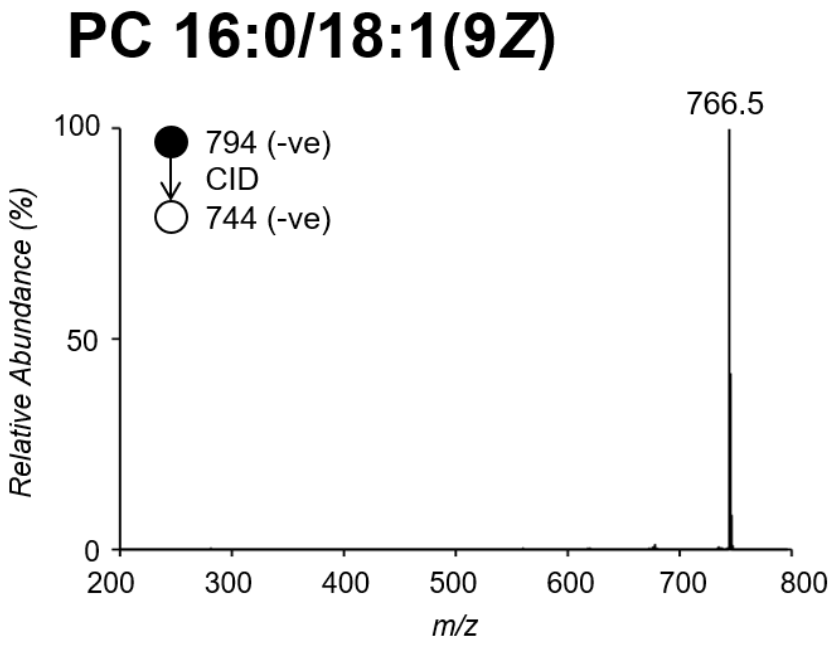

Figure 4.3 Ion-trap CID spectrum resulting from collisional activation of [PC 16:0/18:1(9Z) + $Cl]^-$ (*m/z* 794.5).

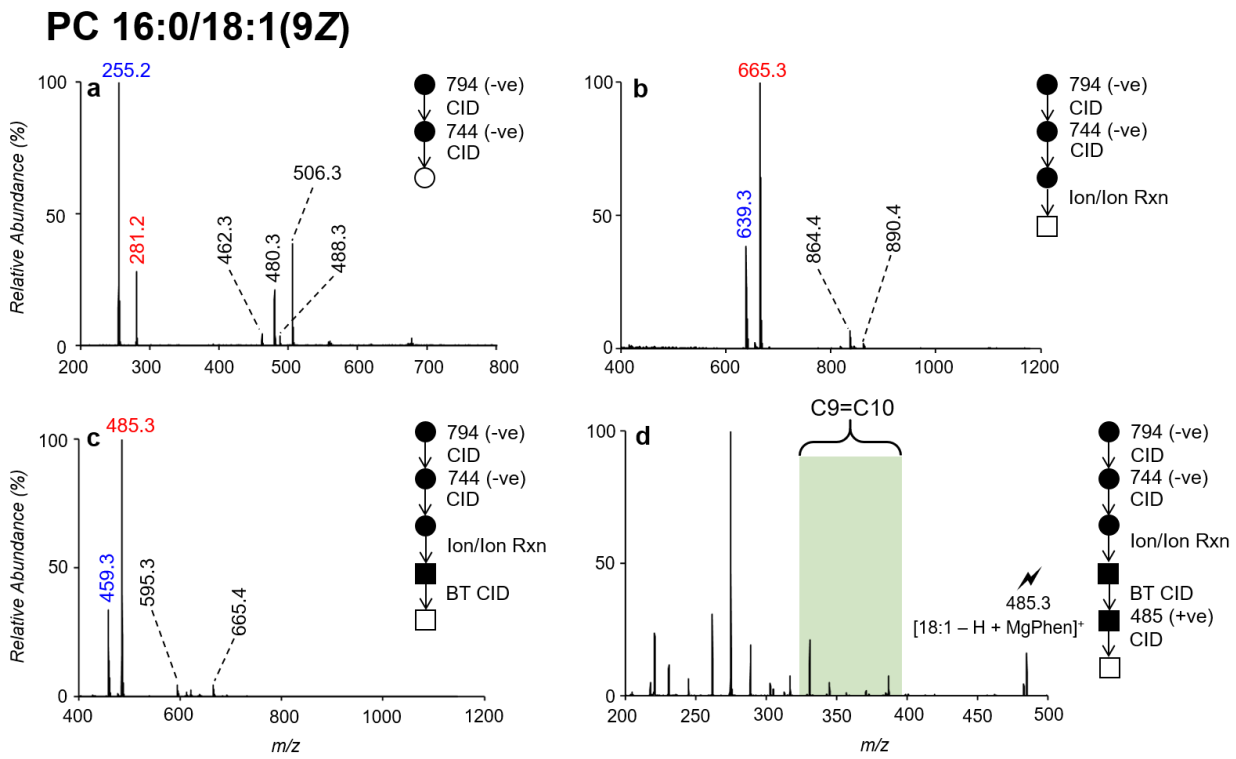

Figure 4.4 Sequence of MS events used to provide in-depth structural identification for synthetic PC 16:0/18:1(9*Z*) standard. (a) Ion-trap CID spectrum of [PC 16:0/18:1(9*Z*) – CH_3]$^-$ (*m/z* 744.5). (b) Charge inversion spectrum generation via the gas-phase ion/ion reaction between product ions generated from CID of the [PC 16:0/18:1(9*Z*) – CH_3]$^-$ precursor ion as shown in (a) and [$MgPhen_3$]$^{2+}$ dications. (c) Subsequent beam-type (BT) CID spectrum generated post-ion/ion reaction. (d) Ion-trap CID product ion spectrum following monoisotopic mass-selection and collisional activation of [18:1(9Z) – H + MgPhen]$^+$ (*m/z* 485.3).

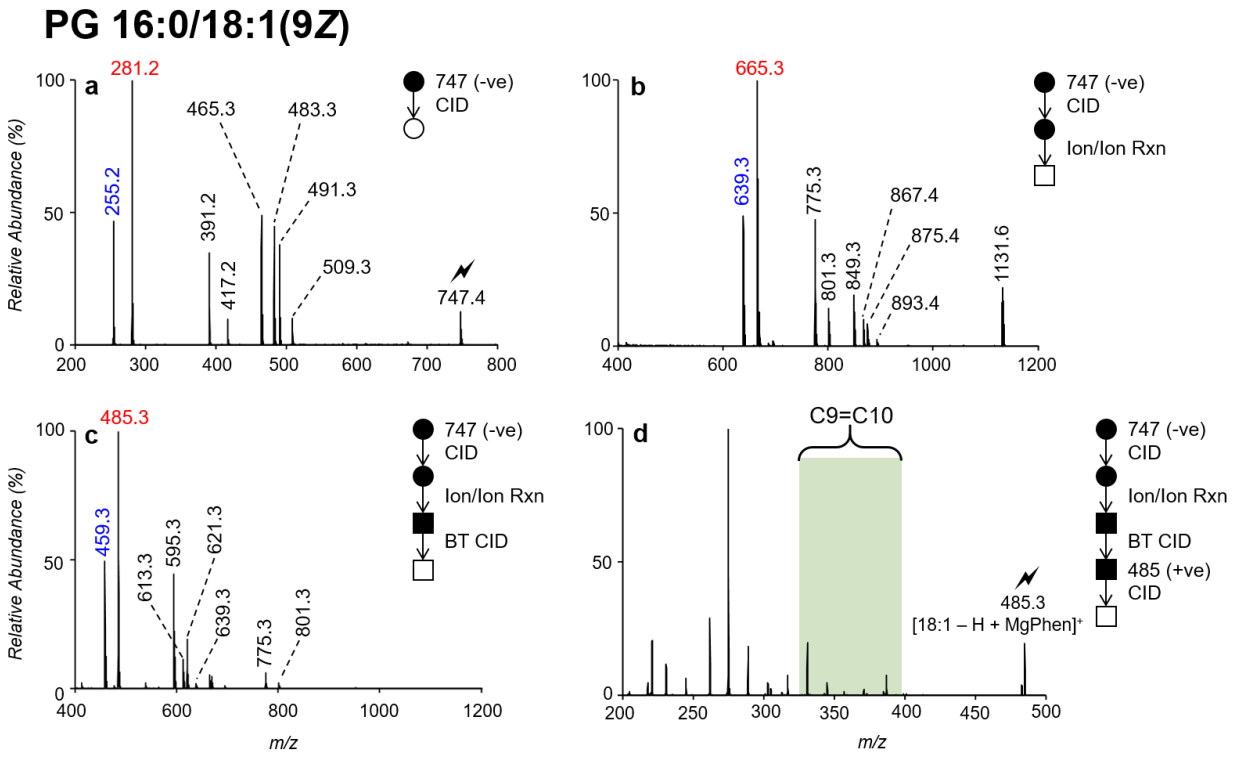

Figure 4.5 Sequence of MS events used to provide in-depth structural identification for synthetic PG 16:0/18:1(9Z) standard. (a) Ion-trap CID spectrum of $[PG\ 16:0/18:1(9Z) - CH_3]^-$ (*m/z* 747.5). (b) Charge inversion spectrum generation via the gas-phase ion/ion reaction between product ions generated from CID of the $[PG\ 16:0/18:1(9Z) - H]^-$ precursor ion as shown in (a) and $[MgPhen_3]^{2+}$ dications. (c) Subsequent beam-type (BT) CID spectrum generated post-ion/ion reaction. (d) Ion-trap CID product ion spectrum following monoisotopic mass-selection and collisional activation of $[18:1(9Z) - H + MgPhen]^+$ (*m/z* 485.3).

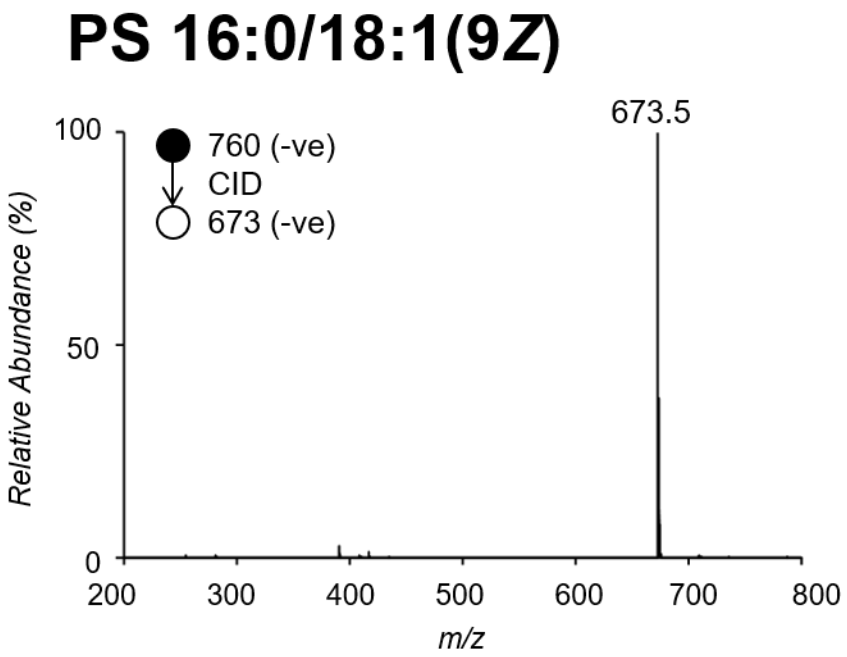

Figure 4.6 Ion-trap CID spectrum resulting from collisional activation of [PS 16:0/18:1(9Z) – H]$^-$ (*m/z* 760.5).

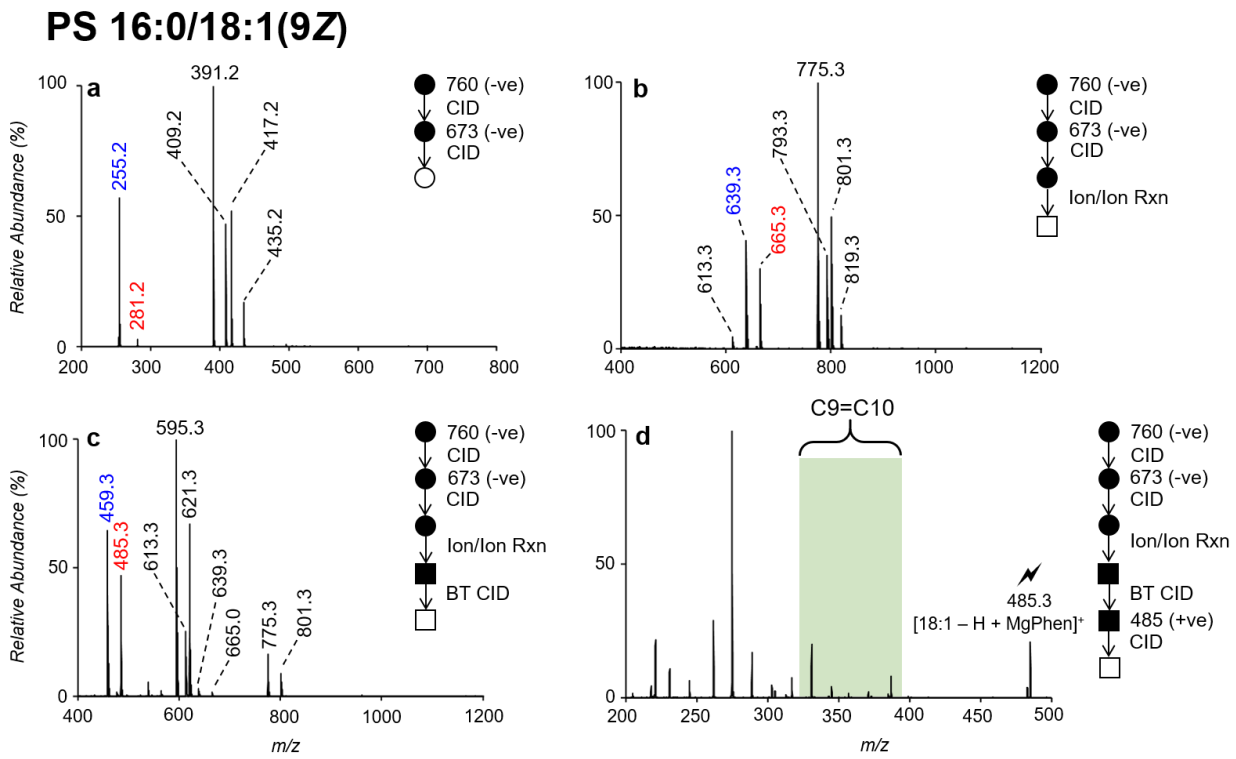

Figure 4.7 Sequence of MS events used to provide in-depth structural identification for synthetic PS 16:0/18:1(9*Z*) standard. (a) Ion-trap CID spectrum of [PS 16:0/18:1(9*Z*) – serine]$^-$ (*m/z* 760.5). (b) Charge inversion spectrum generation via the gas-phase ion/ion reaction between product ions generated from CID of the [PS 16:0/18:1(9*Z*) – serine]$^-$ precursor ion as shown in (a) and $[MgPhen_3]^{2+}$ dications. (c) Subsequent beam-type (BT) CID spectrum generated post-ion/ion reaction. (d) Ion-trap CID product ion spectrum following monoisotopic mass-selection and collisional activation of [18:1(9Z) – H + MgPhen]$^+$ (*m/z* 485.3).

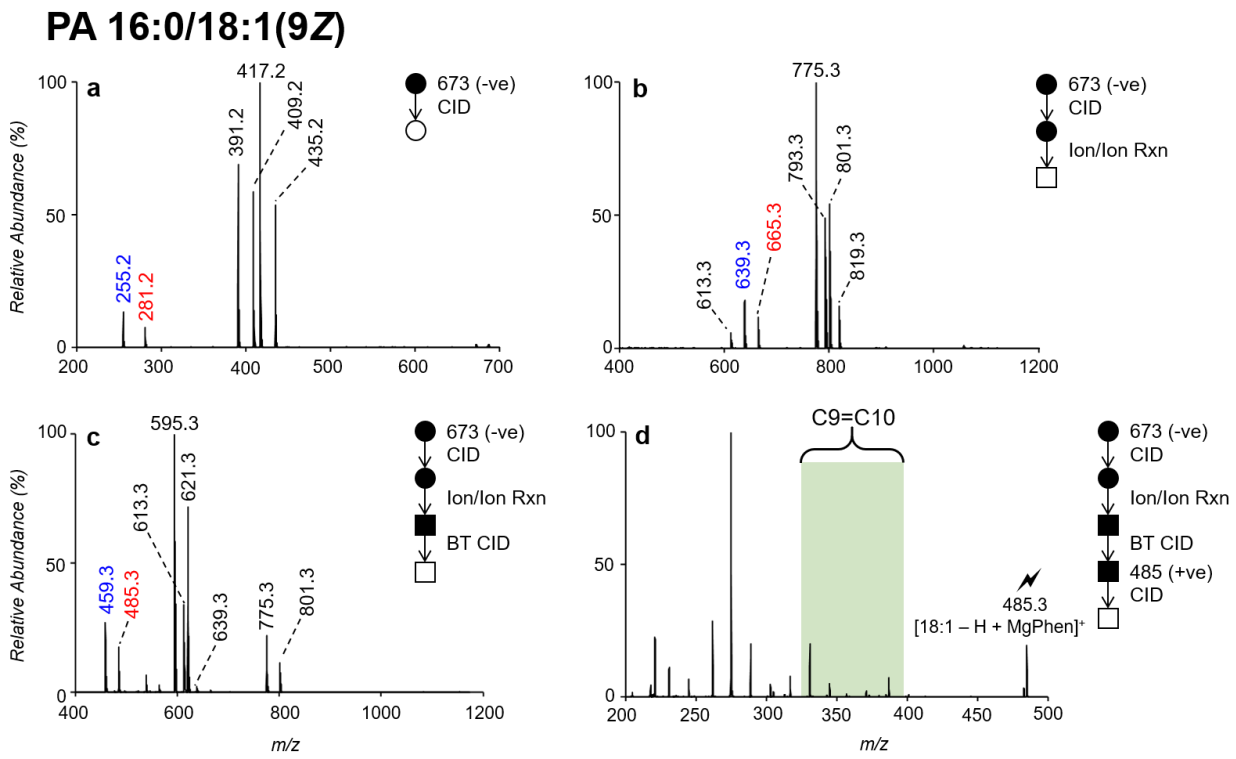

Figure 4.8 Sequence of MS events used to provide in-depth structural identification for synthetic PA 16:0/18:1(9Z) standard. (a) Ion-trap CID spectrum of $[PA\ 16:0/18:1(9Z) - CH_3]^-$ (*m/z* 673.5). (b) Charge inversion spectrum generation via the gas-phase ion/ion reaction between product ions generated from CID of the $[PA\ 16:0/18:1(9Z) - H]^-$ precursor ion as shown in (a) and $[MgPhen_3]^{2+}$ dications. (c) Subsequent beam-type (BT) CID spectrum generated post-ion/ion reaction. (d) Ion-trap CID product ion spectrum following monoisotopic mass-selection and collisional activation of $[18:1(9Z) - H + MgPhen]^+$ (*m/z* 485.3).

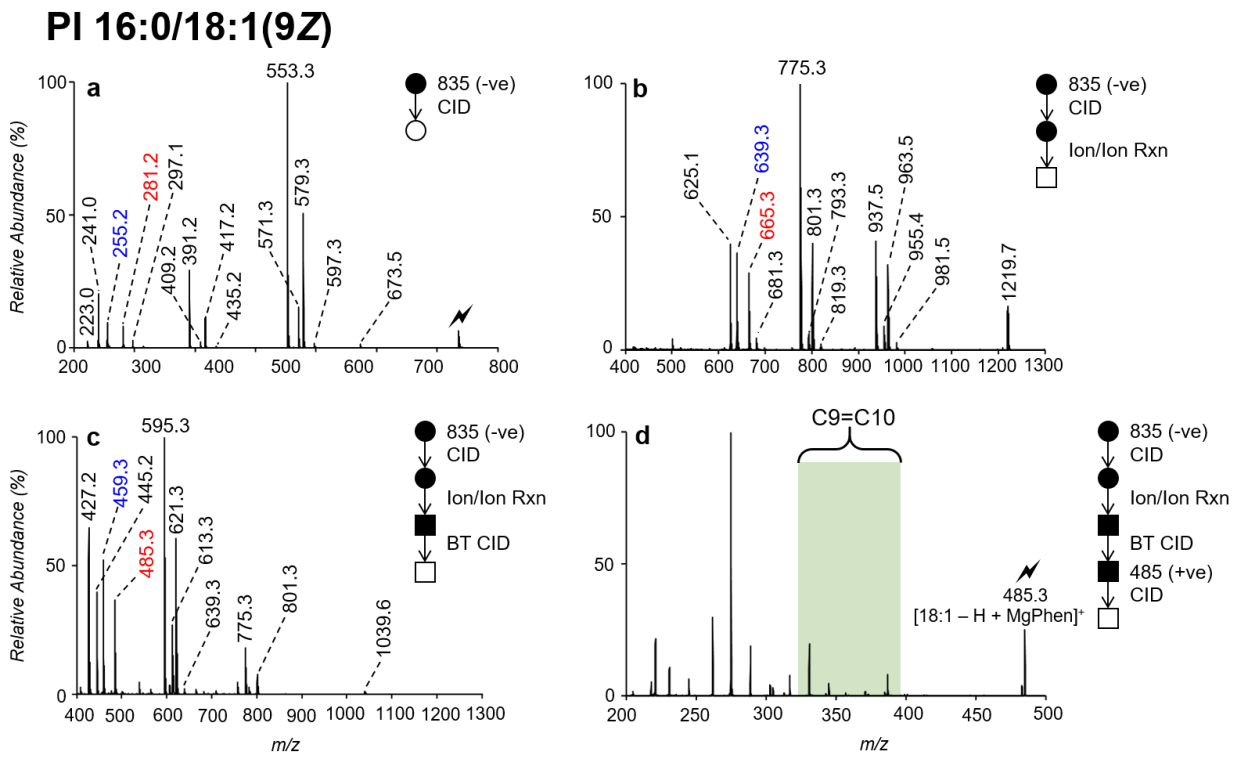

Figure 4.9 Sequence of MS events used to provide in-depth structural identification for synthetic PI 16:0/18:1(9*Z*) standard. (a) Ion-trap CID spectrum of [PI 16:0/18:1(9*Z*) – CH_3]$^-$ (*m/z* 835.5). (b) Charge inversion spectrum generation via the gas-phase ion/ion reaction between product ions generated from CID of the [PI 16:0/18:1(9*Z*) – H]$^-$ precursor ion as shown in (a) and [$MgPhen_3$]$^{2+}$ dications. (c) Subsequent beam-type (BT) CID spectrum generated post-ion/ion reaction. (d) Ion-trap CID product ion spectrum following monoisotopic mass-selection and collisional activation of [18:1(9Z) – H + MgPhen]$^+$ (*m/z* 485.3).

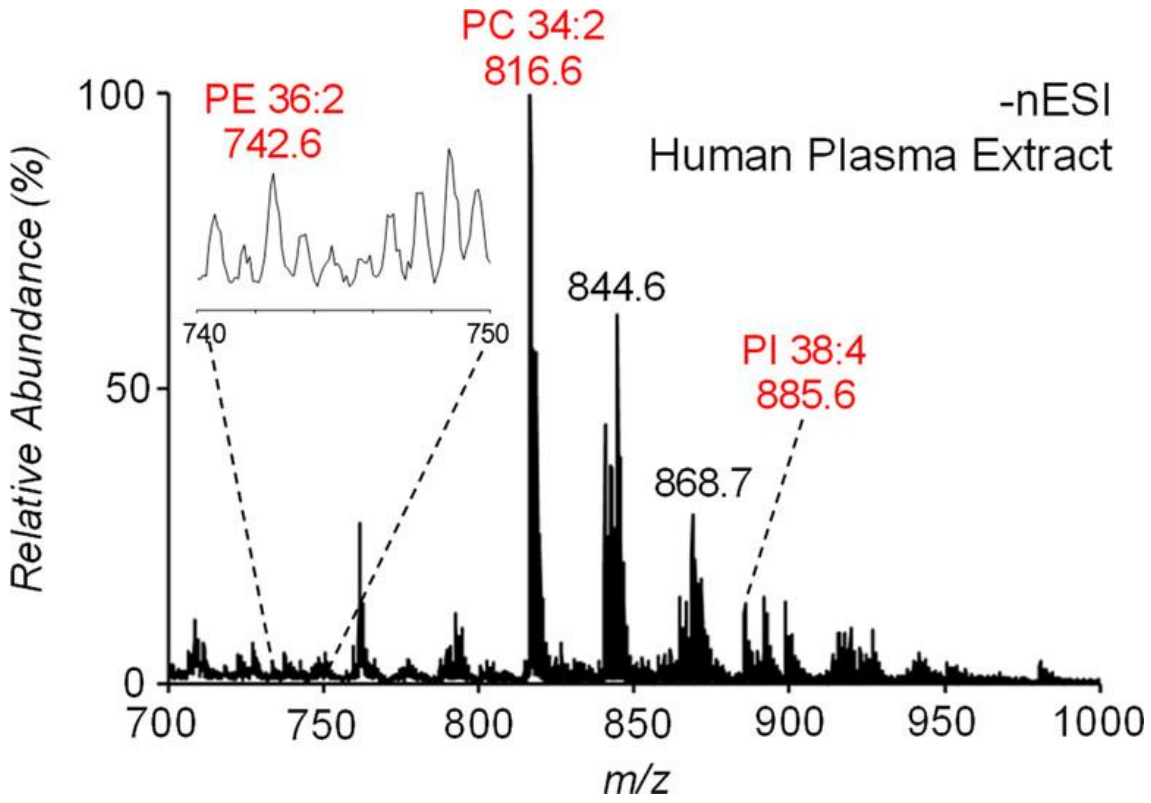

Figure 4.10 Direct infusion negative ion mode nESI mass spectrum of human plasma extract.

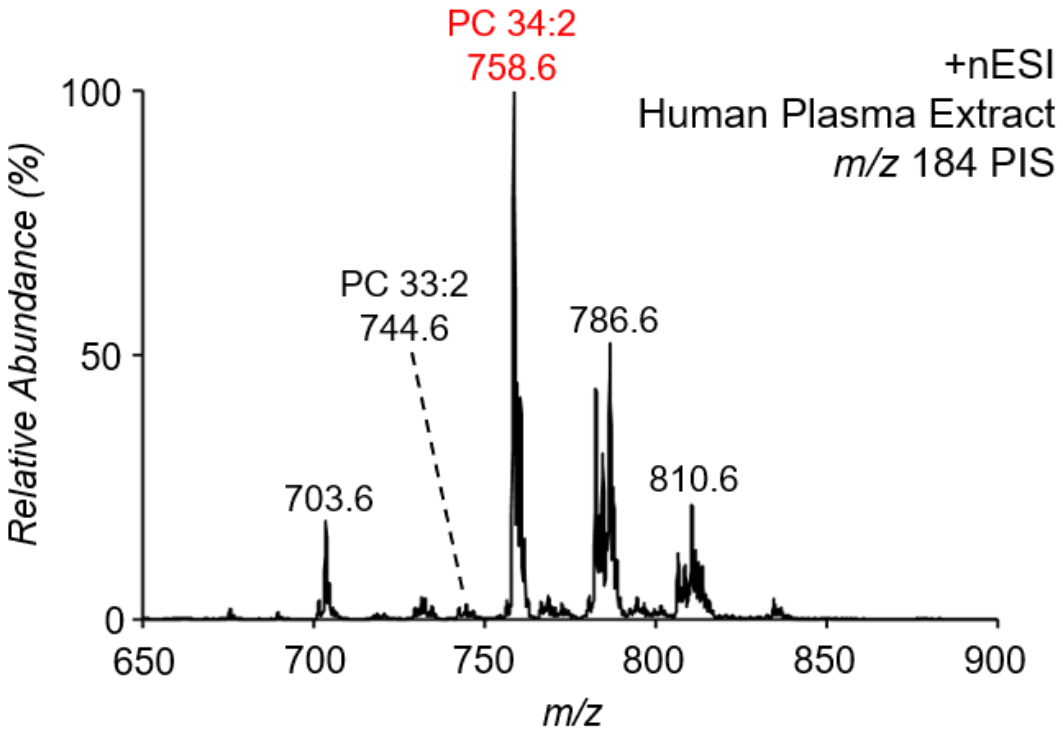

Figure 4.11 Precursor ion scan of *m/z* 184 in positive ion mode used to identify PC lipids in human plasma extract. This scan also includes other choline-bearing lipids such as the $[M + H]^+$ ion of sphingomyelin SM (d34:1) at *m/z* 703.6

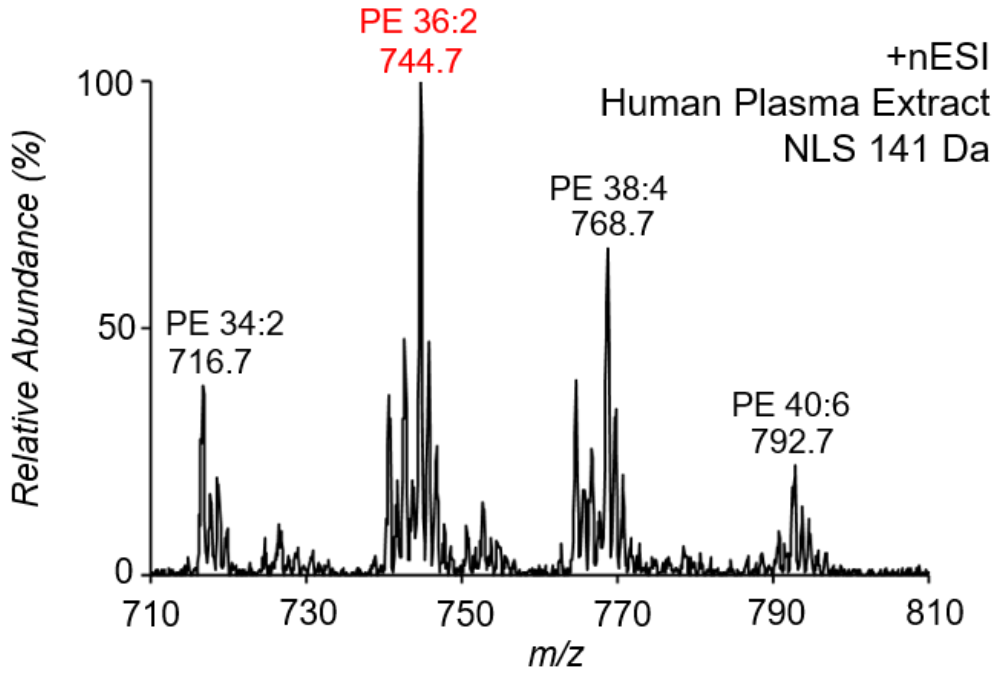

Figure 4.12 141 Da neutral loss scan in the positive ion mode used to identify PE lipids in human plasma extract.

Table 4.1 Summary of Lipids Identified in Human Plasma Extract Using Gas-Phase Charge Inversion Ion/Ion Chemistry

GPL Sum Composition	Precursor Ion (*m/z*)	Fragment Ion (*m/z*)	GPL Structure
PC 36:2	816.6	255.2, 279.2	PC 16:0_18:2(9,12)**
		253.2*, 281.2*	PC 16:1_18:1
PI 38:4	885.6	283.2, 303.2	PI 18:0_20:4(5,8,11,14)
PE 36:2	742.6	283.2, 279.2	PE 18:0_18:2(9,12)
		281.2	PE 18:1_18:1 18:1(9) = 92 ± 2 18:1(11) = 8 ± 2
		255.2*, 307.3*	PE 16:0_20:2

**Unable to identify double bond position(s) via charge inversion ion/ion chemistry due to low ion abundance*
*** Major isomer PC 16:0/18:2(9,12) – see text for discussion*

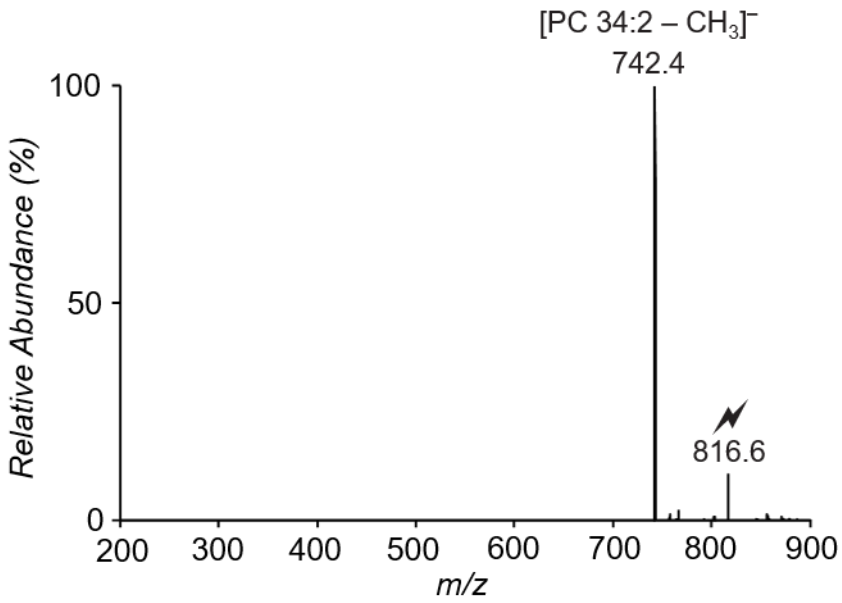

Figure 4.13 Ion-trap CID spectrum resulting from collisional activation of $[PC\ 34:2 + OAc]^-$ (*m/z* 816.6) found in human plasma extract.

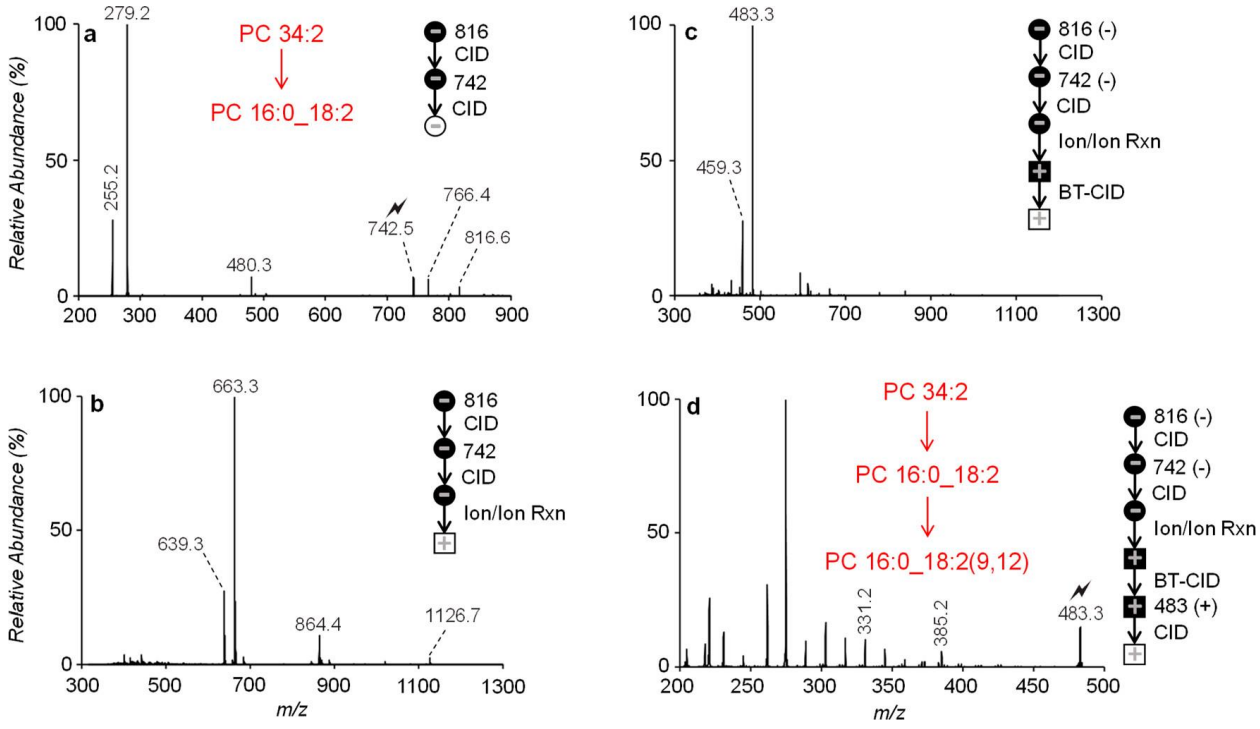

Figure 4.14 Demonstration of gas-phase charge inversion ion/ion chemistry for the analysis of PC 34:2 in human plasma extract. (a) Ion-trap CID spectrum resulting from activation of [PC 34:2 – CH_3]$^-$. (b) Product ion spectrum following ion/ion reaction of fragment ions generated via activation of [PC 34:2 – CH_3]$^-$ and [$MgPhen_3$]$^{2+}$ dications. (c) Beam-type CID product ion spectrum post-ion/ion reaction. (d) CID spectrum of [18:2 – H + MgPhen]$^+$.

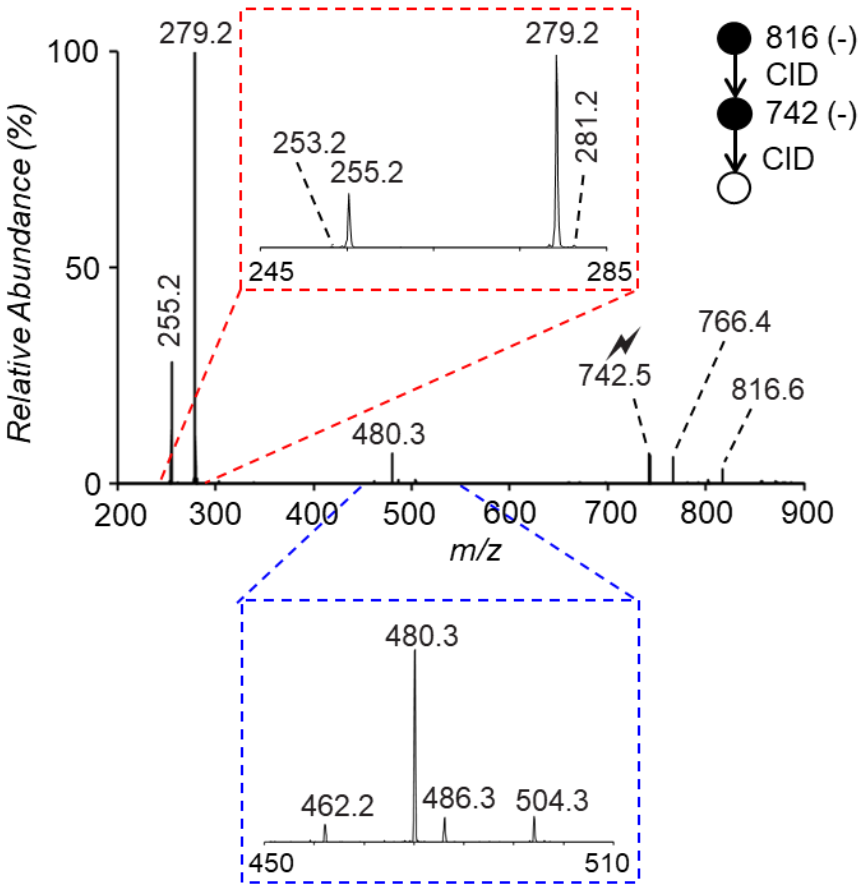

Figure 4.15 CID spectrum resulting from collisional activation of [PC 34:2 – CH_3]$^-$ (*m/z* 742.5) found in human plasma extract. Enlargement of the spectrum from m/z 245 – 285 shows the major FA anions [16:0 – H]$^-$ (*m/z* 255.2) and [18:2 – H]$^-$ (*m/z* 279.2) and the minor FA anions [16:1 – H]$^-$ (*m/z* 253.2) and [18:1 – H]$^-$ (*m/z* 281.2).

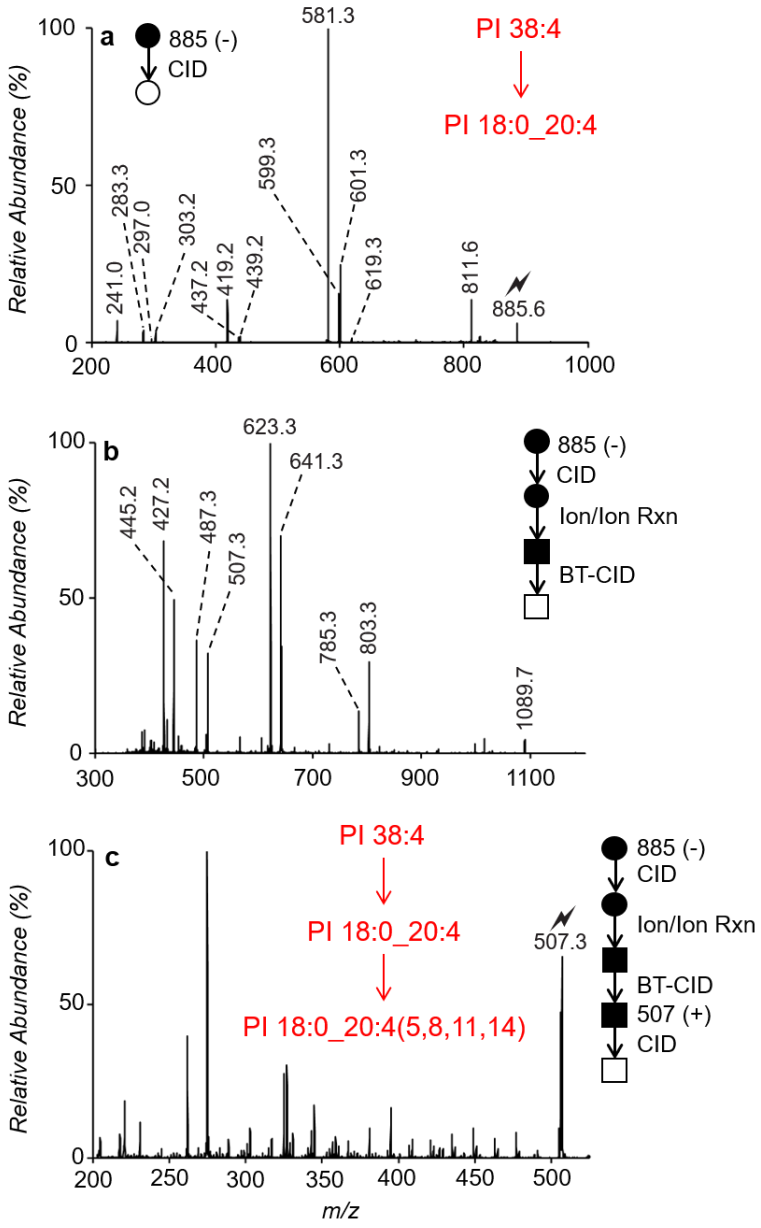

Figure 4.16 Demonstration of gas-phase charge inversion ion/ion chemistry for the analysis of PI 38:4 extracted from human plasma. (a) Ion-trap CID spectrum resulting from activation of $[PI\ 38:4 - H]^-$ (*m/z* 885.5). (b) Product ion spectrum following ion/ion reaction of fragment ions generated via activation of $[PI\ 38:4 - H]^-$ and $[MgPhen_3]^{2+}$ dications and subsequent beam type CID. (c) CID spectrum of $[20:4 - H + MgPhen]^+$ (*m/z* 507.3).

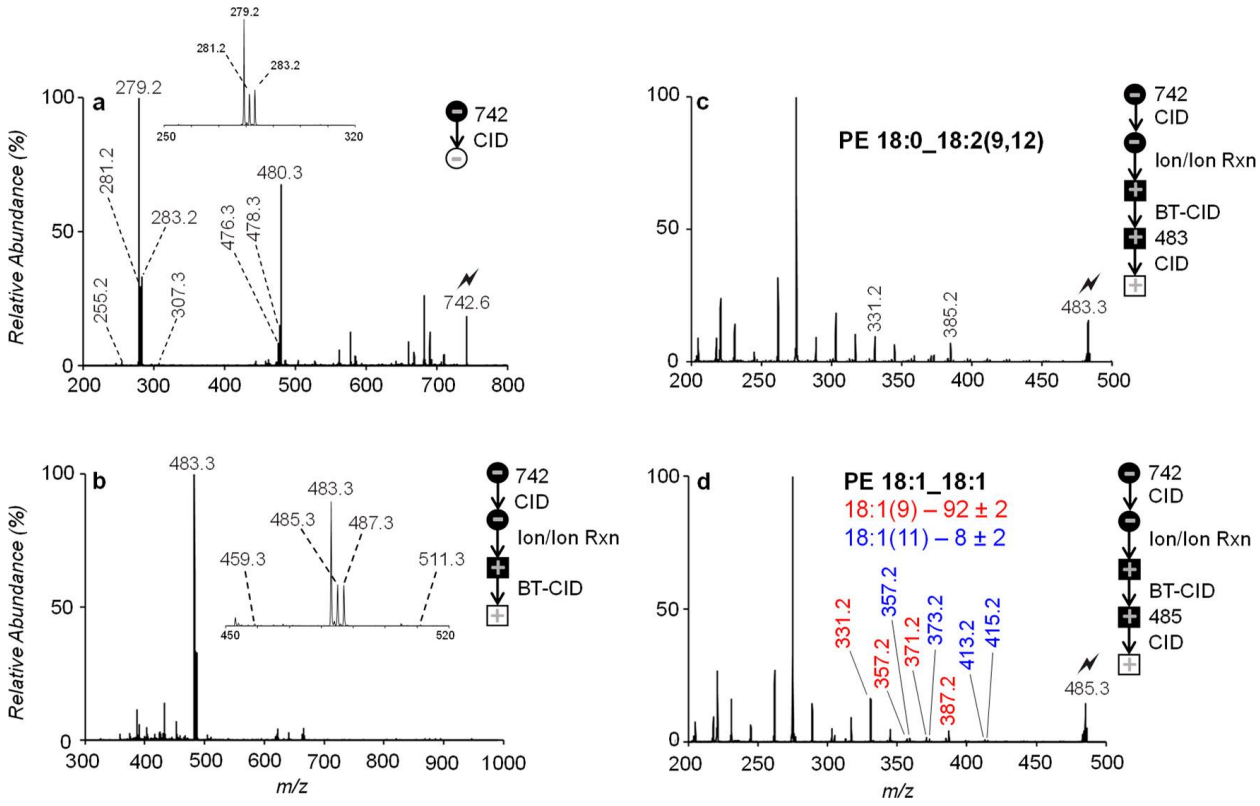

Figure 4.17 Demonstration of gas-phase charge inversion ion/ion chemistry for the analysis of PE 36:2 in human plasma extract. (a) Ion-trap CID spectrum resulting from activation of $[PE\ 36:2 - H]^-$. (b) Product ion spectrum following ion/ion reaction of fragment ions generated via activation of $[PE\ 36:2 - H]^-$ and $[MgPhen_3]^{2+}$ dications and subsequent beam-type CID. (c) CID spectrum of $[18:2 - H + MgPhen]^+$. (d) CID spectrum of $[18:1 - H + MgPhen]^+$.

CHAPTER 5. STRUCTURAL ELUCIDATION OF ETHER GLYCEROPHOSPHOLIPIDS USING GAS-PHASE ION/ION CHARGE INVERSION CHEMISTRY

5.1 Introduction

Ether lipids are peroxisome-derived glycerophospholipids (GPLs) that play significant roles in health and disease.[1,2] In contrast with the more common diacyl GPL structures, which incorporate two fatty acyl chains esterified at both the *sn*-1 and *sn*-2 positions of the central glycerol backbone, ether-linked GPLs are characterized by a hydrocarbon chain linked at the *sn*-1 position via an ether bond. Specifically, while a fatty acid moiety remains esterified at the *sn*-2 position, the plasmanyl and plasmenyl (i.e., plasmalogen) GPL subclasses contain a 1- *O*-alkyl or a 1-*O*-alk-1'-enyl group, respectively, at the *sn*-1 position. Despite constituting only approximately 20% of the mammalian phospholipidome, ether lipids serve diverse structural and functional biological roles.[2] In particular, ether lipids contribute unique structural characteristics to biological membranes, influencing membrane dynamics and physical properties.[3] For example, membrane fluidity is known to be altered by the incorporation of ether-linked GPLs, as alkyl chains at the *sn*-1 position permit increased packing efficiency of membrane phospholipids.[3,4] Furthermore, ether GPLs are suggested to function as endogenous antioxidants while also performing roles in membrane trafficking and cellular signaling.[2,5,6] Recently, alterations to ether GPL production and composition have been associated with several genetic peroxisomal disorders (e.g., rhizomelic chondrodysplasia punctata,[7] Zellweger syndrome[8]) and multiple common disease pathologies including several types of cancer,[9–11] Alzheimer's disease,[12] and multiple metabolic disorders (e.g., obesity,[13] type 1 diabetes,[14] hypertension[15]). In turn, increasing evidence of the critical functional roles of ether lipids in health and disease has highlighted the need for analytical strategies to provide unambiguous structural assignment of these lipids in complex biological mixtures.

Electrospray ionization mass spectrometry (ESI-MS) has emerged as a useful tool to assess changes in GPL structure and composition.[16,17] However, due to the structural similarities of the two GPL subclasses, differentiation between ESI-MS methods.18 As conventional lipidomics strategies like liquid chromatography−mass spectrometry (LC−MS) often fail to achieve chromatographic separation of isomeric ether GPLs,[19,20] direct infusion ESI-MS (commonly referred to as shotgun lipidomics) has been widely adapted for ether GPL analysis. Following lipid

ionization, in either positive or negative ion mode, ether lipids are detected and identified at a sum compositional level via accurate mass measurements (i.e., observed mass-to-charge (*m/z*) ratios).[21] Further structural elucidation can be achieved using tandem MS (MS/MS).[16] Explicitly, low-energy collision-induced dissociation (CID) of mass-selected ether lipid ions permits identification of the polar headgroup and the fatty acid substituent esterified at the *sn*-2 position. Specifically, GPL classes can be individually detected via exploitation of class-specific fragmentations. For instance, in positive ion mode, glycerophosphocholines (PCs) can be identified using precursor ion scanning of *m/z* 184, while glycerophosphoethanolamines (PEs) are detected via neutral loss (NL) scanning of 141 Da.[22] In negative ion mode, low-energy CID readily cleaves the ester bond at the *sn*-2 position, yielding abundant carboxylate anions reflective of the *sn*-2 fatty acyl constituent. However, in either ion polarity, MS/MS alone does not provide direct information regarding the *sn*-1 bond type, as dissociation of the *sn*-1 ether bond is not observed using low-energy CID.[18] Thus, only in specific instances can the *sn*-1 bond type be assigned when exploiting product ion spectra of GPL ions. For example, one can argue that if a monounsaturated ether GPL (e.g., PE *O*-32:1) loses an unsaturated fatty acyl chain from the *sn*-2 position (e.g., loss of 18:1) upon CID of the $[PE - H]^-$ anion, the ether GPL must be a saturated plasmanyl. Aside from this specific case, assignment of GPL subclass can become a difficult task – most notably as the degree of unsaturation increases. In turn, MS^2 product ion spectra are most often insufficient to distinguish an unsaturated alkyl group from a saturated alkenyl moiety at the *sn*-1 position in isomeric ether-linked structures, and thus, most shotgun analyses report ether lipids at the sum compositional level, indicating the need for analytical strategies affording unambiguous ether GPL structural assignment.

Several MS-based approaches have been employed to differentiate GPL subclasses. Widely adopted for plasmalogen identification, Murphy et al. described a combination of mild acid hydrolysis and MS/MS.[23] Acid treatment selectively hydrolyzes the labile 1-*O*-alk-1'-enyl bond found in plasmalogens, and thus, direct spectral comparison before and after acid treatment permits identification and differentiation of various subclasses. Despite its usefulness, this approach is inherently destructive and requires multiple analyses of each sample, which can act as a constraint on throughput. Alternate solution-based strategies, often in combination with tandem MS, permit discrimination among GPL subclasses. For example, Reid and co-workers developed a selective chemical derivatization of the 1-*O*-alk-1'-enyl bond in plasmalogens that enables confident

differentiation among GPL subclasses.[24,25] In a different example, lithium adducted GPL ions (i.e., $[M + Li]^+$) were found to fragment to structurally informative product ions, leading to unambiguous structural assignment.[26] While effective, these approaches are reliant on wet-chemical modification prior to MS analysis or ionization of the sample under conditions that do not maximize detection sensitivity. In a multiple-stage ion-trap MS approach, Hsu and Turk described an MS^n platform to characterize GPL that facilitates structural differentiation among GPL subclasses independent of GPL headgroup composition.[18,27] Unfortunately, as all methods described above are reliant on low-energy CID, these techniques do not pinpoint carbon−carbon double-bond positions in unsaturated fatty acyl chains at the *sn*-2 position.[17,28] As a consequence, resulting experimental signals likely represent a mixture of unresolved isomers. Failing to clearly define structural features, such as double-bond location(s), is problematic, as increasing evidence suggests alterations in lipid isomer relative abundances could serve as sensitive biomarkers for numerous pathologies.[29–32]

While a number of strategies have been established to pinpoint carbon−carbon double bonds in unsaturated lipids, few are capable of identifying the site(s) of unsaturation in intact phospholipids. Furthermore, of these methods, most fail to assign the unsaturation to a particular fatty acyl chain within the complex lipid structure, and in turn, this problem is confounded in ether lipids where different types of carbon−carbon double bonds exist (i.e., conventional unsaturation vs vinyl ether). To our knowledge, only three approaches have demonstrated near-complete ether GPL structure elucidation.[33,34] Specifically, Baba et al. used electron impact excitation of ions from organics (EIEIO) to characterize ether GPLs extracted from animal tissues.[35] While affording assignment of GPL subclass and the site(s) of unsaturation in radyl substituents, EIEIO ultimately suffers from spectral complexity due to a large number of both even- and odd-electron product ions and limited fragmentation efficiency, potentially hindering confident assignment of low-abundance lipids or mixtures of isomeric species. The combination of CID with UV photodissociation in an MS^n workflow can also yield product ions characteristic of acyl chain and double-bond positions in GPLs.[36] In an alternate approach, ozone-induced dissociation (OzID) exploits ion/molecule reactions between mass-selected unsaturated lipid ions and ozone vapor within the trapping region of a mass spectrometer to pinpoint carbon−carbon double-bond locations.[37] Using OzID and/or a combination of OzID and CID (i.e., OzID/CID), confident, high-level lipid structural identification can be achieved, as only double-bond stereochemistry remains

unassigned. Nevertheless, ion/ion reactions offer an alternative approach to gas-phase lipid characterization with shorter reaction times leading to potential advantages in duty cycle compared to ion/molecule chemistries.[38–40]

Recently, gas-phase charge inversion ion/ion reactions have been shown to facilitate lipid characterization.[38–41] Betancourt et al. exploited charge inversion ion/ion reactions between isomeric singly protonated PC and PE cations (i.e., $[PE + H]^+$, $[PC + H]^+$) and doubly deprotonated dicarboxylic acid dianions to charge invert lipid cations, yielding singly charged lipid anions that can be further interrogated to identify fatty acyl subsituents.[41] Importantly, this approach facilitated chemical separation of isomeric/isobaric PC and PE lipid ions on the *m/z* scale due to distinct reactivities of the lipid cations arising from variations in the polar headgroup. Thus, mixture complexities from an isolated lipid precursor cation population can be minimized by employing ion/ion charge inversion chemistry, further improving mixture analysis performance. In an additional example, charge inversion ion/ion reactions have been shown to provide near-complete structural elucidation of lipids.[38–40] Briefly, fatty acid (FA) anions, derived from non-esterified (i.e., free) FA or complex lipid precursors, are reacted with tris-phenanthroline magnesium complex dications (i.e., $[MgPhen_3]^{2+}$) within the high-pressure collision cell of a mass spectrometer to generate charge-inverted FA complex cations (i.e., $[FA - H + MgPhen]^+$). Interrogation of the $[FA - H + MgPhen]^+$ ion facilitates unambiguous isomeric distinction, localization of carbon−carbon double bonds and, in some cases, relative quantitation of isomeric FA.[38,39]

Herein, we report the combination of multiple mass spectrometric workflows to characterize ether GPLs. Specifically, we incorporate MS^n experiments with two discrete gas-phase charge inversion ion/ion chemistries to unravel ether GPL molecular structures. In total, the combination of MS^n and ion/ion reactions facilitates in-depth structural identification of ether GPLs, including differentiation of plasmenyl and plasmanyl subclasses and assignment of carbon−carbon double-bond (C=C) positions within the fatty acyl constituent. Application of the presented method to human plasma extract unveiled ether GPLs previously unresolved using conventional approaches. The demonstration of ether lipids present as isomeric mixtures highlights the remarkable structural diversity of these lipid species and the complexity of the human plasma lipidome.

5.2 Experimental

5.2.1 Materials

All lipid standards were purchased from Avanti Polar Lipids, Inc. (Alabaster, AL). HPLC-grade methanol, water, acetonitrile, ammonium hydroxide, and chloroform were purchased from Fisher Scientific (Pittsburgh, PA). Magnesium chloride, ammonium acetate, 1,10-phenanthroline (Phen), 1,4-phenylenedipropionic acid (PDPA), and citrated human blood plasma were purchased from Sigma-Aldrich (St. Louis, MO).

5.2.2 Lipid Extraction and Preparation of nESI Solutions

Solutions of lipid standards were prepared in methanol to a final concentration of 5 μM. Magnesium chloride and 1,10-phenanthroline were combined in methanolic solution to a final concentration of 20 μM. A solution of PDPA was prepared at a concentration of ~200 μM in 48.5:48.5:3 (v/v/v) acetonitrile/methanol/ammonium hydroxide. Lipids were extracted from human plasma in an identical fashion as previously described.[40]

5.2.3 Nomenclature

When possible, we adopt the shorthand notation recommended by Liebisch et al.[42] For example, glycerophosphoethanolamine and glycerophosphocholine are abbreviated as PE and PC, respectively. In general, 1-*O*-alkyl ether and 1-*O*-alk-1′-enyl ether glycerophospholipids are referred to as the plasmanyl and plasmenyl (plasmalogen) subclasses, correspondingly. Acyl chains are described by the total number of carbons and degree(s) of unsaturation (e.g., 18:1 indicates a fatty acyl chain with 18 carbons and 1 double bond). If known, double-bond position and stereochemistry (*Z* for *cis* or *E* for *trans*) are indicated within parentheses following the degree of unsaturation (e.g., 18:1(9*Z*)). If sn-positions are known, radyl substituents are separated by a forward slash (i.e., PC 16:0/18:1), but if unknown, radyl substituents are separated by an underscore (i.e., PC 16:0_18:1). To indicate ether lipids, proven *O*-alkyl bond (plasmanyl) and *O*-alk-1′-enyl bonds (plasmenyl) are indicated with "*O*" and "*P*", respectively. Where an ether linkage is identified but the adjacent carbon−carbon bond cannot be defined, the general "O" classification is used. For example, the sum composition PE *O*-36:2 can represent either the

plasmanyl PE *O*-18:1(9*Z*)/18:1 or the isomeric plasmenyl species PE *P*-18:0/18:1(9*Z*) or a mixture of both.

5.2.4 Mass Spectrometry

All data were collected on a Sciex QTRAP 4000 hybrid triple quadrupole/linear ion-trap mass spectrometer (SCIEX, Concord, ON, Canada) with modifications analogous to those previously described.[43] Instrument modifications are illustrated with Figure 5.1. The essential hardware modification to enable the mutual storage of oppositely charged ions is the application of auxiliary RF signals to the containment lenses of the q2 quadrupole array.

Two types of charge inversion ion/ion experiments were used in this study for lipid characterization. To aid in mixture analysis, the charge inversion approach developed by Betancourt et al.[41] was implemented prior to negative ion mode MS^n . In short, alternately pulsed nESI emitters enable the sequential injection of lipid cations and reagent anions.[44] First, lipid cations were ionized in positive ion mode via direct infusion positive nESI prior to mass selection in Q1 and subsequent storage in q2. Next, doubly deprotonated reagent PDPA dianions, denoted $[PDPA - 2H]^{2-}$, were ionized in negative ion mode, isolated during transmission through Q1, and accumulated in q2. Once in q2, lipid cations and reagent dianions were reacted under mutual storage conditions for 500 ms. Resulting product lipid anions were then transferred to Q3, isolated using unit resolution, and activated via ion-trap CID (q = 0.25). Product ions generated from CID were analyzed via mass-selective axial ejection (MSAE).[45]

A second experiment employing charge inversion ion/ion chemistry was used to identify sites of unsaturation within the *sn*-2 fatty acyl chain.[40] Direct infusion negative ion nESI was first used to generate the lipid anion. The lipid anion was then isolated during transit through Q1 and sent to the high-pressure collision cell, q2, for storage. Collisional activation of the lipid anion in q2 was employed to generate the *sn*-2 fatty acyl carboxylate anion, denoted $[FA - H]^-$. Now using direct infusion positive ion nESI, the charge inversion reagent dications, $[Mg(Phen)_3]^{2+}$, were generated, mass-selected in Q1, and transferred to q2 for storage. In the high-pressure collision cell, reagent dications and product ions resulting from CID of the mass-selected lipid anion were simultaneously stored for 500 ms. Immediately following the ion/ion reaction period, all product ions were collisionally activated using beam-type CID and transferred to Q3. Once in Q3,

monoisotopic charge-inverted FA complex cations (i.e., $[FA - H + MgPhen]^+$) were isolated and activated via single-frequency resonance excitation (q = 0.383).

5.3 Results and Discussion

5.3.1 Differentiation of Plasmenyl and Plasmanyl Glycerophospholipids

In negative ion mode, diacyl and ether GPLs can be readily differentiated via MS/MS. However, negative ion mode MS2 experiments are usually insufficient for distinguishing isomeric plasmenyl and plasmanyl GPLs. Specifically, CID of the ether GPL anion predominantly results in cleavage of the *sn*-2 fatty acyl ester bond, revealing structural information pertaining only to the *sn*-2 fatty acyl moiety. As mentioned above, Hsu and Turk developed an MS^n multiple-stage ion-trap MS approach for the characterization of ether lipids.[18,27] Herein, we employ this workflow on a modified hybrid triple quadrupole/linear ion-trap mass spectrometer. Our results are analogous to those previously reported,[18,27] noting subtle differences between the data sets, likely due to instrument geometry and resulting differences in ion energetics. Ultimately, we obtained PE subclass differentiation by exploiting MS^3 product ion spectra of the $[PE - H - R_2'CH=C=O]^-$ ions, while MS^4 product ion spectra of $[PC - CH_3 - R_2'CH=C=O]^-$ permitted identification of PC subclasses. For brevity, results from negative ion mode MS^n experiments are detailed in the (see Figures 5.2 and 5.3).

While the approach described previously[18,27] was performed exclusively in negative ion mode, PE and PC analysis is often conducted in positive ion mode, as these species yield abundant singly protonated lipid cations upon direct positive ionization. In particular, a common strategy to identify PEs and PCs entails scanning for neutral fragment losses of a 141 Da NL scan and *m/z* 184 precursor ions in positive ion mode, respectively. However, interrogation of singly protonated PE and PC cations does not provide information pertaining to acyl chain composition. In turn, lipid cation signals likely represent a mixture of isomeric/isobaric molecular species, as the GPL subclass cannot be unambiguously assigned. Notably, isobaric odd-chain diacyl and ether GPL cations can be discriminated via high-resolution mass analysis. For example, the unambiguous discrimination of the isobaric odd-chain diacyl and ether GPL cations such as [PE *P*-18:0/18:1 + $H]^+$ (theoretical *m/z* 730.5745) and [PE 17:0/18:2 + $H]^+$ (theoretical *m/z* 730.5381) can be accomplished if mass resolution exceeds ~20,000 $M/\Delta M_{fwhm}$. However, differentiation of

isomeric ether GPL cations such as [PE *P*-18:0/18:1 + H]$^+$ (theoretical *m/z* 730.5745) and [PE *O*-18:1/18:1 + H]$^+$ (theoretical *m/z* 730.5745) cannot be achieved. Importantly, charge inversion ion/ion chemistry can also be employed to deal with such ambiguities without recourse to high resolution.

To illustrate, synthetic PE *P*-18:0/18:1(9*Z*), PE *O*-16:0/ 18:1(9*Z*), and PE 16:0/18:1(9*Z*) monocations were subjected to ion/ion reaction with doubly deprotonated PDPA dianions to generate structurally informative [PE − H]$^-$ product ions. We note that isomeric GPL standards of varying subclass are not commercially available, and therefore, we must draw conclusions using the synthetic standards presented herein. Explicitly, mass-selected [PE + H]+ cations undergo charge inversion via double-proton transfer to the two carboxylate moieties in doubly deprotonated PDPA to yield [PE − H]$^-$ anions. Results of the ion/ion reaction for PE *P*-18:0/ 18:1(9*Z*), PE *O*-16:0/18:1(9*Z*), and PE 16:0/18:1(9*Z*) are illustrated in Figure 5.4, and all cases exhibited a dominant [PE − H]$^-$ product ion.

The product ion spectra of charge-inverted [PE − H]$^-$ ions derived from synthetic PE *P*-18:0/18:1(9*Z*), PE *O*-16:0/18:1(9*Z*), and PE 16:0/18:1(9*Z*) standards are shown in Figure 5.5a−c, respectively. CID of charge-inverted [PE *P*-18:0/ 18:1(9*Z*) − H]$^-$ (*m/z* 728.5) yielded an abundant 18:1(9*Z*) carboxylate anion observed at *m/z* 281.2 and two additional product ions generated via neutral losses of the *sn*-2 fatty acyl moiety as a fatty acid (i.e., [PE *P*-18:0/18:1(9*Z*) − H − R_2COOH]$^-$, *m/z* 446.3) and as a ketene (i.e., [PE *P*-18:0/18:1(9*Z*) − H − R_2′CH=C=O]$^-$, *m/z* 464.3) (see Figure 5.5a). Similarly, interrogation of [PE *O*-16:0/18:1(9*Z*) − H]$^-$ (*m/z* 702.5) generated via ion/ion reaction gave rise to the [18:1(9*Z*) − H]$^-$ (*m/z* 281.2) and [PE *O*-16:0/18:1(9*Z*) − H − R_2′CH=C=O]$^-$ (*m/z* 438.3) product ions (Figure 5.5b). Thus, as low-energy CID primarily results in ester bond cleavage, MS/MS experiments alone would be inadequate to distinguish isomeric plasmenyl and plasmanyl GPL that differ only in the location of carbon−carbon double bonds in the ether-linked chain. In contrast, the CID spectrum of charge-inverted [PE 16:0/18:1(9*Z*) − H]$^-$ (*m/z* 716.5) displays prominent [16:0 − H]$^-$ (*m/z* 255.2) and [18:1(9*Z*) − H]$^-$ (*m/z* 281.2) anions, along with the [PE 16:0/18:1(9*Z*) − H − R_2COOH]$^-$ (*m/z* 452.3) and [PE 16:0/18:1(9*Z*) − H − R_2′CH=C=O]$^-$ (*m/z* 478.3) product ions (Figure 5.5c). The examples in Figure 5.5 clearly demonstrate that ether GPLs can be readily differentiated from their diacyl counterparts, as the

latter generate abundant fatty acyl carboxylate anions derived from *sn*-1 and *sn*-2 ester bond cleavages. Such negative ion CID analysis can be used to distinguish ether lipids from isobaric odd-chain diacyl GPLs (e.g., [PE *P*-18:0/18:1 − H]$^-$ and [PE 17:0/18:2 − H]$^-$) without the requirement for high-resolution mass spectrometry.

To assign the *sn*-1 bond type in ether PEs, further dissociation of the [PE − H − R_2'CH=C=O]$^-$ product ion is required.[18] To demonstrate, the [PE *P*-18:0/18:1(9*Z*) – H − R_2'CH=C=O]$^-$ (*m/z* 464.3) product ion from Figure 5.5a was re-isolated in the LIT and subjected to ion-trap CID, giving rise to the product ion spectrum depicted in Figure 5.5d. Dominating the MS^3 product ion spectrum of [PE *P*-18:0/ 18:1(9*Z*) − H − R2′CH=C=O]− (*m/z* 464.3) is a product ion observed at *m/z* 196.0 that arises from the neutral loss of the *sn*-1 substituent as a vinyl alcohol (−268 Da). Additionally from Figure 5.5d, the complementary alkoxide product ion [O−CH=CH−$C_{16}H_{33}$]$^-$ is detected at *m/z* 267.2, providing confirmation of the identify of *sn*-1 substituent and the nature of the ether bond at this position. Interrogation of [PE *P*-18:0/18:1(9*Z*) − H − R_2'CH=C=O]$^-$ (*m/z* 464.3) by MS^3 also generated a product ion at *m/z* 403.3 produced via the 61 Da neutral fragment loss of the ethanolamine headgroup (i.e., [PE *P* - 18:0/18:1(9*Z*) − H − R_2'CH=C=O − $HOCH_2CH_2NH_2$]$^-$). In comparison, the MS^3 spectrum of [PE *O*-16:0/18:1(9Z) − H − R_2'CH=C=O]$^-$ (*m/z* 438.3) is defined by a dominant [PE *O*-16:0/18:1(9Z) − H − R_2'CH=C=O − $HOCH_2CH_2NH_2$]$^-$ ion (*m/z* 377.2). Importantly, further dissociation of [PE *O*-16:0/18:1(9Z) − H − R_2'CH=C=O]$^-$ (*m/z* 438.3) does not generate a prominent ethanolamine headgroup product ion at *m/z* 196.0 as previously observed within the CID spectrum of [PE *P*-18:0/18:1(9Z) − H − R_2'CH=C=O]$^-$ (m/z 464.3) (*cf.* Figure 5.5d,e). For completeness, interrogation of the [PE 16:0/18:1(9*Z*) − H − R_2'CH=C=O]$^-$ (*m/z* 452.3) anion induced cleavage of the *sn*-1 ester bond, yielding an abundant 16:0 fatty acyl carboxylate anion (*m/z* 255.2), as illustrated in Figure 5.5f. In sum, implementing MS^3 on analogous charge-inverted [PE − H]$^-$ ions that have undergone neutral fragment losses of the *sn*-2 fatty acyl substituent as a ketene yielded significant mass spectral differences, which consequently enabled structural distinction among GPL subclasses and confident assignment of the *sn*-1 bond type.

[PC + H]$^+$ cations also can be transformed in the gas-phase via charge inversion in reactions with doubly deprotonated PDPA reagent dianions. Explicitly, the charge inversion reaction between [PC + H]$^+$ cations derived from synthetic PC *P*-18:0/18:1(9*Z*), PC *O*-16:0/18:1(9*Z*), and PC 16:0/18:1(9*Z*) and PDPA reagent dianions gives rise to [PC + PDPA – H]$^-$ adduct anions that

can subsequently dissociate via ion-trap CID to yield demethylated PC anions (Figure 5.6).[41,46] Following the gas-phase transformation of PC monocations, dissociation of the $[PC - CH_3]^-$ ion produces $[PC - CH_3 - R_2'CH{=}C{=}O]^-$ ions that can be further probed via ion-trap CID, facilitating identification of radyl constituents and subclass discrimination (see Figure 5.7). Briefly, ion-trap CID of $[PC - CH_3]^-$ yielded information regarding only the *sn*-2 fatty acyl substituent, and therefore, MS^3 product ion spectra would again be insufficient to differentiate isomeric plasmanyl and plasmenyl PCs. Once more, ion-trap CID of mass-selected $[PC - CH_3 - R_2'CH{=}C{=}O]^-$ ions derived from PCs facilitated identification of the *sn*-1 bond type. Specifically, the MS^4 spectra of analogous $[PC - CH_3 - R_2'CH{=}C{=}O]^-$ ions derived from plasmenyl, plasmanyl, and diacyl PCs presented unique mass spectral features paralleling those described above for PE lipids. It is key to note that while the headgroup product ion observed at *m/z* 196.0 can be exploited to identify plasmenyl PE, the phosphocholine-derived ion detected at *m/z* 224.0 confirms the plasmenyl PC structure (Figure 5.7).

Importantly, the combination of charge inversion reactions and the negative ion mode MS^n experiments outlined herein offer a number of benefits when compared to the negative ion mode multiple-stage MS approach alone. Namely, the charge inversion strategy relies on the use of positive ionization for lipid analytes. Particularly for PCs, positive ionization can be more efficient, leading to lower detection limits. Second, PC and PE cations undergo distinct charge inversion processes with PDPA reagent dianions due to differences in the polar headgroups (i.e., primary amine for PEs and quaternary ammonium for PCs). In turn, the net result of the charge inversion ion/ion reaction permits chemical separation of isomeric/isobaric PE and PC lipids entirely in the gas phase.[41] Thus, charge inversion ion/ion chemistry reduces mixture complexities arising from isomeric/isobaric interferences within a single isolated precursor cation population, which can enhance complex mixture analysis performance, especially when considered in combination with negative ion mode MS^n experiments outlined herein.

5.3.2 Identification of Fatty Acyl Double-Bond Position(s) in Ether GPL

While the MS^n experiments described above afford confident assignment of *sn*-1 bond type, low-energy CID alone cannot localize carbon−carbon double-bond positions in radyl substituents. To pinpoint sites of unsaturation in the *sn*-2 fatty acyl moiety, we employed gas-phase ion/ion charge inversion chemistry. Following ionization via direct negative nESI,

collisional activation of mass-selected [PE *P*-18:0/18:1(9*Z*) − H]$^-$ (*m/z* 728.5) liberated the *sn*-2 fatty acyl substituent, generating the 18:1 carboxylate anion. Note that the resulting CID spectrum for [PE *P*-18:0/18:1(9*Z*) − H]$^-$ was identical to that shown above in Figure 5.5a. Next, the MS^2 product ions arising from CID of [PE *P*-18:0/18:1(9*Z*) − H]$^-$ were allowed to react in the gas-phase with [MgPhen$_3$]$^{2+}$ reagent diactions, yielding the product ion spectrum shown in Figure 5.8a. The ion/ion reaction favored formation of the [18:1(9*Z*) − H + MgPhen$_2$]$^+$ (*m/z* 665.4) complex cation, but additional [PE *P*-18:0/18:1(9*Z*) − H + MgPhen$_2$]$^+$ and [PE *P*-18:0/18:1(9*Z*) − H − R$_2$′CH=C=O + MgPhen$_2$]$^+$ product ions were also observed at *m/z* 1112.7 and 848.4, respectively (Figure 5.8a). Ensuing beam-type (BT) CID, arising from collisions during energetic transfer of ions from q2 to Q3, produced the CID spectrum shown in Figure 5.8b, characterized by an abundant [18:1(9*Z*) − H + MgPhen]$^+$ (*m/z* 485.3) product ion. Also depicted in Figure 5.8b are the [PE *P*-18:0/18:1(9*Z*) − H + MgPhen]$^+$ (*m/z* 932.6), [PE *P*-18:0/18:1(9*Z*) − H − R$_2$COOH + MgPhen]$^+$ (*m/z* 650.4), [PE *P*-18:0/18:1(9*Z*)− H − R$_2$′CH=C=O − CH$_2$CH$_2$NH + MgPhen]$^+$ (*m/z* 625.3), and [PE *P*-18:0/18:1(9*Z*) − H −R$_2$COOH − CH$_2$CH$_2$NH + MgPhen]$^+$ (*m/z* 607.3) product ions. As described in previous reports,[38,39] CID of charge-inverted FA complex cations enables unambiguous isomeric distinction and confident assignment of double-bond position(s) either via direct spectral interpretation or automated spectral matching. In this example, ion-trap CID of [18:1(9*Z*) − H + MgPhen]$^+$ (*m/z* 485.3) generated a spectral gap, as highlighted by the blue shading in Figure 5.8c, corresponding with the carbon−carbon double-bond position. In particular, the characteristic spectral gap is flanked by product ions arising from carbon−carbon cleavage allylic to the double bond (i.e., *m/z* 331.2 and 387.2) and displays interruption of the usual 14 Da spacing, as the *m/z* difference between product ions at *m/z* 345.2 and 357.2 is 12 Da, confirming the C9=C10 double bond position in the *sn*-2 acyl chain of synthetic PE *P*-18:0/18:1(9*Z*). In an identical fashion, the site(s) of unsaturation can be localized in the fatty acyl substituent of plasmanyl PE. This process for PE *O*-16:0/18:1(9*Z*) is illustrated with Figure 5.9. Furthermore, charge inversion ion/ion chemistry can be employed to pinpoint carbon−carbon double-bond positions in unsaturated ether GPL regardless of polar headgroup composition. This is demonstrated with the analysis of synthetic PC *P*-18:0/18:1(9*Z*) and PC *O*-16:0/18:1(9Z), as illustrated with Figures 5.10 and 5.11, respectively. In total, through the combination of MS^n in negative ion mode with charge inversion and activation of the ester-linked fatty acyl chain, we achieve confident assignment of the nature of the ether linkage at *sn*-1 and the site(s) of unsaturation on the *sn*-2 chain. We note that in the

case of plasmanyl lipids, where unsaturation is detected in the ether-linked chain but where double bond(s) are not localized at the ether (e.g., PE *O*-18:1(9*Z*)/18:1(9*Z*)), this strategy is unable to directly localize sites of unsaturation carried by the *sn*-1 radyl substituent, and auxiliary data would be required for full characterization.

5.3.3 Identification of Ether Lipids in Human Plasma

As changes in both plasma lipid content and composition have been linked with numerous pathologies, the human plasma lipidome has been extensively explored with the aim of identifying lipid biomarkers.[47] Comprised of thousands of distinct lipid molecular structures, the inherent complexity of the human plasma lipidome presents distinct analytical challenges. Unfortunately, LC-based techniques often fail to provide chromatographic separation of isomeric/isobaric plasmenyl and plasmanyl GPLs. If chromatographic separation is not achieved, both structural analogues must be reported, leading to structural ambiguity.[19,20] Furthermore, as double bond position(s) cannot be assigned using conventional lipidomics workflows, most plasma lipids are identified only at the sum compositional (e.g., PC *O*-36:2) or molecular lipid level (e.g., PC *O*-18:0/18:2). Thus, it is plausible that reported plasma lipids, including proposed biomarkers, exist not as a single species but as an unresolved mixture of isomeric structures.

In this study, we interrogated two ether-linked GPLs previously identified in human plasma at the sum compositional level, exploiting class-specific fragmentations (Figure 5.12). First, we examined the sum composition PE *O*-38:5 detected as a protonated cation at *m/z* 752.5 upon nESI of a human plasma extract (Figure 5.13). To reduce mixture complexities, mass-selected [PE *O*-38:5 + H]$^+$ (*m/z* 752.5) cations were generated by direct infusion positive nESI and subsequently charge-inverted in the gas phase via ion/ion reactions with PDPA reagent dianions to produce lipid anions as summarized above. The resulting ion/ion reaction spectrum shown in Figure 5.14a reveals the presence of at least two isomeric or isobaric components present in the original *m/z* 752.5 ion population, as two prominent charge-inverted product ions were observed. Explicitly, the product ion observed at *m/z* 750.5 in Figure 5.14a corresponds to the singly deprotonated [PE *O*-38:5 − H]$^-$ anion and likely represents an ion population composed of exclusively of PE lipid(s), while the product ion detected at *m/z* 972.5 signifies the [PC 34:5 + PDPA − H]$^-$ complex anion. Subsequent mass selection and ion-trap CID of charge-inverted [PE *O*-38:5 − H]$^-$ (*m/z* 750.5) yields the [20:4 − H]$^-$ (*m/z* 303.2), [20:4 − H − CO_2]$^-$ (*m/z* 259.2), and [PE *O*-38:5 − H −

$R_2'CH=C=O]^-$ (*m/z* 464.2) product ions, which imply the presence of either PE *O*-18:1/20:4 or PE *P*-18:0/20:4 (Figure 5.14b). These structures are further supported by the absence of 18:0 and 18:1 carboxylate anions. Unfortunately, interrogation of the product ion at *m/z* 464.2 shown in Figure 5.14b could not be conducted due to low signal levels. Relative to PCs, PEs can suffer from ionization suppression in the positive ion mode, leading to the low abundance of the [PE *O*-38:5 + H]$^+$ precursor ion prior to ion/ion reaction. Thus, low product ion abundances are not inherently due to charge inversion but, instead, are related to low ether GPL abundance in plasma extract and/or PE ionization suppression in positive ion mode.

To interrogate the [PE *O*-38:5 − H − $R_2'CH=C=O]^-$ (*m/z* 464.2) product ion and determine the nature of the *sn*-1linkage, we turned to direct negative MS^n experiments, in which PE ionization will be less prone to ionization suppression. Following direct negative nESI of plasma extract (Figure 5.13), dissociation of the [PE *O*-38:5 − H]$^-$ ion (*m/z* 750.5) generated product ions analogous to those observed in Figure 5.14b; yet, the CID spectrum obtained in the absence of charge inversion ion/ion reactions contains abundant product ions not originating from the [PE *O*-38:5 − H]$^-$ precursor ion, suggesting isomeric/isobaric interferences (Figure 5.15a). For example, the CID spectrum of [PE *O*-38:5 − H]$^-$ ion (*m/z* 750.5) contains a dominant product ion at *m/z* 480.2 (Figure 5.15a). Re-isolation and ion-trap CID of the product ion at *m/z* 480.2 revealed an abundant [16:0 − H]$^-$ (*m/z* 255.2) carboxylate anion (Figure 5.16), suggesting that the MS^2 product ion observed at *m/z* 480.2 in Figure 5.15a likely originated from an isobaric odd-chain diacyl PC (i.e., [PC 13:0_16:0 + OAc]$^-$ adduct ion with theoretical *m/z* 750.5291). Note that this isobaric interference is absent when using charge inversion ion/ion chemistry (*cf.*, Figures 5.14a and 5.15a).

To differentiate among the PE *O*-18:1/20:4 and PE *P*-18:0/20:4 structures, we applied negative ion mode MS^n. Following CID of [PE *O*-38:5 − H]$^-$ (*m/z* 750.5), the [PE *O*-38:5 – H − $R_2'CH=C=O]^-$ (*m/z* 464.2) product ion was isolated in Q3 and subjected to ion-trap CID. Figure 5.15b illustrates the MS^3 product ion spectrum of [PE *O*-38:5 − H − $R_2'CH=C=O]^-$ (*m/z* 464.2). Exploiting the CID spectrum of [PE *O*-38:5 – H − $R_2'CH=C=O]^-$ (*m/z* 464.2), the major isomeric contributor proved to be PE *P*-18:0/20:4, as an abundant product ion characteristic of plasmalogen PE was observed at *m/z* 196.0 (Figure 5.15b). Also observed in Figure 5.15b are product ions at *m/z* 267.0 and 403.2 corresponding to the $[O{-}CH{=}CH{-}C_{16}H_{33}]^-$ and [PE *O*-38:5 − H − $R_2'CH=C=O$ − $HOCH_2CH_2NH_2]^-$ ions, respectively. Using this approach, it is important to note that we cannot exclude minor isomeric contributions from PE *O*-18:1/20:4 due to the lack of

unique product ions indicative of the plasmanyl subclass upon CID of the [PE *O*-38:5 − H − $R_2'CH{=}C{=}O]^-$ ion.

Additional minor isomeric components are suggested by the [PE *O*-38:5 − H]$^-$ product ion spectra obtained with and without charge inversion (see Figures 5.14a and 5.15b). In particular, the [22:4 − H]$^-$ (*m/z* 331.2), [22:5 − H]$^-$ (*m/z* 329.2), and [20:3 − H]$^-$ (*m/z* 305.2) carboxylate anions indicate potential minor isomeric contributions from – but not limited to – PE *O*-16:0/22:5, PE *O*-16:1/22:4, PE *P*-16:0/22:4, and PE *P*-18:1/20:3. Unfortunately, these suggested structures cannot be corroborated via interrogation of the corresponding [PE *O*-38:5 − H − $R_2'CH{=}C{=}O]^-$ ion(s), as signal levels were too low.

To pinpoint carbon−carbon double bonds in the *sn*-2 fatty acyl constituent of PE *P*-18:0/20:4, we employed gas-phase ion/ion chemistry. The product ions depicted in Figure 4a were transformed in the gas phase via ion/ion reaction with $[MgPhen_3]^{2+}$ dications. The product ion spectrum shown in Figure 5.15c represents the results of the ion/ion reaction and subsequent collisional activation via BT CID. Isolation and ion-trap CID of charge-inverted FA complex cations in the LIT permitted unambiguous assignment of unsaturation site(s).[38] Exploiting the [20:4 − H + MgPhen]$^+$ (*m/z* 507.3) product ion spectrum (Figure 5.17), the major ether structure was confidently assigned as PE *P*-18:0/20:4(5,8,11,14) via spectral matching to an arachidonic acid standard in the previously constructed fatty acid library.[38]

The plasma-derived sum composition PC *O*-38:5 was also interrogated in this study. Recently, serum PC *O*-38:5 has been suggested as a potential biomarker for prostate cancer.[48] However, it is likely that this proposed biomarker exists as an isomeric mixture. Once more, charge inversion of the [PC *O*-38:5 + H]$^+$ cation proceeds via ion/ion reaction with PDPA reagent dianions, generating the product ion spectrum displayed in Figure 5.18a. The ion/ion reaction yields an abundant [PC *O*-38:5 + PDPA − H]$^-$ (*m/z* 1014.7) complex anion likely comprised exclusively of PC lipid(s). Upon collisional activation, [PC *O*-38:5 + PDPA − H]$^-$ (*m/z* 1014.7) fragments to form the demethylated PC *O*-38:5 anion detected at *m/z* 778.6 (Figure 5.18b). Ensuing dissociation of the product ion at *m/z* 778.6 revealed a dominant [20:4 − H]$^-$ (*m/z* 303.2) anion and [PC *O*-38:5 − CH3 − $R_2'CH{=}C{=}O]^-$ (*m/z* 492.3) ion (Figure 5.19a). Together, these product ions indicate the presence of either PC *O*-18:1/20:4 or PC *P*-18:0/20:4. The MS^4 product ion spectrum of [PC *O*-38:5 − CH3 − $R_2'CH{=}C{=}O]^-$ (*m/z* 492.3) contains an abundant product ion corresponding to the neutral loss of dimethylamine observed at *m/z* 403.3, indicative of a plasmanyl PC, while

the diagnostic plasmenyl ions at *m/z* 224.0 and 267.2 were present only at low abundance in the spectrum (Figure 5.19b). Consequently, the alkyl ether linked PC *O*-18:1/20:4 was assigned as the major isomeric contributor to the PC *O*-38:5 sum composition in human plasma. Furthermore, PC *P*-18:0/20:4 was identified as a minor isomeric component based on the presence of low-abundance MS^4 product ions detected at *m/z* 224.0 (i.e., polar headgroup ion) and *m/z* 267.0 (i.e., $[O{-}CH{=}CH{-}C_{16}H_{33}]^-$). Using ion/ion chemistry (Figure 5.20), the 20:4 fatty acyl linked at the *sn*-2 position was identified as 20:4(5,8,11,14) via matching to an arachidonic acid reference standard in the fatty acid database.[38] In total, PC *O*-18:1/20:4(5,8,11,14) and PC *P*-18:0/20:4(5,9,11,14) can be assigned as the major and minor isomeric contributors, respectively. While the site of unsaturation in the ether-linked 18:1 chain of PC *O*-18:1/20:4(5,8,11,14) could not be directly determined from these experiments, recent ozone-induced dissociation measurements on plasma-derived PC *O*-38:5 find a double bond at the 9-position in the ether-linked chain.[34] Taken together, these data suggest a more complete structural assignment for the dominant isomer as PC *O*-18:1(9)/20:4(5,8,11,14). The $[22{:}4 - H]^-$ (*m/z* 331.2) and $[22{:}5 - H]^-$ (*m/z* 329.2) fatty acyl anions provide evidence for additional ether PC isomers, but these additional minor isomeric contributors could not be confidently assigned due to low abundances of the corresponding $[PC - CH_3 - R_2'CH{=}C{=}O]^-$ product ions (Figure 5.19a).

Qualitatively, our findings indicate that despite the presence of a common *O*-38:5 sum composition in PE and PC subclasses in human plasma, the major isomeric contributors vary in *sn*-1 linkages between classes. That is, the plasmenyl PE (i.e., PE *P*-18:0/20:4(5,8,11,14)) was assigned as the primary isomeric contributor to the PE *O*-38:5 sum composition, while a plasmanyl PC (i.e., PC *O*-18:1/20:4(5,8,11,14)) represented the dominant isomer of PC *O*-38:5. Collectively, these data allude to the different underlying mechanisms for PC and PE plasmalogen biosynthesis and regulation.[49] Therefore, the method presented herein could provide an increased understanding of plasmalogen biosynthetic pathways and regulatory factors across different cell types or tissues. Furthermore, as demonstrated with the analysis of human plasma PC *O*-38:5, it is evident that biomarkers identified only at the sum compositional level may very well exist as a mixture of isomeric structures.

5.4 Conclusions

In this work, we pair MS^n with two distinct gas-phase ion/ion charge inversion chemistries to facilitate high-level structural elucidation of ether GPL. Performed on a modified hybrid triple quadrupole/linear ion-trap mass spectrometer, distinction of ether GPL subclasses is ultimately based on substantial differences in negative ion mode MS^3 (or MS^4) product ion spectra of ions arising from losses of the *sn*-2 fatty acyl substituent as a ketene. In particular, the MS^n (n = 3, 4) product ion spectrum from a plasmenyl GPL is dominated by an alkenoxide anion that represents the radyl moiety at the *sn*-1 position and a product ion generated via the consecutive loss of the *sn*-1 radyl group from the mass-selected $[M - H - R_2'CH=C=O]^-$ precursor anion. Conversely, the plasmanyl GPL MS^n (n = 3, 4) product ion spectrum is characterized by a product ion reflecting the neutral loss of a polar headgroup. The combination of positive to negative charge inversion ion/ion chemistry via gas-phase ion/ion reactions between PC and PE lipid monocations and doubly deprotonated PDPA dianions with the reported negative ion mode MS^n platform enhances mixture analysis performance, reducing complexities arising from isomeric or isobaric interferences. However, as this technique is reliant on low-energy CID, sites of unsaturation cannot be assigned using this tactic alone. Thus, to pinpoint carbon−carbon double-bond position(s) in the *sn*-2 fatty acyl moiety, ion/ion charge inversion reactions were employed. Specifically, fatty acyl anions liberated from ether GPL precursor anions were transformed in the gas-phase via ion/ion reaction with charge inversion dications to generate $[FA - H + MgPhen]^+$ complex cations. Predictable fragmentation patterns of charge-inverted FA complex cations permit unambiguous isomeric distinction and confident identification of double-bond position(s). The entirely gas-phase shotgun approach presented herein was successfully applied to identify ether GPL extracted from human plasma, ultimately exposing several isomeric contributors. In turn, the combination of MS^n experiments and ion/ion chemistry enabled confident assignment of all major and some minor isomeric contributors present in plasma ether GPL. As demonstrated with the analysis of plasma PC *O*-38:5, a proposed biomarker for prostate cancer, these data reinforce the need for analytical techniques capable of achieving isomeric resolution and facilitating detailed lipid structural assignments in biomarker discovery. More broadly, the method illustrated here has the potential to provide insight into plasmalogen biosynthetic pathways and regulatory factors dependent on not only headgroup composition but also biological origin. Lastly, application of the

developed approach could advance our understanding of plasmalogen roles in various metabolic processes and pathologies.

5.5 References

1. Maeba, R.; Nishimukai, M.; Sakasegawa, S.; Sugimori, D.; Hara, H. *Adv. Clin. Chem.* **2015**, *70*, 31−94.

2. Dean, J. M.; Lodhi, I. J. *Protein Cell* **2018**, *9* (2), 196−206.

3. Paltauf, F. *Chem. Phys. Lipids* **1994**, *74* (2), 101−139.

4. Han, X. L.; Gross, R. W. *Biochem.* **1990**, *29* (20), 4992−4996.

5. Braverman, N. E.; Moser, A. B. *Biochim. Biophys. Acta, Mol. Basis Dis*. **2012**, *1822* (9), 1442−1452.

6. Brites, P.; Waterham, H. R.; Wanders, R. J. A. *Biochim. Biophys. Acta, Mol. Cell Biol. Lipids* **2004**, *1636* (2−3), 219−231.

7. Malheiro, A. R.; da Silva, T. F.; Brites, P. *J. Inherited Metab. Dis*. **2015**, *38* (1), 111−121.
8. Schrakamp, G.; Schutgens, R. B. H.; Wanders, R. J. A.; Heymans, H. S. A.; Tager, J. M.; Vandenbosch, H. *Biochim. Biophys. Acta, Lipids Lipid Metab*. **1985**, *833* (1), 170−174.

9. Messias, M. C. F.; Mecatti, G. C.; Priolli, D. G.; de Oliveira Carvalho, P. *Lipids Health Dis*. **2018**, *17*, 41.

10. Skotland, T.; Ekroos, K.; Kauhanen, D.; Simolin, H.; Seierstad, T.; Berge, V.; Sandvig, K.; Llorente, A. *Eur. J. Cancer* **2017**, *70*, 122−132.

11. Chen, X. L.; Chen, H. K.; Dai, M. Y.; Ai, J. M.; Li, Y.; Mahon, B.; Dai, S. M.; Deng, Y. P. *Oncotarget* **2016**, *7* (24), 36622−36631.

12. Han, X. L.; Holtzman, D. M.; McKeel, D. W. *J. Neurochem*. **2001**, *77* (4), 1168−1180.

13. Donovan, E. L.; Pettine, S. M.; Hickey, M. S.; Hamilton, K. L.; Miller, B. F. *Diabetol. Metab. Syndr*. **2013**, *5*, 24.

14. Oresic, M.; Simell, S.; Sysi-Aho, M.; Nanto-Salonen, K.; Seppanen-Laakso, T.; Parikka, V.; Katajamaa, M.; Hekkala, A.; Mattila, I.; Keskinen, P.; Yetukuri, L.; Reinikainen, A.; Lahde, J.; Suortti, T.; Hakalax, J.; Simell, T.; Hyoty, H.; Veijola, R.; Ilonen, J.; Lahesmaa, R.; Knip, M.; Simell, O. *J. Exp. Med*. **2008**, *205* (13), 2975−2984.

15. Graessler, J.; Schwudke, D.; Schwarz, P. E. H.; Herzog, R.; Shevchenko, A.; Bornstein, S. R. *PLoS One* **2009**, *4* (7), e6261.

16. Pulfer, M.; Murphy, R. C. *Mass Spectrom. Rev*. **2003**, *22* (5), 332−364.

17. Blanksby, S. J.; Mitchell, T. W. *Annu. Rev. Anal. Chem*. **2010**, *3*, 433−465.

18. Hsu, F. F.; Turk, J. *J. Am. Soc. Mass Spectrom*. **2007**, 18 (11), 2065−2073.

19. Bowden, J. A.; Heckert, A.; Ulmer, C. Z.; Jones, C. M.; Koelmel, J. P.; Abdullah, L.; Ahonen, L.; Alnouti, Y.; Armando, A. M.; Asara, J. M.; Bamba, T.; Barr, J. R.; Bergquist, J.; Borchers, C. H.; Brandsma, J.; Breitkopf, S. B.; Cajka, T.; Cazenave-Gassiot, A.; Checa, A.; Cinel, M. A.; Colas, R. A.; Cremers, S.; Dennis, E. A.; Evans, J. E.; Fauland, A.; Fiehn, O.; Gardner, M. S.; Garrett, T. J.; Gotlinger, K. H.; Han, J.; Huang, Y. Y.; Neo, A. H. P.; Hyotylainen, T.; Izumi, Y.; Jiang, H. F.; Jiang, H. L.; Jiang, J.; Kachman, M.; Kiyonami, R.; Klavins, K.; Klose, C.; Kofeler, H. C.; Kolmert, J.; Koal, T.; Koster, G.; Kuklenyik, Z.; Kurland, I. J.; Leadley, M.; Lin, K.; Maddipati, K. R.; McDougall, D.; Meikle, P. J.; Mellett, N. A.; Monnin, C.; Moseley, M. A.; Nandakumar, R.; Oresic, M.; Patterson, R.; Peake, D.; Pierce, J. S.; Post, M.; Postle, A. D.; Pugh, R.; Qiu, Y. P.; Quehenberger, O.; Ramrup, P.; Rees, J.; Rembiesa, B.; Reynaud, D.; Roth, M. R.; Sales, S.; Schuhmann, K.; Schwartzman, M. L.; Serhan, C. N.; Shevchenko, A.; Somerville, S. E.; St. John-Williams, L.; Surma, M. A.; Takeda, H.; Thakare, R.; Thompson, J. W.; Torta, F.; Triebl, A.; Trotzmuller, M.; Ubhayasekera, S. J. K.; Vuckovic, D.; Weir, J. M.; Welti, R.; Wenk, M. R.; Wheelock, C. E.; Yao, L. B.; Yuan, M.; Zhao, X. Q. H.; Zhou, S. L. *J. Lipid Res.* **2017**, *58* (12), 2275−2288.

20. Quehenberger, O.; Armando, A. M.; Brown, A. H.; Milne, S. B.; Myers, D. S.; Merrill, A. H.; Bandyopadhyay, S.; Jones, K. N.; Kelly, S.; Shaner, R. L.; Sullards, C. M.; Wang, E.; Murphy, R. C.; Barkley, R. M.; Leiker, T. J.; Raetz, C. R. H.; Guan, Z. Q.; Laird, G. M.; Six, D. A.; Russell, D. W.; McDonald, J. G.; Subramaniam, S.; Fahy, E.; Dennis, E. A. J. *Lipid Res.* **2010**, *51* (11), 3299−3305.

21. Bou Khalil, M. B.; Hou, W. M.; Zhou, H.; Elisma, F.; Swayne, L. A.; Blanchard, A. P.; Yao, Z. M.; Bennett, S. A. L.; Figeys, D. *Mass Spectrom. Rev.* **2010**, *29* (6), 877−929.

22. Brugger, B.; Erben, G.; Sandhoff, R.; Wieland, F. T.; Lehmann, W. D. *Proc. Natl. Acad. Sci. U. S. A.* **1997**, *94* (6), 2339−2344.

23. Kayganich, K. A.; Murphy, R. C. *Anal. Chem.* **1992**, *64* (23), 2965−2971.

24. Ryan, E.; Reid, G. E. *Acc. Chem. Res.* **2016**, *49* (9), 1596−1604.

25. Fhaner, C. J.; Liu, S.; Zhou, X.; Reid, G. E. *Mass Spectrom.* **2013**, *2*, S0015.

26. Hsu, F. F.; Turk, J. *J. Mass Spectrom.* **2000**, *35* (5), 595−606.

27. Hsu, F. F.; Lodhi, I. J.; Turk, J.; Semenkovich, C. F. *J. Am. Soc. Mass Spectrom.* **2014**, *25* (8), 1412−1420.

28. Mitchell, T. W.; Pham, H.; Thomas, M. C.; Blanksby, S. J. *J. Chromatogr. B: Anal. Technol. Biomed. Life Sci.* **2009**, *877* (26), 2722−2735.

29. Zhang, W. P.; Zhang, D. H.; Chen, Q. H.; Wu, J. H.; Ouyang, Z.; Xia, Y. *Nat. Commun.* **2019**, *10*, 79.

30. Qiu, Y. P.; Zhou, B. S.; Su, M. M.; Baxter, S.; Zheng, X. J.; Zhao, X. Q.; Yen, Y.; Jia, W. *Int. J. Mol. Sci*. **2013**, *14* (4), 8047−8061.

31. Razquin, C.; Toledo, E.; Clish, C. B.; Ruiz-Canela, M.; Dennis, C.; Corella, D.; Papandreou, C.; Ros, E.; Estruch, R.; Guasch-Ferre, M.; Gomez-Gracia, E.; Fito, M.; Yu, E.; Lapetra, J.; Wang, D.; Romaguera, D.; Liang, L. M.; Alonso-Gomez, A.; Deik, A.; Bullo, M.; Serra-Majem, L.; Salas-Salvado, J.; Hu, F. B.; Martinez-Gonzalez, M. A. *Diabetes Care* **2018**, *41* (12), 2617−2624.

32. Mundra, P. A.; Barlow, C. K.; Nestel, P. J.; Barnes, E. H.; Kirby, A.; Thompson, P.; Sullivan, D. R.; Alshehry, Z. H.; Mellett, N. A.; Huynh, K.; Jayawardana, K. S.; Giles, C.; McConville, M. J.; Zoungas, S.; Hillis, G. S.; Chalmers, J.; Woodward, M.; Wong, G.; Kingwell, B. A.; Simes, J.; Tonkin, A. M.; Meikle, P. J. *Jci Insight* **2018**, *3* (17), e121326.

33. Deeley, J. M.; Thomas, M. C.; Truscott, R. J. W.; Mitchell, T. W.; Blanksby, S. J. *Anal. Chem*. **2009**, *81* (5), 1920−1930.

34. Marshall, D. L.; Criscuolo, A.; Young, R. S.; Poad, B. L.; Zeller, M.; Reid, G. E.; Mitchell, T. W.; Blanksby, S. J. *J. Am. Soc. Mass Spectrom*. **2019**, *30* (9), 1621.

35. Baba, T.; Campbell, J. L.; Le Blanc, J. C. Y.; Baker, P. R. S.; Ikeda, K. *J. Lipid Res*. **2018**, *59* (5), 910−919.

36. Williams, P. E.; Klein, D. R.; Greer, S. M.; Brodbelt, J. S. *J. Am. Chem. Soc*. **2017**, *139* (44), 15681−15690.

37. Thomas, M. C.; Mitchell, T. W.; Harman, D. G.; Deeley, J. M.; Nealon, J. R.; Blanksby, S. J. *Anal. Chem*. **2008**, *80* (1), 303−311.

38. Randolph, C. E.; Foreman, D. J.; Blanksby, S. J.; McLuckey, S. A. *Anal. Chem*. **2019**, *91* (14), 9032−9040.

39. Randolph, C. E.; Foreman, D. J.; Betancourt, S. K.; Blanksby, S. J.; McLuckey, S. A. *Anal. Chem*. **2018**, *90* (21), 12861−12869.

40. Randolph, C. E.; Blanksby, S. J.; McLuckey, S. A. *Anal. Chem*. **2020**, *92* (1), 1219−1227.

41. Rojas-Betancourt, S.; Stutzman, J. R.; Londry, F. A.; Blanksby, S. J.; McLuckey, S. A. *Anal. Chem*. **2015**, *87* (22), 11255−11262.

42. Liebisch, G.; Vizcaino, J. A.; Kofeler, H.; Trotzmuller, M.; Griffiths, W. J.; Schmitz, G.; Spener, F.; Wakelam, M. J. O. *J. Lipid Res.* **2013**, *54* (6), 1523−1530.

43. Xia, Y.; Wu, J.; McLuckey, S. A.; Londry, F. A.; Hager, J. W. *J. Am. Soc. Mass Spectrom*. **2005**, *16* (1), 71−81.

44. Liang, X. R.; Xia, Y.; McLuckey, S. A. *Anal. Chem*. **2006**, *78* (9), 3208−3212.

45. Londry, F. A.; Hager, J. W. *J. Am. Soc. Mass Spectrom*. **2003**, *14* (10), 1130−1147.

46. Stutzman, J. R.; Blanksby, S. J.; McLuckey, S. A. *Anal. Chem*. **2013**, *85* (7), 3752−3757.

47. Vvedenskaya, O.; Wang, Y.; Ackerman, J. M.; Knittelfelder, O.; Shevchenko, A. *TrAC, Trends Anal. Chem*. **2019**, *120*, 115277.

48. Patel, N.; Vogel, R.; Chandra-Kuntal, K.; Glasgow, W.; Kelavkar, U. *PLoS One* **2014**, *9* (3), e88841.

49. Nagan, N.; Zoeller, R. A. *Prog. Lipid Res*. **2001**, *40* (3), 199−229.

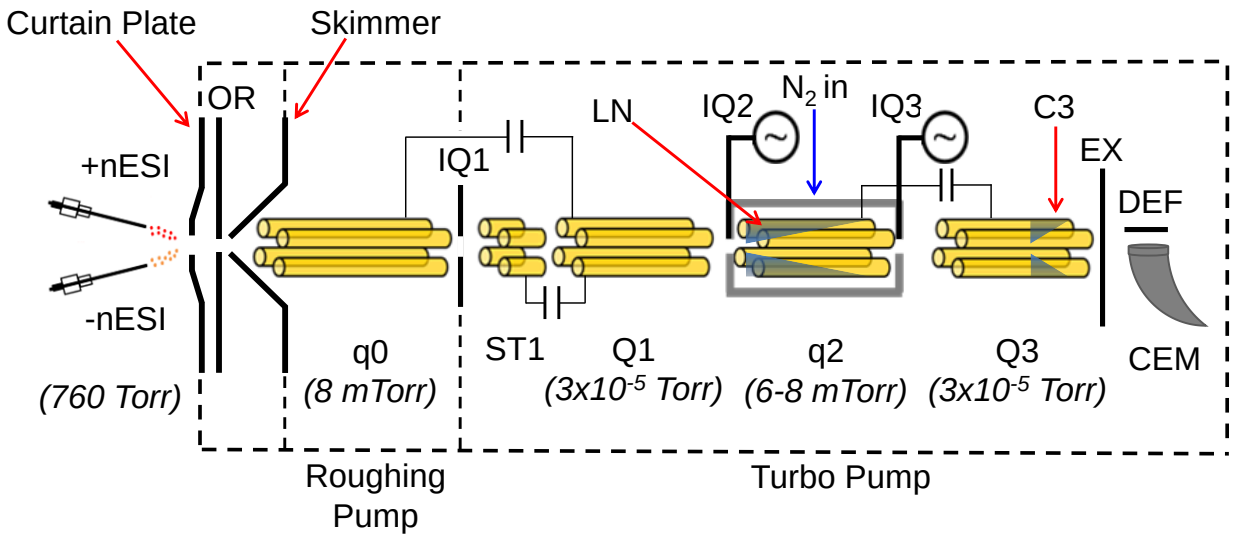

Figure 5.1 Schematic diagram (not to scale) of a QTRAP 4000 hybrid triple quadrupole/linear ion trap mass spectrometer (AB SCIEX, Concord, ON, Canada) previously modified for ion/ion reactions.

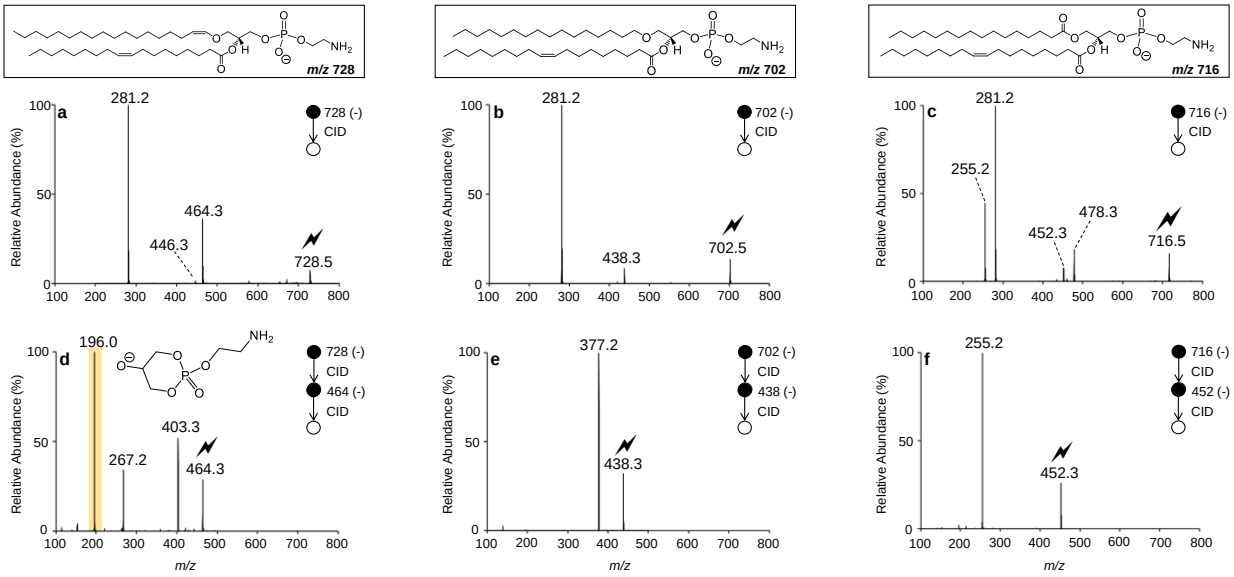

Figure 5.2 MS^2 product ion spectra obtained via ion-trap CID of (a) [PE *P*-18:0/18:1(9Z) – H]$^-$ (*m/z* 728.5), (b) [PE *O*-16:0/18:1(9Z) – H]$^-$ (*m/z* 702.5), and (c) [PE 16:0/18:1(9Z) – H]$^-$ (*m/z* 716.5). MS^3 product ion spectra obtained via ion-trap CID of (d) [PE *P*-18:0/18:1(9Z) – H – R_2'CH=C=O]$^-$ (*m/z* 464.3), (e) [PE *O*-16:0/18:1(9Z) – H – R_2'CH=C=O]$^-$ (*m/z* 438.3), and (f) [PE 16:0/18:1(9*Z*) – H – R_2'CH=C=O]$^-$ (*m/z* 452.3). The lightning bolt (□) indicates the ion subjected to ion-trap CID.

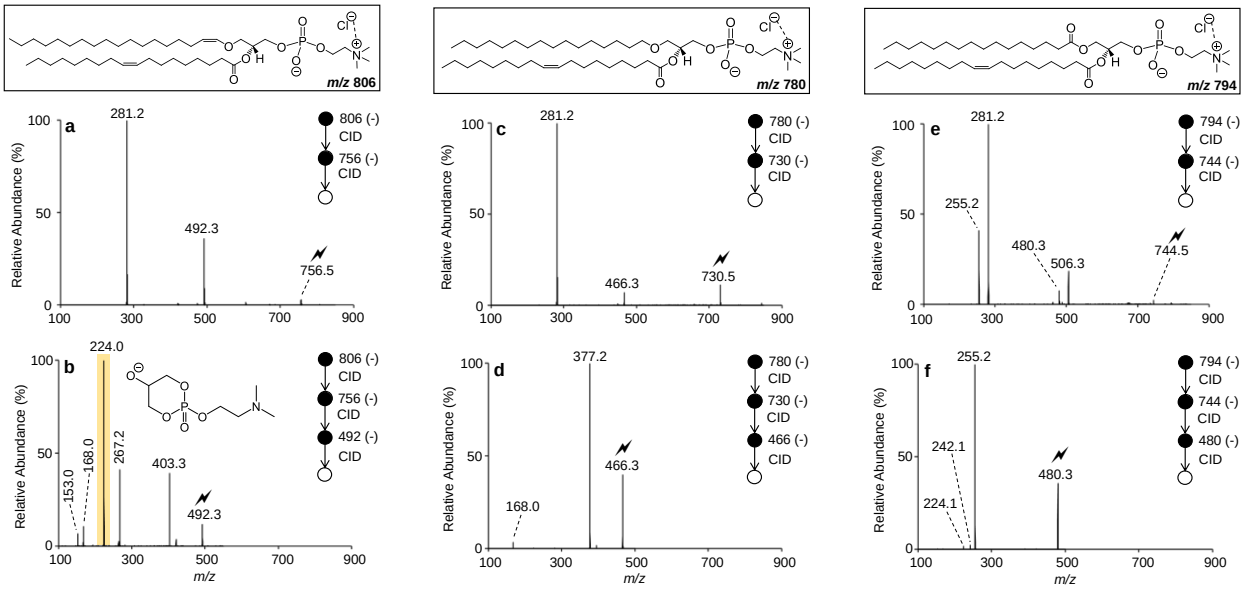

Figure 5.3 MS^2 product ion spectra obtained via ion-trap CID of (a) [PC *P*-18:0/18:1(9Z) – H]$^-$ (*m/z* 806.5), (b) [PC *O*-16:0/18:1(9Z) – H]$^-$ (*m/z* 780.5), and (c) [PC 16:0/18:1(9Z) – H]$^-$ (*m/z* 794.5). MS^3 product ion spectra obtained via ion-trap CID of (d) [PC *P*-18:0/18:1(9Z) – H – $R_2CH{=}C{=}O$]$^-$ (*m/z* 492.3), (e) [PC *O*-16:0/18:1(9Z) – H – $R_2CH{=}C{=}O$]$^-$ (*m/z* 466.3), and (f) [PC 16:0/18:1(9*Z*) – H – $R_2CH{=}C{=}O$]$^-$ (*m/z* 480.3). The lightning bolt (□) indicates the ion subjected to ion-trap CID.

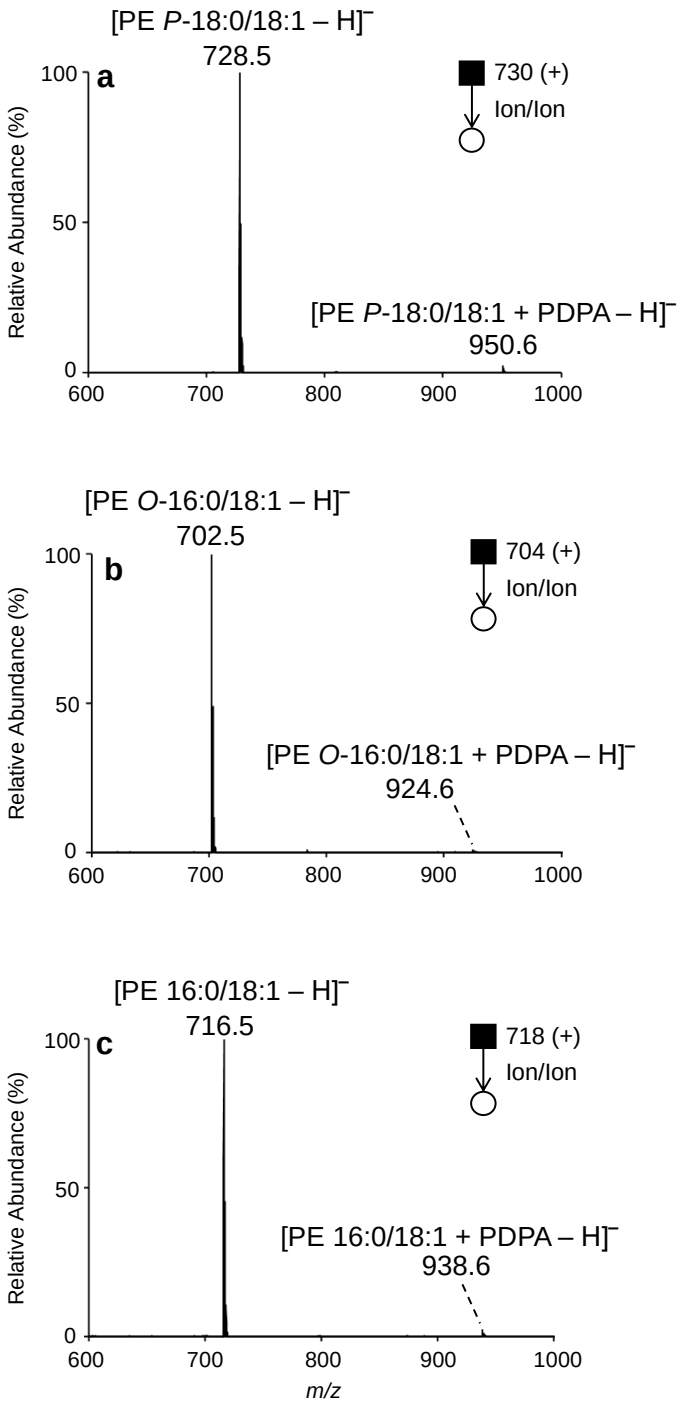

Figure 5.4 Mutual storage product ion spectra resulting from ion/ion reaction between [PDPA – $2H]^{2-}$ dianions and (a) [PE *P*-18:0/18:1(9Z) + $H]^+$ (*m/z* 730.5), (b) [PE *O*-16:0/18:1(9Z) + $H]^+$ (*m/z* 704.5), and (c) [PE 16:0/18:1(9Z) + $H]^+$ (*m/z* 718.5) cations

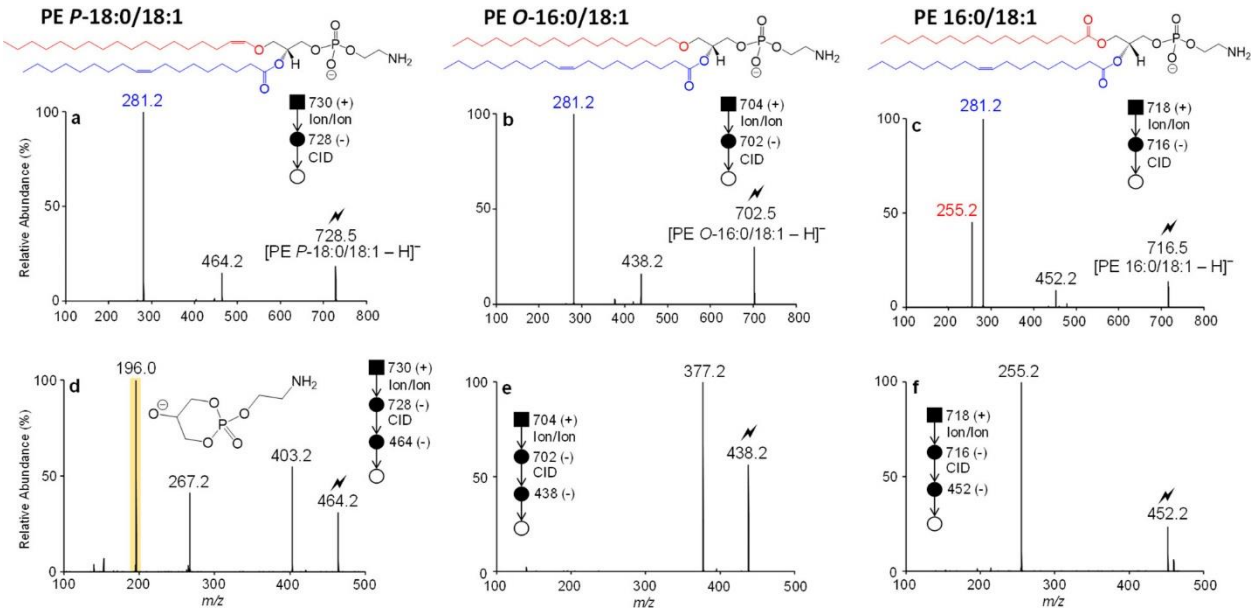

Figure 5.5 CID spectra of (a) [PE *P*-18:0/18:1(9*Z*) – H]$^-$ (*m*/*z* 728.5), (b) [PE *O*-16:0/18:1(9*Z*) – H]$^-$ (*m*/*z* 702.5), and (c) [PE 16:0/18:1(9*Z*) – H]$^-$ (*m*/*z* 716.5) obtained via charge inversion ion/ion reaction. Product ion spectra obtained via ion-trap CID of mass-selected (d) [PE *P*-18:0/18:1(9*Z*) – H – $R_2'CH=C=O$]$^-$ (*m*/*z* 464.3), (e) [PE *O*-16:0/18:1(9*Z*) – H – $R_2'CH=C=O$]$^-$ (*m*/*z* 438.3), and (f) [PE 16:0/18:1(9*Z*) – H – $R_2'CH=C=O$]$^-$ (*m*/*z* 452.3). The lightning bolt indicates the ion that was subjected to ion-trap CID.

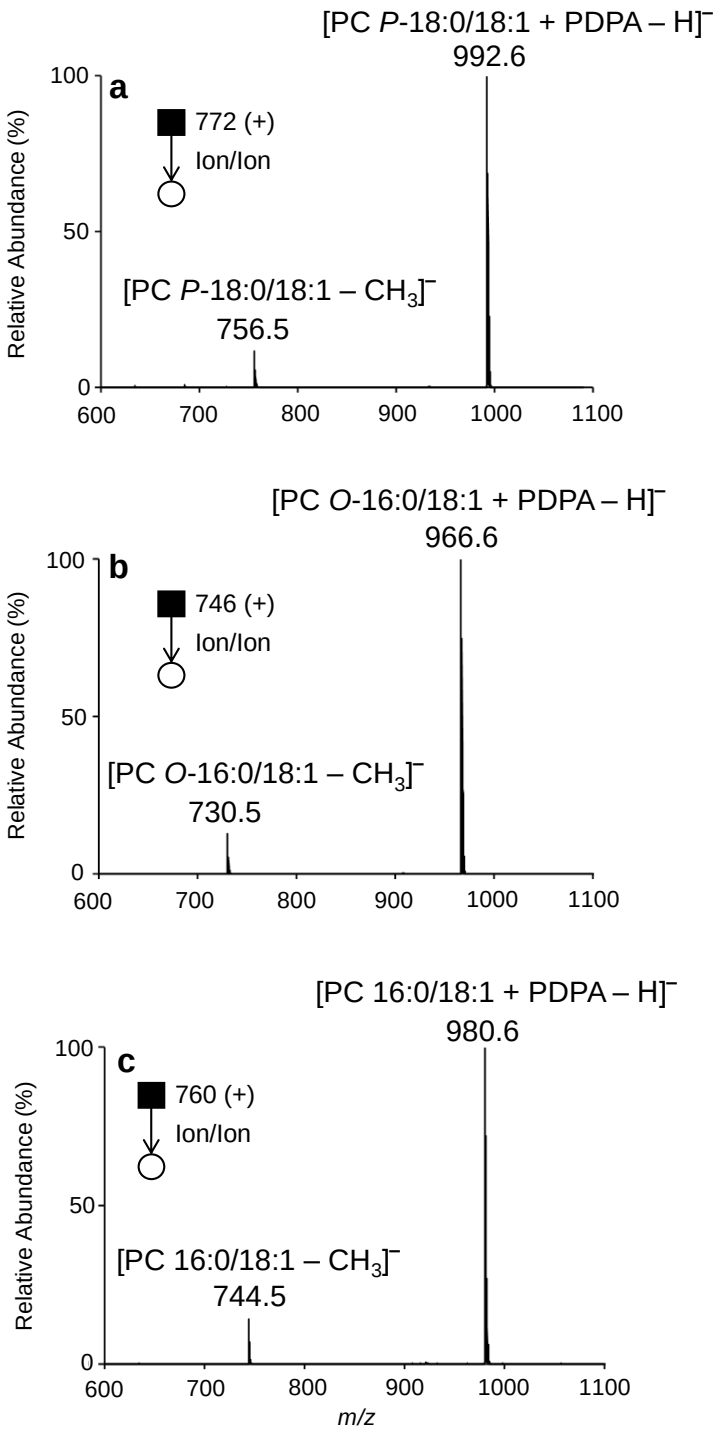

Figure 5.6 Mutual storage product ion spectra resulting from ion/ion reaction between [PDPA – 2H]$^{2-}$ dianions and (a) [PC *P*-18:0/18:1(9Z) + H]$^+$ (*m/z* 772.5), (b) [PC *O*-16:0/18:1(9Z) + H]$^+$ (*m/z* 746.5), and (c) [PC 16:0/18:1(9Z) + H]$^+$ (*m/z* 760.5) cations.

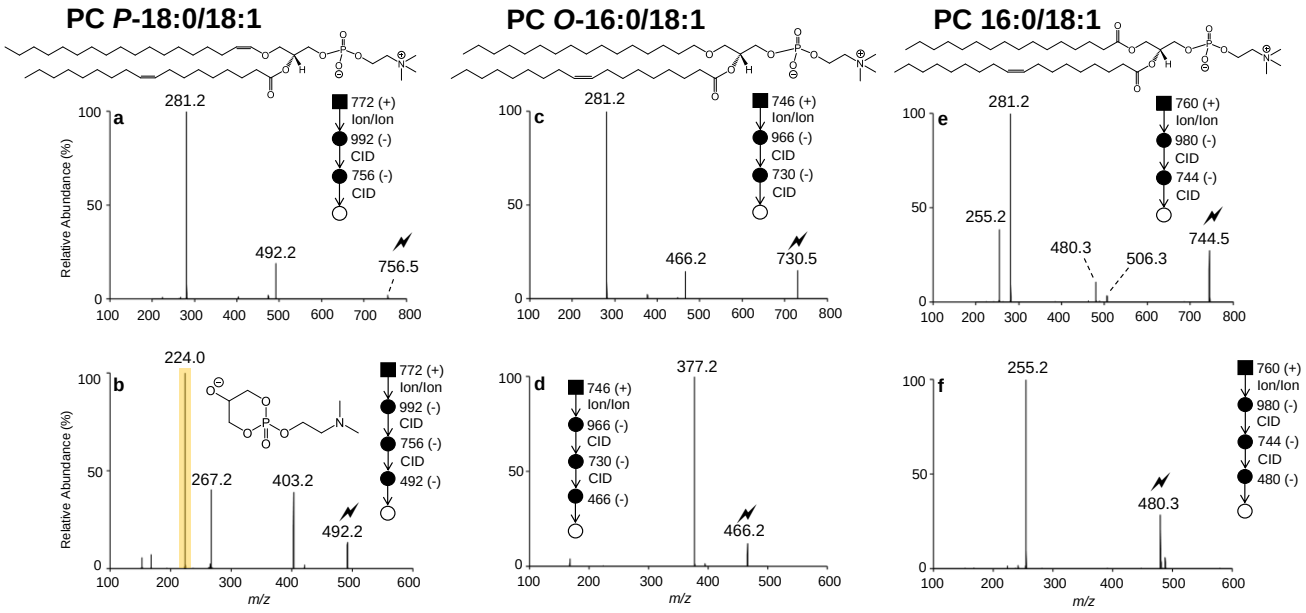

Figure 5.7 CID spectra of (a) [PC *P*-18:0/18:1(9Z) – CH_3]$^-$ (*m/z* 756.5), (b) [PC *O*-16:0/18:1(9Z) – CH_3]$^-$ (*m/z* 730.5), and (c) [PC 16:0/18:1(9Z) – CH_3]$^-$ (*m/z* 744.5) obtained via charge inversion ion/ion reaction. Product ion spectra obtained via ion-trap CID of mass-selected (d) [PC *P*-18:0/18:1(9Z) – CH_3 – R_2'CH=C=O]$^-$ (*m/z* 492.2), (e) [PC *O*-16:0/18:1(9Z) – CH_3 – R_2'CH=C=O]$^-$ (*m/z* 466.2), and (f) [PC 16:0/18:1(9*Z*) – CH_3 – R_2'CH=C=O]$^-$ (*m/z* 480.3).

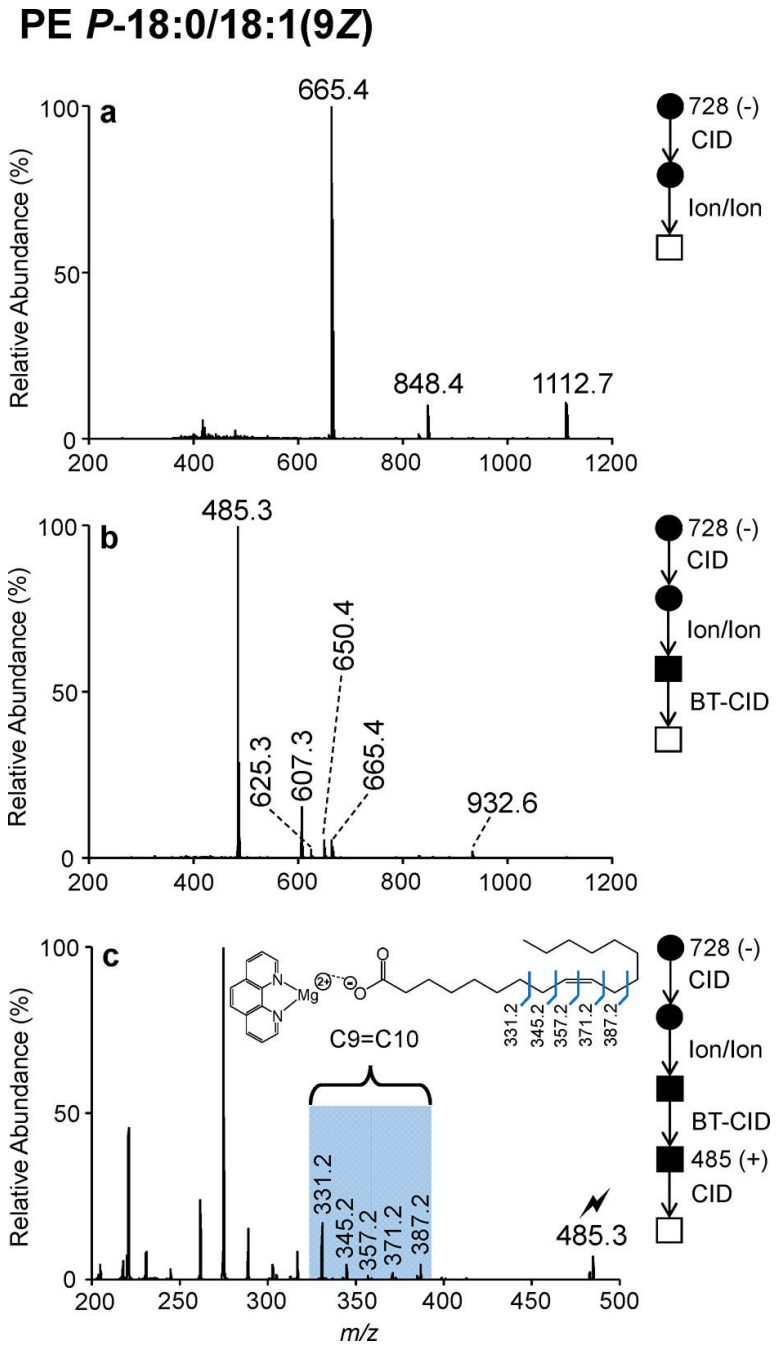

Figure 5.8 Demonstration of ion/ion reactions to identify double-bond position(s) in the fatty acyl substituent of an unsaturated plasmalogen. (a) Product ion spectrum resulting from the ion/ion reaction between $[MgPhen_3]^{2+}$ dications and fragment ions generated via CID of [PE *P*-18:0/18:1(9*Z*) – H]$^-$. (b) Product ion spectrum generated by BT CID of the product ions shown in (a). (c) Ion-trap CID spectrum of mass-selected [18:1(9*Z*) – H + MgPhen]$^+$ (*m*/*z* 485.3).

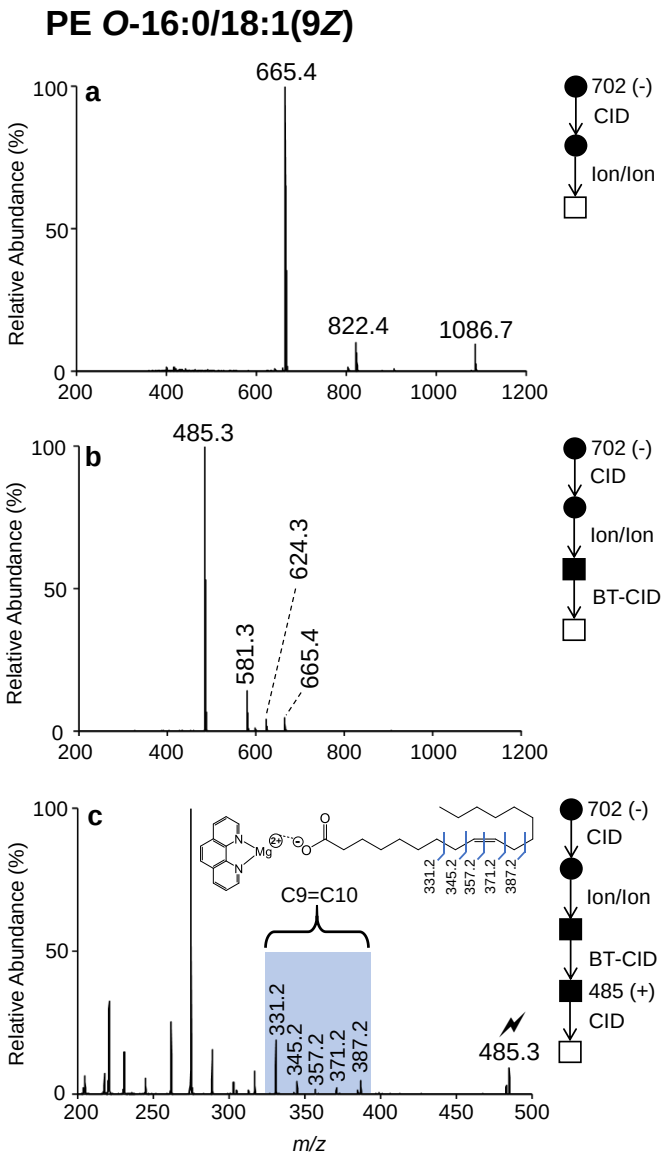

Figure 5.9 Demonstration of ion/ion reactions to identify double bond position(s) in the fatty acyl substituent of unsaturated plasmanyl GPL. (a) Product ion spectrum resulting from the ion/ion reaction between $[MgPhen_3]^{2+}$ dications and fragment ions generated via CID of [PE *O*-16:0/18:1(9Z) – H]$^-$. (b) Product ion spectrum generated by BT CID of the product ions shown in (a). (c) Ion-trap CID spectrum of mass-selected [18:1(9Z) – H + MgPhen]$^+$ (*m/z* 485.3).

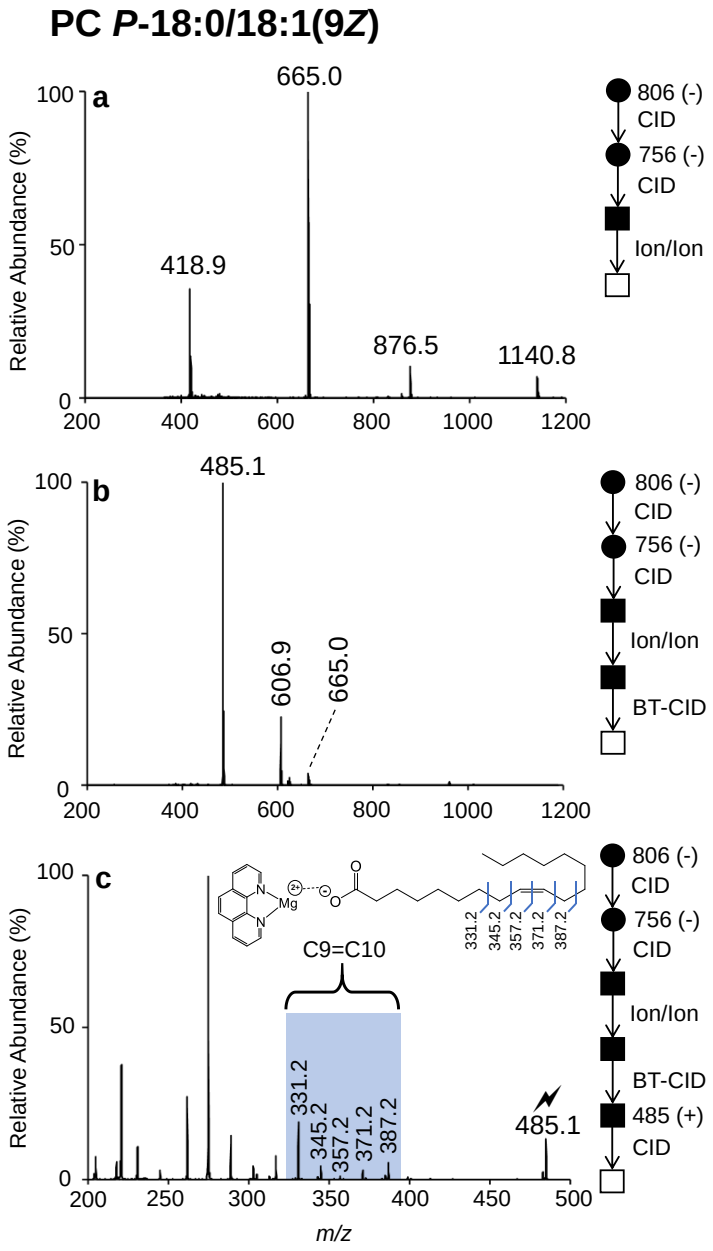

Figure 5.10 Demonstration of ion/ion reactions to identify double bond position(s) in the fatty acyl substituent of unsaturated plasmalogens. (a) Mutual storage product ion spectrum resulting from the ion/ion reaction between $[MgPhen_3]^{2+}$ dications and fragment ions generated via CID of [PC *P*-18:0/18:1(9*Z*) – H]$^-$. (b) Product ion spectrum generated by BT CID of the mutual storage product ions shown in (a). (c) Ion-trap CID spectrum of mass-selected [18:1(9*Z*) – H + MgPhen]$^+$ (*m/z* 485.3).

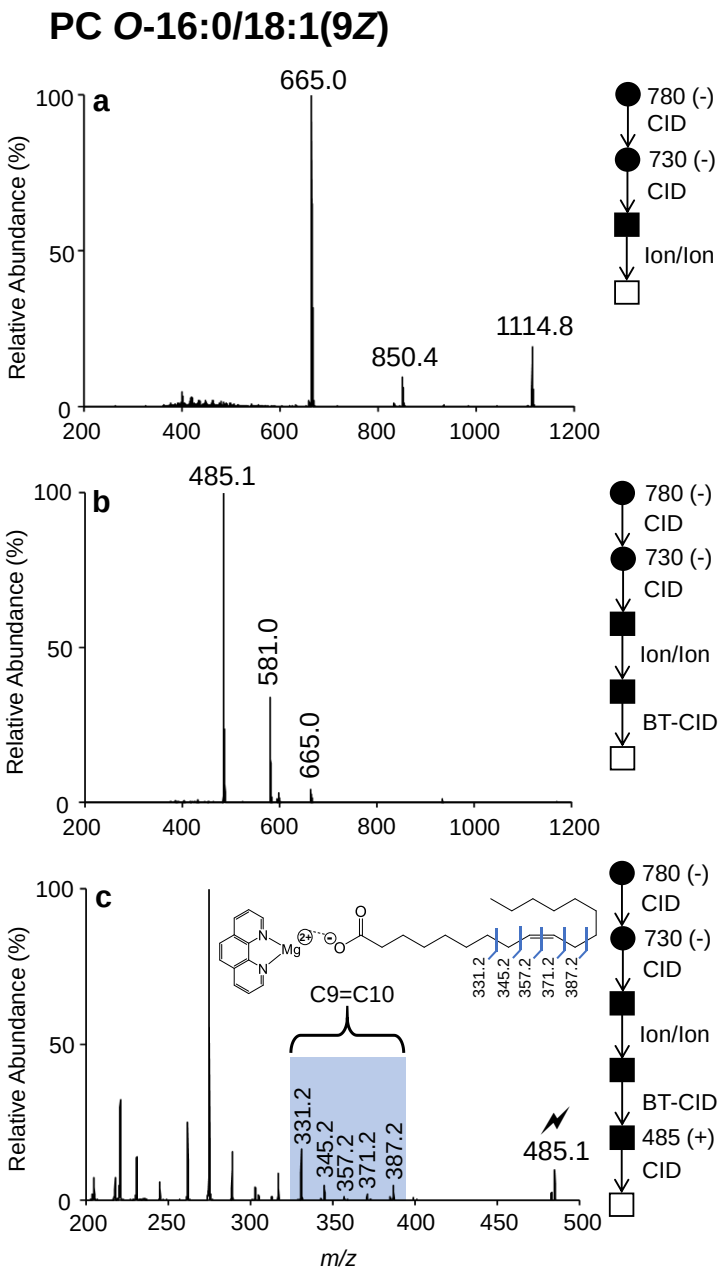

Figure 5.11 Demonstration of ion/ion reactions to identify double bond position(s) in the fatty acyl substituent of unsaturated plasmalogens. (a) Mutual storage product ion spectrum resulting from the ion/ion reaction between $[MgPhen_3]^{2+}$ dications and fragment ions generated via CID of [PC *O*-18:0/18:1(9*Z*) – H]$^{-}$. (b) Product ion spectrum generated by BT CID of the mutual storage product ions shown in (a). (c) Ion-trap CID spectrum of mass-selected [18:1(9*Z*) – H + MgPhen]$^{+}$ (*m/z* 485.3).

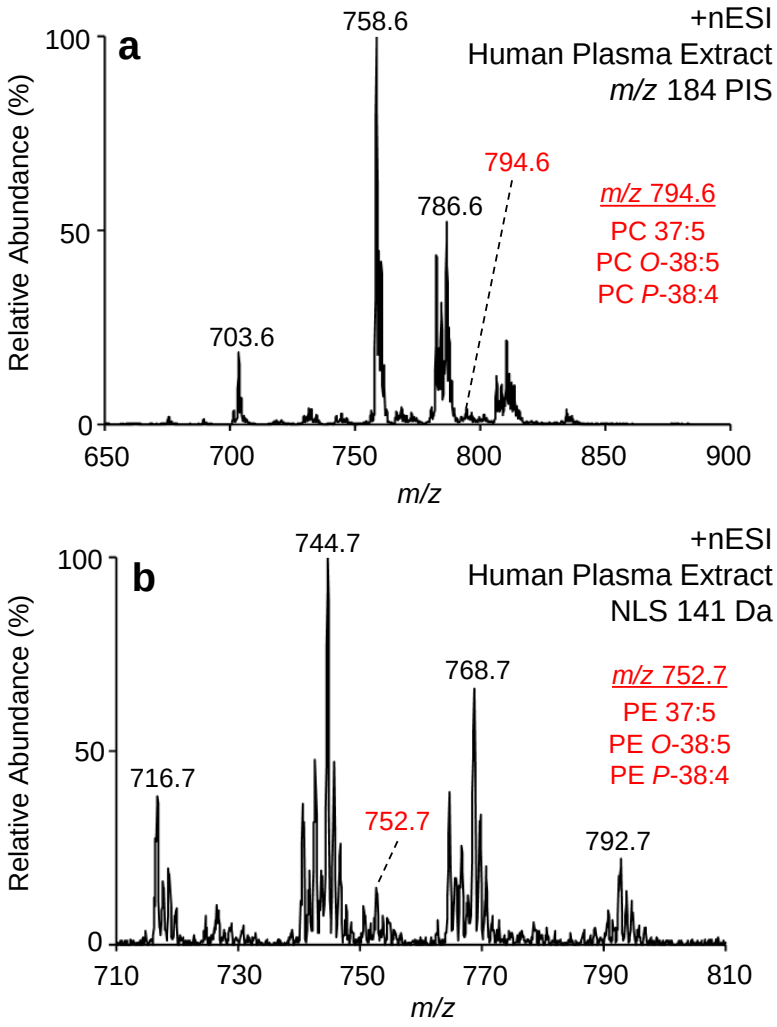

Figure 5.12 (a) Precursor ion scan of *m/z* 184 in positive ion mode used to identify PC lipids in human plasma extract. This scan also includes other choline-bearing lipids such as the $[M + H]^+$ ion of sphingomyelin SM. (b) 141 Da neutral loss scan in the positive ion mode used to identify PE lipids in human plasma extract.

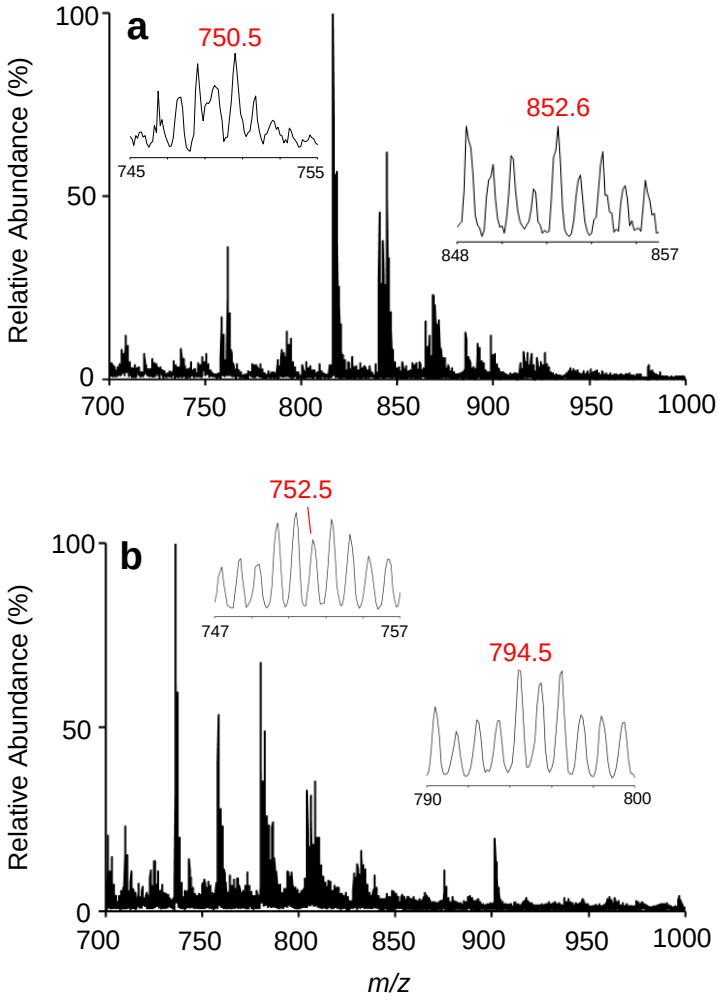

Figure 5.13 Nano-ESI mass spectra of human plasma extract obtained via (a) direct infusion negative ionization and (b) direct infusion positive ionization.

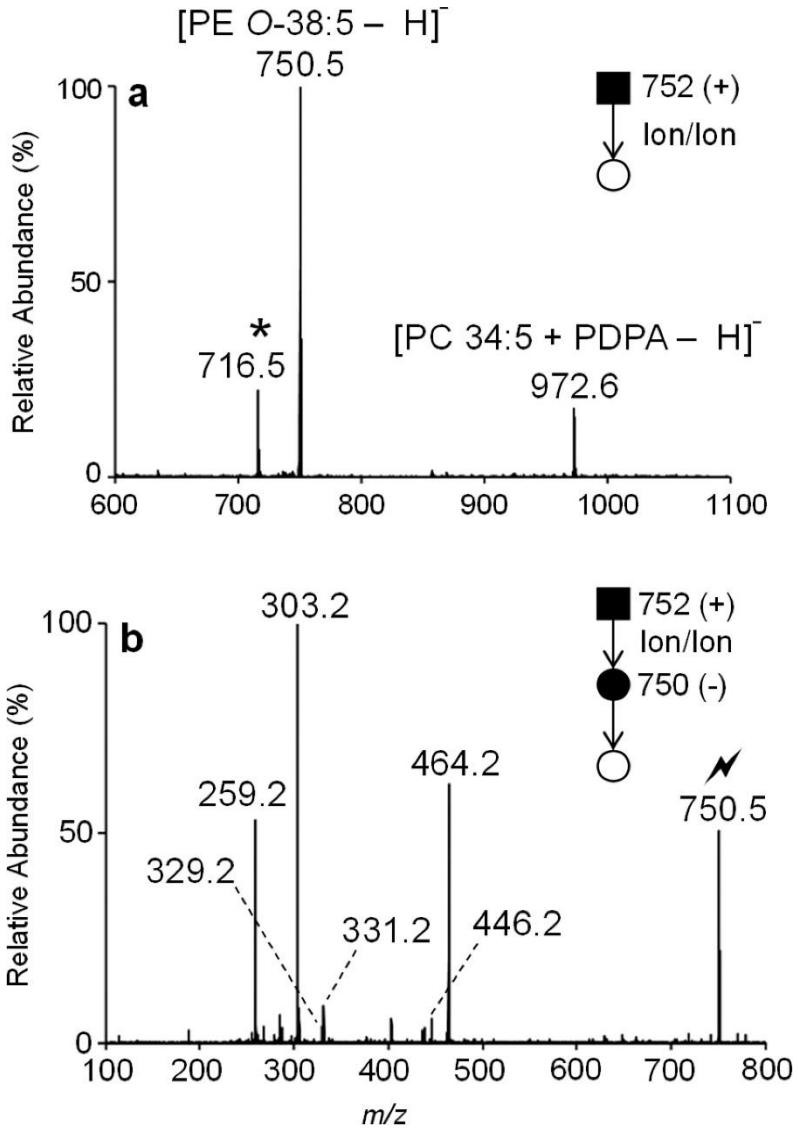

Figure 5.14 (a) Mutual storage product ion/ion spectrum resulting from the charge inversion ion/ion reaction of mass-selected [PE *O*-38:5 + H]$^+$ (*m*/*z* 752.5) cations and [PDPA – 2H]$^{-2}$ dianions. Note that the mutual storage product ion denoted with an asterisk (*) at *m*/*z* 716.5 results from the charge inversion of a precursor ion coisolated with the *m*/*z* 752.5 cation population. (b) MS^3 ion-trap CID spectrum of the ion at *m*/*z* 750.5 obtained after ion/ion reaction

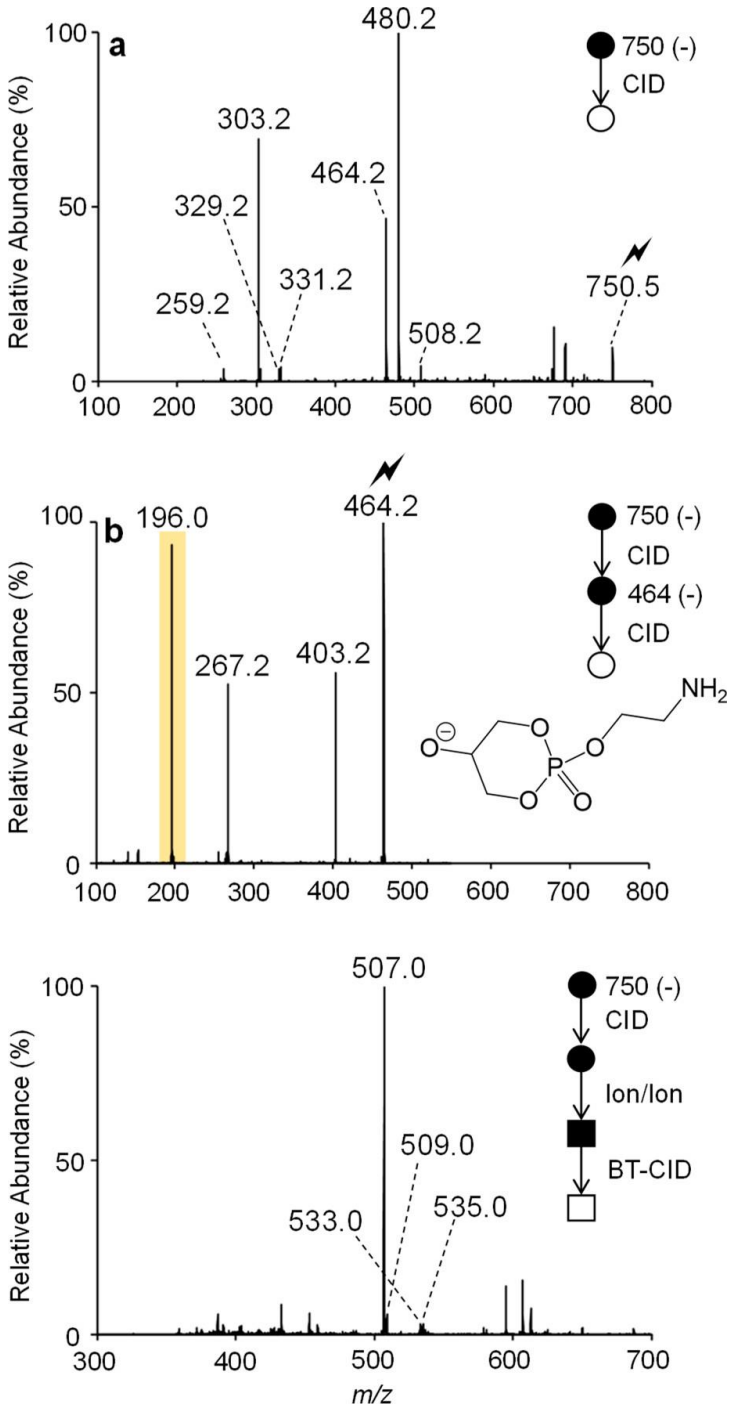

Figure 5.15 (a) Ion-trap CID spectrum of the ether-linked PE *O*-38:5 anion at *m*/*z* 750.5. (b) MS^3 product ion spectrum obtained via ion-trap CID of the mass-selected fragment ion observed at *m*/*z* 464.2 in panel (a). (c) Product ion spectrum obtained following the mutual storage charge inversion ion/ion reaction of the fragment ions observed in panel (a) with $[MgPhen_3]^{2+}$ dications and subsequent collisional activation with beam-type CID.

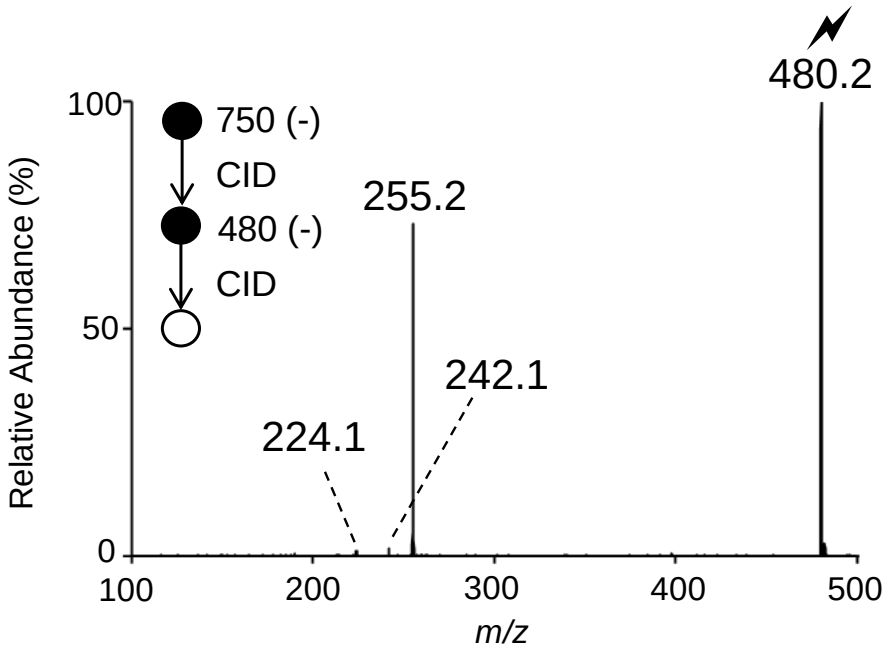

Figure 5.16 MS^3 product ion spectrum of the ion at *m/z* 480.2 derived from collisional activation of the $[PE\ O\text{-}38{:}5 - H]^-$ (*m/z* 730.5) ion from human plasma extract.

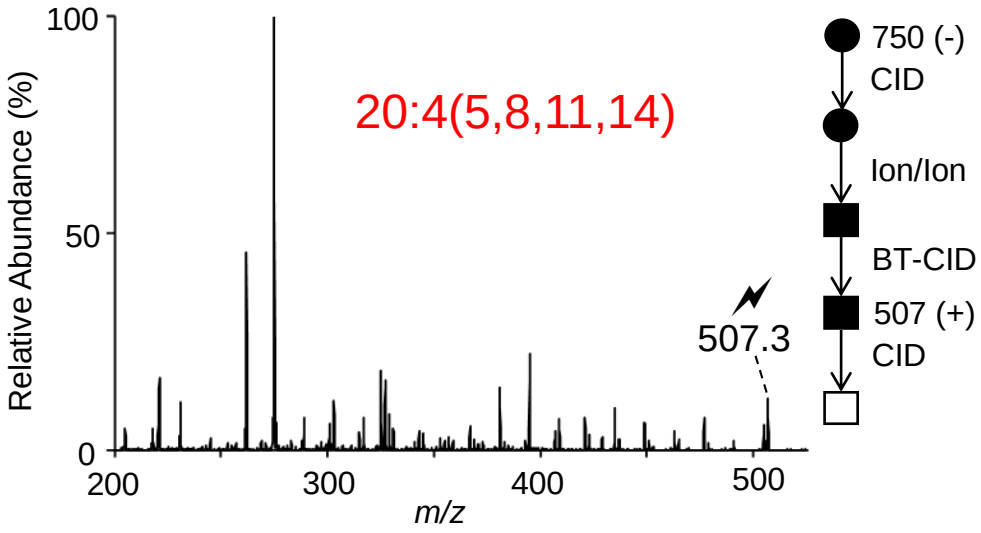

Figure 5.17 Ion-trap CID of mass-selected [20:4 – H + MgPhen]$^+$ from derived from PE *P*-18:0/20:4(5,8,11,14) extracted from human plasma.

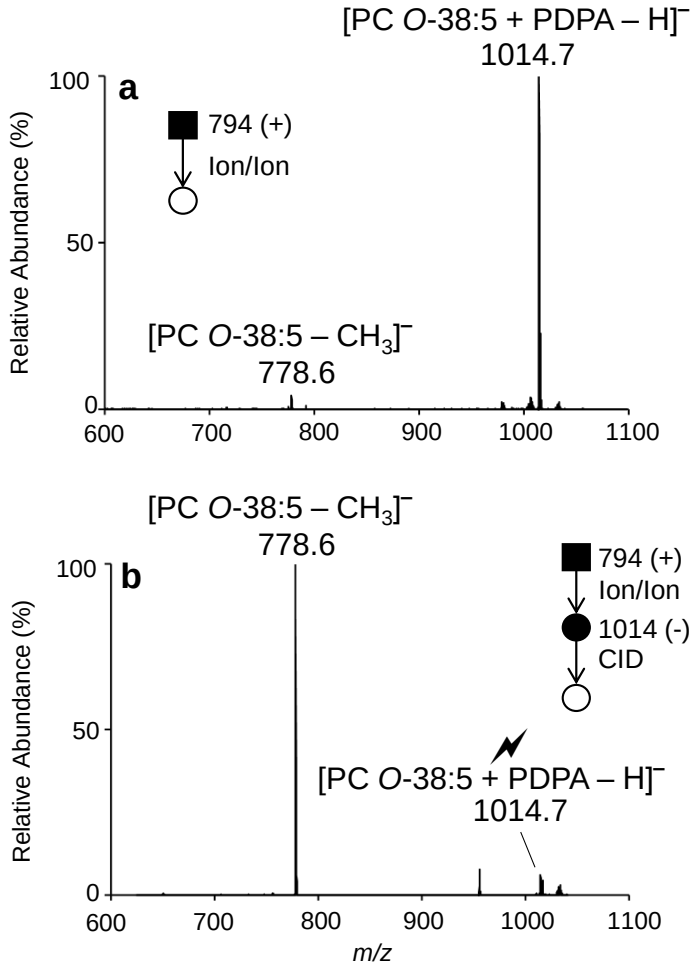

Figure 5.18 (a) Product ion spectrum resulting from ion/ion reaction between $[PDPA - 2H]^{2-}$ dianions and $[PC\ O\text{-}38{:}5 + H]^{+}$ cations. (b) CID spectrum of the charge-inverted $[PC\ O\text{-}38{:}5 + PDPA - H]^{-}$ complex cation (*m/z* 1014.7).

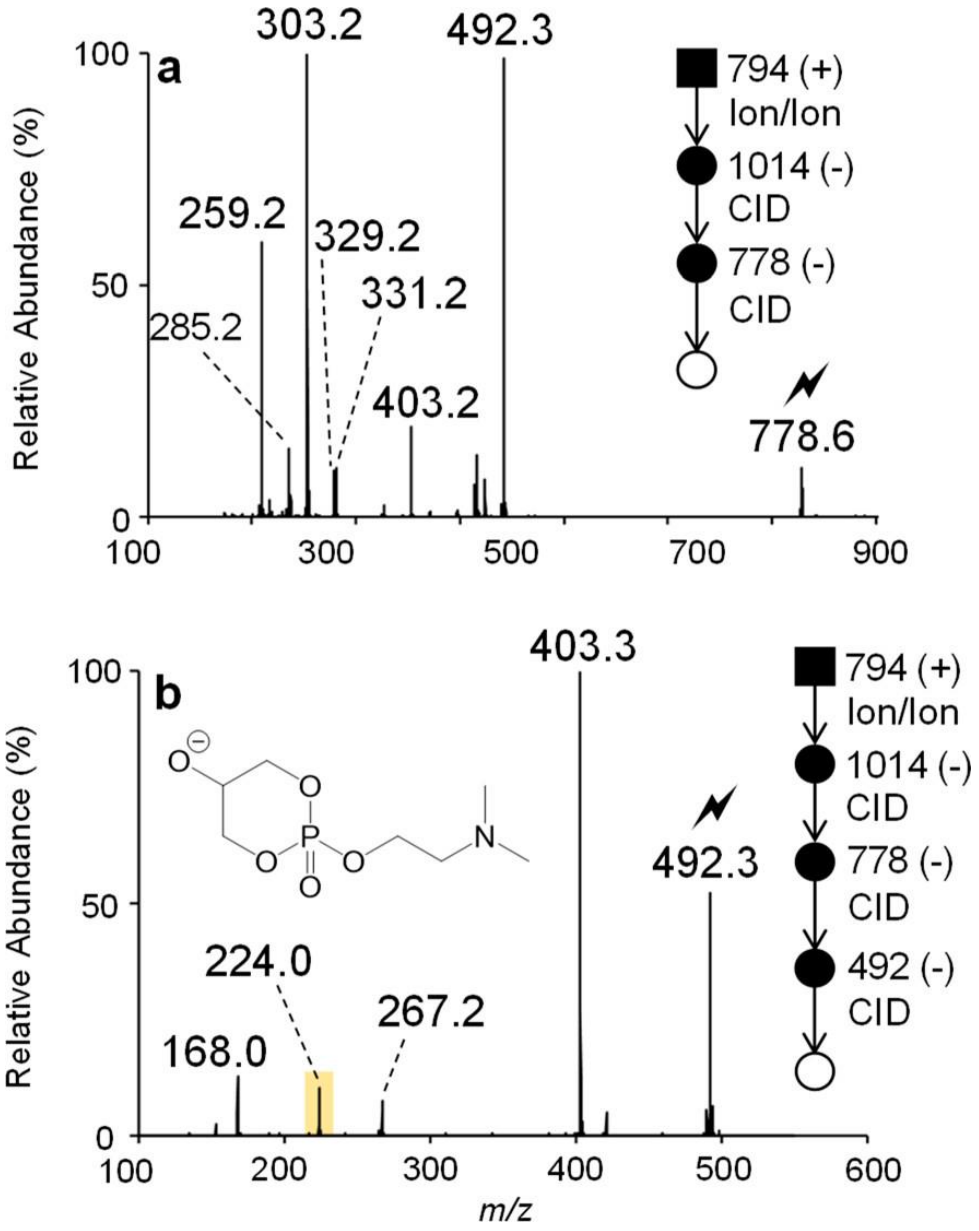

Figure 5.19 (a) Product ion spectrum of [PC *O*-38:5 – CH_3]$^-$ (*m*/*z* 778.6) generated via charge inversion ion/ion reaction of mass-selected [PC *O*-38:5 + H]$^+$ (*m*/*z* 794.5) cations in human plasma and [PDPA – 2H]$^{2-}$ dianions with subsequent CID of the first generation [PC *O*-38:5 + PDPA – H]$^-$ complex anion (*m*/*z* 1014.7). (b) Ion-trap CID spectrum of the ion at *m*/*z* 492.2 shown in panel (a) obtained after ion/ion reaction.

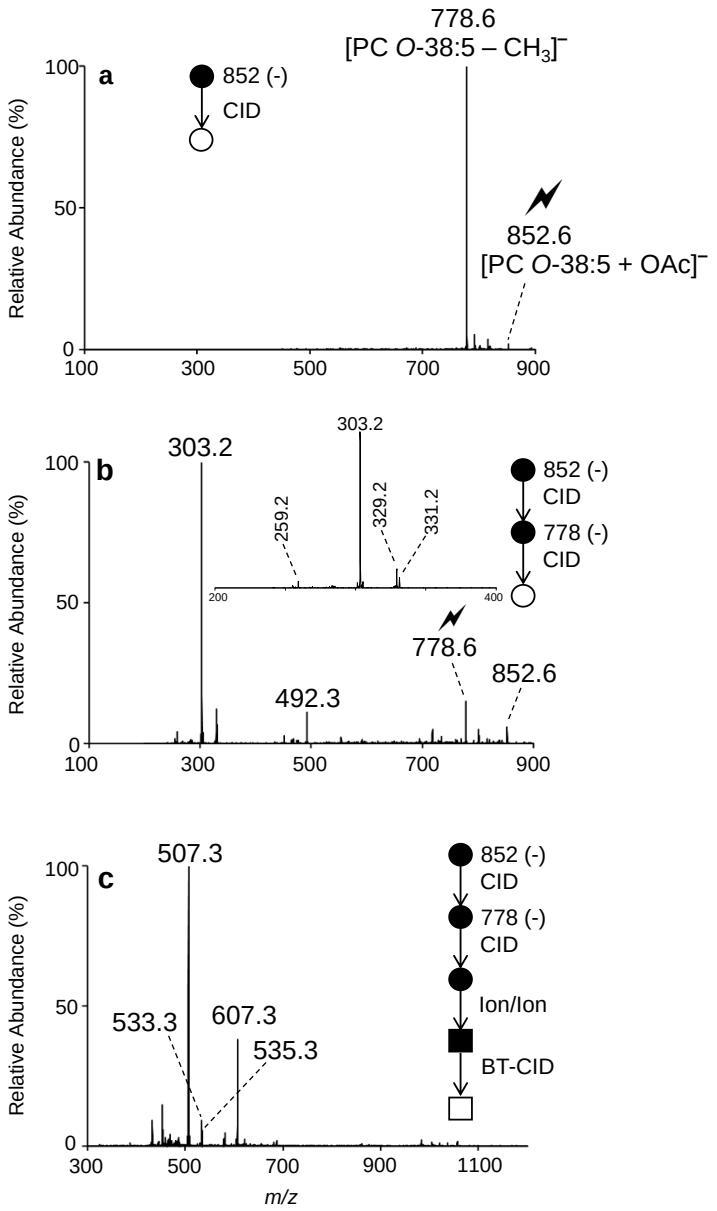

Figure 5.20 (a) Ion-trap CID of mass-selected the [PC-*O* 38:5 + OAc]$^-$ anion (*m/z* 852.6) extracted from human plasma. (b) MS^3 product ion spectrum of [PC-*O* 38:5 – CH_3]$^-$ anion (*m/z* 778.6). (c) Product ion spectrum obtained following the mutual storage charge inversion ion/ion reaction of the fragment ions shown in panel (b) with $[MgPhen_3]^{2+}$ dications and subsequent collisional activation with beam-type CID.

CHAPTER 6. PROTON TRANSFER REACTIONS FOR THE GAS-PHASE SEPARATION, CONCENTRATION, AND IDENTIFICATION OF CARDIOLIPINS

6.1 Introduction

Cardiolipins (CLs) are unique dimeric phospholipids found in bacterial and mitochondrial membranes that exhibit distinct chemical and physical properties.[1] In eukaryotes, following biosynthesis from cytidinediphosphate−diacylglycerol and phosphatidylglycerol, CLs almost exclusively localize in the inner mitochondrial membrane.[1,2] Possessing two phosphatidyl moieties linked to a central glycerol backbone and four fatty acyl substituents, CLs are among the most structurally complex classes of phospholipids. While the roles of CL have not been fully elucidated, CLs are known to serve central functional roles in membrane dynamics, cellular bioenergetics, and apoptosis.[2–5] For example, CLs participate in mitochondrial energetic pathways by providing stabilization to mitochondrial enzymes and are required for optimal enzymatic function, as alternate phospholipid classes cannot substitute for CLs.[6] Thus, CLs are essential to mitochondrial function, and in turn, mitochondrial dysfunction can arise from alterations in CL content and composition. Moreover, recent studies link CL deficiencies and acyl chain remodeling with numerous pathologies[5] such as Barth syndrome,[7] heart failure,[8] diabetes,[9] and several types of cancer.[10,11]

Unfortunately, assessing the modifications to CL structure and production presents considerable challenges, notably due to the high number of CL structural analogues. For instance, thousands of discrete molecular CL structures can be derived from permutations of the four acyl chains, including variations in the esterification site along the glycerol backbones (i.e., *sn*-positional isomers) and fatty acyl composition (i.e., total number of carbons and degree of unsaturation).[12] Over recent decades, mass spectrometry (MS) has emerged as the most widely adopted analytical platform for lipid analysis, and in particular, two distinct MS-based platforms have been deployed in the detection, identification, and quantification of CLs.[4] In the first approach, a lipid extract is admitted to a (tandem) mass spectrometer via liquid chromatography (LC). While CL class isolation from crude lipid extract can be readily achieved using LC-MS, separation of individual CL molecular structures can be chromatographically taxing, as isomeric CL structures frequently exhibit similar chromatographic behaviors.[13,14] In a second approach, a lipid extract is

directly infused into the mass spectrometer using electrospray ionization (ESI). This method, referred to as direct infusion electrospray ionization mass spectrometry (ESI-MS) or shotgun lipidomics, has gained considerable attention.[15–17] Due to the two acidic phosphatidyl moieties, CLs generate abundant deprotonated anions upon direct infusion negative ESI with the potential to form either singly deprotonated $[CL - H]^-$ or doubly deprotonated $[CL - 2H]^{2-}$ dianions, depending on instrument geometry and experimental conditions. To characterize CL molecular species, low-energy collision-induced dissociation (CID) of the CL anion (either singly or doubly deprotonated) has been largely successful. In particular, the tandem (MS^2) mass spectra of deprotonated CL anions (i.e., $[CL - H]^-$ or $[CL - 2H]^{2-}$) facilitate the assignment of individual phosphatidic acid (PA) moieties linked at the 1′ or 3′ position of the central glycerol backbone and fatty acyl substituents.[18] Re-isolation and collisional activation of the $[PA - H]^-$ product ions derived from CL anions yield MS^3 product ion spectra indicative of the fatty acyl composition and regiochemistry of individual PA moieties. Notably, regiochemical assignments based on MS^3 product ion relative abundances do not preclude contributions from minor *sn*-positional isomers, and therefore, such assignments should be made with caution and ideally confirmed with authentic CL standards.[19] In an alternate approach, Hsu and Turk described fragmentation patterns of the $[CL - 2H + Na]^-$ ion, reporting analogous product ion spectra to that of the $[CL - H]^-$ ion.[20] Yet, the principle advantage of interrogating $[CL - 2H + Na]^-$ anions over deprotonated CL ions is the lack of extensive sample preparation prior to analysis, as the generation of $[CL - H]^-$ anions upon direct ESI is often reliant on multiple sample desalting steps. As the methods described above are reliant upon low-energy CID, subtle structural features, such as carbon−carbon double bond locations and geometry, cannot be discerned. In a recent study, Brodbelt and colleagues employed a combination of CID and 193 nm ultraviolet photodissociation (UVPD) on an orbitrap mass spectrometer to pinpoint the site(s) of unsaturation in CLs derived from a biological extract.[21] To date, CID/UVPD has achieved the highest level of structural identification for CL. However, this platform requires high resolving power, yields congested product ion spectra, and suffers from low product ion abundances, primarily due to the limited fragmentation efficiency of UVPD, complicating the analysis of low abundance CLs in biological extracts.

Despite successes, significant challenges associated with CL detection and characterization using shotgun lipidomics remain. First, as CLs represent minor components of the cellular lipidome, CL ions generated via direct infusion negative ESI can be at or below detection limits

for many mass spectrometric methods.[22] Furthermore, the identification of CL molecular species can be exceedingly difficult when examining total lipid extracts. In particular, doubly charged $[CL - 2H]^{2-}$ anions appear in the same mass-to-charge (*m/z*) region that is typically dominated by singly charged anions derived from alternate phospholipid classes (i.e., phosphatidylethanolamine (PE), phosphatidylglycerol (PG), phosphatidylserine (PS), etc.). While high resolving power can aid in the mass assignment of $[CL - 2H]^{2-}$ anions, CL characterization requires tandem-MS (MS/MS). As most MS^2 instruments are unit mass selective at best, $[CL - 2H]^{2-}$ dianions are frequently co-isolated and collisionally activated with isobaric singly charged acidic phospholipid anions leading to composite product ion spectra and ambiguous assignments. Therefore, fractionation of the CL class via condensed-phase separations prior to ESI-MS^2 analysis is often required to achieve unambiguous CL identification. Furthermore, accurate identification of minor and/or overlapping CL molecular species remains an exigent task, especially for analytical platforms employing low-resolution mass spectrometers.[4] Notably, Han et al. established a two-dimensional MS approach, exploiting the marked linoleate enrichment in CL and the doubly charged nature of CL molecular species to both identify and quantify low-abundance CLs directly from biological samples.[23]

Recently, gas-phase ion/ion reactions have been demonstrated in strategies for lipid characterization in complex biological mixtures, including near-complete structural elucidation of phospholipids.[24–28] Moreover, gas-phase proton-transfer ion/ion reactions have been implemented for complex mixture analysis, effectively resolving ions detected at similar mass-to-charge ratios but differing in both mass and charge.[29,30] In this study, we apply proton-transfer ion/ion reactions on a modified hybrid triple quadrupole/linear ion-trap mass spectrometer to separate, concentrate, and identify CLs from a total lipid extract, relying exclusively on gas-phase chemistries.

6.2 Experimental

6.2.1 Materials

HPLC-grade methanol and water were purchased from Fisher Scientific (Pittsburgh, PA). Acetic acid and 8-bis-(dimethylamino)naphthalene (i.e., Proton-Sponge) were purchased from MilliporeSigma (St. Louis, MO). All CL standards and *E. coli* lipid extract (polar) were purchased from Avanti Polar Lipids, Inc. (Alabaster, AL). Solutions of CL standards were prepared in

methanol to a final concentration of 1 μM. A solution of Proton-Sponge solution was prepared in water/methanol/acetic acid (79.5/19.5/1.0) to a final concentration of 0.1 mg/mL.[31] To prepare the lipid extract solution, *E. coli* extract was diluted 50-fold in methanol.

6.2.2 Mass Spectrometry

Experiments were conducted on a Sciex QTRAP 4000 hybrid triple quadrupole/linear ion-trap mass spectrometer (SCIEX, Concord, ON, Canada) that has been modified to perform ion/ion reactions.[32] Lipid anions and Proton-Sponge reagent cations were sequentially injected via alternately pulsed nESI.[33] First, lipid anions generated via negative nESI were mass-selected during transit through Q1 prior to storage in the high-pressure collision cell, q2. Next, positive nESI produced singly protonated Proton-Sponge reagent cations, which were subsequently isolated in transit through Q1, were accumulated in the reaction cell q2. Together in q2, the reagent cations and lipid anions were mutually stored for 300 ms. Next, the q2 radio frequency (RF) amplitude was raised to remove low-mass anions, and the remaining charge-reduced lipid anions were transferred to the low-pressure linear ion trap (LIT), Q3, for storage. Multiple iterations of the ion fill and ion/ion reaction steps were conducted, and charge-reduced product ions were accumulated in Q3 until the charge capacity was reached, noting that a single fill cycle requires approximately 800 ms. To perform MSn experiments in Q3, charge-reduced CL anions were isolated with unit resolution and collisionally activated via single frequency resonance excitation (q = 0.2). Product ions were analyzed by mass-selective axial ejection (MSAE).[34]

6.2.3 Nomenclature

When possible, we adopt lipid nomenclature described by Liebisch et al.[35] For example, the cardiolipin subclass is abbreviated as CL. The shorthand notation for CL sum composition indicates the combined number of carbons in the four fatty acyl chains, followed by a colon and the number of carbon−carbon double bonds (e.g., CL 70:3 implies a total of 70 carbons and 3 carbon−carbon double bonds among the four fatty acyl substituents). To describe CL composition at the fatty acyl level, each fatty acyl substituent is listed sequentially utilizing literature recommendations for fatty acyl chain shorthand notations. Furthermore, fatty acyl composition is represented by the total number of carbons and the degree of unsaturation (e.g., 18:1 indicates a

fatty acyl with 18 carbons and 1 carbon−carbon double bond). When known, the regiochemical assignments of the fatty acyl substituents are separated by a forward slash, and when unknown, fatty acyl constituents are separated by an underscore. We also employ analogous modifications to the shorthand CL notation as described by Macias et al.[21] Briefly, these modifications are used to indicate when fatty acyl composition at each PA substituent is known. For instance, CL (16:0_18:0)_(18:1_20:4) denotes that, while individual fatty acyl and PA moiety regiochemical assignments cannot be made, it is known that one PA constituent contains the 16:0 and 18:0 fatty acyl groups, while the other PA is defined as PA 18:1_20:4.

6.3 Results and Discussion

6.3.1 Proton-Transfer Reactions to Facilitate the Characterization of Synthetic CL

As described above, although $[CL - 2H]^{2-}$ anions can be exploited for CL identification, the assignment of doubly charged CL precursor ions can be compromised when examining total lipid extracts due to (1) limited resolving power of quadrupole mass selection, (2) isomeric/isobaric overlap with more abundant phospholipid ions, (3) the inherently low abundances of CL molecular species, and (4) the generation of degenerate signals across both possible charge states.[4,22] Furthermore, while interrogation of the singly deprotonated $[CL - H]^-$ anions enables CL structure elucidation, the abundances of these CL precursor ions are normally low in complex mixtures and thus challenge the instrument dynamic range.[18] In order to separate CLs from other phospholipids on the *m/z* scale, we employ gas-phase proton-transfer reactions.

We first demonstrate this process with synthetic CL 16:0/18:1/16:0/18:1. Negative nESI of CL 16:0/18:1/16:0/18:1 predominantly generated the doubly deprotonated [CL 16:0/18:1/16:0/18:1− 2H]$^{2-}$ anion (*m/z* 702), though a low abundance singly deprotonated [CL 16:0/18:1/16:0/18:1 − H]$^-$ anion (*m/z* 1404) was also detected, as shown in Figure 6.1a. Next, mass-selected [CL 16:0/18:1/16:0/18:1−2H]$^{2-}$ anions were reacted with the singly protonated Proton-Sponge cations in the high-pressure collision cell, q2, for 300 ms, yielding the product ion spectrum shown in Figure 1b. The proton-transfer reaction resulted in charge reduction of the CL dianion, generating a dominant charge-reduced [CL 16:0/18:1/16:0/18:1 − H]$^-$ product ion (*m/z* 1404) as illustrated in Scheme 6.1. In Q3, subsequent mass selection and ion-trap CID of the charge-reduced [CL 16:0/18:1/16:0/18:1 − H]$^-$ (*m/z* 1404) anion facilitated CL molecular

structural identification. Illustrated with Figure 6.1c, ion-trap CID of the [CL 16:0/18:1/16:0/18:1 − H]$^-$ species gave rise to a prominent tricyclic glycerophosphate ester product ion (*m/z* 809) and a dehydrated phosphatidylglycerol ion (*m/z* 729). Also depicted in Figure 6.1c are product ions corresponding to the neutral losses of the fatty acyl substituents as acids (i.e., [PA 16:0/18:1 − H − R_2COOH]$^-$ (*m/z* 391) and [PA 16:0/18:1 − H − R_1COOH]$^-$ (*m/z* 417)) and ketenes (i.e., [PA 16:0/18:1 − H − R'_2CH=C=O]$^-$ (m/z 409) and [PA 16:0/18:1 − H − R'_1CH=C=O]$^-$ (*m/z* 435)). Consistent with previous observations,18 losses of the *sn*-2 (or *sn*-2′) fatty acyl group were favored over those of the sn-1 (or sn-1′) group, as indicated by higher relative abundances of the [PA 16:0/18:1 − H − R_2COOH]$^-$ (*m/z* 391) and [PA 16:0/18:1 − H − R'_2CH=C=O]$^-$ (*m/z* 409) product ions compared to the [PA 16:0/18:1 − H − R_1COOH]$^-$ (*m/z* 417) and [PA 16:0/18:1 − H − R'_1CH=C=O]$^-$ (*m/z* 435) anions. We note that the CID spectra of the charge-reduced [CL 16:0/18:1/16:0/18:1 − H]$^-$ ion and the unreacted, doubly deprotonated CL ion are similar, yet the [PA 16:0/18:1 − H]$^-$ (*m/z* 673) product ion is notably absent from the [CL 16:0/18:1/16:0/18:1 − 2H]$^{2-}$ product ion spectrum (*c.f.* Figures 6.1c and 6.2). Furthermore, the dissociation of the charge-reduced CL 16:0/18:1/16:0/18:1 anion enabled the assignment of CL fatty acyl composition, as the [16:0 − H]$^-$ and [18:1 − H]$^-$ carboxylate anions were detected at *m/z* 255 and *m/z* 281, respectively. Lastly, the dominant product ion observed in the CID spectrum of [CL 16:0/18:1/16:0/18:1 − H]$^-$ reflects the [PA 16:0/18:1 − H]$^-$ (*m/z* 673) ion, arising from ester bond cleavage at the 1′- or 3′-position of the central glycerol backbone. Re-isolation and collisional activation of the [PA 16:0/18:1 − H]$^-$ product ion (*m/z* 673) confirmed the diacylphosphatidyl moiety assignment, as the 16:0 and 18:1 carboxylate anions were observed in the resulting CID spectrum (see Figure 6.3). In agreement with previous studies,18 the *sn*-1 (or *sn*-1′) [16:0 − H]$^-$ fatty acyl carboxylate anion (*m/z* 255) was more abundant than the *sn*-2 (or *sn*-2′) [18:1 − H]$^-$ fatty acid anion (*m/z* 281) in the CID spectrum of [PA 16:0/18:1 − H]$^-$ (*m/z* 673) shown in Figure 6.3, suggesting preferential formation of the acyl anions from the sn-1 position. Collectively, proton-transfer ion/ion reactions readily and rapidly transform doubly deprotonated CL anions in the gas phase, producing charge-reduced [CL − H]$^-$ anions that fragment to yield structurally informative product ion spectra that permit CL molecular structure identification.

6.3.2 Proton-Transfer Reactions for CL Class Separation

The proton-transfer charge reduction approach was used to examine CLs from an *E. coli* lipid extract. The negative nESI mass spectrum of the *E. coli* extract is shown in Figure 6.4a and contains a variety of ions, mostly singly charged, in the phospholipid region (*m/z* 650−900). An enlargement of this mass spectral region illustrates the challenge of distinguishing CL dianions from singly charged isobaric phospholipid ions (see Figure 6.5). Also, the inset provided in Figure 6.4a highlights the low abundances of singly deprotonated $[CL - H]^-$ anions formed upon direct negative ion nESI. Note that interrogation of individually mass-selected $[CL - H]^-$ anions is plausible following direct negative ion nESI, at the expense of extremely long integration/averaging times, particularly for the lower abundance CL components.

To separate $[CL - 2H]^{2-}$ anions from more abundant phospholipid monoanions, all ions derived from direct negative ion nESI of the *E. coli* extract were allowed to react in the gas phase with Proton-Sponge reagent cations. The resulting product ion spectrum is illustrated in Figure 6.4b. The ion/ion reaction resulted in the charge reduction of doubly charged $[CL - 2H]^{2-}$ anions to yield $[CL - H]^-$ anions, as highlighted with the inset shown in Figure 6.4b. Importantly, the ion/ion reaction resulted in nearly a 10-fold increase in the $[CL - H]^-$ anion signal and dramatically reduced spectral complexity in the low-mass region by removing much of the dianion population (*c.f.*, Figure 6.4a,b). Accounting for isotopic contributions,[36] a normalized abundance CL profile for the *E. coli* extract at the sum compositional level was readily obtained even at nominal mass resolution, as summarized in Figure 6.6. Relevant *m/z* values for the identified CLs are reported in Table 6.1. Examples of abundant charge-reduced CLs species identified in the *E. coli* extract include $[CL\ 70{:}3 - H]^-$ (*m/z* 1430), $[CL\ 68{:}3 - H]^-$ (*m/z* 1402), and $[CL\ 66{:}2 - H]^-$ (*m/z* 1376). Highlighting the dynamic range of the developed technique, minor components such as $[CL\ 73{:}4 - H]^-$ (*m/z* 1470), representing just 1% of the CL profile, could also be reliably identified, noting that we restrict CL identification to CL molecular species yielding a charge-reduced $[CL - H]^-$ ions post-ion/ion reaction with signal-to-noise (S/N) greater than 10 (Figure 6.6). The CL profile of *E. coli* shown here is in good agreement with previous reports.[18,21]

As demonstrated above, proton-transfer ion/ion chemistry separates CL dianions from coexisting phospholipid monoanions while concentrating the CL signal into a single charge state. Importantly, this enables the detection of low-level CLs that under conventional workflows are often obscured by much more abundant phospholipid monoanions of the same nominal *m/z* ratio.

For example, direct negative ion nESI of *E. coli* extract generates an ion at *m/z* 693.5 that can be assigned at nominal mass to $[CL\ 67:3 - H]^{2-}$ (theoretical *m/z* 693.4788). Ion-trap CID of the mass-selected ion population at *m/z* 693.5 generates the product ion spectrum shown in Figure 6.7a. The CID spectrum of *m/z* 693.5 exhibits evidence for at least two isobaric lipid structures, including PG 30:0 and CL 67:3 (Figure 6.7a). Explicitly, product ions likely resulting from fragmentation of $[PG\ 30:0 - H]^-$ and $[CL\ 67:3 - H]^-$ are indicated with the green (●) and orange circles (●), respectively. In turn, the presence of multiple isobaric lipid anions complicates CL identification, though tentative structural assignments of PG 14:0_16:0 and CL 16:1_18:1_17:1_16:0 can be proposed from Figure 6.7a. As demonstrated with this example, proton-transfer ion/ion reactions have the major advantage of alleviating ambiguities arising from composite tandem mass spectra. To illustrate, the mass-selected precursor ion at *m/z* 693.5 was reacted with Proton-Sponge reagent cations, giving rise to the product ion spectrum presented in Figure 6.7b. The proton-transfer reaction resulted in a minor product ion population observed at *m/z* 1388 composed entirely of charge-reduced $[CL\ 67:3 - H]^-$ ions (Figure 6.7b). While a minor charge-reduced CL 67:3 anion was observed following the ion/ion reaction, the major lipid contributor to the precursor ion at *m/z* 693.5 can be assigned as $[PG\ 30:0 - H]^-$, as a dominant ion at *m/z* 693.5 is observed after the ion/ion reaction. Following the proton-transfer ion/ion reaction, interrogation of the residual ions at *m/z* 693.5 yields the CID spectrum shown in Figure 6.7c. Notably, this product ion spectrum confirms PG 14:0_16:0 as the predominant contributor to the original *m/z* 693.5 precursor ion population and, importantly, shows no signals characteristic of the CL 67:3 structure. Note that interrogation of charge-reduced CL product ions will be discussed in more detail below. In general, this example confirms the utility of proton-transfer ion/ion chemistry to effectively resolve the CL class from other acidic phospholipid classes, permitting the gas-phase chemical separation of CL ions on the *m/z* scale.

6.3.3 Proton-Transfer Reactions and Refill Experiments to Concentrate Charge-Reduced CL Anions

We note that ion/ion reaction rates have previously been shown to be proportional to the square of the charge on the analyte ion provided the reagent ions are in great excess, and therefore, doubly charged CL anions formed from the *E. coli* extract will react four times faster than singly charged phospholipid anions.[37] Thus, the proton-transfer ion/ion reaction will preferentially charge

reduce the dianions over neutralization of singly charged phospholipid anions in the reaction time available. As a result, these monoanions will continue to dominate the mutual storage product ion spectrum and occupy the largest fraction of the ion storage capacity of Q3 (Figure 6.4b). While the ion/ion reaction successfully separates the CL class from other acidic lipid classes, the resulting $[CL - H]^-$ anions represent a minor fraction of the total ions observed in Figure 6.4b, in part due to their naturally low-levels in lipid extract. Therefore, even after the ion/ion reaction, relatively long integration/averaging times would be required to obtain CID spectra for mass-selected charge-reduced $[CL - H]^-$ anions, particularly for minor CL species. However, the extent of averaging was minimized here by conducting multiple ion fill and ion/ion reaction steps with intervening removal of residual low *m/z* singly charged ions and transfer of the CL monanions to an adjacent ion trap. This process allows for the accumulation trap to be filled to capacity with the CL anions of interest, thereby eliminating deleterious space charge effects arising from the chemical noise. We note that a similar multiple fill and ion/ion reaction approach has been used on hybrid Orbitrap platforms in whole protein characterization applications.[38,39] The net effect in the present context, however, is the gas-phase separation and concentration of the CL anions.

To concentrate charge-reduced CL product ion signal, we developed an approach employing multiple ion fill and ion/ion reaction steps. Charge-reduced $[CL - H]^-$ product ions are first generated using the ion/ion reaction between *E. coli* lipid anions and proton-transfer reagent cations as outlined above. Next, low-mass anions are removed from q2 by increasing the q2 RF value after the ion/ion reaction while charge-reduced CL product ions are retained and transferred to the LIT for storage (Figure 6.8). To accumulate charge-reduced CL anion signal, these steps can be repeated iteratively prior to MS^n experiments and mass analysis in Q3. Figure 5 displays the results of this gas-phase concentration strategy. In comparison to averaging, in which S/N increases as the square root of the number of averages, refill experiments offer the primary benefit of a linear improvement in S/N with the number of refills. For instance, roughly the same S/N can be obtained from a 10 refill experiment or 100 averages of a single fill. A single mutual storage ion/ion reaction step between *E. coli* lipid anions and Proton-Sponge reagent cations (i.e., a single refill experiment) yields the product ion spectrum shown in Figure 6.9a. In comparison to a single fill experiment, the peak area of *m/z* 1430 increased by a factor of 1.9 with two fill cycles (Figure 6.9b), while three fills yielded a 2.6-fold increase in *m/z* 1430 peak area (Figure 6.9c). In general, these results are in good agreement with theory, as the S/N should improve linearly with refill

experiments. After a total of three fill cycles, the peaks corresponding to the low-mass $[CL - H]^-$ product ions are exhibiting significant broadening, which is a hallmark of space-charge effects, indicating that the charge capacity of Q3 has been reached (Figure 6.9c). While data presented in these experiments utilized only a total of three fills, the theoretical limit of this repetitive process is dependent on the ion storage capacity of the LIT. In other words, once the charge capacity of Q3 is reached, there is no additional benefit to continue refilling the trap. However, depending on initial ion abundances, variations in the total number of Q3 refills may be required to attain the LIT charge capacity, and in principle, refill experiments can be conducted as many times as software limitations permit.

6.3.4 Identification of CLs in *E. coli* Extract Using Proton-Transfer Ion/Ion Reactions and Refill Experiments

To assign the fatty acyl composition of CLs present in *E. coli* extract, charge-reduced $[CL - H]^-$ ions were interrogated. Following the proton-transfer ion/ion reaction, $[CL - H]^-$ product ions were accumulated in Q3 using a total of three fill cycles (Figure 6.9c). After the separation and concentration process, individual charge-reduced CL anions were mass-selected with unit resolution and subjected to ion-trap CID. In this work, we examined the charged-reduced [CL 70:3 $- H]^-$ (*m/z* 1430) and [CL 67:3 $- H]^-$ (*m/z* 1388) anions. As shown in Figure 6.10, CID of the mass-selected [CL 70:3 $- H]^-$ ion reveals the presence of at least three isomers. Product ions related to the major CL isomer are denoted with orange (●) circles, while those attributed to the minor isomeric contributors are indicated with the green (●) and purple (●) circles (see Figure 6.10). The lower *m/z* region of the CID spectrum contains the 16:0, 17:1, 18:1, and 19:1 carboxylate fatty acid anions, noting that the carboxylate anions assigned to 17:1 and 19:1 could also represent cyclopropyl fatty acids.[21] However, as cyclopropyl FAs cannot be differentiated from their isomeric straight-chain unsaturated FA counterparts on the basis of the observed *m/z* ratios alone, we resort to reporting these fatty acyl substituents as the sum composition equivalents. While there is evidence for an additional CL 70:3 isomer, as indicated by the $[16:1 - H]^-$ and [18:0 $- H]^-$ ions, these carboxylate anions and the corresponding product ions generated by the neutral losses of the 16:1 and 18:0 fatty acyl groups were not well-defined. Therefore, we only report the presence of three structural isomers of CL 70:3. From Figure 6.10, the product ion observed at *m/z* 699 could correspond to either [PA 18:1_18:1 $- H]^-$ or [PA 19:1_17:1 $- H]^-$, while the ion at *m/z*

673 likely reflects the [PA 16:0_18:1 − H]$^-$ ion. Further dissociation of these PA ions facilitated confident assignment of the fatty acyl constituents (Figures 6.11 and 6.12).

The CID spectrum of *m/z* 673 displays prominent [16:0 − H]$^-$ (*m/z* 255) and [18:1 − H]$^-$ (*m/z* 281) product ions, confirming the PA 16:0_18:1 structure (Figure 6.11). Similarly, re-isolation and ion-trap CID of the product ion at *m/z* 699 corroborated the PA 18:1_18:1 assignment, as a dominant 18:1 carboxylate anion was observed (Figure 6.12). Therefore, the major CL 70:3 isomer was identified as CL (18:1_18:1)_(18:1_16:0). As described by Hsu and Turk,[18] relative abundances of PA and fatty acyl constituent product ions can be exploited to assign regiochemistry. While these assignments should be interpreted with caution in the absence of authentic standards,[19] these data suggest CL 18:1/18:1/16:0/18:1 is the major isomeric contributor to the CL 70:3 sum composition in the *E. coli* extract. Additional minor contributors to CL 70:3 in the *E. coli* extract were identified as CL (18:1_17:1)/(19:1_16:0) and CL (18:1_19:1)/(17:1_16:0). Note that *sn*-positions were not assigned in the case of minor isomeric components, as individual [PA − H]$^-$ ions arising from CID of the charge-reduced CL anions cannot be re-isolated and collisionally activated due to exceedingly low product ion abundances. While these data were obtained through repeated cycles of ion/ion reaction (i.e., Q3 refill), for comparison, analogous information was acquired through signal averaging of repetitive single-fill experiments (Figure 6.13). To achieve a comparable S/N however, signal averaging of single fill spectra required acquisition times 4−5 times longer, highlighting the critical advantages of the multiple-fill sequence.

In an additional example, we examined a minor CL component present in the *E. coli* extract. From Figure 6.6, CL 67:3 represents approximately 2.5% of the CL fraction in the *E. coli* extract. As highlighted above with Figure 6.7, the precursor ion at *m/z* 693.5 contains a mixture of isobaric species present within a nominal *m/z* unit. Specifically, the major contributor to the precursor ion population at *m/z* 693.5 is [PG 14:0_16:0]$^-$, while the minor component was identified as [CL 67:3 − 2H]$^{2-}$. In turn, unambiguous CL identification is not easily achieved when relying on MS/MS of the [CL 67:3 − 2H]$^{2-}$ precursor anion alone (Figure 6.7a). Therefore, we utilized the separation/concentration steps described herein to both separate CL 67:3 from other lipids and enrich the resulting [CL 67:3 − H]$^-$ product ions in the gas phase. Once more, Q3 was filled with proton-transfer product ions a total of three times, and the charge-reduced [CL 67:3 − H]$^-$ (*m/z* 1388) anions were mass-selected with unit resolution and interrogated via ion-trap CID. The

resulting [CL 67:3 − H]$^-$ (*m/z* 1388) CID spectrum is shown in Figure 6.14. In general, CID of the charge-reduced [CL 67:3 − H]$^-$ anion provides acyl chain composition and sum composition of the constituent PA moieties. The low-mass region of the charged reduced CL 67:3 CID spectrum displays abundant [16:1 − H]$^-$ (*m/z* 253), [16:0 − H]$^-$ (*m/z* 255), [17:1 − H]$^-$ (*m/z* 267), and [18:1 − H]$^-$ (*m/z* 281) product ions, while minor [14:0 − H]$^-$ (*m/z* 227) and [19:1 − H]$^-$ (*m/z* 295) anions were also observed (Figure 6.14a). The PA composition of the dominant isomer was given by product ions observed at *m/z* 671 and 659, indicating the PA 34:1 and PA 33:1 constituents, respectively. In turn, dissociation of the charge-reduced CL 67:3 product anion indicates that the dominant isomer is CL (18:1_16:1)_(17:1_16:0). Ultimately, this assignment is in good agreement with previous reports.[20,21] The data also show evidence for multiple minor isomeric structures, as the [PA 31:1 − H]$^-$ (*m/z* 631), [PA 32:2 − H]$^-$ (*m/z* 643), [PA 32:1 − H]$^-$ (*m/z* 645), [PA 34:1 − H]$^-$ (*m/z* 673), [PA 35:2 − H]$^-$ (*m/z* 685), [PA 35:1 − H]$^-$ (*m/z* 687), and [PA 36:2 − H]$^-$ (*m/z* 699) product ions were detected (Figure 6.14b). Explicitly, CL (16:0_18:1)_(16:1_17:1) was identified as a minor isomeric contributor to CL 67:3. Further structural identifications could not be made, as low abundances of constituent PA product anions arising from minor isomeric contributors hindered subsequent re-isolation and interrogation. Importantly, we note that these minor isomeric contributors to CL 67:3 have only been previously identified when employing condensed-phase fractionation of the CL class prior to analysis, highlighting not only the dynamic range of the developed platform but also the ability to improve S/N entirely within the mass spectrometer. In total, proton-transfer ion/ion reactions permit rapid identification of CL from total lipid extract without the need for prior chromatographic separation of the CL class. The approach outlined herein provides an alternative approach to CL profiling conducted entirely in the gas phase. More so, CID of the charge-reduced CL anions enabled detailed structural characterization, including the assignment of fatty acyl groups, PA constituents, and in some cases, regiochemistry. Furthermore, the application of the methods described above enabled CL isomeric discrimination, revealing the presence of multiple isomeric contributors to a CL species in the *E. coli* extract.

6.4 Conclusions

Localized almost exclusively in the inner mitochondrial membrane of eukaryotes, CLs are complex diphosphatidylglycerol phospholipids that carry four fatty acyl chains and serve vital biological roles in mitochondrial energetics and membrane dynamics.[1–5] While recent studies link

CL dysregulation with numerous pathologies, including several types of cancer,[3,5,7,9–11] CL analysis is challenging, in part due to their vast structural complexity. Owing to their dimeric nature, direct negative ion ESI favors the formation of doubly deprotonated $[CL - 2H]^{2-}$ anions, though minor singly deprotonated $[CL - H]^{-}$ anions can be observed. Without prior chromatographic isolation of the CL class, the identification and subsequent characterization of $[CL - 2H]^{2-}$ anions generated via direct negative ESI of total lipid extract can be problematic. Explicitly, the resulting mass spectra are typically dominated by the more abundant singly charged phospholipid anions, and therefore, doubly charged CL anions are often overshadowed by these coexisting lipid monoanions, hindering confident CL identification.

Herein, we described a shotgun lipidomics approach for the separation, concentration, and identification of CLs from total lipid extract utilizing multiple iterations of gas-phase proton-transfer ion/ion reactions. Specifically, $[CL - 2H]^{2-}$ anions were transformed in the gas phase upon reaction with proton-transfer reagent monocations, giving rise to charge-reduced $[CL - H]^{-}$ anions. Exploiting this entirely gas-phase approach, CL dianions are effectively separated on the *m/z* scale from coexisting singly charged phospholipid anions, permitting rapid identification of CLs without recourse to solution-based separations prior to MS analysis. However, as CLs represent minor fractions of the cellular lipidome, charge-reduced CL anions are still observed in low abundance. To concentrate $[CL - H]^{-}$ product ions, we selectively refill the LIT with proton-transfer product ions. Importantly, this iterative process allows for the accumulation of the desired CL product ions and dramatically reduces the averaging time needed to achieve good S/N product ion ratios. The application of this strategy to the analysis of E. coli lipid extract permitted relative quantification of CLs at the sum compositional level with high sensitivity. Furthermore, the interrogation of charge-reduced CLs derived from the E. coli extract enabled the identification of numerous isomeric contributors to a single CL molecular species. Collectively, the primary advantage of CL profiling utilizing proton-transfer ion/ion chemistry is the elimination of condensed-phase CL class isolation prior to MS analysis, reducing both sample volume requirements and analysis time. Consequently, the presented approach provides an alternative strategy to CL identification based entirely on gas-phase chemistries and offers improved mixture analysis performance, explicitly as CL anions are effectively resolved from more abundant, isobaric phospholipid monoanions and subsequently concentrated in the gas phase. Lastly, as demonstrated herein, gas-phase proton-transfer ion/ion reactions in combination with MS^n can be readily applied to elucidate the structural

complexities of CL molecular structures, as interrogation of charge-reduced CL anions revealed the presence of multiple CL isomers within a single mass-selected CL precursor anion population.

6.5 References

1. Schlame, M. *J. Lipid Res*. **2008**, *49* (8), 1607−1620.

2. Houtkooper, R. H.; Vaz, F. M. *Cell. Mol. Life Sci*. **2008**, *65* (16), 2493−2506.

3. Paradies, G.; Paradies, V.; Ruggiero, F. M.; Petrosillo, G. *Antioxid. Redox Signaling* **2014**, *20* (12), 1925−1953.

4. Scherer, M.; Schmitz, G. *Chem. Phys. Lipids* **2011**, *164* (6), 556−562.

5. Chicco, A. J.; Sparagna, G. C. *Am. J. Physiol.: Cell Physiol*. **2007**, *292* (1), C33−C44.

6. Lewis, R.; McElhaney, R. N. *Biochim. Biophys. Acta, Biomembr*. **2009**, *1788* (10), 2069−2079.

7. Schlame, M.; Ren, M. D. *FEBS Lett*. **2006**, *580* (23), 5450−5455.

8. Dudek, J.; Hartmann, M.; Rehling, P. *Biochim. Biophys. Acta, Mol. Basis Dis*. **2019**, *1865* (4), 810−821.

9. Han, X. L.; Yang, J. Y.; Yang, K.; Zhao, Z. D.; Abendschein, D. R.; Gross, R. W. *Biochemistry* **2007**, *46* (21), 6417−6428.

10. Sapandowski, A.; Stope, M.; Evert, K.; Evert, M.; Zimmermann, U.; Peter, D.; Page, I.; Burchardt, M.; Schild, L. *Mol. Cell. Biochem*. **2015**, *410* (1−2), 175−185.

11. Kiebish, M. A.; Han, X. L.; Cheng, H.; Chuang, J. H.; Seyfried, T. N. *J. Lipid Res*. **2008**, *49* (12), 2545−2556.

12. Schlame, M.; Ren, M. D.; Xu, Y.; Greenberg, M. L.; Haller, I. *Chem. Phys. Lipids* **2005**, *138* (1−2), 38−49.

13. Oemer, G.; Lackner, K.; Muigg, K.; Krumschnabel, G.; Watschinger, K.; Sailer, S.; Lindner, H.; Gnaiger, E.; Wortmann, S. B.; Werner, E. R.; Zschocke, J.; Keller, M. A. *Proc. Natl. Acad. Sci. U. S. A.* **2018**, *115* (16), 4158−4163.

14. Minkler, P. E.; Hoppel, C. L. *J. Lipid Res*. **2010**, *51* (4), 856−865.

15. Han, X. L.; Yang, K.; Gross, R. W. *Mass Spectrom. Rev*. **2012**, *31* (1), 134−178.

16. Blanksby, S. J.; Mitchell, T. W. *Annu. Rev. Anal. Chem*. **2010**, *3*, 433−465.

17. Han, X. L.; Gross, R. W. *Mass Spectrom. Rev*. **2005**, *24* (3), 367−412.

18. Hsu, F. F.; Turk, J.; Rhoades, E. R.; Russell, D. G.; Shi, Y. X.; Groisman, E. A. *J. Am. Soc. Mass Spectrom*. **2005**, *16* (4), 491−504.

19. Ekroos, K.; Ejsing, C. S.; Bahr, U.; Karas, M.; Simons, K.; Shevchenko, A. *J. Lipid Res*. **2003**, *44* (11), 2181−2192.

20. Hsu, F. F.; Turk, J. J. Am. Soc. Mass Spectrom. **2006**, 17 (3), 420−429.

21. Macias, L. A.; Feider, C. L.; Eberlin, L. S.; Brodbelt, J. S. *Anal. Chem*. **2019**, *91* (19), 12509−12516.

22. Bird, S. S.; Marur, V. R.; Sniatynski, M. J.; Greenberg, H. K.; Kristal, B. S. *Anal. Chem*. **2011**, *83* (3), 940−949.

23. Han, X. L.; Yang, K.; Yang, J. Y.; Cheng, H.; Gross, R. W. *J. Lipid Res*. **2006**, *47* (4), 864−879.

24. Randolph, C. E.; Foreman, D. J.; Blanksby, S. J.; McLuckey, S. A. *Anal. Chem*. **2019**, *91* (14), 9032−9040.

25. Randolph, C. E.; Blanksby, S. J.; McLuckey, S. A. *Anal. Chem*. **2020**, *92* (1), 1219−1227.

26. Randolph, C. E.; Foreman, D. J.; Betancourt, S. K.; Blanksby, S. J.; McLuckey, S. A. *Anal. Chem*. **2018**, 90 (21), 12861−12869.

27. Rojas-Betancourt, S. K.; Stutzman, J. R.; Londry, F. A.; Blanksby, S. J.; McLuckey, S. A. *Anal. Chem*. **2015**, *87* (22), 11255−11262.

28. Franklin, E. T.; Betancourt, S. K.; Randolph, C. E.; McLuckey, S. A.; Xia, Y. *Anal. Bioanal. Chem*. **2019**, *411*, 4739.

29. Huang, T. Y.; McLuckey, S. A. *Proteomics* **2010**, *10* (20), 3577−3588.

30. Stephenson, J. L.; McLuckey, S. A. *Anal. Chem*. **1996**, *68* (22), 4026−4032.

31. Bowers, J. J.; Hodges, B. D. M.; Saad, O. M.; Leary, J. A.; McLuckey, S. A. *Int. J. Mass Spectrom*. **2008**, *276* (2−3), 153−159.

32. Xia, Y.; Wu, J.; McLuckey, S. A.; Londry, F. A.; Hager, J. W. *J. Am. Soc. Mass Spectrom*. **2005**, *16* (1), 71−81.

33. Liang, X. R.; Xia, Y.; McLuckey, S. A. *Anal. Chem*. **2006**, *78* (9), 3208−3212.

34. Londry, F. A.; Hager, J. W. *J. Am. Soc. Mass Spectrom*. **2003**, *14* (10), 1130−1147.

35. Liebisch, G.; Vizcaino, J. A.; Kofeler, H.; Trotzmuller, M.; Griffiths, W. J.; Schmitz, G.; Spener, F.; Wakelam, M. J. O. *J. Lipid Res.* **2013**, *54* (6), 1523−1530.

36. Han, X. *Lipidomics: Comprehensive Mass Spectrometry of Lipids* **2016**, 1−466.

37. McLuckey, S. A.; Stephenson, J. L.; Asano, K. G. Anal. Chem. **1998**, *70* (6), 1198−1202.

38. Anderson, L. C.; Karch, K. R.; Ugrin, S. A.; Coradin, M.; English, A. M.; Sidoli, S.; Shabanowitz, J.; Garcia, B. A.; Hunt, D. F. *Mol. Cell. Proteomics* **2016**, *15* (3), 975−988.

39. Ugrin, S. A.; English, A. M.; Syka, J. E. P.; Bai, D. L.; Anderson, L. C.; Shabanowitz, J.; Hunt, D. F. *J. Am. Soc. Mass Spectrom.* **2019**, *30* (10), 2163−2173.

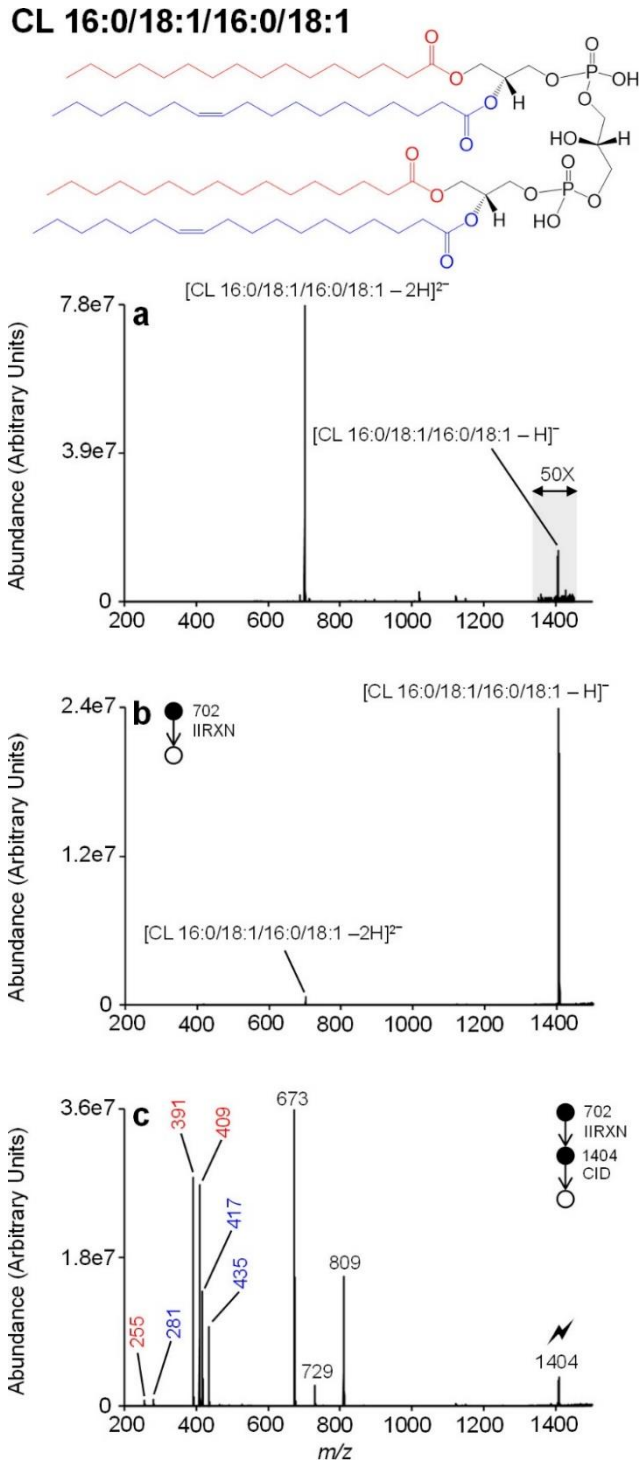

Figure 6.1 Demonstration of proton-transfer reactions for the identification of synthetic CL 16:0/18:1/16:0/18:1. (a) Negative nESI of CL 16:0/18:1/16:0/18:1. (b) Mutual storage product ion spectrum resulting from the proton-transfer reaction between Proton-Sponge cations and CL dianions. (c) Ion-trap CID spectrum of charge-reduced CL 16:0/18:1/16:0/18:1.

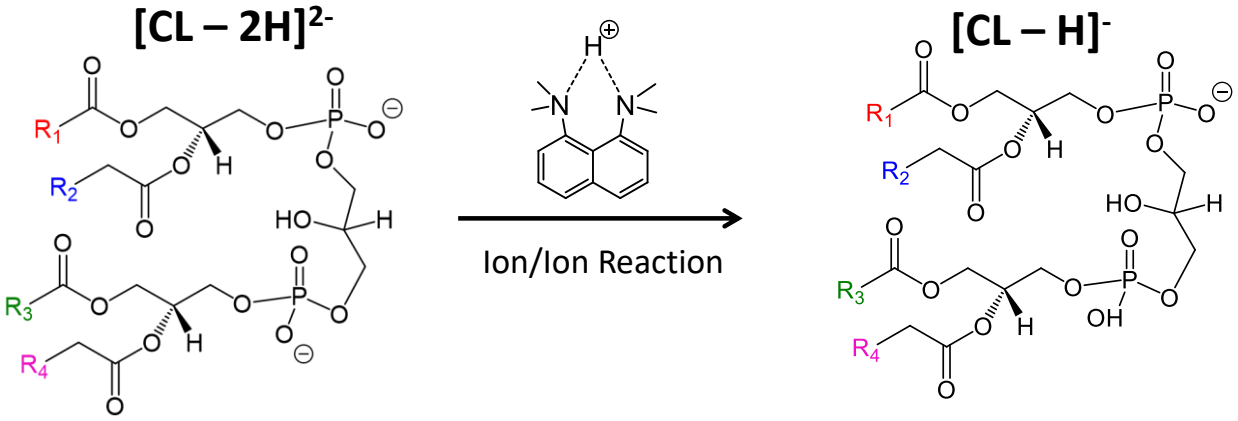

Scheme 6.1 Proton transfer reaction of $[CL - 2H]^{2-}$ anions with singly protonated Proton Sponge® reagent cations to generate charge-reduced $[CL - H]^{-}$ anions.

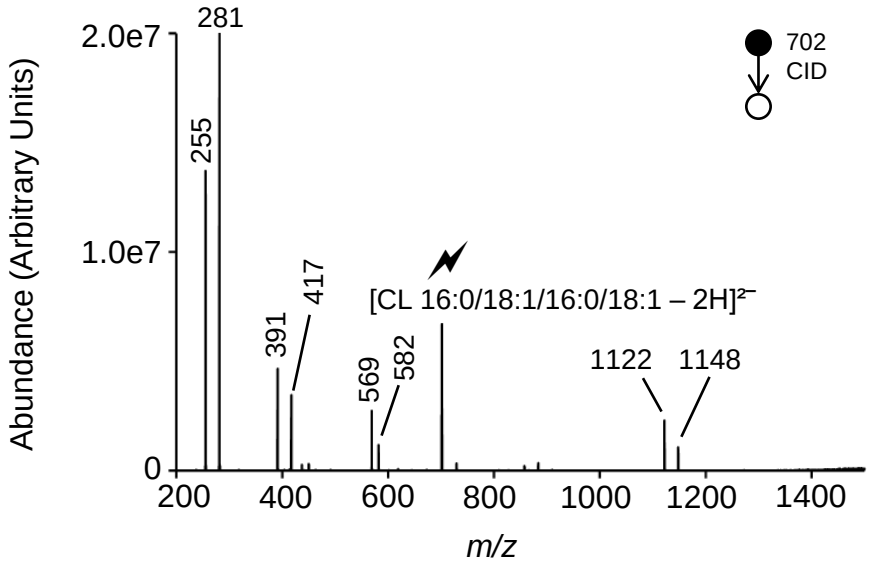

Figure 6.2 MS^2 product ion spectrum of $[CL\ 16:0/18:1/16:0/18:1 - 2H]^{2-}$ (*m/z* 702).

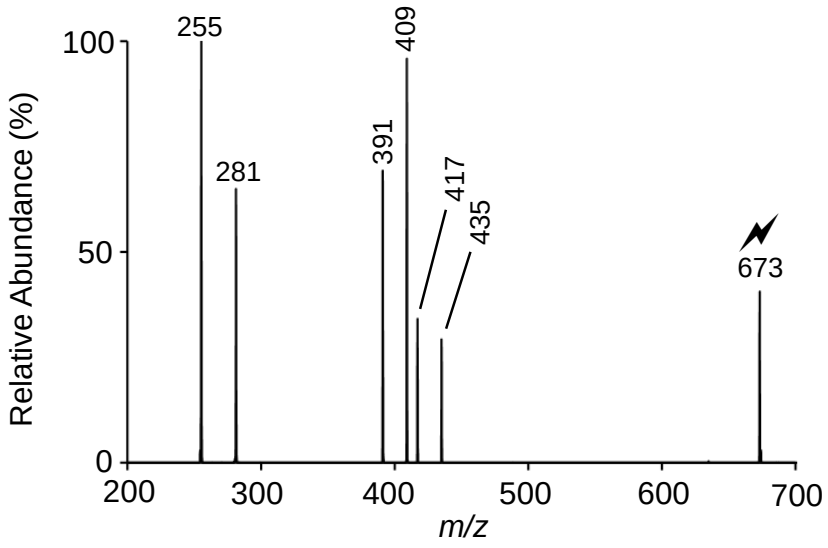

Figure 6.3 MS^3 product ion spectrum of $[PA\ 16:0/18:1 - H]^-$ (*m/z* 673) from CL 16:0/18:1/16:0/18:1.

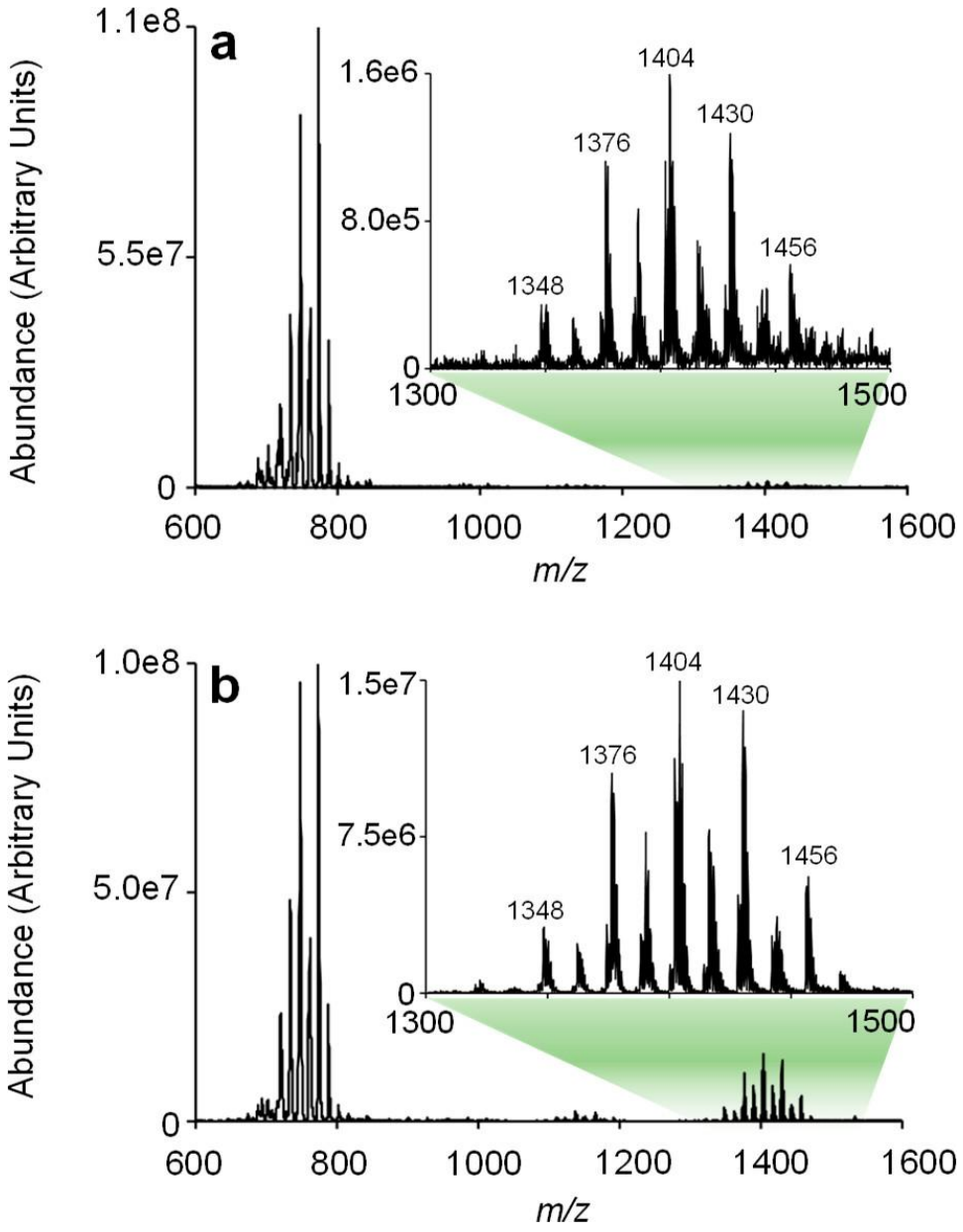

Figure 6.4 Demonstration of gas-phase proton-transfer ion/ion reactions for the identification of CL from *E. coli* extract. (a) Direct negative nESI mass spectrum of *E. coli* extract. (b) Product ion spectrum resulting from the gas-phase proton-transfer ion/ion reaction between anions shown in (a) and Proton-Sponge reagent cations. Note that both spectra represent an average of 20 scans.

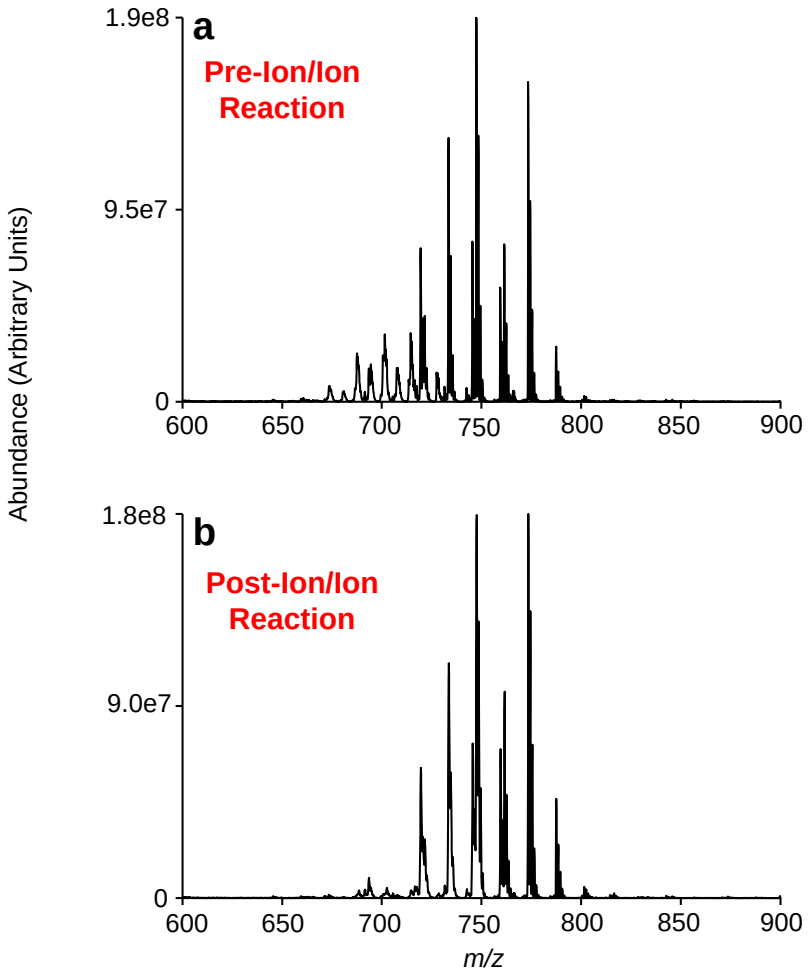

Figure 6.5 Enlargement of *m/z* 600 – 900 region in the (a) direct negative nESI mass spectrum of *E. coli*. extract, and (b) mutual storage product ion spectrum resulting from the gas-phase proton transfer ion/ion reaction between anions shown in (a) and Proton-Sponge® reagent cations.

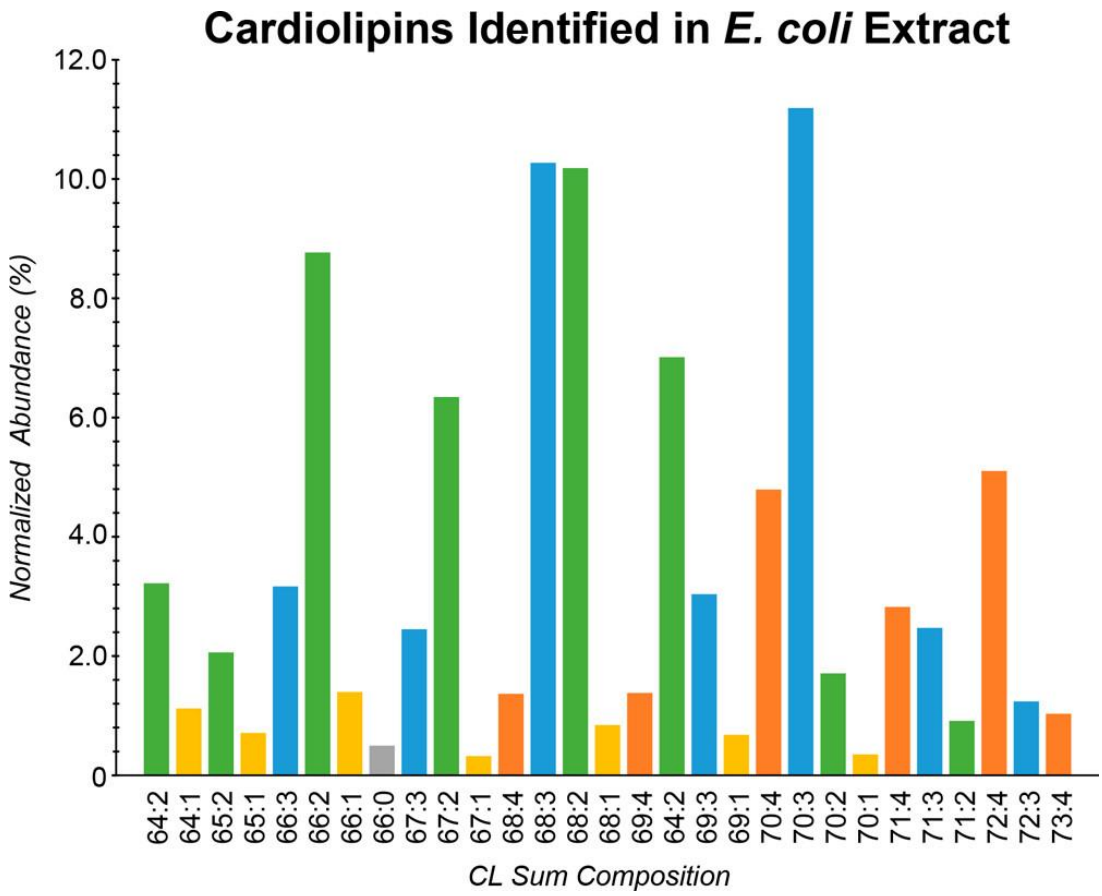

Figure 6.6 Normalized abundance cardiolipin profile for *E. coli* extract at the sum compositional level generated via proton-transfer ion/ion reactions.

Table 6.1 Cardiolipin profile for *E. coli* extract

$[CL - H]^-$ (*m/z*)	CL Identity	Normalized CL Abundance (%)
1348	64:2	3.2
1350	64:1	1.1
1362	65:2	2.1
1364	65:1	0.7
1374	66:3	3.2
1376	66:2	8.8
1378	66:1	1.4
1380	66:0	0.5
1388	67:3	2.5
1390	67:2	6.3
1392	67:1	0.3
1400	68:4	1.4
1402	68:3	10.3
1404	68:2	10.2
1406	68:1	0.8
1414	69:4	1.4
1416	69:3	7.0
1418	69:2	3.0
1420	69:1	0.7
1428	70:4	4.8
1430	70:3	11.2
1432	70:2	1.7
1434	70:1	0.4
1442	71:4	2.8
1444	71:3	2.5
1446	71:2	0.9
1456	72:4	5.1
1458	72:3	1.2
1470	73:4	1.0

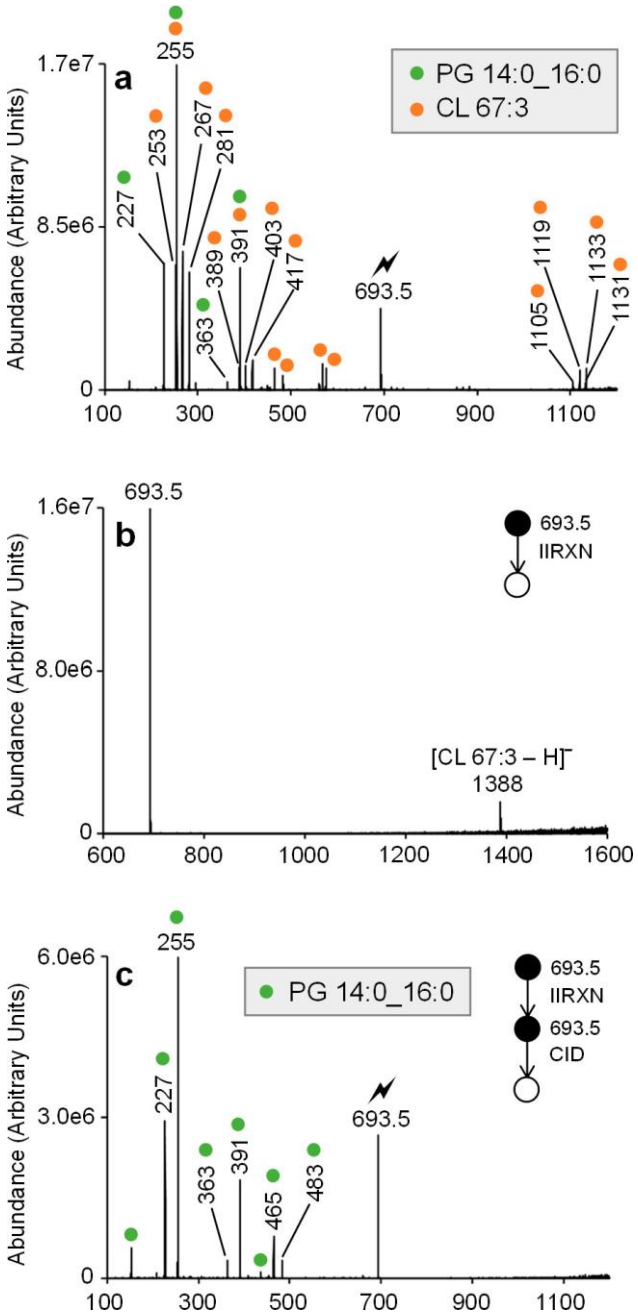

Figure 6.7 (a) Ion-trap CID spectrum of *m*/*z* 693.5 from *E. coli* lipid extract. (b) Mutual storage product ion spectrum resulting from the ion/ion reaction between mass-selected *m*/*z* 693.5 from *E. coli* lipid extract and Proton-Sponge reagent cations. (c) Ion-trap CID spectrum of *m*/*z* 693.5 from *E. coli* lipid extract after the proton-transfer ion/ion reaction. The lightning bolt indicates the ion subjected to ion-trap CID.

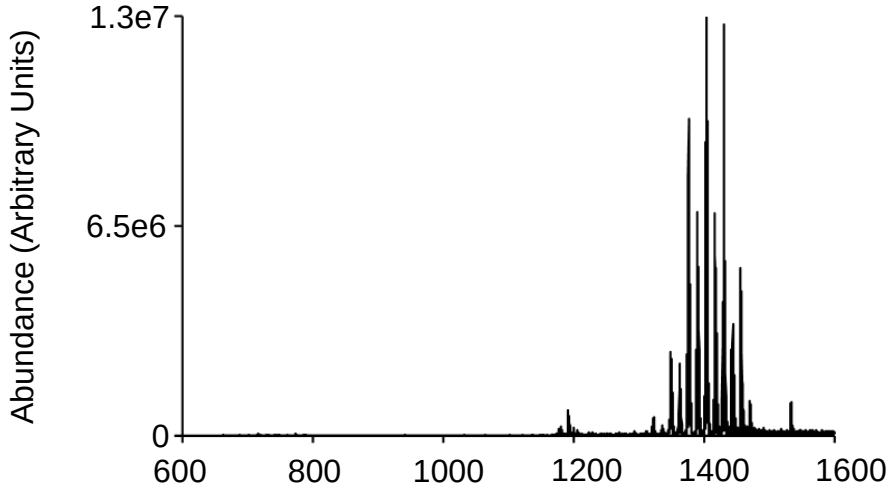

Figure 6.8 Demonstration of selective transfer of charge-reduced $[CL - H]^{-}$ product ions to the LIT for storage following the proton-transfer ion/ion reaction between lipid anions derived from *E. coli*. extract and Proton-Sponge® cations and subsequent increase in q2 RF amplitude.

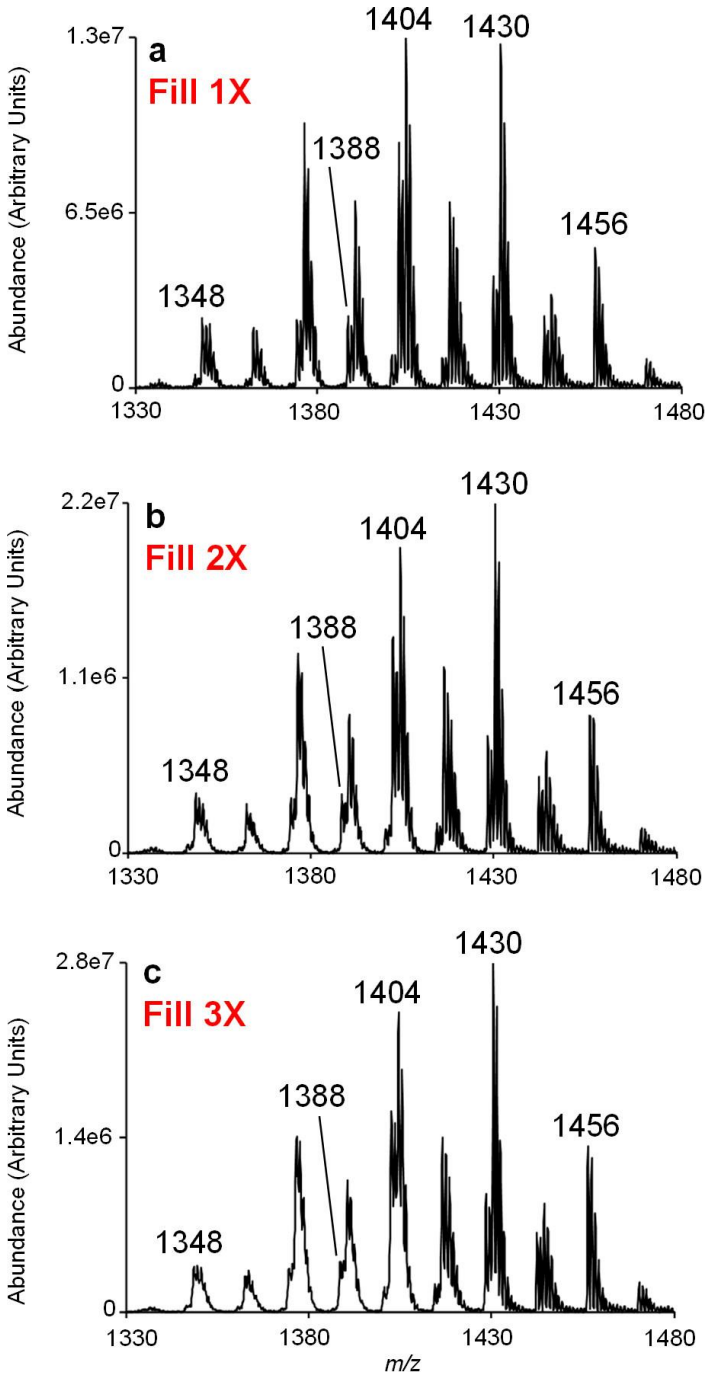

Figure 6.9 Demonstration of refill experiments to concentrate charge-reduced $[CL - H]^-$ product ion signals. All mutual storage product ion spectra result from the ion/ion reaction between lipid anions derived from *E. coli* extract and Proton-Sponge reagent cations, followed by an increase in q2 RF value. Note that all spectra represent an average of 20 scans. Product ion spectra obtained via (a) 1, (b) 2, and (3) 3 fill cycles.

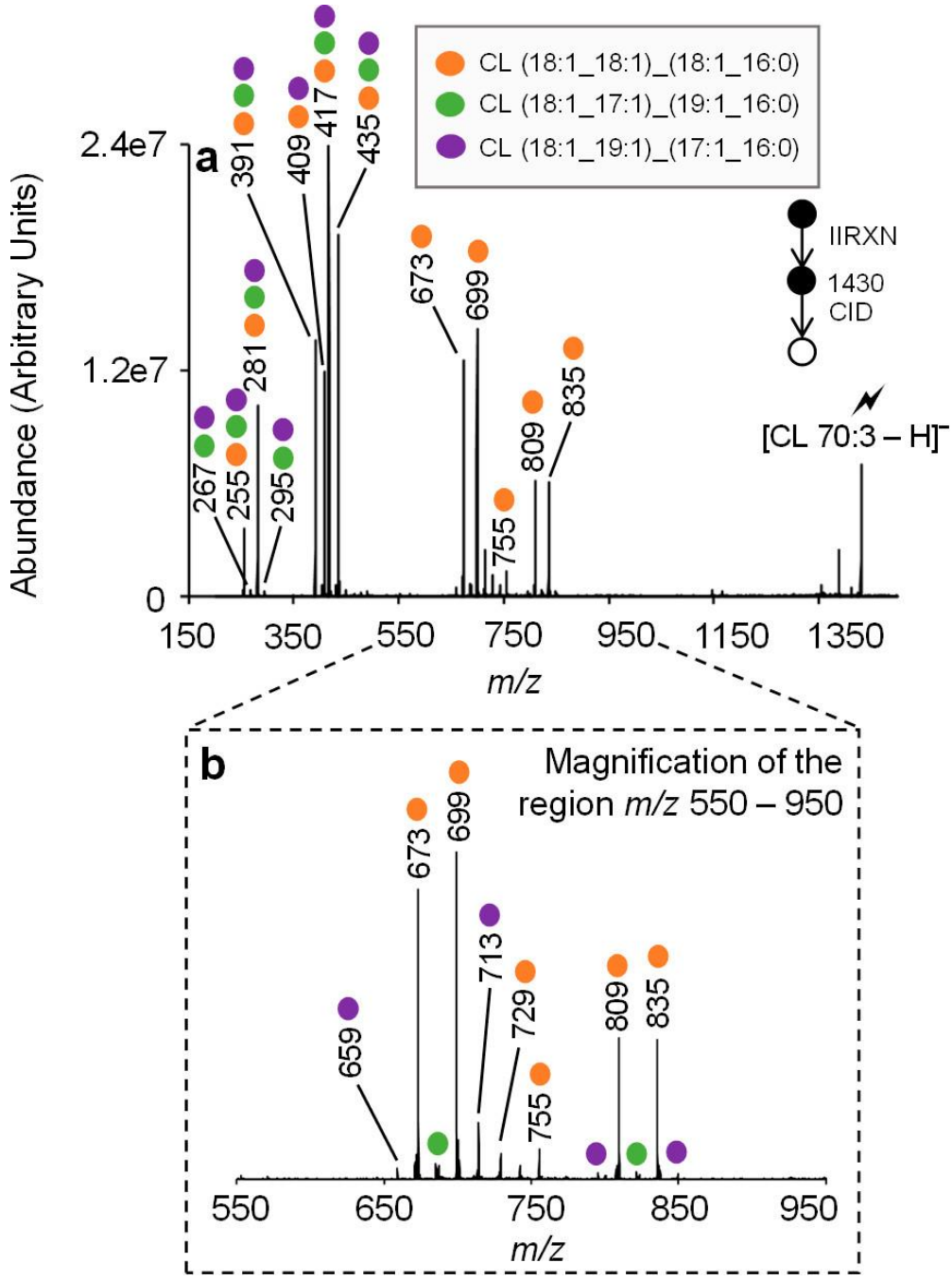

Figure 6.10 (a) Ion-trap CID spectrum of the charge-reduced [CL 70:3 – H]$^-$ ion (*m/z* 1430) that has been concentrated in Q3 using a total of three fill cycles. (b) Enlargement of *m/z* 550–950 mass spectral region shown in (a). The lightning bolt indicates the ion subjected to ion-trap CID.

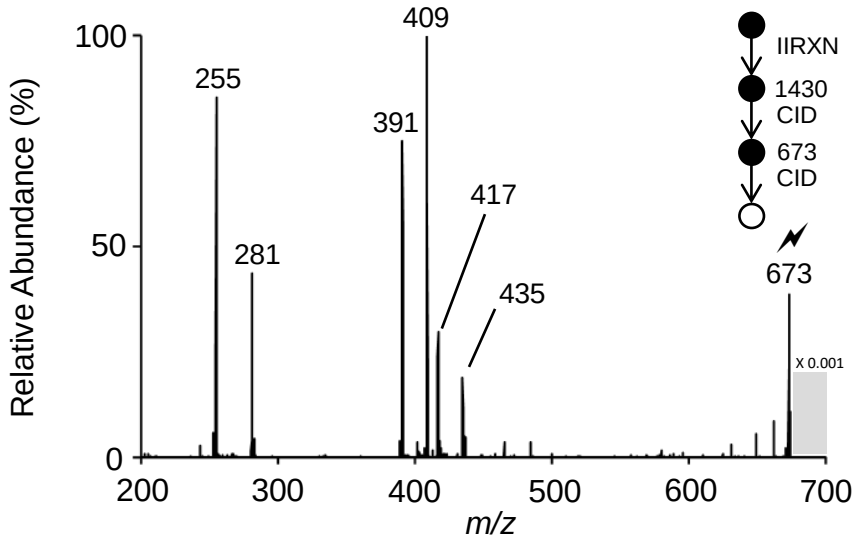

Figure 6.11 MS^3 product ion spectrum of the mass-selected product ion observed at *m/z* 673.

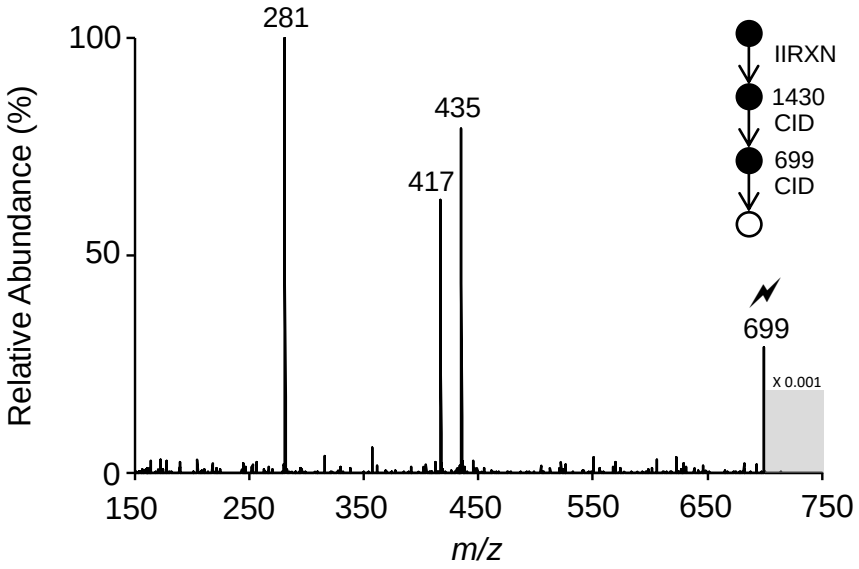

Figure 6.12 MS^3 product ion spectrum of the mass-selected product ion observed at *m/z* 699.

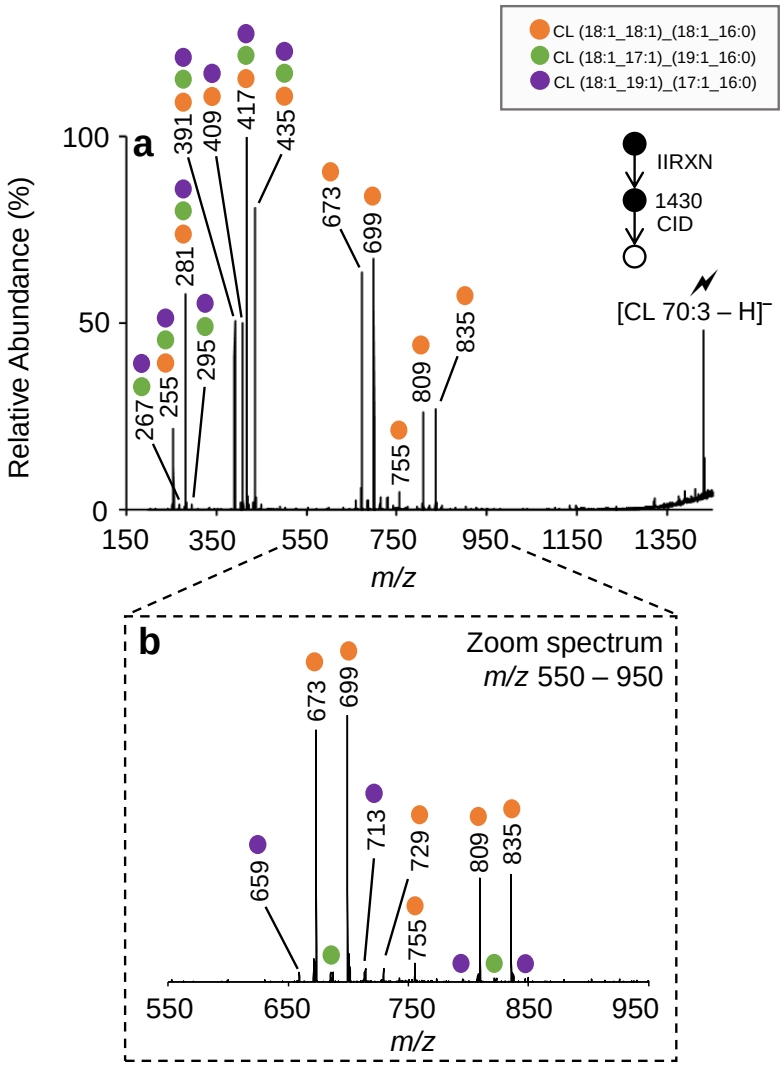

Figure 6.13 (a) Ion trap CID spectrum of the charge-reduced $[CL\ 70:3 - H]^-$ ion (*m/z* 1430) that has *not* been concentrated in Q3 using a refill experiments. (b) enlargement of *m/z* 550 – 950 mass spectral region shown in (a).

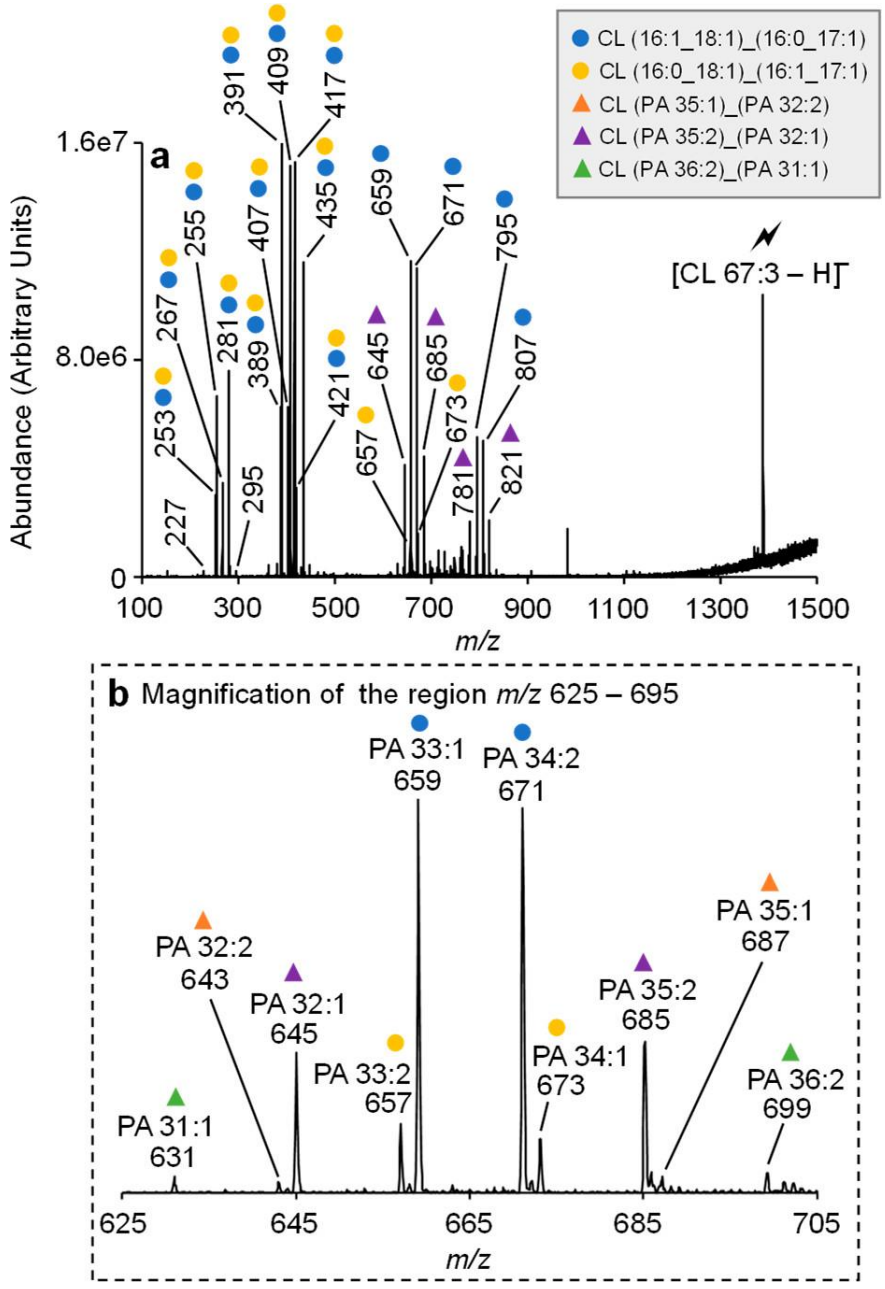

Figure 6.14 (a) Ion-trap CID spectrum of the charge-reduced $[CL\ 67:3 - H]^-$ ion (*m*/*z* 1388) that has been concentrated in Q3 using a total of three refill experiments. (b) Enlargement of the *m*/*z* 625–705 mass spectral region shown in (a).

CHAPTER 7. CHARGE-SWITCH DERIVATIZATION OF FATTY ACID ESTERS OF HYDROXY FATTY ACIDS VIA GAS-PHASE ION/ION REACTIONS

7.1 Introduction

Fatty acid esters of hydroxy fatty acids (FAHFAs), also referred to as (*O*-acyl)-hydroxy fatty acids (OAHFAs), are a newly discovered category of lipids found in mammals and plants.[1,2] Branched FAHFAs are important signaling molecules with potential anti-inflammatory and anti-diabetic effects and have thus received considerable attention as potential therapeutic agents for type 2 diabetes and inflammatory diseases like obesity.[1] FAHFAs are regulated by GLUT4, a major insulin-regulated glucose transporter that serves as a key regulator of whole-body glucose homeostasis, and are suggested to improve glucose tolerance, stimulate insulin secretion, and enhance glucose transport.[1, 3, 4] FAHFAs are found in mammalian serum and tissues as non-esterified (*i.e.,* free) molecules at low concentrations[1], and according to recent studies, FAHFAs can also be incorporated into complex lipid classes like triacylglycerols and sphingolipids.[5, 6] Interestingly, the concentrations of FAHFA-containing triacylglycerols (FAHFA-TGs) in adipose tissue were reported to be 100-fold greater than that of non-esterified FAHFAs, suggesting FAHFA-TGs may serve as a major reservoir of these lipids.[5] In general, FAHFA structure is defined by a fatty acid (FA) esterified to the alcohol of a hydroxy fatty acid (HFA). A large number of distinct FAHFA structural variants arise from modifications to FA and HFA composition, including variations in aliphatic chain length, carbon-carbon double bond number and position, and hydroxylation site. Furthermore, a specific category of isomeric FAHFAs that differ only in the position of the ester linkage along the *n*-HFA backbone, referred to as *n*-FAHFA isomers, have been detected in human adipose tissue and serum, noting that *n* indicates the ester position relative to the HFA carboxyl carbon.[1] Importantly, regulation of *n*-FAHFA isomers levels under insulin-resistant conditions is both tissue-specific and isomer-specific.[1] Consequently, it is imperative to develop analytical tools that provide unambiguous FAHFA structural identification, as the evolution of such technologies is integral to the advancement of biomedical sciences, including the development of new strategies for the treatment and diagnosis of metabolic and inflammatory disorders (*e.g.*, type 2 diabetes and obesity).

Mass spectrometry (MS) has played a pivotal role in the structural elucidation of lipids.[7-9] Even in contemporary MS-based lipidomics workflows, however, there remain significant challenges associated with lipid structural identification. Currently, two main mass spectrometric strategies for FAHFA analysis have been established.[10] In the first approach, FAHFA molecular structures are first separated via liquid chromatography (LC) prior to admission to a tandem mass spectrometer. While LC-tandem mass spectrometry (MS/MS) can provide increased isomeric resolution, FAHFA structural identifications using this strategy are often reliant on comparison of retention times to authentic lipid standards, which, to date, are limited.[1, 11, 12] Notably, Ma *et al.* developed an *in silico* MS/MS library that extends the coverage of FAHFA molecules in LC-MS/MS studies, aiding in the identification of unknown molecular structures when external reference standard compounds are not available.[13]

While many LC-MS/MS approaches for FAHFA identification have been described and successfully used for FAHFA analysis[1, 11], direct infusion electrospray ionization tandem mass spectrometry (ESI-MS/MS), or so-called "shotgun lipidomics", has also emerged as a sensitive and powerful approach for lipid identification and quantification.[14-16] Due to the presence of a carboxylic acid moiety, FAHFAs can be ionized by direct infusion negative polarity ESI, forming abundant singly deprotonated FAHFA anions, denoted $[FAHFA - H]^-$. From accurate mass measurements (*i.e.*, observed mass-to-charge ratio) alone, FAHFA sum composition (*i.e.*, the total number of carbons and degree of unsaturation) can be obtained. Subsequent interrogation of $[FAHFA - H]^-$ ions via low-energy collision induced dissociation (CID) facilitates the assignment of constituent FA and HFA. Explicitly, the $[FA - H]^-$ and $[HFA - H]^-$ product ions are readily observed in resulting $[FAHFA - H]^-$ CID spectra, and in turn, isomeric FAHFAs differing in aliphatic chain length combinations can be discerned.[1, 17] Nevertheless, significant challenges remain for unambiguous FAHFA identification when utilizing conventional shotgun approaches, particularly in distinguishing *n*-FAHFA isomers that vary only in ester regiochemistry. For instance, the MS^2 product ion spectra of isomeric $[n\text{-}FAHFA - H]^-$ ions are remarkably similar, characterized by variations only in product ion relative abundances related to the site of esterification along the HFA backbone. Thus, MS/MS alone is often insufficient to distinguish *n*-FAHFA isomers.[17] Notably, Yore and coworkers exploited low mass product ions observed using a quadrupole-time of flight mass spectrometer to distinguish FAHFA isomers.[1] However, these diagnostic product ions are not consistently observed across various mass spectrometric platforms

and studies, precluding more widespread application of this approach.[13, 17] Deploying a systematic MS^n approach, Marshall *et al.*[17] showed that MS^3 of $[HFA - H]^-$ ions can reveal the esterification site in FAHFA, as diagnostic product ions indicative of ester position were observed.[17] Although, in some cases, significant overlap in predicted diagnostic product ions arising from unique FAHFA isomeric precursors limits FAHFA identification in this manner. Altogether, unambiguous identification of FAHFA isomers continues to be a difficult task when employing low-energy CID alone.

Often in combination with CID, shotgun and LC-MS strategies employing bespoke ion activation or wet-chemical derivatization have enjoyed success for lipid structural identification by permitting the distinction of lipid isomers such as those varying in carbon-carbon double bond position, stereochemical configuration, or acyl chain branching.[9] To our knowledge, only two of these methods have been applied in the study of FAHFAs. The first approach exploits a combination of CID and ozone-induced dissociation (OzID) to pinpoint ester position along the HFA backbone, achieving near-complete FAHFA structural elucidation.[17] In brief, the [*n*-FAHFA – H]$^-$ precursor anion dissociates to form a dehydrated HFA product ion, denoted [*n*-HFA – H – H_2O]$^-$. Subsequent ion/molecule reactions between the [*n*-HFA – H – H_2O]$^-$ product ion and ozone vapor confirms that this unsaturated product ion is composed of two isomeric alkene structures. Importantly, the carbon-carbon double-bond positions of the two isomeric unsaturated FA ions depend on the location of the fatty acyl ester, and in turn, the dehydrated *n*-HFA anion is indicative of the *n*-FAHFA isomer. Specifically, ozonolysis of the MS^2 [*n*-HFA – H – H_2O]$^-$ product ion population reveals that this anion population is comprised of two distinct, isomeric alkene product ions that contain carbon-carbon double bonds at C_n and C_{n+1} positions, respectively. Despite successes, ion-molecule reactions between dehydrated HFA anions and ozone molecules are slow and reaction rates are dependent on the alkene position relative to the carboxylate moiety, impacting sensitivity. In an alternate approach, Han and coworkers employed solution-based charge inversion of FAHFA with *N*-[4-(aminomethyl)phenyl]pyridinium (AMPP) derivatization giving rise to a fixed-charge cation.[18] Upon collisional activation, the $[AMPP\text{-}FAHFA]^+$ cation fragments to form product ions indicative of ester position albeit at low abundance. In general, CID of AMPP derivatized FAHFA provide some insight into the structure of the HFA but little, or no, information on the bonding in the FA portion.[19] Additionally, like all traditional derivatization, this approach is reliant on wet-chemical modification, requiring additional sample

manipulation prior to analysis and is susceptible to matrix effects in complex lipid extracts. It would thus be desirable to exploit the benefits of charge-inversion derivatization of FAHFAs but to enhance both the efficiency and speed of derivatization by exploiting entirely gas phase chemistries within the mass spectrometer.

Recently, we demonstrated the structural elucidation of lipids utilizing gas-phase charge inversion ion/ion chemistry.[20-22] Charge inversion ion/ion reactions can provide a significant reduction in chemical noise associated with mass spectra derived from complex mixtures, including lipid extracts, translating to lower detection limits and enhanced sensitivity.[23, 24] In particular, $[FA - H]^-$ ions originating from direct negative nESI of non-esterified (*i.e.*, free) FA or released from complex lipid precursor anions by ion-trap CID are derivatized within the mass spectrometer. To do so, $[FA - H]^-$ anions are simultaneously stored with tris-phenanthroline magnesium complex dications, denoted $[MgPhen_3]^{2+}$, undergoing a charge inversion ion/ion reaction to yield abundant $[FA - H + MgPhen]^+$ complex cations. Subsequent interrogation of charge inverted FA complex cations permits unambiguous isomeric differentiation and the assignment of carbon-carbon double bond positions(s) in unsaturated FA. Explicitly, monounsaturated and diunsaturated FA are identified by direct spectral interpretation, exploiting reproducible fragmentation patterns, while automated matching to a library developed from authentic FA reference standards permits polyunsaturated FA identification. Herein, we deploy gas-phase charge inversion ion/ion reactions to achieve near-complete FAHFA structure elucidation. Conducted entirely in the gas-phase, this strategy permits the identification of ester position and localization of unsaturation sites in FAHFAs without recourse to condensed phase derivatization or separation. Collectively, while also facilitating high-level FAHFA structural characterization on chromatographically relevant timescales, the method supports *de novo* identification FAHFA molecular structures, in the absence of authentic commercial standards, thereby extending the range of confident FAHFA identification.

7.2 Experimental

7.2.1 Reagents

HPLC-grade methanol was purchased from Fisher Scientific (Pittsburgh, PA). Magnesium chloride and 1,10-phenanthroline (Phen) were purchased from MilliporeSigma (St. Louis, MO).

All lipid standards were purchased from Cayman Chemical, Co. (Ann Arbor, MI). Solutions of FAHFA standards were prepared in methanol to a final concentration of 1 μM. Magnesium chloride and 1,10-phenanthroline were combined in methanolic solution to a final concentration of 20 μM.

7.2.2 Mass Spectrometry

All experiments were conducted on a modified Sciex QTRAP 4000 hybrid triple quadrupole/linear ion trap mass spectrometer (SCIEX, Concord, ON, Canada).[25] Alternately pulsed nanoelectrospray ionization (nESI) emitters permit the sequential injection of lipid anions and reagent dications.[26] Prior to entry into the high-pressure collision cell q2, lipid anions and reagent dications are mass selected in transit in Q1. Next, reagent dications and FAHFA anions were mutually stored for 500 ms. Product cations resulting from the charge inversion ion/ion reaction were then transferred to the low-pressure linear ion trap (LIT), Q3. In Q3, MS^n analysis of charge inverted product ions was performed using single frequency resonance excitation (q = 0.2). Mass analysis was conducted using mass-selective axial ejection (MSAE).[27]

7.2.3 Nomenclature

Lipid nomenclature is based on general literature recommendations by Liebisch *et al.*[28] To describe fatty acyl structure, we employ the *X*:*Y* shorthand notation where *X* and *Y* represent the total number of carbons and the degree of unsaturation, respectively (*i.e.*, the 18:1 fatty acyl has 18 carbons and 1 double bond). Proven double bond position is specified after the degree of unsaturation within parentheses, and if known, double bond geometry is labeled as *Z* for *cis* and *E* for *trans*. For brevity, palmitic acid (FA 16:0) and palmitoleic acid (FA 16:1(9*Z*)) are referred as PA and PO, respectively, while HSA indicates any hydroxystearic acid (FA 18:0_OH). Proven hydroxylation position in HSA structures are indicated in the front of the HFA abbreviation. For example, 10-HSA indicates hydroxstearic acid with a hydroxyl group at C10. To describe FAHFA structure, we adopt the specific nomenclature proposed by Marshall *et al.*[17] and Ma *et al.*[13] Briefly, FAHFA are described using the X_1:Y_1/X_2:Y_2 notation, where the FA and HFA are identified as X_1:Y_1 and X_2:Y_2, respectively. To define the site of esterification, the FAHFA X_1:Y_1-(*n*-O-X_2:Y_2) notation was adopted herein, in which *n* indicates the ester position relative to the carboxyl carbon

of the HFA. Lastly, the *n*-FAHFA abbreviations are also utilized for convenience. To illustrate, the FAHFA 16:0-(10-O-18:0) can be represented as 10-PAHSA. **Table 7.1** details the specific *n*-FAHFA abbreviations used in this study.

7.3 Results and Discussion

7.3.1 Charge Inversion Ion/Ion Strategies to Elucidate Saturated FAHFA Structures

As described above, efforts to discriminate *n*-FAHFA isomers using conventional approaches have been limited, largely due to the formation of identical product ions arising from multiple isomeric precursors.[17] To achieve unambiguous FAHFA structural elucidation, we employ a charge-switch derivatization approach based on gas phase ion/ion reactions. In this approach, singly deprotonated FAHFA anions are charge-inverted with tris-phenanthroline magnesium complex reagent dications, as indicated in Scheme 7.1. To conduct this experiment, $[10\text{-PAHSA} - H]^-$ (*m/z* 537.5) anions were simultaneously stored with $[MgPhen_3]^{2+}$ reagent dications in the high-pressure collision cell q2 and permitted to react. The results of the ion/ion reaction are provided in Figure 7.1a. The $[10\text{-PAHSA} - H + MgPhen_2]^+$ complex cation, detected at *m/z* 921.6, represents the dominant product ion, while a minor $[10\text{-PAHSA} - H + MgPhen]^+$ complex cation (*m/z* 741.5) was also observed (Figure 7.1a). Importantly, the complex cation is observed at a signal level that is roughly a factor of three greater than that of the $[10\text{-PAHSA} - H]^-$ ion in negative ion mode when using the same ion multiplier voltage but opposite conversion dynode voltages (Figure 7.2). We attribute the signal enhancement achieved via charge inversion to the difference in overall gain for detection for each polarity under these conditions. Following the ion/ion reaction, the resulting charge-inverted product ions were energetically transferred from q2 to Q3, giving rise to a 'beam type' (BT) CID spectrum. At lower collision energies, BT CID results in the loss of a single phenanthroline ligand, generating the $[10\text{-PAHSA} - H + MgPhen]^+$ complex cation (*m/z* 741.5) (Figure 7.3). As collision energies are increased, abundant $[PA - H + MgPhen]^+$ (*m/z* 459.3) and $[10\text{-HSA} - H - H_2O + MgPhen]^+$ (*m/z* 485.3) product ions were observed (Figure 7.1b). Note that the $[10\text{-HSA} - H - H_2O + MgPhen]^+$ product ion observed at *m/z* 485.3 can also be represented as an unsaturated FA 18:1 complex cation (*i.e.,* $[18{:}1 - H + MgPhen]^+$). Importantly, the BT CID spectrum shown in Figure 7.1b enables assignment of HFA and FA composition, as the $[PA - H + MgPhen]^+$ (*m/z* 459.3) and $[10\text{-HSA} - H - H_2O + MgPhen]^+$

(*m/z* 485.3) ions were readily observed. The ion-trap CID spectrum of the mass-selected *m/z* 741.5 ion is provided in Figure 7.4 and is in good agreement with the BT CID spectrum shown in Figure 7.1b.

Next, the complex cation of *m/z* 485.3 was mass-selected in the LIT with a 1 *m/z* window and subsequently interrogated via ion-trap CID. The CID spectrum of [10-HSA – H – H_2O + MgPhen]$^+$ (*m/z* 485.3) is displayed in Figure 7.1c. Consistent with the observations reported by Marshall *et al.*,[17] the data suggest that the dehydrated 10-HSA complex cation population is comprised of two isomeric monounsaturated FAs with carbon-carbon double bonds at C9=C10 and C10=C11. Indeed, the formation of a pair of alkenes upon dissociation of [PAHSA + MgPhen]$^+$ cations was independently verified by measuring the OzID mass spectra of the [HSA – H – H_2O + MgPhen]$^+$ product ion population. These data, acquired from solution-formed [*n*-PAHSA + MgPhen]$^+$ cations, confirm that the positions of the carbon-carbon double bonds formed upon dissociation flank the *n*-position of the ester moiety (Figure 7.5). Consequently, the presence of FA 18:1(9) and 18:1(10) confirms the hydroxylation position in the [10-HSA – H – H_2O + MgPhen]$^+$ complex cation, and in turn, establishes ester regiochemistry in the original PAHSA precursor ion. Importantly, the double bond positions in the isomeric alkene product ions are dependent on site of hydroxylation in the HFA constituent, and therefore, relate to the position of the ester linkage along the HFA backbone. From Figure 7.1c, the product ions related to dissociation of [18:1(9) – H + MgPhen]$^+$ and [18:1(10) – H + MgPhen]$^+$ complex cations are denoted with the green (●) and red (●) circles, respectively. As previously described[20, 22], the site of unsaturation in monounsaturated FA can be pinpointed using charge inversion ion/ion chemistry as [FA – H + MgPhen]$^+$ complex cations fragment to generate reproducible spectral patterns indicative of double bond location. Briefly, to localize the double bond in monounsaturated FA, a characteristic spectral gap dependent on carbon-carbon double bond position is exploited. The spectral gap arises from dramatic suppression in product ion abundance related to product ions representing carbon-carbon double bond cleavage and carbon-carbon cleavages vinylic to the double bond. Flanking the spectral gap, carbon-carbon cleavage distal (*i.e.,* on the methyl side) and allylic to the double bond yields a product ion doublet composed of a charge remote fragment ion and a terminally saturated product ion. This product ion doublet represents the two heaviest product ions (*i.e.*, highest *m/z*) in the fragmentation pattern and serves as a key diagnostic marker for double bond position. In the case of 10-PAHSA, the pair of product ions observed at *m/z* 385.2

and 387.2 serve as diagnostic product ions for FA 18:1(9), while the product ion pair detected at *m/z* 399.2 and 401.2 indicate the 18:1(10) isomer (Figure 7.1c). Moreover, in the absence of spectral magnification in Figure 7.1c, the product ion at *m/z* 345.2 serves as a marker for hydroxylation position in the HFA ion. Specifically, carbon-carbon cleavage proximal (*i.e.*, on the carboxyl side) and allylic to the C10=C11 double bond in the FA 18:1(10) isomer predominately contributes to the abundant product ion detected at *m/z* 345.2, though minor contributions to this product ion population are provided by C8-C9 cleavage in the FA 18:1(9) isomer. While the two sets of high-mass product ion doublets confirm the presence of two FA 18:1 isomers, the characteristic product ion at *m/z* 345.2 serves as a key indicator of hydroxylation position, easily facilitating the identification of original ester position in the 10-PAHSA precursor ion.

An alternate strategy for FAHFA identification based on charge inversion of product ions generated from CID of deprotonated precursors is outlined for 10-PAHSA in Scheme 7.2. In this approach, direct infusion negative nESI of 10-PAHSA generates abundant singly deprotonated $[\text{10-PAHSA} - \text{H}]^-$ ions (*m/z* 537.5) with Ion-trap CID of the mass-selected $[\text{10-PAHSA} - \text{H}]^-$ precursor anion (*m/z* 537.5) in q2 generating the product ion spectrum shown in Figure 7.6a. CID of the FAHFA precursor anion enables assignment of the FA and HFA constituents at the sum compositional level. In the case of the CID spectrum of $[\text{10-PAHSA} - \text{H}]^-$, the product ions observed at *m/z* 255.2, 281.2, and 299.3 reflect the $[\text{PA} - \text{H}]^-$, $[\text{10-HSA} - \text{H} - \text{H}_2\text{O}]^-$, $[\text{10-HSA} - \text{H}]^-$ anions, respectively. Notably, these product ions are characteristic of the $[\text{PAHSA} - \text{H}]^-$ precursor ion, differentiating it from isomeric FAHFAs comprised of different chain length combinations in the HFA and FA constituents (Figure 7.6a). However, subtle structural features like ester regiochemistry cannot be easily discerned from this spectrum, and in turn, other *n*-FAHFA isomers are not easily distinguished at the MS^2 level.[17]

Next, all product anions derived from collisional activation of $[\text{10-PAHSA} - \text{H}]^-$ were subjected to ion/ion reaction with $[\text{MgPhen}_3]^{2+}$ reagent dications. The resulting product ion spectrum is illustrated with Figure 7.6b. Dominating the product ion spectrum are the $[\text{PA} - \text{H} + \text{MgPhen}_2]^+$ (*m/z* 639.4), $[\text{10-HSA} - \text{H} - \text{H}_2\text{O} + \text{MgPhen}_2]^+$ (*m/z* 665.4), and $[\text{10-HSA} - \text{H} + \text{MgPhen}_2]^+$ (*m/z* 638.4) product ions (Figure 7.6b). Following the ion/ion reaction, the resulting charge-inverted product ions were collisionally activated via BT CID, giving rise to the BT CID spectrum portrayed in Figure 7.6c. In general, BT CID results in the neutral loss of a single phenanthroline ligand, as the $[\text{PA} - \text{H} + \text{MgPhen}]^+$ (*m/z* 459.3), $[\text{10-HSA} - \text{H} - \text{H}_2\text{O} + \text{MgPhen}]^+$

(*m/z* 485.3), [10-HSA – H + MgPhen]$^+$ (*m/z* 503.3) product ions are predominant (Figure 7.6c). Note that the [10-HSA – H – H_2O + MgPhen]$^+$ product ion observed at *m/z* 485.3 can also be represented as an unsaturated FA 18:1 complex cation (*i.e.*, [18:1 – H + MgPhen]$^+$). In the LIT, CID of [10-HSA – H – H_2O + MgPhen]$^+$ (*m/z* 485.3) generates the product ion spectrum displayed in Figure 7.6d. Interestingly, we note that the CID spectra in Figures 7.1c and 7.6d are *identical*, and once more, this CID spectrum exhibits evidence for two isomeric FA 18:1 complex cations. Exploiting characteristic product ions reflective of carbon-carbon double bond position, the 18:1(9) and 18:1(10) isomers were identified from Figure 7.6d. Additionally, as described above, the product ion at *m/z* 345.2 once more serves as a clear marker for hydroxylation position and, consequently, confirms the original ester location in the 10-PAHSA precursor ion. Moreover, in comparison to the BT CID spectrum shown with Figure 7.1b, Figure 7.6c displays an abundant [10-HSA – H + MgPhen]$^+$ (*m/z* 503.3) product ion that was not previously observed following direct charge inversion and collisional activation of the 10-PAHSA ion (*c.f.* Figures 7.1b and 7.6c). Comparing the two distinct charge inversion ion/ion strategies presented herein (*i.e.*, CID of the FAHFA ion followed by charge inversion *vs*. direct charge inversion of the FAHFA anion), we chose to utilize the direct charge inversion strategy for the analysis of saturated FAHFAs. While both ion/ion approaches afford identification of FA and HFA constituents, the [10-HSA – H – H_2O + MgPhen]$^+$ complex cation is more abundant when utilizing direct charge inversion of the 10-PAHSA precursor anion, leading to reduced integration times and increased sensitivity. Thus, all data presented hereafter for saturated FAHFA analysis employs a direct charge inversion approach.

7.3.2 Differentiation of Isomeric *n*-FAHFAs using Direct Charge Inversion Ion/Ion Strategies

In addition to 10-PAHSA, we examined an array of synthetic *n*-PAHSA isomers including 13-PAHSA, 12-PAHSA, 9-PAHSA, and 5-PAHSA. Ultimately, isomeric FAHFA differing only in the site of esterification can be discerned using gas-phase charge inversion chemistry. Utilizing the direct charge inversion method outlined above, [*n*-PAHSA – H]$^-$ anions were selectively derivatized in the gas-phase via ion/ion reactions with [$MgPhen_3$]$^{2+}$ reagent dications, yielding abundant [*n*-PAHSA – H + MgPhen]$^+$ complex cations. Once more, [*n*-HSA – H – H_2O + MgPhen]$^+$ complex cations were obtained from BT CID of charge-inverted *n*-PAHSA complex cations. We note that the resulting BT CID spectra are insensitive to ester position, as collisional

activation of charge-inverted *n*-PAHSA complex cations yielded nearly identical product ion spectra (Figure 7.7). Individual CID spectra of the charge inverted dehydrated *n*-HSA complex cations originating from the 13-PAHSA, 12-PAHSA, 9-PAHSA, and 5-PAHSA precursor ions are provided in Figure 7.8.

Analogous to the results described above with 10-PAHSA, the individual CID spectra of [*n*-HSA – H – H_2O + MgPhen]$^+$ complex cations derived from the various *n*-PAHSA isomers indicate the presence of two isomeric unsaturated octadecenoic ions. Furthermore, distinct spectral differences confirm that unsaturated [*n*-HSA – H – H_2O + MgPhen]$^+$ complex cations are unique to each *n*-PAHSA isomer (Figure 7.8). While the fragmentation highlighted in the grey shading can be rationalized as indicated above, ester position in isomeric *n*-PAHSA structures are marked by an abundant product ion arising from carbon-carbon cleavage proximal and allylic to the site of unsaturation in the [18:1 – H + MgPhen]$^+$ complex cation. Considering 13-PAHSA, the CID spectrum of [13-HSA – H – H_2O + MgPhen]$^+$ (*m/z* 485.3) provided in Figure 7.8a contains an abundant product ion at *m/z* 387.1 that can be exploited to assign the site of hydroxylation and thus ester bond position. Paralleling results described above, carbon-carbon cleavage proximal and allylic to the C13=C14 in the [18:1(13) – H + MgPhen]$^+$ complex cation is the dominant contributor to the *m/z* 387.1 product ion population. As there is a dramatic suppression in the relative abundances of product ions observed at *m/z* values greater than *m/z* 387.1, the product ion at *m/z* 387.1 is recognized as a key indicator of hydroxylation position, confirming the original ester location in the 13-PAHSA precursor ion. In general, as the ester position in the original *n*-PAHSA precursor ion moves closer to the carboxyl carbon of the HFA constituent, the diagnostic product ion shifts lower in *m/z*. For example, interrogation of the [12-HSA – H – H_2O + MgPhen]$^+$ (*m/z* 485.3) the produces ion at *m/z* 373.1 indicates the 18:1(12) structure, confirming the original ester position in the 12-PAHSA precursor ion (Figure 7.8b). In an additional example, the CID spectrum of [18:1 – H + MgPhen]$^+$ ions derived from 9-PAHSA again illustrates a distinct fragmentation pattern, with the presence of 9-octadecenoate indicated by the product ion at *m/z* 331.1 (Figure 7.8c). Lastly, in the case of 5-PAHSA, the product ion at *m/z* 275.1 from FA 18:1(5) was observed upon dissociation of [5-HSA – H – H_2O + MgPhen]$^+$ (*m/z* 485.3), as shown in Figure 7.8d. Collectively, these data demonstrate the utility of charge inversion ion/ion reactions for the structural elucidation of isomeric FAHFA. As alkene position in unsaturated *n*-HFA complex cations is dependent on the original site of ester linkage along the HFA backbone, the CID spectra

of [*n*-HSA – H – H_2O + MgPhen]$^+$ complex cations will reflect differences in *n*-HSA composition. In turn, interrogation of unsaturated *n*-HFA complex cations reveals distinct, reproducible spectral patterns that enable the unambiguous assignment of hydroxylation position, and consequently, fatty acyl ester location in the initial FAHFA precursor ion.

7.3.3 Structure Elucidation of Unsaturated FAHFAs using Charge Inversion Ion/Ion Reactions

Lastly, we demonstrate the near-complete structure elucidation of unsaturated FAHFA, pinpointing the sites of unsaturation and hydroxylation in the constituent FA and HFA, respectively. This is illustrated with the analysis of 10-POHSA, a synthetic FAHFA in which PO is esterified to 10-HSA. Using the direct charge inversion approach, singly deprotonated 10-POHSA anions were reacted with $[MgPhen_3]^{2+}$ reagent dications and subsequently collisionally activated via BT CID, giving rise to the product ion spectrum shown in Figure 7.9a. Two unsaturated product ions were observed at *m/z* 457.3 and 485.3 indicating the [16:1 – H + MgPhen]$^+$ and [18:1 – H + MgPhen]$^+$ complex cations, respectively. Mass-selection and ion-trap CID of the product ion at *m/z* 485.3 from Figure 7.9a yielded a product ion spectrum portrayed in Figure 7.9b. Once more, CID of the [10-HSA – H – H_2O + MgPhen]$^+$ (*m/z* 485.3) complex cation provides product ions arising from the dissociation of two octadecenoic isomers. Specifically, the product ions at *m/z* 387.1 and 385.1 signify FA 18:1(10), while those at *m/z* 373.1 and 371.1 indicate the 18:1(9) isomer (Figure 7.9b). Importantly, the product ion at *m/z* 345.2 can be exploited identifies the hydroxylation site in the 10-HSA and the original ester position in synthetic 10-POHSA, as formation of this ion occurs via proximal carbon-carbon cleavage allylic to the C10=C11 double bond in the [18:1(10) – H + MgPhen]$^+$ complex cation. Next, ion-trap CID of the [16:1 – H + MgPhen]$^+$ (*m/z* 457.3) complex cation from Figure 7.9b was employed to localize the site of unsaturation in the fatty acyl substituent of 10-POHSA. The product ion spectrum of [16:1 – H + MgPhen]$^+$ (*m/z* 457.3) is provided in Figure 7.9c. Notably, the CID spectrum of the product ion at *m/z* 457.3 exhibits evidence for only a single hexadecenoic acid isomer, as a single high-mass product ion doublet was detected at *m/z* 387.1 and 385.1. Together, these diagnostic ions and the identifiable spectral gap facilitate the assignment of the C9=C10 double bond in the [16:1 – H + MgPhen]$^+$ ion consistent with palmitoleic acid. We note that while the C9=C10 double bond in 16:1 was assigned *de novo* exploiting the reproducible spectral pattern, carbon-carbon

double bond positions, particularly in polyunsaturated FAs, can be assigned by automated spectral matching to the previously developed FA library.[20] Taken together the two sets of CID products ions explicitly confirm the structure of both FA and HFA components, as well as the regiochemistry of the FAHFA.

While for the 10-POHSA standard the above direct charge inversion analysis is unambiguous, in a complex mixture there exists the potential for dehydrated HFA ions (*i.e.*, $[HFA - H - H_2O + MgPhen]^+$) to be isomers of unsaturated FAs. Explicitly, the direct charge inversion strategy is prone to overlapping product ion signals arising from dehydrated HFA and unsaturated FA ions, and in turn, the dehydrated HFA constituent could be misidentified as a FA. Fortunately, this ambiguity to can be removed by implementing the complementary approach, described above, wherein CID of the $[FAHFA - H]^-$ ions can be conducted first followed by charge-switch derivatization of the product ions. In q2, CID of the $[10\text{-}POHSA - H]^-$ anion (*m/z* 535.5) yields an abundant singly deprotonated 16:1 carboxylate anion at *m/z* 253.2, reflecting the FA substituent (Figure 7.10a). Dissociation of the $[10\text{-}POHSA - H]^-$ precursor ion also generated the $[10\text{-}HSA - H]^-$ (*m/z* 299.3) and $[10\text{-}HSA - H - H_2O]^-$ (*m/z* 281.2) product ions that readily facilitate identification of the HFA constituent in the unsaturated FAHFA precursor ion. Charge-inversion of the product ions shown in Figure 7.10a followed by BT CID provides the product ion spectrum illustrated with Figure 7.10b. Following the ion/ion reaction, BT CID results in the generation of the $[16:1 - H + MgPhen]^+$ (*m/z* 457.3) complex cation, along with charge-inverted product ions pertaining to the HSA constituent. Specifically, the product ion observed at *m/z* 485.3 corresponds to the $[10\text{-}HSA - H - H_2O + MgPhen]^+$ complex cation, while the complex cation at *m/z* 503.3 represents $[10\text{-}HSA - H + MgPhen]^+$. Subsequent interrogation of the unsaturated complex cation at *m/z* 485.3 and 457.3 provide *identical* product ion spectra to those shown in Figure 7.9b and 7.9c, respectively. Again, CID of the $[10\text{-}HSA - H - H_2O + MgPhen]^+$ product ion can be used to establish the original ester position along the HFA backbone, while dissociation of the $[16:1 - H + MgPhen]^+$ complex cation facilitates assignment of carbon-carbon double bond position in the unsaturated FA constituent. In total, both charge inversion strategies outlined herein can be utilized to assign ester position in the initial FAHFA precursor ion and localize double bond positions in the unsaturated fatty acyl constituent. However, we note that direct charge inversion of unsaturated FAHFA anions could complicate the task of unambiguous FAHFA structure elucidation, especially if multiple isomers are present in a complex biological sample. Therefore, we find that

by performing CID of the unsaturated FAHFA anion prior to charge inversion, the HFA and FA constituents can be confidently identified, and ensuing charge inversion via ion/ion reactions can be employed to pinpoint subtle – yet key – structural features such as the site(s) of unsaturation and hydroxylation.

7.4 Conclusions

FAHFAs are a newly discovered class of endogenous lipid found in mammalian tissues and serum that have received considerable attention recently due to their anti-inflammatory and anti-diabetic effects. While the general FAHFA structure consists of a FA esterified to the alcohol moiety of a HFA, FAHFAs exhibit extensive structural diversity, including a category of FAHFA isomers differing only in the ester position along the HFA backbone. In this study, we report the use of gas-phase charge inversion reactions to achieve near-complete structure elucidation of FAHFA. Herein, we explored two distinct charge-inversion strategies. In the first approach, the charge inversion of *n*-FAHFA isomers is followed by subsequent interrogation of charge-inverted FAHFA complex cations. In the second strategy, *n*-FAHFA isomers ionized in negative ion mode were first collisionally activated via ion-trap CID and then, the resulting product ions were charge inverted via ion/ion reactions with reagent dications. In general, both strategies permit the identification of hydroxylation position along the HFA backbone and can therefore determine the original ester position in the FAHFA precursor ion. Furthermore, using either charge inversion approach, additional carbon-carbon double bond positions in unsaturated FAHFA can be pinpointed exploiting the CID spectra of $[FA - H + MgPhen]^+$ complex cations generated via ion/ion reactions. Ultimately, we find that *n*-FAHFA structure elucidation is limited by the direct charge inversion strategy, particularly regarding the analysis of unsaturated FAHFAs. Therefore, while direct charge inversion offers increased sensitivity, by performing CID of the FAHFA anion prior to charge inversion we readily achieve unambiguous FAHFA structural elucidation and isomeric discrimination.

Representing a key advantage of the presented method, charge inversion ion/ion chemistry overcomes the difficulties of isomeric FAHFA differentiation when commercial standards are not available. Explicitly, reproducible fragmentation patterns of charge inverted unsaturated FA complex cations can be exploited to localize critical subtle FAHFA structural features like ester position and unsaturation sites, affording unambiguous FAHFA molecular structural assignments.

In turn, as monounsaturated FA identification relies on direct spectral interpretation, only authentic FA standards are required to identify polyunsaturated FAs, many of which are readily commercially available. Noting that as additional unsaturated HFA standards become accessible, this approach could likely be further extended to the analysis of FAHFA incorporating unsaturated HFA. Moreover, utilizing the developed ion/ion approach, complementary information obtained from both polarities can be exploited, constituting a major advantage of the ion/ion chemistry over wet-chemical derivatization. Lastly, this entirely gas-phase approach represents a rapid, sensitive MS-based method, affording high-level FAHFA structural detail. Though yet to be demonstrated, charge inversion ion/ion reactions are likely compatible with orthogonal modes of separation, as experimental timescales are consistent with chromatographic separations. Therefore, when FAHFAs are present in higher abundance, a direct infusion strategy could be employed. However, in other cases, where FAHFAs are present at low concentrations, prefractionation could be required. For example, following lipid extraction, FAHFAs could be enriched using solid-phase extraction (SPE) prior to chromatographic separation utilizing an LC-MS/MS protocol paralleling that established by Kolar *et al*.[11] While experiments done herein were not conducted in the context of LC-MS/MS, the current scan function duration is approximately 1.25 s. While current scan rates are already amendable to LC experiments, shorter scan times could be attained by the appropriate tuning of mutual storage and spray conditions. Thus, in conjunction with separation methods prior to MS analysis, ion/ion charge inversion chemistry could not only reduce mixture complexities arising from biological samples but also represent a viable strategy towards achieving complete FAHFA structural elucidation, with the potential to increase the understanding of FAHFA biological functions and their underlying roles in metabolic and inflammatory diseases.

7.5 References

1. Yore, M. M.; Syed, I.; Moraes-Vieira, P. M.; Zhang, T. J.; Herman, M. A.; Homan, E. A.; Patel, R. T.; Lee, J.; Chen, S. L.; Peroni, O. D.; Dhaneshwar, A. S.; Hammarstedt, A.; Smith, U.; McGraw, T. E.; Saghatelian, A.; Kahn, B. B., Discovery of a Class of Endogenous Mammalian Lipids with Anti-Diabetic and Anti-inflammatory Effects. *Cell* **2014,** *159* (2), 318-332.

2. Zhu, Q. F.; Yan, J. W.; Zhang, T. Y.; Xiao, H. M.; Feng, Y. Q., Comprehensive Screening and Identification of Fatty Acid Esters of Hydroxy Fatty Acids in Plant Tissues by Chemical Isotope Labeling Assisted Liquid Chromatography-Mass Spectrometry. *Anal. Chem.* **2018,** *90* (16), 10056-10063.

3. Zhou, P.; Santoro, A.; Peroni, O. D.; Nelson, A. T.; Saghatelian, A.; Siegel, D.; Kahn, B. B., PAHSAs enhance hepatic and systemic insulin sensitivity through direct and indirect mechanisms. *J. Clinical Invest.* **2019,** *129* (10), 4138-4150.

4. Moraes-Vieira, P. M.; Saghatelian, A.; Kahn, B. B., GLUT4 Expression in Adipocytes Regulates De Novo Lipogenesis and Levels of a Novel Class of Lipids With Antidiabetic and Anti-inflammatory Effects. *Diabetes* **2016,** *65* (7), 1808-1815.

5. Tan, D.; Ertunc, M. E.; Konduri, S.; Zhang, J.; Pinto, A. M.; Chu, Q.; Kahn, B. B.; Siegel, D.; Saghatelian, A., Discovery of FAHFA-Containing Triacylglycerols and Their Metabolic Regulation. *J. Am. Chem. Soc.* **2019,** *141* (22), 8798-8806.

6. Hirabayashi, T.; Anjo, T.; Kaneko, A.; Senoo, Y.; Shibata, A.; Takama, H.; Yokoyama, K.; Nishito, Y.; Ono, T.; Taya, C.; Muramatsu, K.; Fukami, K.; Munoz-Garcia, A.; Brash, A. R.; Ikeda, K.; Arita, M.; Akiyama, M.; Murakami, M., PNPLA1 has a crucial role in skin barrier function by directing acylceramide biosynthesis. *Nat.Comm.* **2017,** *8*.

7. Lee, H. C.; Yokomizo, T., Applications of mass spectrometry-based targeted and non-targeted lipidomics. *Biochem. Biophys. Res. Comm.* **2018,** *504* (3), 576-581.

8. Rustam, Y. H.; Reid, G. E., Analytical Challenges and Recent Advances in Mass Spectrometry Based Lipidomics. *Anal. Chem.* **2018,** *90* (1), 374-397.

9. Hancock, S. E.; Poad, B. L. J.; Batarseh, A.; Abbott, S. K.; Mitchell, T. W., Advances and unresolved challenges in the structural characterization of isomeric lipids. *Anal. Biochem.* **2017,** *524*, 45-55.

10. Holcapek, M.; Liebisch, G.; Elcroos, K., Lipidomic Analysis. *Anal. Chem.* **2018,** *90* (7), 4249-4257.

11. Zhang, T. J.; Chen, S. L.; Syed, I.; Stahlman, M.; Kolar, M. J.; Homan, E. A.; Chu, Q.; Smith, U.; Boren, J.; Kahn, B. B.; Saghatelian, A., A LC-MS-based workflow for measurement of branched fatty acid esters of hydroxy fatty acids. *Nat. Protcol.* **2016,** *11* (4), 747-763.

12. Kolar, M. J.; Nelson, A. T.; Chang, T. N.; Ertunc, M. E.; Christy, M. P.; Ohlsson, L.; Harrod, M.; Kahn, B. B.; Siegel, D.; Saghatelian, A., Faster Protocol for Endogenous Fatty Acid Esters of Hydroxy Fatty Acid (FAHFA) Measurements. *Anal. Chem.* **2018,** *90* (8), 5358-5365.

13. Ma, Y.; Kind, T.; Vaniya, A.; Gennity, I.; Fahrmann, J. F.; Fiehn, O., An in silico MS/MS library for automatic annotation of novel FAHFA lipids. *J. Cheminf.* **2015,** *7*, 5.

14. Han, X. L.; Yang, K.; Gross, R. W., Multi-dimensional mass spectrometry-based shotgun lipidomics and novel strategies for lipidomic analyses. *Mass Spectrom. Rev.* **2012,** *31* (1), 134-178.

15. Han, X. L.; Gross, R. W., Shotgun lipidomics: Electrospray ionization mass spectrometric analysis and quantitation of cellular lipidomes directly from crude extracts of biological samples. *Mass Spectrom. Rev.* **2005,** *24* (3), 367-412.

16. Wang, M.; Wang, C. Y.; Han, R. H.; Han, X. L., Novel advances in shotgun lipidomics for biology and medicine. *Prog. Lipid Res.* **2016,** *61*, 83-108.

17. Marshall, D. L.; Saville, J. T.; Maccarone, A. T.; Ailuri, R.; Kelso, M. J.; Mitchell, T. W.; Blanksby, S. J., Determination of ester position in isomeric (O-acyl)-hydroxy fatty acids by ion trap mass spectrometry. *Rapid Comm. Mass Spectrom.* **2016,** *30* (21), 2351-2359.

18. Hu, C.; Wang, M.; Duan, Q.; Han, X., Sensitive analysis of fatty acid esters of hydroxy fatty acids in biological lipid extracts by shotgun lipidomics after one-step derivatization. *Anal. Chim. Acta*, 2020; Vol. 1105, pp 105-111.

19. Hancock, S. E.; Ailuri, R.; Marshall, D. L.; Brown, S. H. J.; Saville, J. T.; Narreddula, V. R.; Boase, N. R.; Poad, B. L. J.; Trevitt, A. J.; Willcox, M. D. P.; Kelso, M. J.; Mitchell, T. W.; Blanksby, S. J., Mass spectrometry-directed structure elucidation and total synthesis of ultra-long chain (O-acyl)-omega-hydroxy fatty acids. *J. Lipid Res.* **2018,** *59* (8), 1510-1518.

20. Randolph, C. E.; Foreman, D. J.; Blanksby, S. J.; McLuckey, S. A., Generating Fatty Acid Profiles in the Gas Phase: Fatty Acid Identification and Relative Quantitation Using Ion/Ion Charge Inversion Chemistry. *Anal. Chem.* **2019,** *91* (14), 9032-9040.

21. Randolph, C. E.; Blanksby, S. J.; McLuckey, S. A., Toward Complete Structure Elucidation of Glycerophospholipids in the Gas Phase through Charge Inversion Ion/Ion Chemistry. *Anal. Chem.*, **2019**.

22. Randolph, C. E.; Foreman, D. J.; Betancourt, S. K.; Blanksby, S. J.; McLuckey, S. A., Gas-Phase Ion/Ion Reactions Involving Tris-Phenanthroline Alkaline Earth Metal Complexes as Charge Inversion Reagents for the Identification of Fatty Acids. *Anal. Chem.* **2018,** *90* (21), 12861-12869.

23. Hassell, K. M.; LeBlanc, Y. C.; McLuckey, S. A., Chemical Noise Reduction via Mass Spectrometry and Ion/Ion Charge Inversion: Amino Acids. *Anal. Chem.* **2011,** *83* (9), 3252-3255.

24. Rojas-Betancourt, S.; Stutzman, J. R.; Londry, F. A.; Blanksby, S. J.; McLuckey, S. A., Gas-Phase Chemical Separation of Phosphatidylcholine and Phosphatidylethanolamine Cations via Charge Inversion Ion/Ion Chemistry. *Anal. Chem.* **2015,** *87* (22), 11255-11262.

25. Yu, X.; Jin, W.; McLuckey, S. A.; Londry, F. A.; Hager, J. W., Mutual storage mode ion/ion reactions in a hybrid linear ion trap. *J. Am. Soc. Mass Spectrom.* **2005,** *16* (1), 71-81.

26. Xia, Y.; Liang, X. R.; McLuckey, S. A., Pulsed dual electrospray ionization for ion/ion reactions. *J. Am. Soc. Mass Spectrom.* **2005,** *16* (11), 1750-1756.

27. Londry, F. A.; Hager, J. W., Mass selective axial ion ejection from a linear quadrupole ion trap. *J. Am. Soc. Mass Spectrom.* **2003,** *14* (10), 1130-1147.

28. Liebisch, G.; Vizcaino, J. A.; Kofeler, H.; Trotzmuller, M.; Griffiths, W. J.; Schmitz, G.; Spener, F.; Wakelam, M. J. O., Shorthand notation for lipid structures derived from mass spectrometry. *J. Lipid Res.* **2013,** *54* (6), 1523-1530.

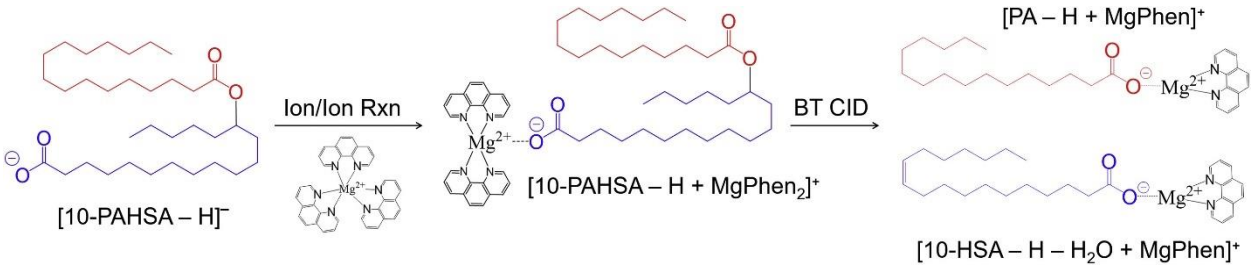

Scheme 7.1 Direct charge inversion of the $[10\text{-PAHSA} - H]^-$ precursor ion via ion/ion reactions with $[MgPhen_3]^{2+}$ reagent dications followed by BT CID, generating the $[10\text{-HSA} - H - H_2O + MgPhen]^+$ and $[PA - H + MgPhen]^+$ complex cations.

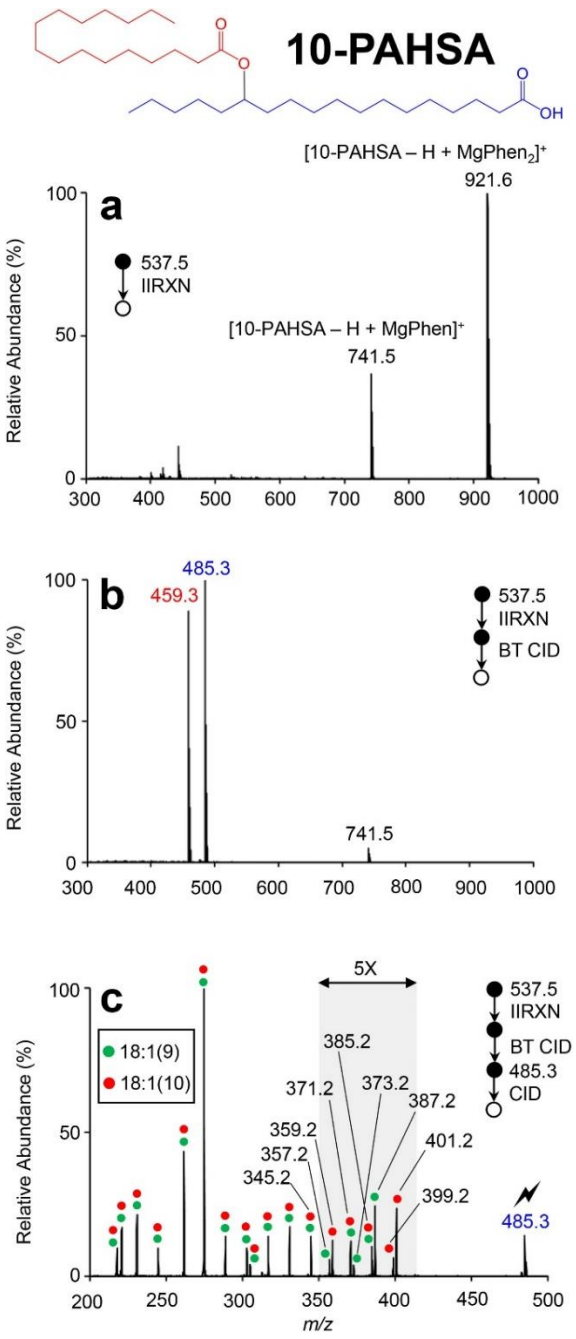

Figure 7.1 Illustration of charge inversion ion/ion workflow used to identify site of esterification in 10-PAHSA. (a) Product ion spectrum resulting from mutual storage ion/ion reaction between $[10\text{-PAHSA} - H]^-$ anions (*m/z* 537.5) and $[MgPhen_3]^{2+}$ reagent dications. (b) Beam type CID spectrum post-ion/ion reaction. (c) Ion trap CID spectrum of mass-selected $[10\text{-HSA} - H - H_2O + MgPhen]^+$ (*m/z* 485.3).

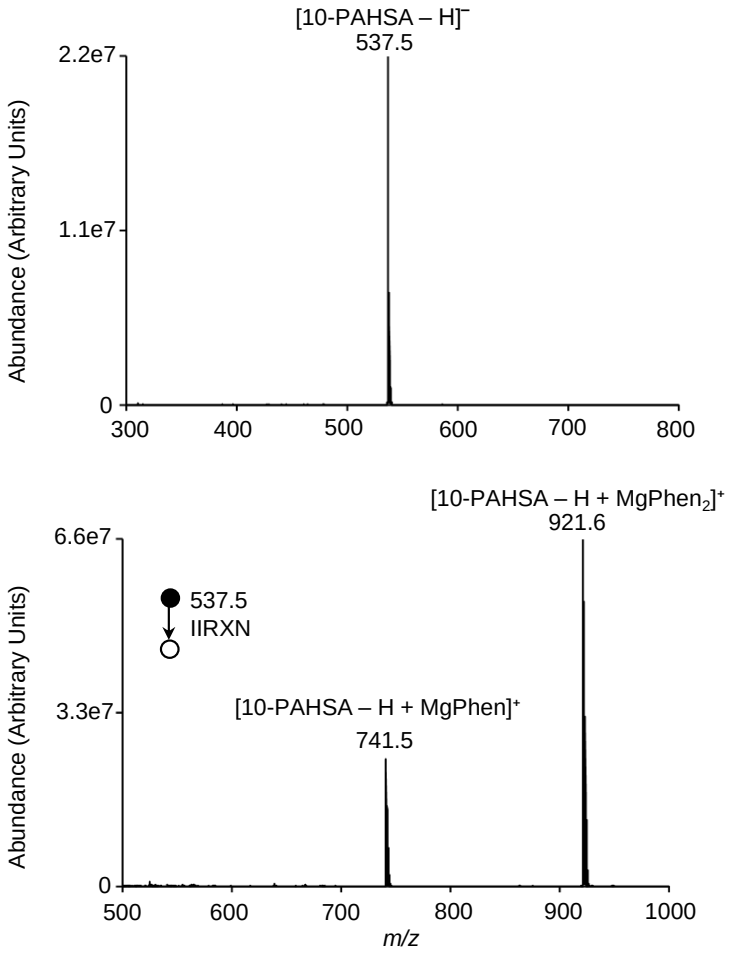

Figure 7.2 (a) Direct negative nESI mass spectrum of 10-PAHSA. (b) Product ion spectrum resulting from the ion/ion reaction between $[MgPhen_3]^{2+}$ reagent dications and $[10\text{-PAHSA} - H]^-$ anions.

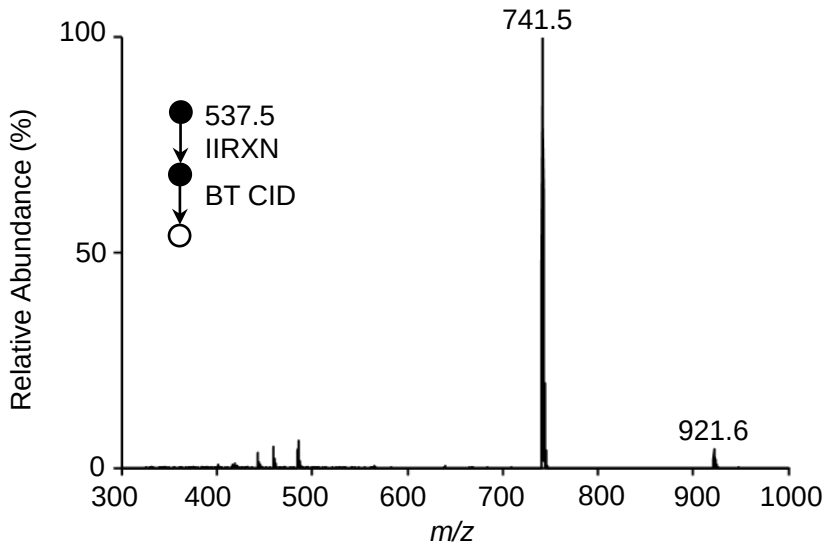

Figure 7.3 BT CID spectrum to generate the [10-PAHSA – H + MgPhen]$^+$ complex cation (*m/z* 741.5).

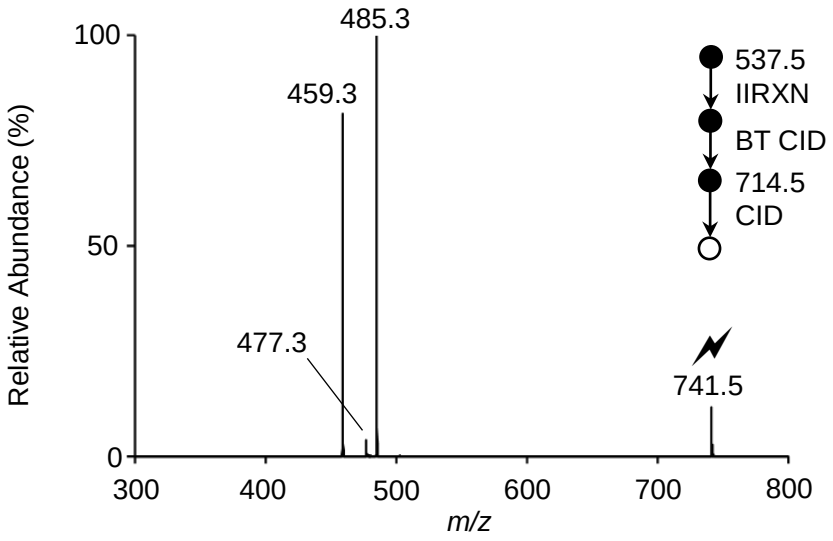

Figure 7.4 Ion-trap CID spectrum of mass-selected [10-PAHSA – H + MgPhen]$^+$ (*m/z* 741.5).

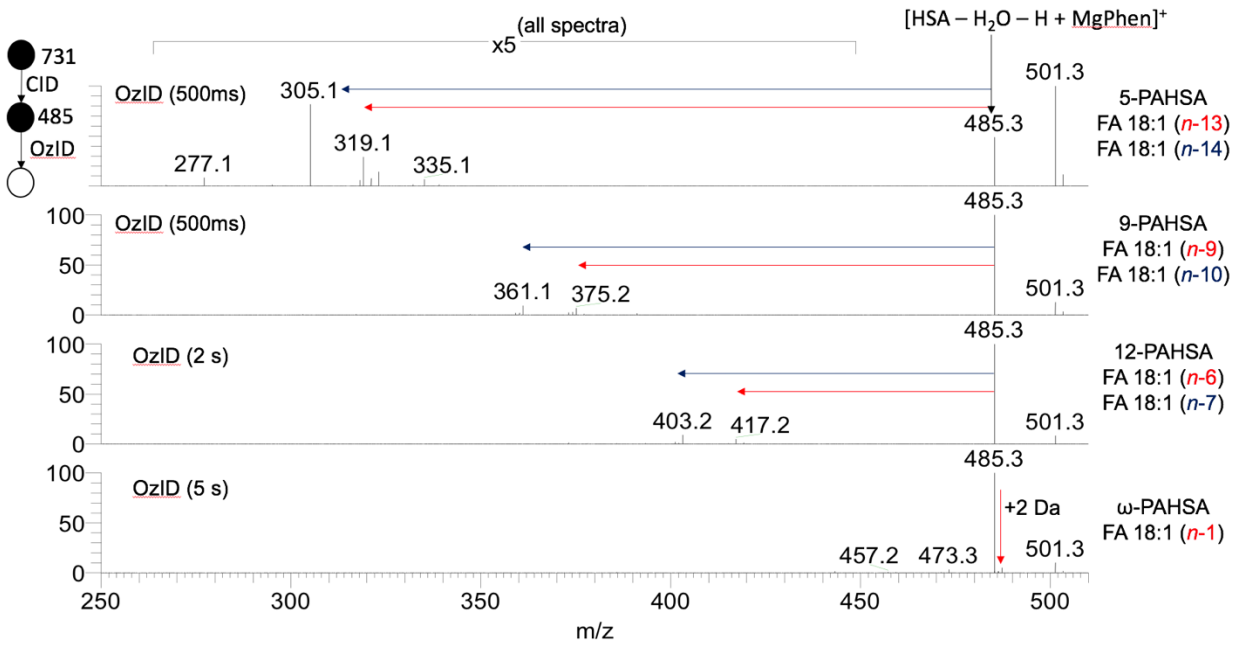

Figure 7.5 Ozone-induced dissociation mass spectra of the [HSA - H_2O - H + MgPhen]$^+$ product ions from CID of *n*-PAHSA isomers where *n* = 5, 9, 12 and 16 (w). Data were obtained on a Thermo Scientific Orbitrap Elite (*R* = 240,000 at *m/z* 400) fitted with a Triversa NanoMate nano-electrospray source operating in positive polarity. [*n*-PAHSA + MgPhen]$^+$ cations were generated by nESI of a mixture of $MgCl_2$, 1,10-phenanthroline and the FAHFA standard. Ozone (220 g/Nm^3, external) was seeded in helium buffer gas and delivered to the segmented ion trap as previously described.[17]

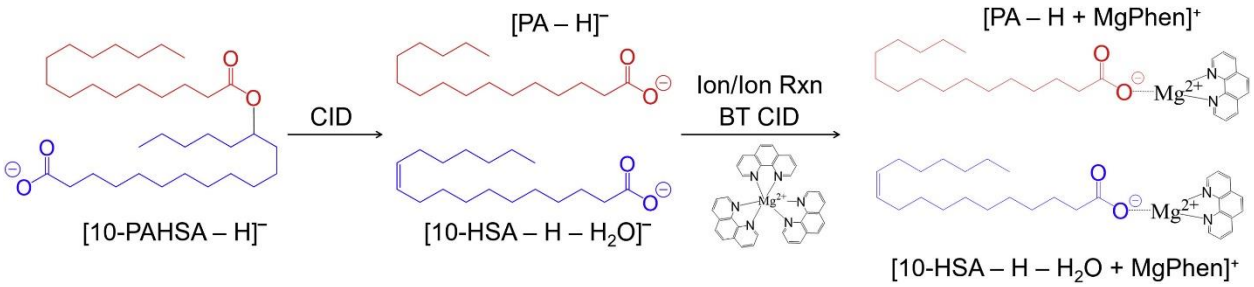

Scheme 7.2 Charge inversion of the product ions generated via CID of the $[10\text{-PAHSA} - H]^-$ precursor ion via ion/ion reactions with $[MgPhen_3]^{2+}$ reagent dications, generating the $[10\text{-HSA} - H - H_2O + MgPhen]^+$ and $[PA - H + MgPhen]^+$ complex cations.

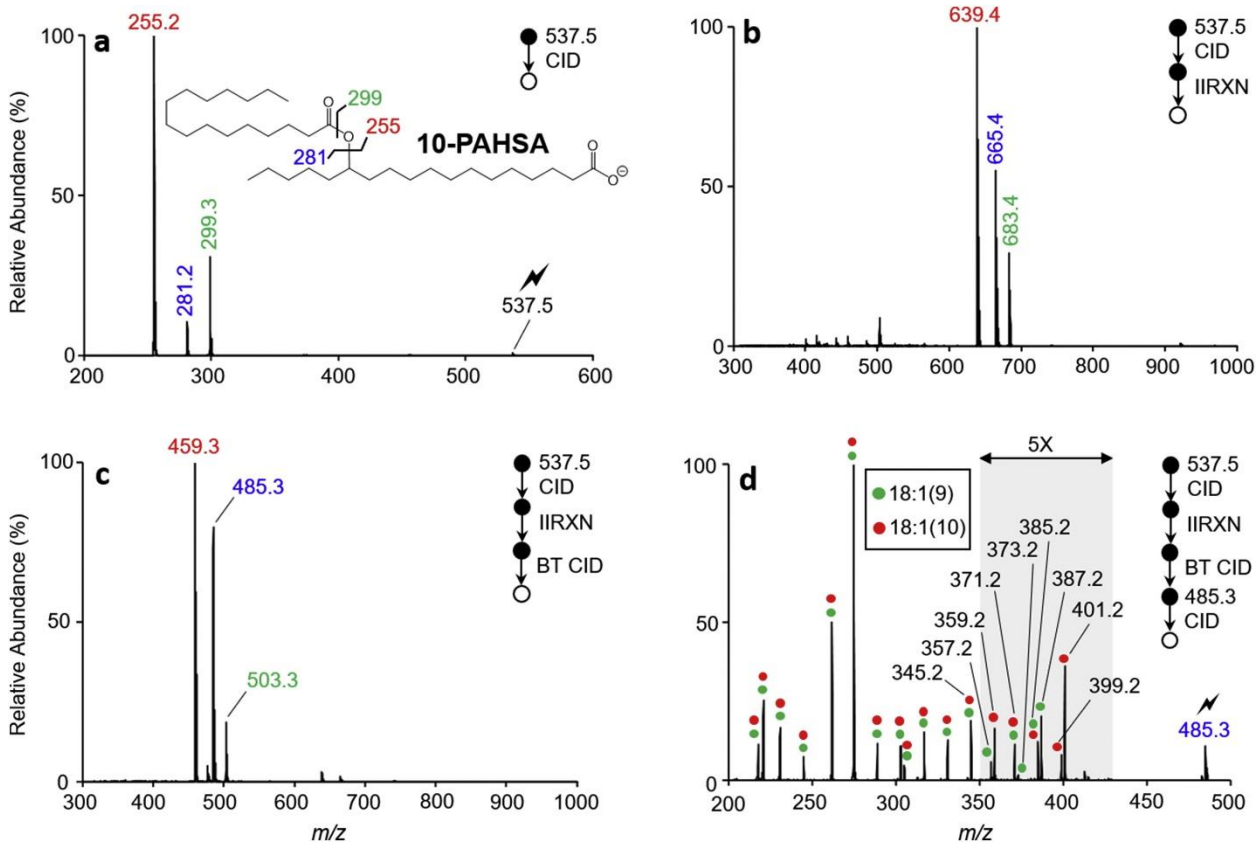

Figure 7.6 Demonstration of charge inversion ion/ion reactions for the identification of ester position in FAHFA. (a) CID spectrum of mass selected [10-PAHSA – H]$^-$ (*m/z* 537.5). (b) Mutual storage product ion spectrum resulting from the charge inversion ion/ion reaction between $[MgPhen_3]^{2+}$ reagent diactions and the product anions shown in panel (a). (c) Product ion spectrum generated via energetic transfer (*i.e.*, beam-type CID) of the mutual storage product cations shown in panel (b) from q2 to Q3. (d) CID spectrum of mass-selected $[10\text{-HSA} - H - H_2O + MgPhen]^+$ (*m/z* 485.3)

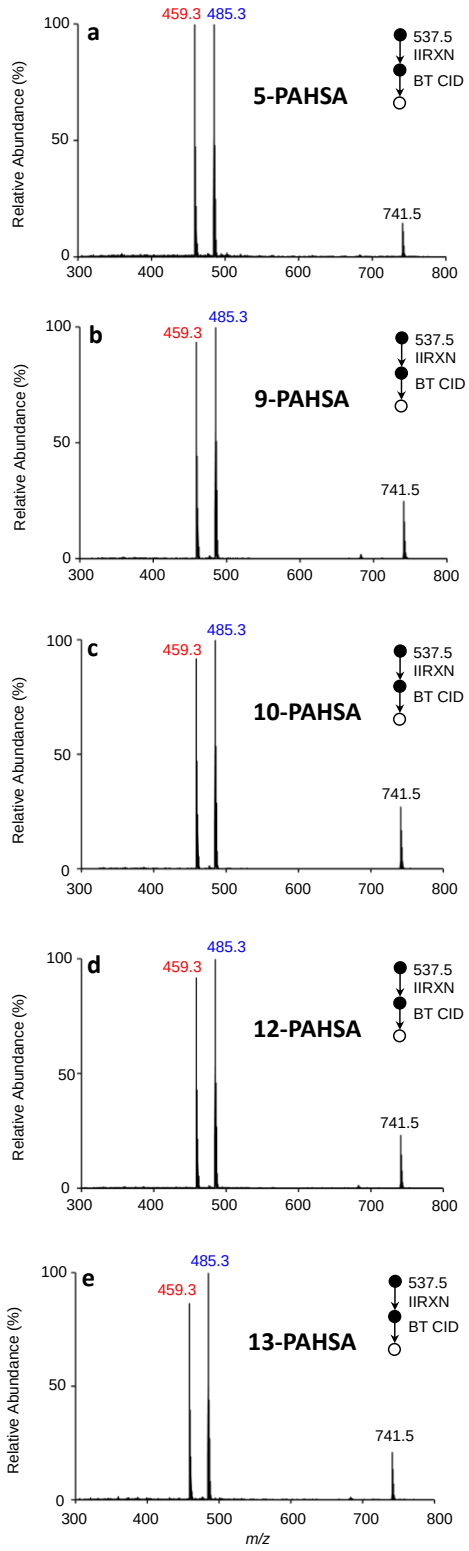

Figure 7.7 BT CID spectra of charge-inverted FAHFA complex cations derived from (a) 5-PAHSA, (b) 9-PAHSA, (c) 10-PAHSA, (d) 12-PAHSA, and (e) 13-PAHSA.

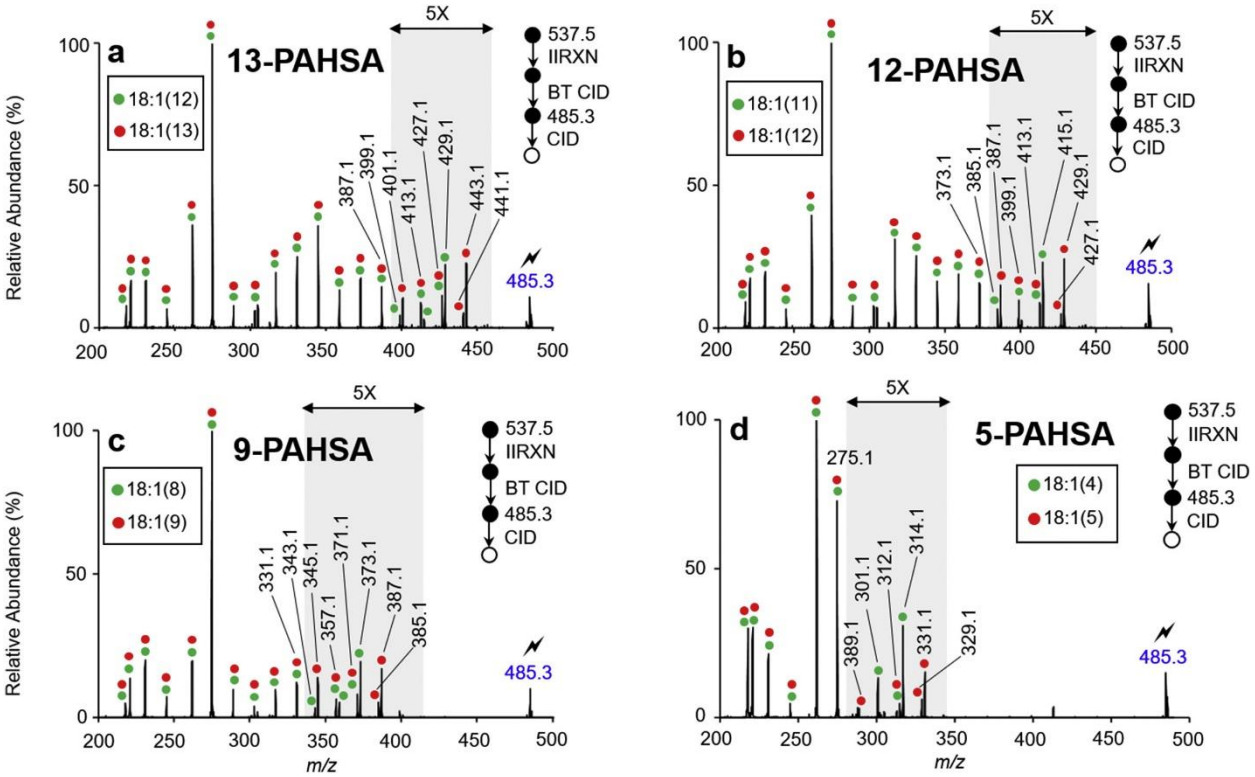

Figure 7.8 CID spectra of isomeric [*n*-HSA – H – H_2O + MgPhen]$^+$ complex cations derived from (a) 13-PAHSA, (b) 12-PAHSA, (c) 9-PAHSA, and (d) 5-PAHSA.

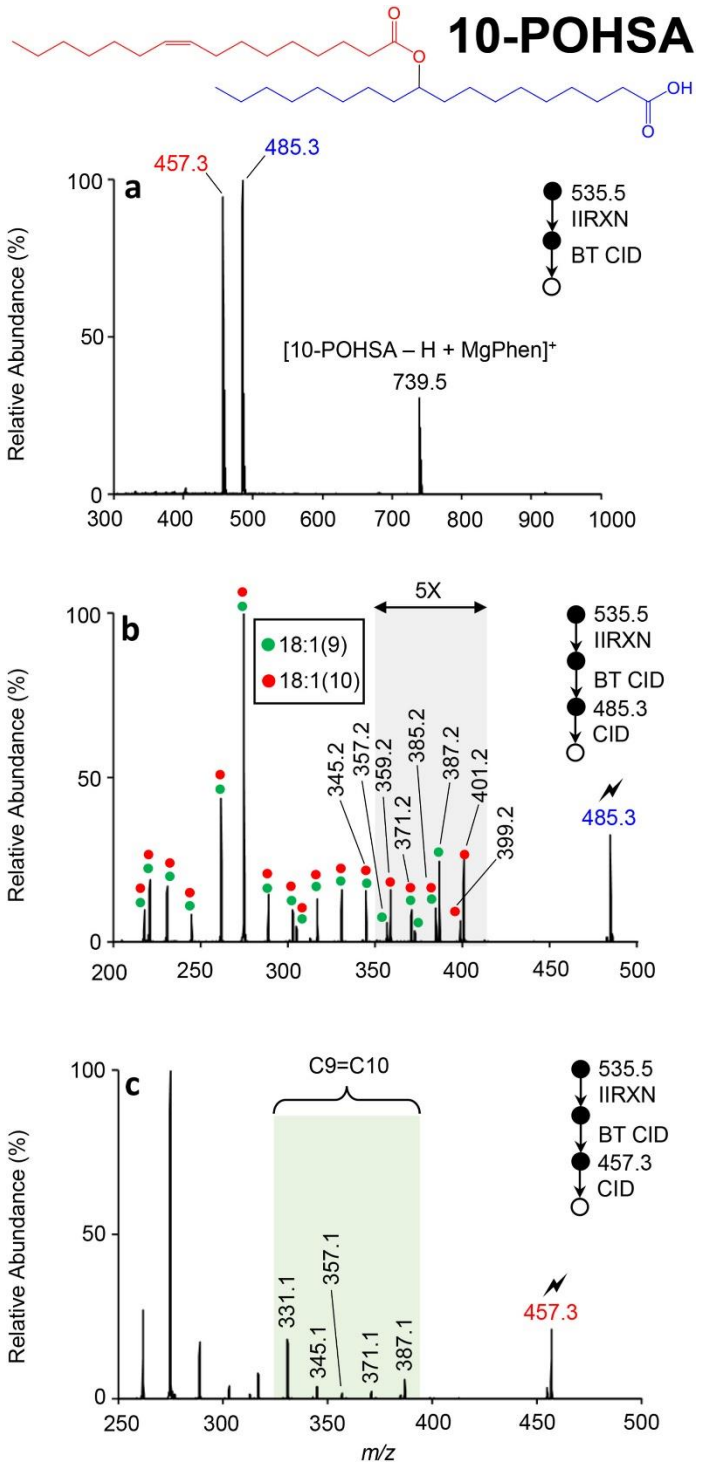

Figure 7.9 (a) Product ion spectrum resulting from ion/ion reaction between $[10\text{-POHSA}]^-$ anions and $[MgPhen_3]^{2+}$ reagent dications and subsequent BT CID. Ion-trap CID spectra of (b) $[10\text{-HSA} - H - H_2O + MgPhen]^+$ (*m/z* 485.3) and (c) $[16{:}1 - H + MgPhen]^+$ (*m/z* 457.3).

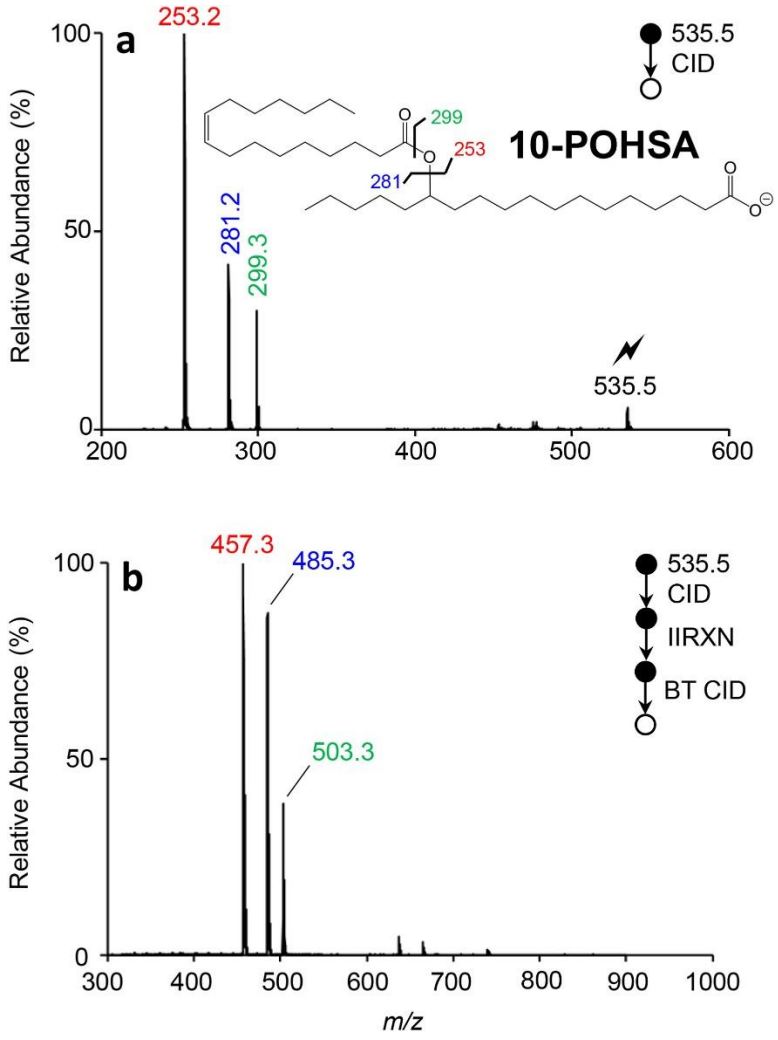

Figure 7.10 (a) CID spectrum of $[10\text{-POHSA}]^-$ (*m/z* 535.5). (b) Product ion spectrum resulting from ion/ion reaction between the $[10\text{-POHSA}]^-$ product anions shown in (a) and $[MgPhen_3]^{2+}$ reagent dications followed by collisional activation via BT CID.

PUBLICATIONS

1. Randolph, Caitlin E., Blanksby, Stephen J., McLuckey, Scott A. "Proton transfer ion/ion reactions for the gas-phase separation, concentration, and identification of cardiolipins." *Anal. Chem., **2020**, 92* (15), 10847–10855.

2. Randolph, Caitlin E., Marshall, L. David, Blanksby, Stephen J., McLuckey, Scott A. "Charge-switch derivatization of fatty acid esters of hydroxy fatty acids via gas-phase ion/ion reactions." *Anal.Chim. Acta, **2020,** 1129,* 31-39.

3. Randolph, Caitlin E., Shenault, De'Shovon M., Blanksby, Stephen J., McLuckey, Scott A. "Structural elucidation of ether glycerophospholipids using gas-phase ion/ion charge inversion chemistry." *J. Am. Soc. Mass Spectrom., **2020**, 31,* 5, 1093–1103.

4. Randolph, Caitlin E., Blanksby, Stephen J., McLuckey, Scott A. "Toward Complete Structure Elucidation of Glycerophospholipids in the Gas Phase through Charge Inversion Ion/Ion Chemistry." *Anal. Chem., **2020**, 92* (1), 1219-1227.

5. Randolph, Caitlin E., Foreman, David J., Blanksby, Stephen J., McLuckey, Scott A. "Generating Fatty Acid Profiles in the Gas Phase: Fatty Acid Identification and Relative Quantitation Using Ion/Ion Charge Inversion Chemistry." *Anal. Chem., **2019**, 91* (14), 9032-9040.

6. Franklin, Elissia T., Betancourt, Stella K., Randolph, Caitlin E., McLuckey, Scott A., Xia, Yu. "In-depth structural characterization of phospholipids by pairing solution photochemical reaction with charge inversion ion/ion chemistry." *Anal. Bioanal. Chem., **2019**, 411* (19), 4739-4749.

7. Randolph, Caitlin E., Foreman, David J., Betancourt, Stella K., Blanksby, Stephen J., McLuckey, Scott A. "Gas-Phase Ion/Ion Reactions Involving Tris-Phenanthroline Alkaline Earth Metal Complexes as Charge Inversion Reagents for the Identification of Fatty Acids." *Anal.l Chem., **2018**, 90* (21), 12861-12869.